

Microwave Electronics

**Design and Development of Compact Circularly
Polarized Multiband and Ultra-wideband
Microstrip Antennas for Wireless Applications**

A thesis submitted by

PRAKASH K. C.

in partial fulfillment of the requirements for the degree of

DOCTOR OF PHILOSOPHY

Under the guidance of

Prof. K. VASUDEVAN



**Department of Electronics
Faculty of Technology
Cochin University of Science and Technology
Cochin-22, India**

May 2019

***Design and Development of Compact Circularly Polarized
Multiband and Ultra-wideband Microstrip Antennas for
Wireless Applications***

Ph.D. Thesis under the Faculty of Technology

Author

Prakash K.C,
Research Scholar ,
Department of Electronics,
Cochin University of Science and Technology,
Cochin- 682022.
Email: keyceepee@gmail.com

Supervising Guide

Dr. K. Vasudevan,
Professor Emeritus,
Department of Electronics,
Cochin University of Science and Technology,
Cochin – 682022.
Email: vasudevankdr@gmail.com

May 2019

The true laboratory is the mind, where behind illusions we uncover the laws of truth.

– Sir Jagadish Chandra Bose

“When wireless is perfectly applied the whole earth will be converted into a huge brain, which in fact it is, all things being particles of a real and rhythmic whole. We shall be able to communicate with one another instantly, irrespective of distance”.

Nikola Tesla

Dedicated to the Almighty,

My Parents,

My Teachers

and my loving Wife and Daughter.....



**DEPARTMENT OF ELECTRONICS
COCHIN UNIVERSITY OF SCIENCE AND
TECHNOLOGY
COCHIN-22, INDIA.**

Dr. K.Vasudevan

Professor Emeritus

E-mail: vasudevankdr@cusat.ac.in, Ph: 0484 2576418

Certificate

This is to certify that, this thesis entitled “**Design and Development of Compact Circularly Polarized Multiband and Ultra-wideband Microstrip Antennas for Wireless Applications**”, is the outcome of the original work done by the candidate **Mr. Prakash K.C**, under my supervision in the Department of Electronics, Cochin University of Science and Technology. The work did not form part of any dissertation submitted for the award of any other degree, diploma, associateship or any other title or recognition from any University/ Institution.

I further certify that the corrections and modifications suggested by the audience during the pre-synopsis seminar and recommended by the Doctoral Committee of the candidate, are incorporated in the thesis.

*Kochi-22,
Vasudevan
May 2019.*

Dr. K.
(Supervising guide)

Declaration

I hereby declare that the work presented in this thesis entitled **“Design and Development of Compact Circularly Polarized Multiband and Ultra-wideband Microstrip Antennas for Wireless Applications”** is the outcome of the original work done by me, under the supervision of **Dr. K. Vasudevan**, Professor Emeritus, Department of Electronics, Cochin University of Science and Technology, India, in the Department of Electronics, Cochin University of Science and Technology. The work did not form part of any dissertation submitted for the award of any other degree, diploma, associateship or any other title or recognition from any University/ Institution.

*Kochi-22,
May 2019.*

Prakash K.C
Research Scholar

Acknowledgement

I remember with sincere gratitude deep from the heart.....

My supervisor and guide Prof. K. Vasudevan, for his constant encouragement and excellent guidance throughout the tenure of the work. His simplicity, way of life, elegant thoughts and positive approach has influenced me a lot. I consider it a great honour and fortune to have worked under his supervision. I am very much indebted to his efforts of helping me to complete this dissertation.

Prof. K. G. Nair, Former HOD and Founder of this Research Centre CREMA, for his vision, boundless effort in the development of this Department and for lighting the lamp of knowledge in us, without which we would not have entered the path of successful life. He remains as a role model in our minds.

Prof. C.S Sridhar (the late), veteran academician, embodiment of pleasant character, for the inspiration imparted to me.

I am grateful to Prof. C. K. Aanadan, Head, Department of Electronics for his whole-hearted support, friendly approach and extending the facilities of the Department of Electronics for my research.

Prof. P. Mohanan, UGC-BSR Professor, Dept. of Electronics for his special care, concern and great encouragement all throughout my years in this Department.

Prof. P. R. S. Pillai, Prof. K. T. Mathew and Prof. Tessamma Thomas, former Professors, Dept. of Electronics for their support and blessings.

Prof. Supriya M.H., former Head, Dept. of Electronics for her great support and help rendered to me and Prof. James Kurian, for his co-operation.

Sri. Arun Balakrishnan A, Sri. Mithun Haridas T.P, Dr. Bijoy and all other Faculty members of the department of Electronics for their goodwill and assistance.

The Librarian, all the technical, administrative and non-teaching staff of the department for the warm and cordial relations shared and invaluable helps.

Senior researchers Dr. Dinesh R, Dr. Sarin V.P, Dr. Nijas C.M., Dr. Shameena V.A, Dr. Sumitha Mathew, Dr. Anitha R, Dr. Deepak U. Mrs. Roshna T.K for sharing their sound technical and scientific knowledge with me.

My fellow researchers Jayakrishnan M.P, Vinesh P.V, Manoj M, Mohammed Ameen, Lindo Ouseph who helped me with their technical expertise, skills and knowledge at various junctures during the tenure of my research. Those moments are really memorable.

Vivek R, Libimol V.A, Dr. Sajitha, Dr. Sarah Jacob, Anju P. Mathews, Sreekala P.S, Dibin Mary, Neeraj, Tittu, Nelson, Tony D, Paulbert Thomas, and Cyriac M.O for their research discussions and memorable moments in the department.

Prasanth P.P, Suraj Kamal, Satheesan, Aji, Athul, Midhun and all other colleagues at the Centre for Ocean Electronics (CUCENTOL), Microwave Material Research Lab (MMRL), Audio and Image Research Lab (AIRL), Advanced Signal Processing & Instrumentation Research Lab (ASPIRE) and Intelligent Machine Systems Lab (IMSL), Department of Electronics, Cochin University of Science and Technology for their whole-hearted co-operation.

Beloved Beenachechi (Librarian, Central Library), who has been a source of inspiration since my M.Sc days here.

Hon'ble Chairman, University Grants Commission, New Delhi, Hon'ble President Board Members and the Secretary, Travancore Devaswom Board, Hon'ble Vice Chancellor, the Registrar and the Director of College Development Council, University of Kerala, The Director of Collegiate Education, Dr. K.S. Anilkumar, Principal, Sree Ayyappa College, Eramallikkara, for facilitating my research through Faculty Development Programme, without which my dream would not have been materialised.

Dr. S. Devaki Antharjanam, Sri. Jayachandran, Smt.S. Lekha, Dr. S. Gopalakrishnan Unnithan and Dr. K.Mohanakumar former Principals of Sree Ayyappa College, who provided me timely support and enthusiasm.

My Pappa, N. Chellappan (who is no more), Amma Smt. L.Thankamma and elder brother Sri. C.Vijayakumar who gave the highest priority to my education in spite of all hardships.

My Achan, Navaneethalal T.S (who is no more) for his love, support, care, blessings showered upon me and being a true mentor for me.

My lovely wife Adv. Sreekala T.N and daughter Aryasree P, for their boundless constant support, love, care, patience, sacrifice and being adorable, leaving behind all sorts of their personal sufferings. My dream would not have been materialised without their support and I am deeply indebted to them.

My Amma Sreedevi Lal, in-laws Lekha and Prasad, lovely kids Ammu and Ambady, loving brother Vijayan Chettan and all other well-wishers of Palluruthy, who loved me very much and provided me wholehearted support.

My sisters Smt. Sukumari, Bindu, Ambily, in-laws and their kids, family members and relatives who supported me.

Dr. Suresh S, Dr. N. Madhavan, Sri. Deepu G.P, Smt. JishaNair B.J Dr. S. Sreedevi, Smt. Ushakumary K.L, Smt. P.K. Sobha, Sri. Rejithakumar, Sri. Ganesan, Sri. Muralidharan Namboothiri, all other colleagues, friends, nonteaching staff and students of Sree Ayyappa College, Eramallikkara, my M.Sc classmates Dr. Jobin K, Antony , Dr. Jacob George, Paul V. John, Girish K and Deepukumar M. Nair for their support and encouragement.

K.G. Balakrishna Pillai Sir and M.N. Ramachandran Nair Sir, for their blessings, in the absence of their physical presence in this world.

All my friends and well-wishers of Kairali Grandhasala, Mampra.

Above all I thank Almighty, whose blessings and kindness helped me a lot to finish this thesis.

Prakash K.C

Abstract

Circular polarization is an important polarization scheme of electromagnetic waves, used extensively in wireless communication systems, like radar and satellite systems owing to its useful characteristics. Immunity to Faraday rotation, mitigation of multipath propagation, lack of polarisation losses due to misalignment are some of the attractive features of circular polarisation. These features make them widely useful in versatile wireless applications. Typically, circularly polarized antennas may be developed as microstrip patch antenna, slot antenna, spiral antenna and dielectric resonator antenna. However, the important challenges faced by these antennas are, difficulty in achieving omnidirectional radiation pattern, wideband radiation, manufacturability and miniaturization etc. Absolutely wide band electromagnetic pulses of very short duration, in the range of nanoseconds, are of great concern to the communication engineers and used extensively for military and biotechnological applications. Whereas, obtaining CP characteristics in the entire ultrawide band spectrum is challenging. Enhancement of CP bandwidth is a challenging task to the antenna designers, without compromising size of the antenna. In this context, compact single band, multiband and ultrawide-band circularly polarised microstrip antennas with enhanced bandwidths play a significant role in wireless communication systems.

The aim of this research work is to design and develop compact single band, multi band and ultrawide band circularly polarised antennas. This thesis presents a detailed study on the design, development and

characterisation of eight different types of single band, one dual band and four different types of ultrawide-band circularly polarised antennas, intended for wireless applications.

The single band CP antennas developed are polygonal shaped patch antennas, designed to be operated in the 2.4 GHz ISM band. The maximum 3 dB axial ratio band width obtained was 180 MHz, in the operating band. One of the major highlights of the thesis is, the achievement of significant impedance bandwidth (IBW) and 3 dB axial ratio bandwidth (ARBW) spanned over two frequency bands by a dual band circularly polarised antenna. It offered 10 dB IBW of 4.72 GHz (2.63–7.35 GHz, 94.6%), corresponding 3 dB ARBW of 2.12GHz (3.62–5.74 GHz, 45.3%) in Band I, IBW of 0.98 GHz (7.86 – 8.84 GHz, 117.4%) corresponding ARBW of 1.82GHz (7.06 – 8.88 GHz, 22.84 %) in Band II. Another significant achievement is, by a compact UWB antenna. It offered a 10 dB IBW of 10.05GHz (2.55–12.6GHz, 132.7%), 3 dB ARBW of 7.3GHz (3.9–11.2GHz, 96.7%), with an antenna size of $30 \times 33.5 \times 0.8 \text{ mm}^3$. This constitutes a wide coverage of over 88% of the ultra-wideband (UWB) spectrum (3.1–10.6GHz). Omni directional radiation patterns and marginal group delays are the other features these antennas. One of the highlights of the thesis is, the analysis of circular polarisation behaviour of a dual band CP antenna, by using Characteristic Mode Analysis tool of CST Microwave studio. The analysis of the patch geometries, is done through mathematical methods and simulation tools. The evolution of the antennas developed was thoroughly studied to have a deep insight into their circular polarisation behaviour.

Contents

Chapter 1

INTRODUCTION	01-29
1.1 Introduction.....	02
1.2 Broadband and UWB technologies.....	03
1.2.1 Ultrawide band Technology	05
1.2.2 Advantages of UWB	06
1.2.3 Development of UWB antennas.....	06
1.3 Microstrip antennas	07
1.3.1 Radiation mechanism	09
1.3.2 Printed slot antennas.....	11
1.3.3 Printed wide slot antenna	11
1.4 Feeding Techniques	12
1.4.1 Microstrip line feed	13
1.4.2 Coaxial probe feed	13
1.4.3 Proximity coupled feed	13
1.4.4 Aperture coupled feed.....	13
1.5 Polarisation.....	14
1.5.1 Circular polarization.....	14
1.5.2 Benefits of CP	16
1.5.3 Challenges of CP antenna	17
1.6 Models of analysis.....	19
1.6.1 Transmission line model	20
1.6.2 The cavity model.....	20
1.6.3 The multiport network model.....	20
1.6.4 Characteristic Mode Analysis	21
1.6.5 Method of moments	21
1.6.6 Finite element method.....	22
1.6.7 Spectral domain analysis.....	22
1.6.8 FDTD method	22
1.7 Motivation of the current research work.....	22
1.8 Thesis organisation	24
References	26

Chapter 2

LITERATURE REVIEW.....	31-81
2.1 Single band Circularly polarized antenna.....	32
2.2 Dual band and wide band CP microstrip antennas	44
2.3 Wide band/ UWB CP antennas	54

References	63
------------------	----

Chapter 3

METHODOLOGY..... 83 -97

3.1 Ansys HFSS Antenna simulation tool	84
3.2 Characteristic Mode Analysis using CST	85
3.3 Antenna fabrication procedure	86
3.3.1 Selection of substrate	86
3.3.2 Photolithography	87
3.4 Antenna Measurement Facilities	88
3.4.1 Performance Network Analyser	88
3.4.2 Anechoic Chamber	89
3.4.3 Hardware and software set up	90
3.5 Experimental Techniques	90
3.5.1 Measurement of S parameters	91
3.5.2 Radiation pattern	92
3.5.3 Antenna Gain and efficiency	92
3.5.4 Polarisation.....	93
3.5.5 Axial ratio.....	94
3.5.6 Group delay	95
3.6 Conclusion	95
References	96

Chapter 4

SINGLE BAND CIRCULARLY POLARISED MICROSTRIP

ANTENNAS..... 99-176

Introduction.....	100
4.1 Circularly Polarised Hexagonal patch antenna with polygonal slot	101
4.1.1 Antenna Geometry	102
4.1.2 Design equations and CP mechanism	104
4.1.3 Results and analysis	107
4.1.3.1 Measurement of $ S_{11} $ characteristics	108
4.1.3.2 Axial ratio	109
4.1.3.3 Radiation patterns.....	110
4.1.3.4 Measurement of Gain and efficiency.....	111
4.1.3.5 Surface current pattern.....	111
4.1.3.6 Confirmation of sense of polarization	112
4.1.3.7 Confirmation of sense of polarization using Smith Chart	113
4.1.4 Appropriateness of the antennas	116
4.1.5 Analytical treatment	116

4.1.5.1	Modal expansion	116
4.1.5.2	Orthogonal near degenerate modes	120
4.2	CP Dodecagonal patch antenna with polygonal slot	125
4.2.1	Antenna geometry	125
4.2.2	Design equations	127
4.2.3	Results and discussion.....	128
4.3	Hexagonal CP patch antenna with elliptical and circular slots.....	134
4.3.1	Antenna geometry	134
4.3.2	Design equations	136
4.3.3	Results and discussion.....	138
4.4	Dodecagonal CP patch antenna with elliptical slot	142
4.4.1	Antenna geometry	142
4.4.2	Results and discussion.....	145
4.5	CP decagonal patch antenna with polygonal slot	148
4.5.1	Antenna geometry	148
4.5.2	Results and discussion.....	150
4.6	CP Tridecagonal patch antenna with polygonal slot	154
4.6.1	Antenna geometry	154
4.6.2	Design equations	156
4.6.3	Results and discussion.....	156
4.7	CP Tetradeccagonal patch antenna with polygonal slot.....	160
4.7.1	Antenna geometry	160
4.7.2	Design equations	161
4.7.3	Results and discussion.....	162
4.8	CP Hexadecagonal patch antenna with polygonal slot	166
4.8.1	Antenna geometry	166
4.8.2	Design equations	167
4.8.3	Results and discussion.....	168
	Summary of the Chapter	171
	References	173

Chapter 5

DUAL BAND CIRCULARLY POLARISED

MICROSTRIP ANTENNA 177-244

5.1	A Printed Dual band Circularly Polarized Slot Antenna for Wireless Applications	180
5.2	Antenna Geometry	180
5.3	Measurement and simulation results.....	183
5.3.1	Measurement of $ S_{11} $ and Axial Ratio.....	183
5.3.2	Measurement of Gain and Efficiency	184

5.3.3	Radiation pattern	185
5.4	Study of surface current and electric field patterns	188
5.5	Evolution of the antenna DBCPA1	201
5.6	Characteristic Mode Analysis of the antenna DBCPA1	224
5.6.1	Characteristic modes evaluated with a sorting frequency 2.5 GHz	225
5.6.1.1	Orthogonal modes at 2.984 GHz.....	228
5.6.1.2	Orthogonal modes at 3.512 GHz.....	230
5.6.1.3	Orthogonal modes at 4.16 GHz	231
5.6.2	Characteristic modes evaluated with a sorting frequency 8.7 GHz	232
5.6.2.1	Orthogonal modes at 6.179 GHz.....	234
5.6.2.2	Orthogonal modes at 6.234 GHz.....	235
5.6.2.3	Orthogonal modes at 6.19 GHz.....	237
5.6.2.4	Orthogonal modes at 8.082 GHz.....	239
	Chapter summary	241
	References	241

Chapter 6

ULTRA WIDE BAND CIRCULARLY POLARISED MICROSTRIP ANTENNAS..... 245-287

6.1	A Compact UWB Circularly Polarized Hexagonal Slot Antenna for Wireless Applications	247
6.1.1	Antenna Design	247
6.1.2	Results and Discussion	249
6.2	A Compact UWB Circularly Polarized Penta Decagonal Slot Antenna for Wireless Applications.....	253
6.2.1	Antenna Design.....	253
6.2.2	Results and discussion.....	255
6.3	Circularly Polarised UWB Antenna	259
6.3.1	Antenna Geometry and Design	259
6.3.2	Study of simulated surface current.....	260
6.3.3	Measured results and discussion	262
6.3.3.1	Measurement of S11 and axial ratio	262
6.3.3.2	Measurement of gain and efficiency	263
6.3.3.3	Measurement of radiation pattern	264
6.4	Printed Circularly Polarised Asymmetric Ultra- wideband Antenna	265
6.4.1	Antenna geometry and design	266
6.4.2	Study of surface current and electric field patterns.....	270
6.4.3	Measured results and discussion	276
	Chapter summary	283

References	283
Chapter 7	
CONCLUSION	289-297
7.1 Thesis summary and conclusion	289
7.2 Inferences from the investigations on the various antennas described	291
7.3 Suggestions for future work in the field	296
PUBLICATIONS	299
RESUME OF THE AUTHOR	305

List of Abbreviations

AR	Axial Ratio
ARBW	Axial Ratio Band Width
BW	Band Width
CP	Circular Polarisation
CPW	Co-planar Waveguide
C-SRR	Complementary-Split Ring Resonator
CST	Computer Simulation Technology
DGS	Defected Ground Structure
DSSS	Direct Sequence Spread Spectrum
EBG	Electromagnetic Band Gap
EMI/EMC	Electromagnetic Interference/ Compatibility
FCC	Federal Communication Commission
FDTD	Finite Difference Time Domain
FWHM	Full Width Half Maximum
Gbps	Giga bits per second
HFSS	High Frequency Structure Simulator
HF	High Frequency
IFFT	Inverse Fast Fourier Transform
IRA	Impulse Radiating Antennas
IBW	Impedance Band Width
LHCP	Left Hand Circular Polarisation
LNA	Low Noise Amplifier
LOS	Line of Sight
MEMS	Micro Electro Mechanical Systems
MMIC	Monolithic Microwave Integrated Circuits

NLOS	Non-LOS
OFDM	Orthogonal Frequency Division Multiplexing
PAM	Pulse Amplitude Modulation
PCB	Printed Circuit Board
PNA	Performance Network Analyser
PPM	Pulse Position Modulation
PSD	Power Spectral Density
RF	Radio Frequency
RFID	Radio Frequency Identification
RHCP	Right Hand Circular Polarisation
RL	Return loss
SNR	Signal to Noise Ratio
SRR	Split-Ring Resonator
UWB	Ultra-wide Band
VNA	Vector Network Analyser
VSWR	Voltage Standing Wave Ratio
Wi Fi	Wireless Fidelity
WiMAX	Worldwide Interoperability for Microwave Access
WLAN	Wireless Local Area Networks
WPAN	Wireless Personal Area Networks

.....❧.....

Chapter 1

INTRODUCTION

<i>Contents</i>	1.1 <i>Introduction</i>
	1.2 <i>Broadband UWB Technologies</i>
	1.3 <i>Microstrip antennas</i>
	1.4 <i>Feeding Techniques</i>
	1.5 <i>Polarisation</i>
	1.6 <i>Models of analysis</i>
	1.7 <i>Motivation of the present thesis</i>
	1.8 <i>Organization of the thesis</i>

This chapter gives a brief account of the history of modern wireless communication. In comparison to other types of antennas, the importance of microstrip antennas and progressive research work going on in modern times has been emphasised. Theoretical explanation and mathematical analysis methods have been dealt with. The motivation behind the curious study, analysis, design and development of new antennas is furnished. The conclusion of this chapter is an overview of the organisation of the thesis.

1.1 Introduction

Antenna is “that part of a transmitting or receiving system that is designed to radiate or to receive electromagnetic waves” as per IEEE definition [1].

Any wireless communication system needs antenna as the most inevitable component. In the beginning, dipole antenna was used for various applications [2]. It should be approximately one half the wavelength ($\lambda/2$) at the operating frequency, in order to have effective reception as well as transmission (or multiples of this length). Hence, at low frequencies of operation, the antenna length will be fairly high. Whereas at higher frequencies, it is not quite desirable due to its protruding nature. When Yagi- Uda antenna was introduced in 1920s, it was a breakthrough because of its high gain (8–14dB) [3]. Antennas based on different wire geometries like dipole antenna, Yagi-Uda antenna, log-periodic antenna, spiral antenna, horn antenna, reflectors, slot antenna and their arrays were used till the late 1970s. The antenna designer was free to modify an antenna depending upon certain antenna parameters like gain, bandwidth, input impedance, sidelobe levels and beam width. Extensive experimental investigations were required for the validation of an antenna design. Recently, exponential growth is observed in computing speed and efficient computational techniques for realistic antenna design has catalysed in the economical antenna development. There has been an explosive growth in wireless communication technologies, microwave sensors, microwave imaging techniques, and radars. A breakthrough which led to the miniaturisation of communication

technologies was the introduction of microstrip antennas by Deschamps in 1953. In another span of 30 years it evolved as a vibrant area. The development of low loss substrates and easy photolithographic techniques mobilised its developmental growth. Even though the idea behind microstrip antennas was proposed by Deschamps, patent with regard to the first practical microstrip antenna development goes to the credit of Munson and Howell [4]-[7]. Need for non-protruding type antennas for airborne systems, enhanced bandwidth needs, and multifunctionality resulted in large scale exploitation of printed (microstrip patch) antennas and slot-type antennas. The powerful computational tools aided the design of such antennas [8].

The recent explosive growth in antenna design needs were rendered chiefly by the commercial mobile communications industry. The past decade has witnessed substantial use of antennas for Radio Frequency ID (RFID) devices, Bluetooth devices, cellular systems, GPS systems, satellite communication, Wi-Fi, WiMAX, etc. However, in the forthcoming era of automation, the need for antennas may get multiplied. In the area of military applications, extensive demand is there for compact and conformal multifunctional antennas [3].

1.2 Broad Band and Ultra-wide Band (UWB) Wireless Technologies

The technology that deals with point to point and point to multipoint communication services for the transmission of signals between hub and end-users is referred to as wireless broad band technology. It ensures high-speed. The advantages of higher frequencies

over lower frequencies are wider bandwidth and compact antenna size and hence ease of installation. But the disadvantage is range limitations under bad weather conditions [9].

Based on the features broad band wireless technologies are classified. Each class has a specific application. Data rate, range and power are the requirements for each application. Classification of wireless technologies based on the range [10] is shown in Fig. 1.1.

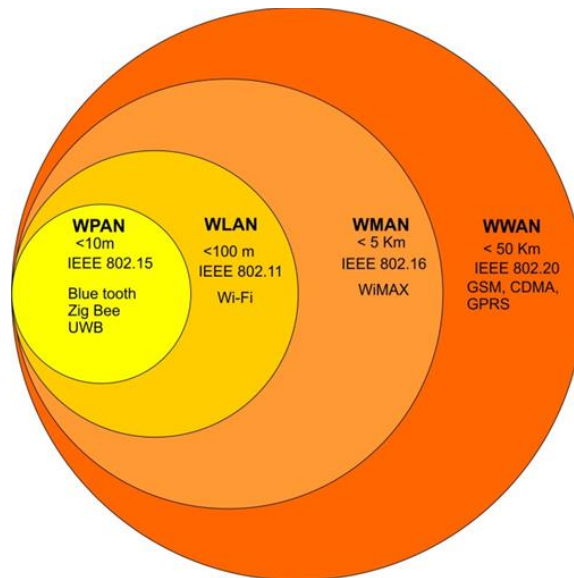


Figure 1.1. Classification of broadband wireless technologies

The transmission radius of Wireless Local Area Networks (WLANs), is a few hundreds of meters and that of Wireless Personal Area Networks (WPANs) is tens of meters or less. These two are popular applications of wireless technology. For these networks, the data rate requirement is increasing day by day [11]. There is a wide variety of wireless networking

applications for home and commercial needs, rather than IEEE 802.11, WLAN (Wi-Fi) applications and IEEE 802.15 WPAN (Bluetooth) applications [12]. Recently, the aim of WPAN is to establish wireless connections between computers, portable devices and consumer electronics gadgets with high reliability, speed and data rate, within a short radius. Whereas to achieve high data rate, large bandwidth is a necessary requirement. Spectral scarcity will be a crisis due to the hike in mobile devices day by day. The co-existence of wireless devices will be cumbersome. The issues of high data rate and co-existence of wireless devices may be solved by an alternative high-rate physical layer that is achievable with Ultra-wide Band technology (UWB) [13].

1.2.1 Ultra-wide Band (UWB) Technology

UWB terminology in wireless communication technology is used to transmit huge data using low power, short duration (a few nanoseconds) radio pulses/ impulses. As there is no carrier required for its transmission over a short distance, carrier-free, impulse or base-band radio are the other names of this system [11].

Federal Communication Commission (FCC) defines UWB as a system for which the fractional bandwidth is greater than 20% or occupying an instantaneous bandwidth of at least 500 MHz [14]. The signal of UWB system has a wide band width of 7.5 GHz (3.1–10.6 GHz as per FCC regulations) and a power spectral density of -41.3 dBm/ MHz.

UWB devices are encompassed in three groups; namely communication, imaging and vehicular radar, as per FCC regulations.

The number of Personal communication devices get multiplied every year. Large scale use of UWB devices in home, offices and public places catalysed this growth.

1.2.2 Advantages of UWB

There are several advantages for UWB systems over other communication systems like narrow band and wide band systems; due to the spectral properties of narrow pulses used here [15]-[17].

- High channel capacity
- Operate with low SNR:
- RF spectrum sharing:
- Immunity to intercept and detection:
- Robustness against multipath propagation:
- Ranging and imaging capability:
- Simple transceiver design:

1.2.3 Development of UWB Antennas

UWB antenna belongs to the class of broad band antennas which operate over wide bandwidth. In 1898, It was Oliver Lodge who introduced the concept of UWB antenna design in 1898. He introduced various types of dipoles such as square plate dipoles, triangular or “bow-tie” dipoles, spherical dipoles and biconical dipoles [18]. Later several types of UWB antennas were introduced by researchers. This include conical monopole, biconical dipole, coaxial horn etc. [18]

The first UWB antenna introduced by Oliver Lodge was biconical dipole antenna. This design was modified and improved by Carter in 1939[19]. It was the stepping stone towards the development of broadband antennas. Further modification resulted in Discone antenna; which has a disk and a cone. During 1940's, coaxial horns became the popular UWB antenna. L. N. Brillouin [20] developed omni-directional and directional coaxial horns, But the bulky structure made it less attractive. In 1940, J. D. Kraus [21] introduced an antenna known as volcano smoke antenna. Though these UWB antennas were used in communication systems, they are not convenient to be used in modern communication systems. Their structure, size, cost and incompatibility in integration with the systems, were the disadvantages.

1.3 Microstrip Antennas

Microstrip antennas, comprises of a very thin metallic strip (patch), which is thinner than free space wavelength. This patch is placed on one side of a dielectric sheet called substrate with height 'h'. 'h' is very small compared to free space wavelength and the other side of the substrate is the ground plane as shown in Figure 1.2 [2]. The microstrip patch is designed as a broadside radiator, its pattern maximum will be normal to the plane of the patch, by choosing the mode of excitation below the patch. The proper mode selection is important.

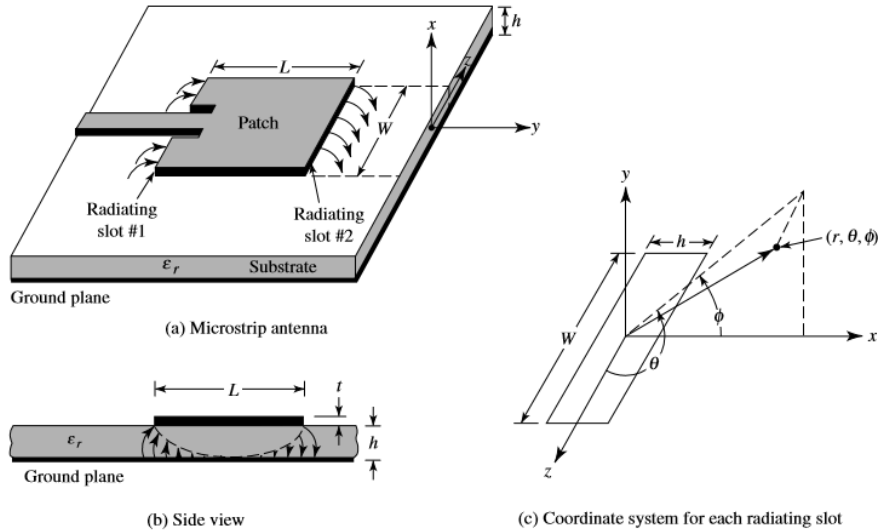


Figure 1.2. Microstrip antenna and coordinate system [2]

The range of dielectric constants of different substrates is between 2.2 and 12. Substrates with lower dielectric constants and higher thickness provide good efficiency, wider bandwidth. Thin substrates with larger values of dielectric constants need tightly bound fields, which help to minimize unwanted radiation and coupling and are preferred for microwave circuitry. They lead to smaller sizes but they are having minimum efficiency and with bandwidths of smaller values and greater losses, [22].

Microstrip antennas are having advantages like low profile, conformable to planar and nonplanar surfaces, compatible with printed-circuit technology and hence simple and inexpensive to manufacture, on rigid surfaces. It is mechanically robust, easily compatible with MMIC designs. Versatile as far as resonant frequency, impedance, pattern, and polarization are considered. There are certain demerits like less efficient,

high quality factor, minimum values of power, purity of polarization, and less bandwidth [2]. It is possible to overcome these disadvantages using a wide variety of techniques.

Photolithography is used to print various shapes of elements on microstrip antennas or patch antennas. The radiating patch may have different shapes. Some shapes are depicted in Figure 1.3.

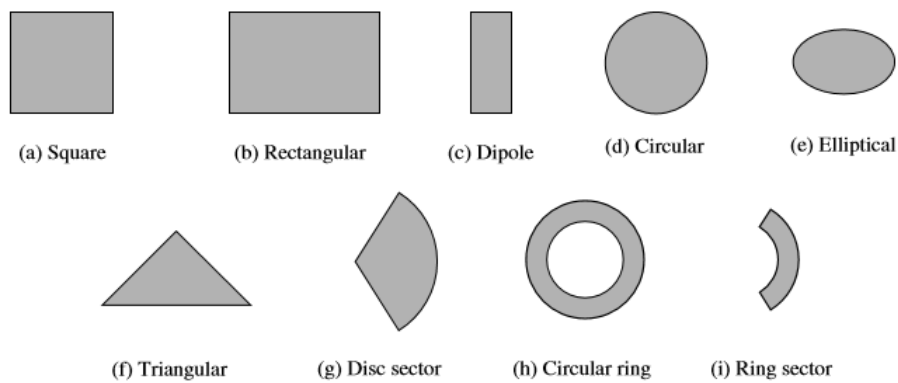


Figure 1.3. A few shapes of microstrip patch elements [2].

1.3.1 Mechanism of radiation

The fields along the edges of the patch are subjected to fringing as the patch finite length and width. This is illustrated along the length. From the Figures 1.2 (a) and 1.2 (b) it can be inferred from the two radiating slots of the rectangular patch. The same is applicable along the width of the patch. The values of L , W and h and dielectric constant affect the amount of fringing.

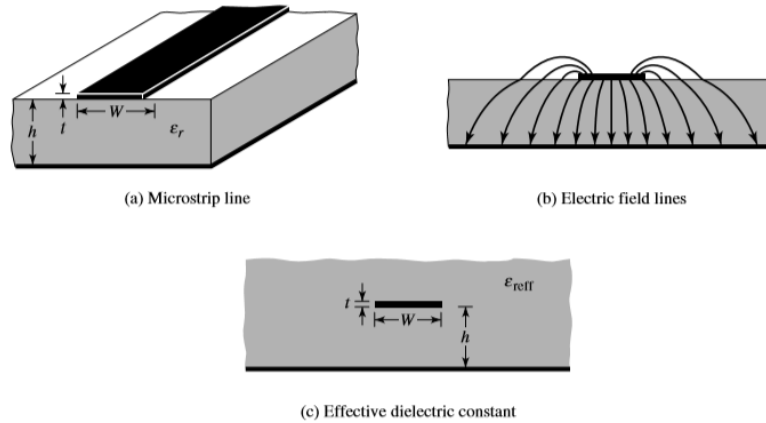


Figure 1.4. Microstrip line and its electric field lines, and effective dielectric constant geometry [2].

As $W/h \gg 1$ and $\epsilon_r \gg 1$, almost all electric field lines are concentrated in the substrate. The microstrip line looks electrically wider in comparison to its physical dimensions due to the fringing mechanism in this case. Now the term effective dielectric constant ϵ_{reff} is introduced due to the fringing mechanism and the wave propagation along the microstrip line, on account of the fact that some waves propagate in the substrate and some in the other substrate (air).

A thick dielectric substrate with lower dielectric constant values provides better efficiency, radiation and larger bandwidth, while, the antenna size becomes large. Whereas high value of dielectric constant decreases the size of the antenna. Demerits are lower efficiency and bandwidth.

1.3.2 Planar slot antennas

For applications like a miniaturised antenna is a major requirement. Here slot antenna is a good candidate in mobile handsets and other wireless applications, as it is having simple structure. The slot antenna comprises of a straight slot having very small thickness and fed electromagnetically by a transmission line. The straight slot can be altered [23], [24]. The structures are depicted in Figure 1.5 (a)–(c).

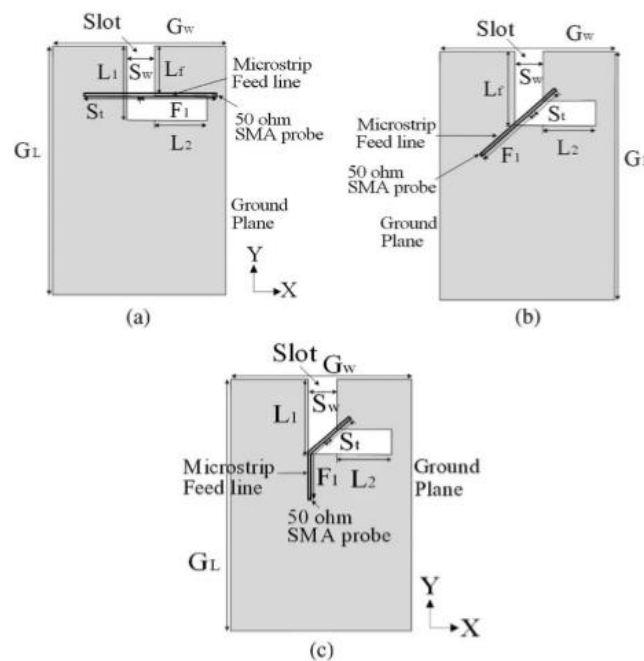


Figure 1.5. L-slot antenna, with feed lines: (a) straight, (b) inclined, and (c) bent [23]

1.3.3 Printed Wide-Slot Antenna:

The antenna configuration of this type of antenna is shown in Figure 1.6 [25]. This wide slot and stub can assume any shape and as such, a wide varieties of antennas are there. A slot antenna usually

generates a bidirectional radiation pattern as it radiates on upper and lower sides of the slot. A reflector plate situated below one side of the slot, can generate a unidirectional pattern.

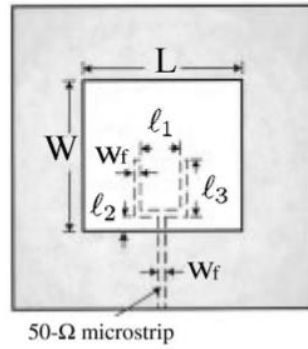


Figure 1.6. Planar wide-slot antenna [25]

1.4 Feeding Techniques

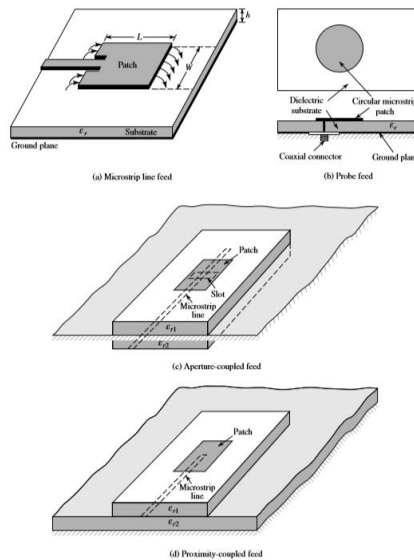


Figure 1.7. Typical feeds for microstrip antennas [2]

There are many methods which are used to feed patch antennas as shown in Figure 1.7.

1.4.1 Microstrip line feed

This is a simplest feeding method as shown in Figure 1.7 (a). The feedline and patch are fabricated together. The disadvantages are spurious radiations which adversely effect the side-lobe level and cross-polarization of the antenna.

1.4.2 Coaxial probe feed

This is the most popular feeding technique. The SMA connector is used for feeding the signal input. The outer conductor of the connector touches with ground plane and the centre conductor touches the top patch element as shown in Figure 1.7b. Here the feed location is selected to yield best impedance matching. Fabrication simplicity and minimum spurious radiation are the two merits of this feed method.

1.4.3 Proximity coupled feed

The feed technique is shown in Figure 1.7c. The advantages are less spurious feed radiation and high bandwidth, due to the overall increase in the thickness of the microstrip patch antenna. Two different dielectric materials, may also be used. But fabrication will be more difficult [26].

1.4.4 Aperture coupled feed

A microstrip line etched on the lower substrate is electromagnetically coupled to the patch through a slot or aperture in the ground plane, as in Fig.1.7d. Spurious radiations are minimum. Fabrication is difficult.

1.5 Polarization

The polarization is one of the important features of electromagnetic wave. This is the locus traced by the extremity or tip of the time-varying electric field vector \mathbf{E} with respect to an observation point, which is fixed. The trigonometric form of the field vector of a wave propagating towards the z direction may be expressed as [27]

$$\mathbf{E} = \hat{x} A \cos(\omega t - \beta z) + \hat{y} B \sin(\omega t - \beta z) \quad (1)$$

where A represent the amplitude of the field component in the X direction and B , that in the y direction, respectively. this expression represents a linearly polarized wave; If A or $B = 0$. If $A \neq B \neq 0$, the wave becomes an elliptically polarized. if $A = B$, it then represents a circularly polarized wave, the focal topic of this thesis.

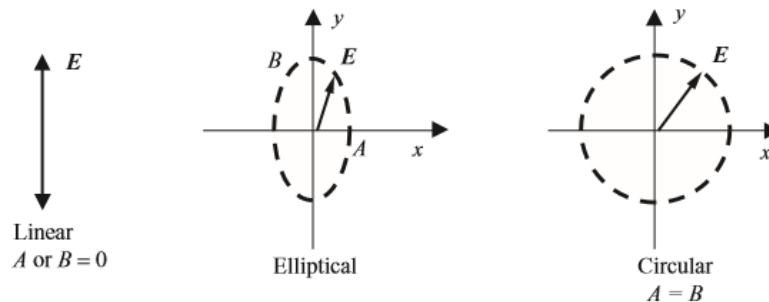


Figure 1.8. Wave polarisations [27]

1.5.1 Circular polarisation

The combination of two orthogonally polarized (one vertical and one horizontal) waves gives rise to a circularly polarized wave. As such the two senses or types of circular polarization are RHCP and LHCP. The two senses of polarisation are generated when phase of one linearly

polarized wave is ahead of or behind the other linearly polarised wave by 90 degrees. When the thumb is pointed in the direction of propagation and the tip of the E vector is in the direction of the right-hand fingers, it is RHCP. Otherwise, it is LHCP. If $A = B > 0$, equation (1) is one for a right-hand circularly polarized wave. The corresponding equation for left-hand polarized wave may be written as follows [27]

$$\mathbf{E} = \hat{x}A \cos(\omega t - \beta z) - \hat{y} B \sin(\omega t - \beta z) \quad (2)$$

The only difference between equations (1) and (2) is only in a sign. ‘+’ is changed to ‘-’ for the y component, and a phase lag for this component. The ratio of amplitudes A to B, that is the amplitude of one linearly polarised wave to the amplitude of the other linearly polarised wave is called the axial ratio:

$$AR = A/B$$

The value of axial ratio for a circularly polarized wave, is unity. Whereas for a linearly polarized wave, its value will be either zero or infinity. infinite or zero, thus $0 \leq AR \leq +\infty$. Therefore, a plane wave can have any of the three polarisations namely linearly polarization, circularly polarization or elliptical polarization.

$$\mathbf{E} = \hat{x} E_0 e^{j(\omega t - \beta z)} \quad (3)$$

Equation (3) [27] represents a linearly polarized plane wave, whilst Equations (1) and (2) represent circularly polarized plane waves. Circular polarization (CP) is a case of elliptical polarisation, when the minor axis and major axis of the ellipse become equal. Co-

polarization is the polarization, antenna is intended to radiate (receive) while cross polarization is the polarization orthogonal to the co-polarization.

Circular polarisation is having inherent unique properties, which are employable in high performance wireless communication systems.

1.5.2 Benefits of Circularly Polarised Antennas

Immunity to Faraday rotation. The Faraday effect is a phenomenon which causes the plane of polarisation to rotate. The extent of rotation is proportional to the magnetic field component in the propagation direction. The thickness and temperature of the ionosphere, as well as the frequency affects the extent of rotation –the rotation is more at lower frequencies but less at higher frequencies [27]. Highly ionized plasma generates strong magnetic fields in ionosphere [28]. In the case of linearly polarised waves it will result in polarisation mismatch of the signal. As the ionosphere causes Faraday rotation to an EM wave, there is a chance for a linearly polarized EM wave to be rotated by an unknown amount. A very important fact is that circularly polarised waves have high immunity to this effect, as both orthogonal components have equal magnitude and rotation occurs equally for both the components by the same angle. Hence CP is used in almost all earth–satellite communication systems, GPS (global positioning system) etc., particularly due to this advantage.

Mitigation of multipath propagation. Reflection from a conducting surface causes the sense of polarisation of a circularly polarised wave, to change and gets counter polarised (RHCP becomes LHCP and vice

versa). Hence reflected signal is filtered out [29] and is a major benefit for satellite based and other navigation systems. This avoids interference between direct and reflected signals. It is highly beneficial for large data rate communication especially in indoor applications.

Polarisation losses due to misalignment. In order to avoid polarisation mismatch, the receiving and transmitting antennas in communication systems must be properly aligned when the waves are linearly polarised. In the case of circular polarisation, this alignment is not at all required [30]. The loss is 3 dB, irrespective of receiving antenna orientation, if linearly polarised antenna receives ideal CP signal. In the case of RFID systems, it ensures the detection of portable tag irrespective of its orientation [31]. This is a very useful property here in the case RFID systems. Because of the above advantages there is large demand for CP antennas.

1.5.3 Challenges for Circularly Polarised Antennas

Despite the features mentioned above, many features exhibited by linearly polarised antennas are not available for CP antennas. The challenges are:

Omnidirectional Radiation Pattern: Achieving omnidirectional radiation pattern with circularly polarized antennas seems to be difficult [32]. The reason is that the requirement of two electric field components having same magnitude and $\pm 90^\circ$ phase difference. For wider angles, it is not easily achievable. The ground plane of a microstrip patch antenna attenuates the electric field component parallel to it. This results in the

deterioration of the axial ratio. Now, multiple radiators or complex polarisers are used for omnidirectional CP antennas. It is quite inconvenient and new methods are to be devised to address this issue. However, this is mandatory to develop omnidirectional CP antennas, as they find numerous applications. Some are listed below.

- **Point-to-multipoint communication.** A node located at the center broadcast RF signals to surrounding units.
- **In RFID systems, the omnidirectional pattern mitigates the chance of not detection of a tag due to nulls in radiation pattern.** A tag is detected irrespective of the direction of its orientation in CP systems. This is more useful in security systems.
- **For many remote tracking applications.** Tracking object rotates with antenna. Omnidirectional RHCP antenna is used in satellite navigation systems and therefore this problem can be rectified.
- **Currently antennas for TT&C are complex, expensive and heavy.** For telemetry, tracking and command (TT&C) applications if CP antenna is used, omnidirectional pattern is required. CP is applied to minimise the effect of Faraday rotation in the ionosphere.

Omnidirectional Radiation Pattern It is difficult to maintain pattern reconfigurability in CP antennas, as maintaining orthogonality of the individual components for all switched beams is not that easy. However

to have a wide scanning angle, each antenna element in an array should be either omnidirectional or radiate within a wide beam width.

Wideband Radiation

As described already, a 90° phase shift between the individual electric field components is required for a CP antenna. However this introduces a serious limitation on the bandwidth of these CP antennas.

Manufacturability and Miniaturization

Manufacturability is an important factor as far as an antenna design is considered. Miniaturization of antennas and accommodating multiple radio systems in CP antennas is a major requirement. But it is not that easy to realise with CP antennas, as two orthogonal components need space requirements. Current miniaturization techniques applied for linearly polarised antenna, would mitigate the polarisation purity. If high permittivity substrate is used, bandwidth will be reduced.

Cost factor

At present CP antennas with good axial ratio performance are not cost effective.

1.6 Models of analysis

The antenna analysis techniques help us to have an understanding of the underlying principles which are meaningful for the development of a novel design and configuration and also to incorporate modifications. The analysis yields different radiation characteristics and parameters of the antenna. Major analytical methods used are [33], [34] and [35]

Transmission line, multiport network and cavity models and Characteristic mode analysis methods.

The first three methods are suitable analytical methods for simple geometries with common patch shapes. Though they provide simplicity and easy analysis the results are less accurate. Whereas numerical techniques based on full wave methods are the most accurate but procedure is lengthy.

1.6.1 Transmission line model

The primitive method to analyse a rectangular microstrip antenna was developed by Munson [36]. A transmission line is used to model inner portion of the antenna. Two narrow slots situated at each end of the line resonator are used to model the radiator element. Mutual conductance represents the above said interaction between the two slots. The occurrence of fringing fields is mainly at the open circuited ends.

1.6.2 The cavity model

The interior of the patch is modelled as a cavity [37]. The patch is modelled as combination of various resonant modes, for regular patch shapes such as rectangular, circular and triangular etc. Whereas for irregular geometrical shapes, regular shapes are derived from the patch and then modelled.

1.6.3 The multiport network model

The electromagnetic fields in and outside the patch are patterned. With a two-dimensional planar network, the patch of any geometrical shape is modelled with numerous ports arranged around the edges. The

segmentation method is used for evaluation. The voltage distribution helps to calculate the radiated fields [38].

1.6.4 Characteristic Mode Analysis

The characteristic mode analysis of the antenna helps us to have a clear understanding of the theory behind the CP performance of the antenna. This enables us to explore new design strategies for improved performance. In this method of analysis, two quantities are used to describe the performance. They are Characteristic Angle (CA) and Modal Significance (MS); both are described in terms of the eigen value (λ). They are defined as follows [35]

$$\text{Characteristic Angle (CA) , } \alpha = 180^\circ - \tan^{-1}(\lambda)$$

$$\text{Modal Significance MS} = \frac{1}{|1+j\lambda|}$$

The characteristic angle is the phase angle between a characteristic current and the associated characteristic field. Hence, a mode is at resonance When the characteristic angle of a mode is nearly 180° , it is inferred that this mode is at resonance. The modal significance value of a mode describes its contribution to the total radiation when a source or excitation is applied. When the characteristic angle value difference between two resonant modes is 90° and their MS values are equal; then those modes are said to contribute for CP performance. These modes are said to be orthogonal modes [35].

1.6.5 Method of moments

Microstrip antennas of rectangular and nonrectangular shape can be analysed by the method of moments. The method of moments is used to solve the integral equation [39].

1.6.6 Finite element method

This is a numerical technique for solving a integral or differential equation. In a microstrip antenna, depending upon the dimensions of the interior region, the region of interest is subdivided into tiny areas or volumes, the inner fields of the antenna cavity is estimated. The small regions are chosen as polygons for 2D problems and tetrahedral elements for 3D problems.. The wave equations with inhomogeneous boundary conditions may be solved [40]. This method is applicable to patches with irregular shapes also.

1.6.7 Spectral domain analysis

2-D Fourier transforms and basis functions are used for the evaluation of different antennas [41].

1.6.8 Finite difference time domain (FDTD) method

By providing a straight forward solution to Maxwell's equations in differential form, the FDTD is a strongest electromagnetic tool capable of analysing complex antenna structures [41], [42]. The transient current's Fourier transform gives the frequency dependence of different parameters. Computational cost is high and requires large memory requirements for complex structures.

1.7 Motivation behind the current research work

- The printed antenna technology is attractive to the antenna designer due to many reasons.
- Growing interest is observed in accommodating several operating frequencies in a single antenna which provide high IBW and ARBW. UWB electromagnetic pulses of nanosecond duration are very useful in communication field and widely explored for military and biotechnological applications. CP antennas provide better mobility, weather penetration, insensitive to orientation of mobile device, reduced multi path loss.
- Benefits of Circularly Polarised Antennas like immunity to Faraday rotation, mitigation of multipath propagation and non requirement of alignment between transmitter and receiver.
- Single feed systems require no external polarizers or power divider networks
- Challenge of CP antenna in yielding omni directional radiation pattern, which is highly useful in point-to-multipoint communication, In radio frequency identification (RFID), remote tracking applications
- Slot antennas with large radiating aperture yield wider bandwidth without increasing the size and thickness.
- The highest percentage ARBW coverage of the UWB spectrum obtained by the antennas under study is 64%.
- Asymmetric design strategy for CP slot antennas

- Compact structure that provides maximum percentage CP band coverage of the UWB spectrum.

Issues to be addressed

- Preserve compactness while applying the modifications
- Achieve CP in the dominant mode
- Maintain optimum ARBW and maximum impedance matching and achieve high ARBW in UWB with a compact structure
- Asymmetric slot structure has not been much explored
- The ultra wide band is to be focused upon
- Slits, slots and stubs were to be suitably combined
- Omni directional radiation pattern in CP antennas

1.8 Thesis organization

Aim of this research work is to develop compact circularly polarised single band, multi band and ultrawide band microstrip antennas employing novel patch modification techniques and geometrical shapes. The design, fabrication, characterization and theoretical analysis of different circularly polarised patch geometries for use at single resonant frequency, dual bands and ultrawide band operating frequencies yielding good results are presented in this thesis. Investigations on the effects of the asymmetrical structure on the circular polarisation is carried out. Parametric analyses are done and experimentally proved.

Introduction to microstrip antennas, feeding mechanisms, analysis approaches and theory of circular polarization are briefly explained in Chapter 1.

A comprehensive review of literature related to circularly polarised microstrip antennas working in single band, dual band and ultrawide band antennas are described in Chapter 2.

Chapter 3 presents experimental methods availed. The simulation tool which is also used for the preliminary design has been explained. Measurements techniques of various antenna parameters and fabrication steps are described.

Chapter 4 investigates single band CP antennas developed. The polygonal shaped patches are embedded with polygonal slot. The parametric study of the slot in the centre of the patch boundary has been conducted.

Chapter 5 presents the design, development, measurements and analysis of compact dual band circularly polarised patch antenna. The slots, slits and metallic strips are added at different positions. The circular polarization performance is analysed through characteristic mode analysis. Different modes have been identified through characteristic mode analysis. Excitations of higher order degenerate modes are analysed.

Chapter 6 elucidates the design and development of novel circularly polarised ultrawide band microstrip antenna with an asymmetric design strategy. The design strategy based on combination of slits, slots and stubs have been studied extensively.

A brief summary of investigations on the performances of developed CP antennas are emphasised in Chapter 7. A few suggestions for the future study are also incorporated here.

References

- [1] “IEEE Standard Definitions of Terms for Antennas”, The Institute of Electrical and Electronics Engineers, Inc 345 East 47th Street, Newyork, NY10017, USA, 1983.
- [2] C. A. Balanis, Antenna Theory: Analysis and Design, 2nd Ed. (New York: John Wiley & Sons, Inc., 1996).
- [3] Thomas F. Eibert and John L. Volakis, “Antenna Engineering Handbook”, McGraw-Hill
- [4] Deschamps G. A., “Microstrip Microwave Antennas”, III rd USAF symposium on Antennas, 1953.
- [5] Ramesh Garg, Prakash Bhartia and Inder Bahl, “Microstrip Antenna Design Handbook”, 1st ed. MA Artech House, 2001.
- [6] Pozar, D.M, “Microstrip antennas”, Proceedings of the IEEE Volume 80, Issue 1, pp 79 –91, Jan. 1992.
- [7] J.R. James and P.S.Hall, Handbook of Microstrip antennas-volume I, Peter Peregrinus Ltd., U.K.
- [8] D. Pozar and D. Schaubert, Microstrip Antennas (Piscataway: IEEE Press, 1995).
- [9] [http:// www.tutorialspoint.com](http://www.tutorialspoint.com) “Wireless Introduction”.
- [10] R. Prasad, OFDM for Wireless Communications Systems, Artech House Publishers, 2004.
- [11] L. Miller, “Why UWB? A Review of Ultra wideband Technology” National Institute of Standards and Technology, 2003.
- [12] <http://www.wlana.com/direct/matrix.htm>, web pages of the Wireless LAN Association (WLANA)

- [13] <http://www.ieee802.org/15/pub/TG3a.html>, web pages of the alternate high-rate physical layer Task Group of IEEE 802.15
- [14] Federal Communications Commission, “Revision of Part 15 of the Commission's Rules Regarding Ultra-Wideband Transmission Systems,” First Report and Order, ET Docket 98-153, FCC 02-48, 2002. <http://www.fcc.gov>.
- [15] F. Nekoogar, “Ultra-Wideband Communications: Fundamentals and Applications”, Prentice Hall, 2005.
- [16] M. Ghavami, L. B. Michael and R. Kohno, “Ultra Wideband Signals and Systems in Communication Engineering”, John Wiley and Sons, 2004.
- [17] D. Porcino and W. Hirt, “Ultra-wideband radio technology: potential and challenges ahead”, IEEE Commun. Mag., vol. 41, no. 7, pp. 66–74, 2003.
- [18] Lodge, “Electric telegraphy”, U.S. Patent 609, 154, August 1898.
- [19] P.S. Carter, “Wideband, short wave antenna and transmission line system”, U.S. Patent 2, 181, 870, December 1939.
- [20] L.N. Brillouin “Broad Band Antenna”, U.S. Patent 2, 454, 766, November 1948
- [21] L. Paulsen, J.B West, W.F Perger and J. Kraus, “Recent investigations on the volcano smoke antenna”, IEEE Antennas and Propagation International Symposium (Digest), 2003.
- [22] D. M. Pozar, “Microstrip Antennas,” Proc. IEEE, Vol. 80, No. 1, pp. 79–81, January 1992.
- [23] S. I. Latif, L. Shafai, and S. K. Sharma, “Bandwidth enhancement and size reduction of microstrip slot antennas”, IEEE Trans. Antennas Propag., vol. 53, no. 3, pp. 994–1003, Mar. 2005.

- [24] S. K. Sharma and L. Shafai, "Investigation of wide-band microstrip slot antenna," *IEEE Trans. Antennas Propag.*, vol. 52, no. 3, pp. 865–872, Mar. 2004.
- [25] J.-Y. Sze and K.-L. Wong, "Bandwidth enhancement of a microstrip-line-fed printed wide-slot antenna", *IEEE Trans. Antennas Propag.*, vol. 49, no. 7, pp. 1020–1024, Jul. 2001.
- [26] J.R. James and P.S.Hall, *Handbook of Microstrip antennas-volume I*, Peter Peregrinus Ltd., U.K.
- [27] Y. Huang and K. Boyle, "Antennas from Theory to Practice", 2008 John Wiley & Sons Ltd.
- [28] K. Davies and E. K. Smith, "Ionospheric effects on satellite land mobile systems," *IEEE Antennas and Propagation Magazine*, vol. 44, no. 6, pp. 24–31, Dec 2002.
- [29] J. L. Volakis, R. C. Johnson, and H. Jasik, *Antenna Engineering Handbook*, 4th ed. McGraw—Hill Book Company, 2007.
- [30] B. R. Elbert, *Introduction to Satellite Communication*, 2nd ed. Artech House, 1999.
- [31] J. Garcia, A. Arriola, F. Casado, X. Chen, J.I. Sancho, and D.Valderas, "Coverage and read range comparison of linearly and circularly polarised radio frequency identification ultra-high frequency tag antennas," *IET Microwaves, Antennas and Propagation*, vol. 6, no. 9, pp. 1070–1078, 2012.
- [32] Narbudowicz, A. Z. : *Advanced Circularly Polarised Microstrip Patch Antennas*. Doctoral Thesis. Dublin Institute of Technology, 2013.
- [33] Y. Yoshimura, "A microstrip line slot antenna", *IEEE Transactions on Microwave theory and techniques*, November 1972, pp. 760-762.

- [34] K.R Carver, “Description of a Composite Hex cell Microstrip Antenna”, Private Communication to J.W. Mink, 1979.
- [35] Yikai et. al, “Characteristic Mode-Based Improvement of Circularly Polarized U-Slot and E-Shaped Patch Antennas”, IEEE Antennas and wireless propagation letters, Vol.11, 2012
- [36] R.E Munson, “Conformal Microstrip Antennas and Phased Arrays,” IEEE Trans. Antennas & Propagation, Ap-22, pp. 74-77, 1974.
- [37] Y. T. Lo, D. Solomon and W. F. Richards, “Theory and experiments on microstrip antennas,” IEEE Transactions on Antennas and propagation, vol-AP-27, 137-145, 1979.
- [38] Abdelaziz Benella and K.C.Gupta, “Multiport Network Model and Transmission Characteristics of Two-Port Rectangular Microstrip patch antennas,” IEEE Transactions on Antennas and propagation, vol-36, no.10, pp. 1337–1342, October 1988.
- [39] E. H. Newman, “Analysis of Microstrip Antennas Using Moment Methods,” IEEE Transactions on Antennas and propagation, vol-AP-29, no. 1, pp. 47– 53, January 1981.
- [40] P. Silvester, “Finite Element Analysis of Planar Microwave Network,” IEEE Trans. Microwave Theory Tech., Vol. MTT-21, pp.104–108, 1973.
- [41] K.S. Yee, “Numerical solution of initial boundary value problems involving Maxwell's equations in isotropic media,” IEEE Trans. Antennas Propagat., vol.14, pp.302-307, May 1966.
- [42] A. Taflove, Computational electrodynamics, Finite difference time domain method, Artech house, MA, 1995.

.....✂.....

Chapter 2

LITERATURE REVIEW

Contents

- 2.1 *Single band circularly polarised microstrip antennas*
- 2.2 *Multi band circularly polarised microstrip antennas*
- 2.3 *Wideband/UWB circularly polarised antennas*

This chapter deals with a comprehensive literature review of various antennas which seem to have significance in the realm of circularly polarised microstrip antennas operated in various bands. Different techniques and methodologies applied for the development of these antennas are explained in brief. The recent research works are also explained.

2.1 Single band circularly polarised microstrip antennas

This section is a brief review of major research works pertaining to circularly polarised single band patch antennas. A wide variety of antennas have been developed with CP radiation. Each of them have peculiar geometries and can be divided into three classes according to their CP operating principles. The first one is a class of microstrip patch antennas, which uses the two orthogonal modes of TM_{10} and TM_{01} to obtain CP radiation. This class include patch antennas, co axial fed wide slot antennas and wide slot structure with CPW feed. The second class is originated from the definition of a CP wave, which aims to produce two orthogonal electric fields with quadrature phase difference. Dipole structures belong to this class. The third class is the widely used spiral antennas and helical antennas, which take the advantage of travelling wave current along curved structures.

2.1.1 Methods of design of CP antennas

By the excitation of two orthogonal, linearly polarised, equal amplitude waves which are in phase quadrature, circularly polarised waves are possible to be generated. This can be accomplished by adjusting the physical dimensions of the patch antenna and using either single, two, or more feed [1]. The simplest and popular method to yield CP radiation in the case of a square patch antenna, is to feed the element at two adjacent edges with waves having a phase difference of 90° , as shown in Figure 1. The feeding at one edge excites the TM_{010} mode and that at the other edge excites TM_{001} . A phase difference of 90° is achieved by using a power divider or a 90° hybrid.

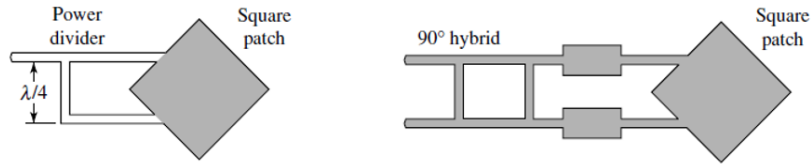


Figure 1. (a) Feed using a power divider (b) using 90° hybrid

The above method results in good CP radiation. But the usage of external 90° power divider or the 90° hybrid increases the complexity. It is possible to achieve CP radiation with a single feed in patch antennas. The advantage of single feed is lack of complexity, simple feed technique and eliminates the need of phase shifters and power dividers. However the two orthogonal modes with 90° phase shift and equal amplitude are to be generated through the antenna geometry alone. In order to accomplish this, one has to feed the patch at a specific feeding point, such that two orthogonal degenerate modes are excited. These modes will have slightly different resonant frequencies, when appropriate asymmetry is incorporated to the patch. One mode can lead by 45° , in its radiated electric field while that of the other can lag by 45° and thus a quadrature phase difference is possible to obtain between these two degenerated modes at some frequencies [2].

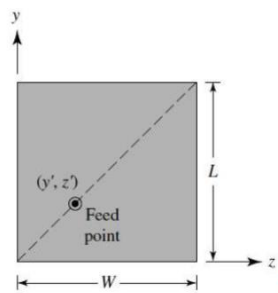


Figure 2. Diagonal feed

Consider a nearly square patch, where L is nearly equal to W , as shown in Figure 2. The two orthogonal modes TM_{010} and TM_{001} can be excited once the feeding point is in the diagonal line of the patch. Better CP radiation is achievable at boresight if a nearly square patch with the length and width ratio given by [3]

$$\frac{L}{W} = 1 + \frac{1}{Q_t}$$

is excited with a diagonal feed, where Q_t represents the total quality factor. Thus by making a small difference in length and width, required phase difference is achieved between the resonating modes, which resonate at slightly different frequencies. A small difference Δ between patch length and width of the antenna is very critical in the circular polarisation behaviour of the antenna. This difference is inversely proportional to antenna quality factor. In the vicinity of resonant frequency, the Smith chart shifts from the lower half to upper half. i.e from capacitive reactance to inductive reactance. One mode will have positive and the other will have negative reactance between the two resonant frequencies. The CP operating frequency is between the two resonant frequencies of the TM_{010} and TM_{001} modes. Here impedance bandwidth is wider than that of equivalent linearly polarised patch. Whereas the axial-ratio bandwidth is inversely proportional to Q and hence narrow [4].

Other methods applied to excite the two orthogonal degenerate modes are by using a corners-truncated patch [5] as shown in Figure 3.

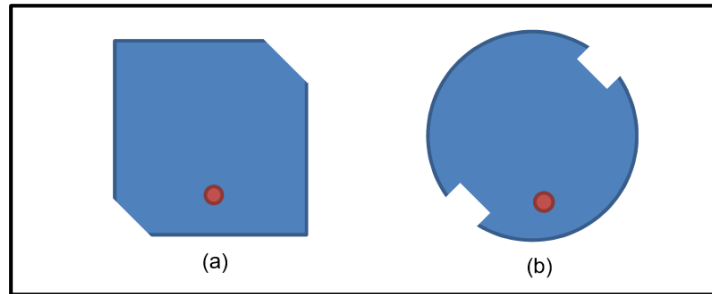


Figure 3. (a) Corner truncations (b) Notches in circular patch

The corner truncated patch is developed by removing two diagonally opposite corners of the rectangular patch. The perturbation introduced should have right amount at the desired frequency to produce two orthogonally polarized waves having the same amplitude and a 90° phase difference. An example is the truncated square patch shown in Figure 3(a) The feed is selected to be at the middle of one of the edges. It excites one mode and the other is excited due to the irregularity in the geometry. The truncated corners decide the sense of polarisation. The solutions for polarisation reconfigurability have been proposed by covering and uncovering the truncation, by Hsu and Chang in [6]. The method of introducing notches in a circular patch at the two opposing edges is depicted in Figure 3(b).

The other method is cutting slots on the patch [7] as shown in Figure 4.



Figure 4. Diagonal slot

Like the truncated corner, the narrow diagonal slot introduced splitting the energy into two orthogonal modes with appropriate phase shift. The diagonal modes are the two orthogonal modes. [8].

M.S. Nishamol et.al described a cross patch CP antenna in which two V shaped slots are embedded. The V-slots in it contribute to enhanced IBW and ARBW [9].

H. Chen, S. Kuo, C. Sim, and C. Tsai presented a UHF square patch RFID tag antenna [10]. The square patch and the cross slot, contribute for compact size and CP radiation characteristics. Obtained IBW of the tag antenna is 50 MHz (904–954 MHz), and ARBW is 6 MHz (922–928 MHz) [10].

Nasimuddin et.al explained the design of symmetric-slit microstrip antennas which exhibit CP radiation [11]. By varying the slit's circumference, Circularly polarized radiation gets affected. IBW and ARBW are 3.85% and 1.5%, respectively, with a peak gain of around 0.8 dBic, when the substrate selected is FR4. When it is R04003 substrate, these values are 1.5% and 0.5%, respectively, with a peak gain of around 3.4 dBic.

Nasimuddin et.al in [12] proposed four microstrip antennas which have asymmetric-slits. Asymmetrical slits along diagonals antenna yields circularly polarized radiation. IBW and ARBW are around 2.5% and 0.5%, respectively.

S. Maddio, A. Cidronali, and G. Manes in [13] explained a circular disc antenna having a central elliptical cut with coaxial feed and analysed through mathematical methods.

Nasimuddin, Zhi Ning Chen, and Xianming Qing in [14] described CP patch antenna with a cross-shaped slot and this slot contributes to size reduction and CP. ARBW is 6.0MHz and IBW is 18.0 MHz The gain is 3.8 dBic in the operating frequency range [14].

Sumitha Mathew et.al, introduced a fan shaped CP microstrip antenna [15]. The corner truncation is for CP characteristics, and size reduction. Obtained ARBW was 1.3%, and size is reduced by 55%, with reference to the reference antenna [15].

S. K. Lee et.al, described the analysis and design of a nearly-square-patch CP antenna using a cavity model [16]. Based on the cavity model, simple linear equations have been derived. The design of a simple matching network has also been presented.

Stefano Maddio introduced a switched beam antenna with operating frequency at 2.45GHz [17]. There are two disc-based patches in a concentric structure. An axial ratio below 3dB for the entire beam-set and correlation coefficients of 0.17 are also observed at center frequency.

We-Shyang Chen et.al, described square-ring microstrip antenna with truncated corners [18]. Two antennas were proposed, with certain dimensional changes, but with the same basic structure. One produced an IBW of 4.51% and ARBW of 1.37% with reference to the centre frequency 2.330 GHz. Second antenna produced, an IBW of 4.62% and ARBW of 1.33% with reference to the centre frequency 2.247 GHz.

J. Lu, H. Yu, and K. Wong proposed spur lines antenna [19]. The resonant frequency of the triangular microstrip patch is significantly lowered with increasing spur-line length.

J. Lu, C. Tang and K. Wong proposed another CP antenna [20]. It is demonstrated that CP is obtained using a single feed. For the design with a cross slot, its CP radiation is improved.

H. Chen, K. Wong, and Kin-Lu Won proposed annular ring CP microstrip antennas [21]. Inserting a pair of slits at the inner boundary of the annular ring patch contribute to CP. Obtained size reduction is 32–42%.

W. Chen, C. Wu and K. Wong proposed a cross strip embedded square ring microstrip CP antenna [22]. By incorporating a small tuning stub compact CP operation was obtained.

Liang C. Shen proposed a single fed elliptical microstrip CP antenna [23]. Sense of polarisation gets affected when eccentricity of the ellipse is small. Mathieu functions are used to express currents, internal fields and radiated fields.

J. Lu and Y. Wang proposed a single feed triangular microstrip CP antenna [24]. Triangular slots are embedded in triangular microstrip antennas. narrow slit of proper length gives rise to CP radiation. The size reduction is 30.

K. Wong, C. Huang, and W. Chen proposed a printed ring slot CP antenna [25]. Asymmetry gives rise to Circular polarization (CP) radiation. ARBWs obtained for the square and annular ring slot antennas are 4.3% and 3.5%, respectively.

Lei, H. Chu, and Y. Guo proposed a ground radiation CP antenna for biomedical applications [26]. A measured impedance bandwidth of 621 MHz is achieved in the 2.4-2.48 GHz band.

Hui Gu et.al proposed a frequency reconfiguration antenna [27]. It has a rectangular patch with a rectangular-ring slot. The resonant frequencies are changed by varying the capacitance values of the four pairs of varactor diodes with single DC voltage.

Z. Tu, Q. Chu, and S. Dong proposed square-ring patch CP antenna with an unequal cross-slot ground plane [28]. It was fabricated on 35mm×35mm×0.8mm FR4 substrate. Obtained axial ratios were 0.55dB and 0.63dB at 1.995GHz and 2.105GHz respectively.

J. Liu, Y. Li, Z. Liang, and Y. Long proposed a planar quasi-magnetic–electric CP antenna [29] . It is based on a quarter-wave shorted patch connected with two printed strips. IBW is 4.3%, with an average axial ratio below 1.5 dB and a gain between 2.4 and 3.3 dBi.

X. Zhang and L. Zhu proposed CP microstrip patch with loading of shorting pins and having high gain [30]. Two sets of metallic pins symmetrically placed along the two orthogonal diagonals of a square patch radiator give rise to CP radiation.

Nasimuddin, Z. N. Chen and X. Qing presented microstrip patch antennas with various slot shapes which are diagonally symmetric. These antennas are circularly polarised [31]. It is established that any arbitrarily shaped slot in an antenna gives rise to circularly polarized radiation. A cross shaped diagonally symmetric slotted microstrip-patch antenna which is circularly polarised has also been presented [31].

H. Chen, S. Kuo, C. Sim, and C. Tsai presented coupling-feed RFID tag antenna with CP radiation and mountable on metallic surface [32]. A square patch passive RFID tag antenna within the operating frequency UHF band is introduced. A cross slot is introduced in a square patch and then, one L-shaped open-ended microstrip line linked to a tag-chip and terminated by a shorting pin, is capacitively coupled to the patch. IBW obtained is 50 MHz (904–954 MHz), and ARBW obtained is 6 MHz (922–928 MHz) [32].

K. Maamria and T. Nakamura proposed a simple, single fed structure consisting of a pair of crossed dipoles connected to two angular branches which easily produces circular polarisation [33]. This antenna, with a director, placed over a ground plane was analysed and a design example was realised and measured at 2 GHz.

B. Kim et al., proposed a circular microstrip antenna with reconfigurable polarization [34]. Y.T. Lo.B. et al., introduced simple

design formulas for circularly polarised microstrip antennas [35]. The cavity model theory is used for its derivation.

Chihyun Cho et al., introduced a tag antenna which uses CP radiation and capable of increasing RFID reading range [36]. It comprises of a radiating patch, a shorting plate, and a ground plane. The operating frequency range is UHF RFID band. It is estimated that RHCP gain of the tag antenna affects the reading range rather than the AR. Loading an additional parasitic patch on the top increase the RHCP gain [36].

Z. Wang et al., proposed a CP antenna [37]. Good results are obtained by means of the horizontally meandered strip feed technique. IBW of 25.8% (758–983MHz), ARBW of 13.5% (838–959 MHz), are the important results obtained.

Nasimuddin, X. Qing, and Z. N. Chen proposed symmetric-slit square CP microstrip-patch antennas [38]. A symmetric slit initiates circularly polarized radiation. By slightly varying the slit's circumference along one of the diagonal axes CP properties are changed.

J. P. Shinde et al., proposed four structures for CP generation in hexagonal shaped patch antenna, with a centre frequency 2 GHz [39]. Four such hexagonal antenna configurations are introduced. IBW, ARBW and axial ratio are found to be 2.58%, 1.71 % and 0.1615 dB respectively [39].

B. Zheng and Z. Shen described the effect of the ground plane. It has been demonstrated that there is small effect on radiation pattern in the forward direction due to the size of the ground plane, and it has

significant effect on the front-to-back ratio. By introducing a finite ground plane, the axial ratio can be greatly modified [40].

Sanyog Rawat and K. K. Sharma proposed a circularly polarized microstrip patch antenna with T-Shaped slot [41]. The length and width of slots and air gap in proposed antenna geometry affects ARBW.

Yogesh Kumar Gupta, R.L.Yadava and R.K.Yada proposed a truncated pentagonal shaped microstrip patch antenna, which is circularly polarized. The extent of truncation affects CP properties [42].

S.K. Lee et al., described the design and theoretical study of a circularly polarized, nearly square patch antenna using an offset microstrip feed operating at 2.45 GHz. The effect of the offset on the perturbation segment and the design of a simple matching network are discussed [43].

K.P Ray et. al., proposed suspended hexagonal microstrip antenna of circular polarization. Perturbations are introduced along two opposite sides of the suspended hexagonal microstrip antenna. IBW of 70 MHz and ARBW of 16.2 MHz has been achieved for this antenna which is designed at 915 MHz [44].

A. Ramadan et al., proposed a CP decagonal slot antenna [45]. The antenna is based on a 0.762mm-thick 5 cm × 8 cm RO3203 substrate and a decagonal slot in the ground plane. A Wilkinson power divider, was used to couple the electromagnetic energy to the above slot.

M. D. Deshpande and N. K. Das proposed Ichmond's reaction integral equation method to design a CP rectangular microstrip patch. Circular polarization characteristics was obtained by the rectangular patch with the aspect ratio in the range 1.015- 1.02 and comer fed by a microstrip line. For substrate with thickness $d = 0.16$ cm, $a = 1.017$ the nearly square patch gives maximum bandwidth [46].

C. Yen, D. Sim, K. Lin, and J. Row proposed the design of circularly polarised annular-ring microstrip antenna [47]. The design parameters of the ring largely affect the CP characteristics.

Chow Yen Desmond Sim et al, proposed a new perturbation segment that controls the CP operation for the annular-ring microstrip antenna. It is this extent of perturbation, which accounts for CP radiation properties [48].

M. Samanta and Santanu Das proposed circularly polarized hexagonal microstrip antenna for blue tooth application [48]. By inserting perturbations along two opposite vertices of a diagonal of hexagonal patch, CP characteristics have been changed..

X. Yang, Y. Z. Yin, W. Hu and S. L. Zuo, introduced circularly polarized inverted L antenna with double-folded arms. The double-folded structure plays a major role in enhancing impedance matching and radiation characteristic s [49].

J. Row and S. Wu in their work, found that two adjacent CP modes can be simultaneously excited by the proximity coupling of an L-shaped

feedline. By tuning the dimensions of this L-shaped feed line, improved CP bandwidth was obtained [50].

2.2 Dual band and wide band circularly polarised microstrip Antennas

Circular polarization was preferred in more bands due to its peculiarity of insensitivity to transmitter receiver orientation and the least multipath fading. In this section, major contributions towards the development of multiband CP antennas are reviewed.

S. Maddio et al. presented a dual band CP antenna [51]. There is a principal patch and four parasitic patches around it. TM_{11} and TM_{12} modes contribute to circular polarisation generation.

Z. Harouni et al., proposed an antenna with two crossed slots on the ground plane and coupled microstrip feed line generate CP in dual bands [52].

X. Bao and M. Ammann proposed a dual frequency dual circularly-polarised patch antenna [53]. It has a two-layer structure which has circular patches with offset circular slots and rectangular slots. Both senses of polarisations RHCP and LHCP are realised in the lower and upper bands, respectively. For elevations greater than 10° , the axial-ratio is less than 3 dB for both bands [53].

W. Liao and Q.-X. Chu explained the dual-band performances due to a circular patch and a narrow annular-ring, which differ in radii slightly. Unequal cross-slot on the circular patch and linear stubs contribute to the CP characteristics [54].

K. Kandasamy and B. Majumder proposed a square slot antenna which is loaded with split ring resonators. This provides CP response in dual bands [55]. CP upper band is generated by outer ring connected SRRs which are placed on the back side of the slot. Diagonally opposite truncated corners of the slot with the SRRs give CP response in the lower band. The proposed antenna is designed to operate at 3.1 and 4.7 GHz.

Z. Liang et al., in their antenna used two eccentric rings intended to produce single-band circular polarization [56]. Arc-shaped strip excites these rings. It has ARBW of 9 and 21 MHz at 2.1 and 3.6 GHz respectively.

M. Bod and H. R. Hassani proposed a multi-band circularly polarized slot antenna [57]. The antenna has a wide circular slot in the ground plane. Four L-shaped slot arms are attached loaded with smaller ring slots have been attached to this wide slot. L-shaped arms provide size reduction. This circular-slot antenna is fed through a microstrip-fed circular patch situated on the reverse side of the substrate.

Sanjay Kumar, B.Ramachandran, and S.Bashyam proposed the design of dual-band circularly polarized antenna [58]. Two rectangular loops with parasitic rectangular elements are there for the antenna. Antenna structure is situated above a finite ground plane. The position of gap and the height of the rectangular loop from the ground plane are adjusted to have impedance match and good ARBW.

S. Maddio, et al., introduced a dual band circularly polarized patch antennas having small frequency ratio [59]. The proposed antenna is a disc patch loaded by 2 pairs of parasitic crown segments. This design

gives dual band configurations with small frequency ratio; from 4% to 16%.

X. Rui, J. Li, and K. Wei proposed an antenna, which comprises of L shaped patch, wide slot ground along with two rectangular strips around two opposite corners. This structure yielded ARBW of 37.4% and 16.3% in two bands [60].

X. L. Bao and M. J. Ammann proposed a monofilar spiral slot antenna. This antenna gives dual-frequency dual-sense circular polarization [61] characteristics. It generates right-hand circular polarization in one band and the counter polarization in the second band. The coupled spiral slots are fed by a 50 microstrip line. Oppositely-directed current rotation for the two frequency bands produce dual-sense circularly-polarized performance. The 3 dB axial-ratio bandwidths are 4.5% and 3.5% for the RHCP and LHCP bands, respectively [61].

Q. Liu, J. Shen, H. Liu, and Y. Liu proposed a dual-band 0.92/2.45GHz CP unidirectional antenna with the aid of dual-feed network, asymmetric H-shape slots, and annular-ring patches which is stacked for RF identification (RFID) applications [62].

X. Bao and M. J. Ammann introduced a dual CP antenna obtained by four unequal linear slots [63].

Y. Shao, and Z. Chen developed an antenna, which is composed of an annular slot and a cross slot, which produce two different frequency bands. The lower band and the upper band are controlled by the annular

slot and the cross slot respectively. The asymmetry on both annular slot and cross slot, CP radiation at the two frequencies is obtained [64].

S. Zuo, L. Yang, and Z. Zhang developed antenna with stacked cone-patches; small patch and a large patch; small patch for upper band and large patch for lower band yield the dual-band CP characteristics [65].

W. Cao, A. Liu, B. Zhang, and T. Yu proposed a dual-band spiral patch-slot antenna. This antenna provides omnidirectional CP characteristics in one band and unidirectional CP properties in another band [66].

Y. Sung proposed a dual-band pentagonal slot antenna with CP characteristics [67]. The circular polarization (CP) radiation characteristics are achieved by loading with asymmetry. For this, the corner cut is used as a perturbation [67].

J. Lu and C. Liou proposed a planar monopole antenna with dual-band circular polarization properties [68]. Dual-band CP properties are achieved by introducing an inverted L-shaped strip-sleeve shorted to the ground plane. IBWs of 1932/339 MHz and ARBWs of 250/360 MHz in 2.4/5.2-GHz bands are obtained [68].

U. Mashayak and V. G. Kasabegoudar proposed an antenna with branched microstrip feed which is Circularly polarised in two bands. The first band is 2.61-2.93 GHz and the second band from 4.244.41 GHz. Reasonably good axial ratio bandwidths are obtained in these bands [69].

S. M. Noghabaei et al., proposed asymmetric slot antenna which is CP in two bands, intended for WiMAX applications [70]. Measured results show that values of IBW and ARBW are 7.2% and 2 % in band 1(2.53 GHz) and 3.6 % and 3.2 % in band2 (5.73 GHz).

Y. Chen et. al, proposed a dual-band circularly polarized slot antenna with dual-sense and having a C - shaped grounded strip. The slots in two opposite corners account for the CP performance in lower band. The C-shaped grounded strip provides a current path for the upper band and enhances the axial ratio bandwidth [71].

D. Yu et.al, proposed an antenna which is dual-band dual circularly polarized Using TM_{01} and TM_{02} Modes. The horizontal polarisation is due to the currents flowing on the patch and vertical polarisation is due to the coaxial probe [72].

W. Li et.al, introduced a U-Shaped Structure in Dual-Band Circularly Polarized Slot Antenna Design. It is a coplanar waveguide fed antenna which has got a single metallic layer. It has a small frequency ratio of the upper band to the lower band [73].

Y. Cai et.al, demonstrated an antenna which is circularly polarized in dual-bands. The proposed antenna has an annular slot radiator on a square substrate and the ground plane is a high impedance surface (HIS) [74].

C. Wanget.al, proposed an antenna which is a wideband open-slot structure with dual-band circular polarization. There are T-shaped and two inverted-L topologies in the ground plane. A bent feeding structure

along with three slots are designed to excite a right-hand circularly polarized (RHCP) wave at 1.57 GHz and left-hand circularly polarized (LHCP) wave at 2.33 GHz [75].

C. Wu et.al., demonstrated an antenna which is CPW-Fed Slot structure with Dual Band and circularly polarised in both bands. The obtained bands are 2.10GHz with LHCP and 2.90GHz with RHCP. Axial radio bandwidths obtained are 100MHz (2.05GHz-2.15GHz) and 200MHz (2.82GHz-3.02GHz) [76].

J. Zhang et.al, introduced a CP patch antenna with a control over polarisation in two frequency bands [77].

Yi Liu et.al, introduced an antenna which is dual-polarized with omni directional radiation patterns in two bands. It has a circular patch with eight open slots, eight shorted metal pins. It has impedance bandwidths of 18MHz (1566MHz-1584MHz) and 32MHz (2440MHz-2472MHz) with axial ratios less than 3dB [78].

C. Chen and E. K. N. Yung proposed a CPW fed slot antenna, which is dual-band and dual-sense circularly-polarized and loaded with two spiral slots. The T-shape strip accounts for dual-band operation. 3dB axial-ratioband widths are measured to be 8.4% and 19.24%, with respect to 1.6 GHz (RHCP) and 2.2 GHz (LHCP), in two bands respectively [79].

F. Alizadeh et. al., proposed slots mutual coupling based ring-shaped dual-band / multi-band circularly polarized microstrip antenna. The impedance band width of the antenna is influenced by embedding pairs of asymmetrical ring-shaped arc slots to the boundary of both

planes. It gives dual-band/multi-band CP radiation by extending the ring-shaped arc slots out with narrow slots [80].

R. Xu, J. Li, and G. Yang introduced a dual band dual sense Circularly Polarized Antenna with a printed dipole structure. Its structure is derived from a linear polarized bow-tie dipole antenna, and the rotational symmetry geometry accounts for its dual-band dual-sense CP generation [81].

J. Lin et al., proposed an AMC based dual-band dual-mode and dual-polarized antenna. Antenna comprises of a pair of double-printed crossed dipoles. Incorporating vacant quarter-rings it has dual-band dual-polarized property but strong back radiation. Artificial magnetic conductor layer is used for performance improvement [82].

D.D. Wang et al., introduced a conceptual design of a square loop antenna, which is dual band circularly polarised under even mode resonance. The dual band CP operation is realised by first order and third order even modes within a single loop radiator [83].

Hu Rack Lee et al., proposed a microstrip antenna for installation into satellite mobile phones which is circularly polarised in two bands. Initially to reduce size and to produce CP waves, four edges of the microstrip antenna were folded. Then, two such antennas were fabricated having different sizes and then stacked vertically on a phone-shaped ground, which gives dual-band capability [84].

Y. Zhang proposed an annular-ring microstrip antenna for GNSS applications which is circularly polarized in dual-bands. The coupling

between the microstrip lines and the rings is improved by a lotus-shaped aperture. To achieve good axial ratio and impedance band width three wideband planar baluns are applied [85].

T. Chang proposed that by adding sleeves to the monopole dual band CP antenna may be designed. A truncated patch in addition with two sleeves is sufficient to generate circularly polarized antenna with dual-band response and having high boresight gains[86].

Y. Hu et al., proposed an antenna which is circularly polarised in dual bands and applicable for GPS and dedicated short-rang communication (DSRC) applications. It has two sections. A truncated square patch, operates around 5.888 GHz, which is left-hand circularly polarised and usable for DSRC applications. The second part is having two open-loop square ring resonators with a T-shaped feed structure applicable for GPS system at 1.575 GHz, which is right-hand circularly polarised [87].

R. Caso et al., introduced a dual band circularly polarized antenna for portable RFID readers and usable in UHF-RFID / WLAN bands. A circular array of four inverted-F meandered monopoles, is the radiating element for the UHF-RFID band. The array elements are excited with a 90° phase offset [88].

Qiang Liu et al., proposed dual CP antenna usable in 0.92/2.45-GHz bands. It has a wideband dual-feed network and two stacked concentric patches [89].

K. Qian et al., proposed a hexagonal microstrip antenna which is circularly polarized in dual bands. This is a multilayer microstrip antenna for 3.5/5.2-GHz applications. The stacked-patch configuration accounts for the dual-bands and the CP performance is obtained by the truncated corners and inserted slits [90].

Xiao-Yu He et al., proposed a dual band dual CP antenna which has a multifunction broad beam. It comprises of a crossed dipole and four inclined monopole antennas. They share a common aperture [91].

F. Samadi, et al., proposed an antenna with parasitic element for gain enhancement. This is also a dual band CP antenna. A fork type parasitic element and a rectangular stub account for CP dual band characteristics [92].

Q. Wu, et. al., demonstrated a L / S-Band antenna which is fed by 3-dB coupler and circularly polarised in both bands. It has two concentric ring patches, two planar L-probes and a dual-band 3-dB SICL branch-line coupler. This antenna is applicable for the Beidou-1 regional navigation system [93].

S. Zhou, P. Li, and Y. Wang proposed a square-ring slot antenna, which is circularly polarised in dual bands. This is achieved by notching technique of two square-ring slots as well as changing the gap width. A dual-sense CP radiation is achieved by the perturbations of the two slots about the microstrip feeding line [94].

M. Matsunaga proposed a spiral antenna which offers circularly polarised radiation in two bands. It consists of spiral elements and a dipole feeder. The spiral elements bent like a cross shape accounts for

circularly polarized radiation. The dipole feeder contributes CP waves in two bands [95].

R. Xu et al., proposed a square slot antenna with a simple structure and dual sense circularly polarised in dual bands. The lower band RHCP radiation is obtained by an inverted L-shaped strip. LHCP radiation is achieved by an offset feed structure [96].

The-Nan Chang et al., proposed an antenna, which is dual band CP through the method of line coupling to a patch and a ring. The polarizations are made of the same sense by the line between the two radiation elements. Opposite sense polarizations were obtained when both elements were situated on the same side [97].

K. G. Tan et al., proposed the design of stacked antenna, which is dual band CP. Its dual band CP operation is realized by the stacked arrangement with a truncated edge technique. Two edges of the geometry are truncated. The feed position is chosen to be at an angle between X-Y axes [98].

B. Mubarak, et al., introduced a planar monopole antenna which is circularly polarized with a novel radiator/ground. The CP performance is produced by a horizontal stub from a vertical monopole. Then a slot is formed on the ground plane below the protruded stub [99].

J. Wu et al., proposed a differential feeding method employed to a dual band CP antenna. A gap-feeding structure produces sufficient axial-ratio bandwidth. On the other side parasitic square ring is placed [100].

2.3 Wide band/Ultrawide band Circularly polarised Antennas

Recently numerous research works have been with regard to the design of wideband CP antennas with necessary attributes to fulfil the requirements of wireless communication systems. Rigorous work is going on to accommodate several operating frequencies in a single antenna, which has high bandwidths in terms of impedance and circular polarisation characteristics. UWB pulses of shortest duration are richly used in communication field and widely applied for military and biotechnological applications.

There is large demand for higher capacity and higher data rate in wireless systems. Hence CP antennas are required to have wider bandwidth. Therefore a lot of works have been reported in the area of wideband CP antennas. Following is the comprehensive overview of such antennas.

Jianjun Wu et al., introduced a square slot antenna which gives broad IBW and ARBW. Modified edged square slot antennas are used. The perturbations due to the stubs and notches account for AR bandwidth. Introduction of conducting reflector further enhances CP performance [101].

L. Zhang et al., introduced an inverted-S antenna, which offers large IBW and ARB. It consists of two curved arms or inverted “S.” It has an impedance bandwidth of 63% and ARBW of 42%. It is extendable to an array antenna to get more ARBW [102].

K. Hirose et al., demonstrated a comb line antenna which gives wider impedance bandwidth and circular polarisation characteristics in that band. Initially a loop antenna is used for CP radiation. Then the loop element is applied for a comb-line antenna for CP radiation mechanism [103].

Mehrdad Nosrati et al., used antipodal Y-strip for the design of CP Square Slot Antenna, which has wide IBW and ARBW. The U-shaped microstrip feed line is used for improved IBW. Obtained ARBW is 41.3% (from 4.4 to 6.67 GHz) [104].

S. Karamzadeh et al., used crooked T-Shape technique and designed a square slot antenna with wide bandwidths. The antenna is CPW fed. L-shape and crooked T-shape grounded strips are used at the slots' opposite corners [105].

T. Mondal et. al., designed perturbed psi-shaped antenna, which has wider bandwidth. The modified TM₀₁, TM₂₀, and TM₂₁ modes with three slots account for wide bandwidths [106].

J. Wei et al., proposed an antenna with Double-Y-Shape Slot which is a high gain antenna with wider band widths. It is made of two patches, an aperture coupling-fed layer and a metallic reflector [107].

R. U. I. Xu et al., introduced an antenna in which C-shaped slot and a microstrip-fed port yield left-hand circular polarization. The band widths are greatly widened by off-center sword structure [108].

A. Narbudowicz, et al., explained the design method for wideband CP slot antennas. The slot structure uses compact UWB phase shifter.

Advanced optimization algorithm is used and uses spline curves for CP radiation [109].

R. Joseph and T. Fukusako proposed microstrip line fed circular slotted CP broadband antenna. The orthogonal components of the L-shaped probe are placed on two sides of the substrate [110].

K. Ding et al., proposed a monopole antenna which is CPW-Fed and with open loop/asymmetric ground plane. This antenna exhibits wideband CP performance. The asymmetric ground plane contributes to CP in the upper band. A rectangular open loop yields wide IBW and ARBW [111].

K. Ding et al., proposed a slot antenna with backed FSS reflector which exhibits wideband CP performance. The antenna has two slots with crescent shape, a feed-line with L shape and an FSS reflector. Initially CP radiation is obtained the single crescent-shaped slot structure. There are two benefits for the FSS reflector. Unidirectional radiation and improved axial ratio bandwidth [112].

Shing Lung et al., proposed an antenna with L-shaped slot and exhibits wideband CP characteristics, obtained due to truncation of one of the corners. ARBW of 46.5% is obtained [113].

S. L. S. Yang et al., discussed the design and study of CP antennas with single feed. It is inferred that thickness of the substrate affects the axial ratio bandwidth [114].

H. Huang and B. Wang proposed Slot Antenna with V-shape. This also exhibits wideband circular polarization. There is Z-shaped feedline ,

stub and a patch and two right-angled V-shaped. The stub provides broadband [115].

Z. Wu et al., proposed designed a wide slot antenna based on a bent feed, which has wider bandwidth and wide CP bandwidth. It has a corner-truncated patch which is square-ring shaped. The CP radiation is due to bent strip. Wide bandwidths are attributed by several open stubs [116].

S. Trinh-van et al., proposed a multiple-circular-sector patch loaded slot antenna which exhibits broadband CP characteristics. S-shaped strip introduces CP radiation. The ARBW is widened by a patch, comprises of 12 numbers of circular-sectors having central angles of 30° each and varied radii [117].

X. L. Bao et al., introduced a microstrip antenna with enhanced bandwidths. It has an asymmetrical dipole and a ground plane with slit. It has L-shaped microstrip feedline. The surface currents on dipole, feedline and ground plane contribute to CP characteristics [118].

C. F. Zhou et al., used $1 - \lambda$ resonant mode in a crossed slot antenna with a single feed. It has got wideband CP characteristics. It has two crossed slot radiators with equal length. It is microstrip line fed. By loading reactive elements on each slot it produces CP radiation [119].

J. Chen and J. Row designed an antenna with a reflector, which has got slotted patch. This has got wideband CP characteristics. Initially a slotted patch antenna is designed and obtained ARBW of of 53% is obtained. The metallic reflector is used for unidirectional radiation [120].

X. Gao and Z. Shen proposed a novel circularly polarised UHF / UWB tag antenna. For the optimization of CP properties, design and analysis have been evaluated at both UHF and UWB. [121].

N. Ghassemi et al., proposed a CPW fed spiral antenna which has wide band widths. Antenna's substrate is having high dielectric constant. The proposed spiral antenna has an axial ratio band width 11.4–17.5 GHz [122].

S. Mohammadi et al., proposed a slot antenna having two elliptical slots which are linked and having wider impedance and axial ratio band widths. Two rectangular stubs and four rectangular slits in the ground plane, the IBW and ARBW got enhanced [123].

S. Mao and S. Chen studied the time-domain characteristics of loop antennas which are tapered and covers ultrawide band [124].

S. Mao and J. Yeh proposed a spiral antenna, which is ultrawideband CP antenna. It used integrated balun, i.e., a tapered microstrip balun is integrated into one of the arms. The IBW is 3.75 to 18.6 GHz and the ARBW is 3 to 14.5 GHz [125].

A. S. A. El-hameed et al., introduced a CPW fed square slot antenna which is UWB CP. CP performance is contributed by a fork-shaped feed line. A pair of inverted-L, and inverted-F grounded strips enhance the ARBW [126].

R. Kumar, B. Huyart, and J. Cousin designed an antenna which is dumbbell-shaped crossed-dipole structure. It is a UWB CP antenna. It has circular patches on the ends of dipoles on two planes of the substrate [127].

M. S. Ellis et al., introduced a wideband CP antenna for C-band applications. The CP performance is due to a horizontal stub protruded up to the center of the wide slot and microstrip feedline placed to the side below the protruded stub [128].

K. Hung and Y. Lin demonstrated a cavity-backed aperture antenna which has broadband CP radiation characteristics and travelling wave excitation. An array formed gave the results of IBW of 70%, ARBW of 50% [129].

Q. Chen proposed a CPW fed antenna with equiangular tapered-feedline, having UWB CP characteristics. This special feedline, the axial an ARBW of 61.9% (2.9–5.5GHz) is achieved [130].

S. Karamzadeh et al., designed a UWB CP antenna. It is a square slot antenna with corners connected by a long strip line and it provides an additional current path. It provides IBW of 130.38% and ARBW of 35.7% [131].

J. P. Shinde et al., proposed a UWB CP rectangular slot antenna having trapezoidal tuning stub, located at the slot centre and fed by a coplanar waveguide. The orthogonal surface currents in the slot and feed line contribute to CP. Enhanced ARBW is due to the trapezoidal tuning stub [132].

Y. Shen and C. L. Law introduced a quasi-spiral UWB CP antenna which is microstrip fed [133].

J. Pourahmadazar et al., proposed a square slot antenna with inverted L strips. It is a CP antenna usable for UWB applications. The square ground plane along with two unequal-size inverted-L strips generate a resonant mode CP radiation. It has enhanced impedance bandwidth and the axial ratio bandwidth [134].

J. Pourahmadazar and S. Mohammadi proposed a UWB CP slot antenna with stubs and strips. It has ARBW of 38.2% [135].

H. Tang et al., proposed a monopole antenna with tilted branch. It has IBW of 97.4% and ARBW of 59.1%. This is achieved by slotted rectangular patch on the tilted monopole and the ground plane [136].

P. Tendolkar et al., described the study of a slot antenna which is CPW and usable for UWB applications [137].

Y. Zhong et al., introduced a UWB CP antenna with archimedean spiral structure. It is an Archimedean spiral antenna. A circular reflector with cross slots enhances ARBW [138].

J. Wei et al., proposed an antenna with double-Y-shape slots. It exhibits UWB CP characteristics. The antenna has an aperture coupling-fed layer. To enhance the gain and unidirectional radiation properties, a metallic reflector is placed beneath [139].

Raghupatruni V et al., described the design of slot antenna which is temple shaped. The antenna is circularly polarised and applicable for Ultra Wideband applications. The temple shaped slot is formed by half trapezoidal and half semi-circular slots and fed by CPW feed. IBW is

108%, (2.75GHz to 9.25GHz). ARBW is 51.6% (4.6GHz to 7.8GHz) [140].

M. Shokri et al., proposed a UWB – CP antenna with modified ground plane. It has two rectangular notches located at two opposite corners meant for enhanced IBW. Pair of reverse L shaped arms meant for enhanced ARBW [141].

J. Sze et al., introduced a design for increased axial-ratio bandwidth with asymmetric-CPW-fed square slot antenna, which offers UWB – CP performance. It offers ARBW of 35% and IBW of 35% in UWB [142].

S. Fu et al., proposed a slot antenna array. It is Fed by Asymmetric CPW and usable for L-Band Applications. It is a CP slot antenna array with an inverted L-shaped strip for L-band applications [143].

J. Pourahmadazar proposed a UWB - CP slot antenna for L- and S-band applications [144].

T. Chang used two linked annular slots for making a UWB- CP antenna. By tuning the distance between two corners IBW and ARBW may be adjusted [145].

S. Du and Q. Chu proposed UWB CP square slot Antenna with ground plane having E- shaped slits. E shaped slits in the ground plane of ground plane account for a good CP bandwidth [146].

T. Li et al., proposed a CPW-Fed circularly polarized square Slot antenna . It has a stepped feeding strip, L-shaped patch, an inverted-L

strip and an asymmetric ground with an L-shaped slot as well as two horizontal slots. It has better IBW and ARBW. [147].

J. Jan et al., proposed a broadband CP antenna with an open slot.

CP performance is obtained by slot at the lower left of slot. Achieved ARBW is 27 % [148].

S. H. Yeung et al., proposed a slot antenna using slot made of multiple circular sectors. It provides an ARBW of 57.4% [149].

R. Xu et al., described the design of dual - wideband antenna. It has a square slot with CP radiation having dual sense. The CP performance is obtained by a halberd-shaped metal strip [150].

This chapter, which gives a brief account of the literature reviewed imparts a clear picture of the current trends in the design and development of compact single band, multiband and ultra-wide band circularly polarised microstrip antennas. It also gives a clear indication that the design and development of circularly polarised antennas is major topic for research and highly relevant in the perspective of contemporary wireless communication applications. In the piece of research work described in this thesis, wide variety of circularly polarised antennas incorporating novel design techniques have been presented. The review of literature as described in this chapter has helped qualitatively in the design and development of above said antennas.

References

- [1] C. A. Balanis, *Antenna theory: analysis and design*: John Wiley & Sons, 2016.
- [2] K. Carver and J. Mink, "Microstrip antenna technology," *IEEE Transactions on Antennas and Propagation*, vol. 29, pp. 2-24, 1981.
- [3] W. Richards, Y. Lo, and D. Harrison, "An improved theory for microstrip antennas and applications," *IEEE Transactions on Antennas and Propagation*, vol. 29, pp. 38-46, 1981
- [4] W. L. Langston and D. R. Jackson, "Impedance, axial-ratio, and receive-power bandwidths of microstrip antennas," *IEEE Transactions on Antennas and Propagation*, vol. 52, no. 10, pp. 2769–2774, Oct 2004.
- [5] P. Sharma and K. Gupta, "Analysis and optimized design of single feed circularly polarized microstrip antennas," *IEEE Transactions on Antennas and Propagation*, vol. 31, pp. 949-955, 1983.
- [6] S.-H. Hsu and K. Chang, "A novel reconfigurable microstrip antenna with switchable circular polarization," *IEEE Antennas and Wireless Propagation Letters*, vol. 6, pp. 160–162, 2007.
- [7] H. Iwasaki, "A circularly polarized small-size microstrip antenna with a cross slot," *IEEE Transactions on Antennas and Propagation*, vol. 44, pp. 1399-1401, 1996.
- [8] P.C Sharma, K.C.Gupta,"Analysis and Optimized Design of Single Feed Circularly Polarized Antennas Microstrip," *IEEE Transactions On Antennas And Propagation.*, Ap-31, No. 6, November 1983.
- [9] M. S. Nishamol, V. P. Sarin, D. Tony, P. Mohanan and K. Vasudevan, "Single Feed Circularly Polarized Cross patch Antenna", 978-1-4244-4819-7/2009 IEEE.

- [10] H. Chen, S. Kuo, C. Sim, and C. Tsai, “Coupling-Feed Circularly Polarized RFID Tag Antenna Mountable on Metallic Surface,” *IEEE Transactions On Antennas And Propagation*, vol. 60, no. 5, pp. 2166–2174, 2012.
- [11] Nasimuddin, X. Qing, and Z. N. Chen, “Compact Circularly Polarized Symmetric-Slit Microstrip Antennas,” *IEEE Antennas and Propagation Magazine* vol. 53, no. 4, pp. 63–75, 2011.
- [12] Nasimuddin, X. Qing and Z. N. Chen, “Compact Asymmetric-Slit Microstrip Antennas for Circular Polarization,” *IEEE Transactions on Antennas and Propagation*, vol. 59, no. 1, pp. 285–288, 2011.
- [13] S. Maddio, A. Cidronali, and G. Manes, “A New Design Method for Single- Feed Circular Polarization Microstrip Antenna with an Arbitrary Impedance Matching Condition,” *IEEE Transactions on antennas and propagation* vol. 59, no. 2, pp. 379–389, 2011.
- [14] Nasimuddin, Zhi Ning Chen, and Xianming Qing, “A compact circularly polarised and cross shaped slotted microstrip antenna,” *IEEE Transactions on antennas and propagation*, Vol. 60, no. 3, pp. 1584–1588, 2012.
- [15] S. Mathew, R. Anitha, T. K. Roshna, and C. M. Nijas, “A Fan-Shaped Circularly Polarized Patch Antenna for UMTS Band,” *Progress In Electromagnetics Research C*, Vol. 52, no. June, pp. 101–107, 2014.
- [16] S. K. Lee, A. Sambell, E. Korolkiewicz, and S. F. Ooi, “Analysis and design of a circular-polarized nearly- square-patch antenna using a cavity model,” *Microwave and optical technology letters*, Vol. 46, No. 4, August 20 2005 vol. 46, no. 4, pp. 406–410, 2005.
- [17] S. Maddio, “A Circularly Polarized Switched Beam Antenna With Pattern Diversity for WiFi Applications,” *IEEE Antennas and Wireless Propagation Letters*, Vol. 1225, no. c, pp. 2–5, 2016.

- [18] We-Shyang Chen, Chun-Kun Wu and Kin-Lu Wong, “Single-feed square-ring microstrip antenna with truncated corners for compact circular polarisation operation,” *Electronics letters*, Vol. 34 No. 11 vol. 34, no. 11, pp. 1045–1047, 1998.
- [19] J. Lu, H. Yu, and K. Wong, “Compact circular polarisation design for equilateral-triangular microstrip antenna with spur lines,” *Electronics letters*, vol. 34, no. 21, pp. 1989–1990, 1998.
- [20] J. Lu, C. Tang and K. Wong, “Single-Feed Slotted Equilateral-Triangular Microstrip Antenna for Circular Polarization,” *IEEE Transactions on antennas and propagation*, vol. 47, no. 7, pp. 1174–1178, 1999.
- [21] H. Chen, K. Wong, and Kin-Lu Won, “On the circular polarization operation of annular ring microstrip antennas,” *IEEE Transactions on antennas and propagation*, vol. 47, no. 8, pp. 1289–1292, 1999.
- [22] W. Chen, C. Wu and K. Wong, “Square-Ring Microstrip Antenna with a Cross Strip for Compact Circular Polarization Operation,” *IEEE Transactions on antennas and propagation*, vol. 47, no. 10, pp. 1566–1568, 1999.
- [23] Liang C. Shen, “The elliptical microstrip antenna with circular Polarization,” *IEEE Transactions on antennas and propagation*, no. 1, pp. 90–94, 1981.
- [24] J. Lu and Y. Wang, “Single-Feed Triangular Microstrip Antenna with Compact Circular Polarization” *Proceedings of APMC2001*, Taipei, Taiwan, R.O.C., pp.1032–1035, 2001.
- [25] K. Wong, C. Huang, and W. Chen, “Printed Ring Slot Antenna for Circular Polarization”, *IEEE Transactions On Antennas And Propagation*, vol. 50, no. 1, pp 75-77, January 2002.

- [26] Lei, H. Chu, and Y. Guo, “Design of a Circularly Polarized Ground Radiation Antenna for Biomedical Applications,” DOI 10.1109/TAP.2016.2552551, IEEE Transactions on Antennas and Propagation, no. c, pp. 1–7, 2016.
- [27] H. Gu, J. Wang, and L. Ge, “Circularly Polarized Patch Antenna With Frequency Reconfiguration,” IEEE Antennas and wireless propagation letters, vol. 14, pp. 1770–1773, 2015.
- [28] Z. Tu, Q. Chu, and S. Dong, “A Novel Compact Single-feed Dual-band Circular Polarization Antenna” 978-1-4244-2642-3/08/IEEE, pp. 25–28, 2008.
- [29] J. Liu, Y. Li, Z. Liang, and Y. Long, “A Planar Quasi-Magnetic – Electric Circularly Polarized Antenna,” IEEE Trans. Antennas Propag., vol. 64, no. 6, pp. 2108– 2114, 2016.
- [30] X. Zhang and L. Zhu, “High-Gain Circularly Polarized Microstrip Patch Antenna With Loading of Shorting Pins,” IEEE Trans. Antennas Propag., vol. 64, no. 6, pp. 2172–2178, 2016.
- [31] Nasimuddin, Z. N. Chen and X. Qing, “Slotted Microstrip Antennas for Circular Polarization with Compact Size,” IEEE Antennas and Propagation Magazine, vol. 55, no. 2, pp. 124–137, 2013.
- [32] H. Chen, S. Kuo, C. Sim, and C. Tsai, “Coupling-Feed Circularly Polarized RFID Tag Antenna Mountable on Metallic Surface,” IEEE Transactions on Antennas and propagation, vol. 60, no. 5, pp. 2166–2174, 2012.
- [33] K. Maamria and T. Nakamura, “Simple antenna for circular polarisation,” IEE proceedings-h, Vol. 139, No. 2, pp. 157–158, 1992.
- [34] B. Kim Boyon Kim, Bo Pan, Symeon Nikolaou, Young-Sik Kim, John Papapolymerou, and Manos M. Tentzeris, “A Novel Single-Feed Circular Microstrip Antenna With Reconfigurable Polarization Capability,” IEEE transactions on antennas and propagation, vol. 56, no.3, pp. 630–638, 2008.

- [35] Y.T. Lo, B. Engst, R.Q. Lee, "Simple Design Formulas For Circularly Polarised Microstrip Antennas," *IEEE Proceedings*, vol. 135, no. 3, pp. 4–6, 1988.
- [36] Chihyun Cho, Ikmo Park, and Hosung Choo "Design of a Circularly Polarized Tag Antenna for Increased Reading Range," *IEEE Transactions on antennas and propagation*, vol. 57, no. 10, pp. 3418–3422, 2009.
- [37] [37] Z. Wang, S. Fang, S. Fu, and S. Jia, "Single-Fed Broadband Circularly Polarized Stacked Patch Antenna With Horizontally Meandered Strip for Universal UHF RFID Applications," *IEEE Transactions On Microwave Theory And Techniques* vol. 59, no. 4, pp. 1066–1073, 2011.
- [38] Nasimuddin, X. Qing, and Z. N. Chen, "Compact Circularly Polarized Symmetric Slit Microstrip Antennas," *IEEE Antennas and Propagation Magazine*, vol. 53, no. 4, pp. 63–75, 2011.
- [39] J. P. Shinde and M. D. Uplane, "Circular Polarization in Stacked Hexagonal Shaped Microstrip Antennas," *IJAREEIE*, vol. 2, no. 7, pp. 3376–3384, 2013.
- [40] B. Zheng and Z. Shen, "Effect of a Finite Ground Plane on Circularly Polarized Microstrip Antennas," *0-7803-8883-6/05IEEE*, pp. 238–241, 2005.
- [41] Sanyog Rawat and K. K. Sharma, "Circularly Polarized Microstrip Patch Antenna with T-Shaped Slot," *IJECT*, vol. 7109, pp. 65–69, 2013.
- [42] Yogesh Kumar Gupta, R L Yadava, R.K.Yada, "Circularly polarized truncated pentagonal shaped microstrip patch antenna," *International Journal of Microwaves Applications*, vol. 2, no. 6, pp. 6–9, 2013.

- [43] S.K. Lee, A. Sambell, E. Korolkiewicz, S.F. Loh, S.F. Ooi and Y. QIN, “A Design Procedure For A Circular Polarized, Nearly Square Patch Antenna,” *Microwave Journal* January, 2005.
- [44] K. P. Ray, D. M. Suple, and N. Kant, “Suspended Hexagonal Microstrip Antennas for Circular Polarization,” *International Journal Of Microwave And Optical Technology*, vol. 5, no. 3, pp. 1–5, 2010
- [45] A. Ramadan, M. Al-husseini, K. Y. Kabalan, and A. El-hajj, “A Circularly Polarized Decagonal Slot Antenna,” 978-1-4244-6830-0/10/IEEE, pp. 545–548, 2010.
- [46] M. D. Deshpande and N. K. Das, “Rectangular Microstrip Antenna for Circular Polarization,” 0018-926X/86/0500-0744\$01.00 0 IEE,no. 5, pp. 744–746, 1986.
- [47] C. Yen, D. Sim, K. Lin, and J. Row, “Design of An Annular-Ring Microstrip Antenna for Circular Polarization,” 0-7803-8302-8/04/\$20.00 02004 IEEE, pp. 471–474.
- [48] M. Samanta,Santanu Das, “Circularly Polarized Hexagonal Microstrip Antenna for Bluetooth Application,” 2011 Indian Antenna Week, pp. 1–3, 2011.
- [49] X. Yang, Y. Z. Yin, W. Hu and S. L. Zuo, “Low-Profile , Small Circularly Polarized Inverted-L,” *IEEE Antennas And Wireless Propagation Letters*, vol. 9, pp. 767–770, 2010.
- [50] J. Row and S. Wu, “Circularly-Polarized Wide Slot Antenna Loaded With a Parasitic Patch,” *IEEE Transactions On Antennas And Propagation*, vol. 56, no. 9, pp. 2826–2832, 2008.
- [51] S. Maddio, G. Pelosi, M. Righini, and S. Selleri, “A Circularly Polarized Antenna for Dual Band Operation at 2.45 GHz and 5.10 GHz,” *Progress In Electromagnetics Research C*, vol. 74, pp. 1–8, 2017.

- [52] Z. Harouni, L. Cirio, L. Osman, A. Gharsallah and O. Picon, "A Dual Circularly Polarized 2.45 GHz Rectenna for Wireless Power Transmission," *IEEE Antennas and Wireless Propagation Letters*, vol. 10, pp. 306–309, 2011.
- [53] X. Bao and M. Ammann, "Dual Frequency Dual Circularly-polarised Patch Antenna with Wide Beam width," *Electronics Letters*, Vol. 44, No. 21 pp. 2008–2010, 2008.
- [54] W. Liao and Q.-X. Chu "Dual-Band Circularly Polarized Microstrip Antenna With Small Frequency Ratio", *Progress In Electromagnetics Research Letters*, Vol. 15, 145–152, 2010.
- [55] K. Kandasamy and B. Majumder, "Dual-Band Circularly Polarized Split Ring Resonators Loaded Square Slot Antenna," *IEEE Transactions on Antennas and Propagation*, vol. 64, no. 8, pp. 3640–3645, 2016.
- [56] Z. Liang, D. Yang, and X. Wei, "Dual-Band Dual Circularly Polarized Microstrip Antenna With Two Eccentric Rings and an Arc-Shaped Conducting Strip," *IEEE Antennas and Wireless Propagation Letters*, vol. 15, pp. 834–837, 2016.
- [57] M. Bod and H. R. Hassani, "Multi-Band Circularly Polarized Slot Antenna for GPS, Bluetooth and WiMAX Bands," *Progress In Electromagnetics Research C*, vol. 49, pp. 171–178, 2014.
- [58] Sanjay Kumar, B.Ramachandran, and S.Bashyam, "Design and Implementation of Dual-Band Circularly Polarized Antenna," *IEEE ICCSP 2015 conference*, 978-1-4799-8081-9/152015 IEEE pp. 1242–1246, 2015.
- [59] S. Maddio, A. Cidronali, G. Manes, and V. S. Marta, "Compact Dual Band Circularly Polarized Patch Antennas with Small Frequency Ratio," *Proceedings of the 44th European Microwave Conference*, pp. 1679–1682, 2014.

- [60] X. Rui, J. Li, and K. Wei, “Dual-band dual-sense circularly polarised square slot antenna with simple structure,” *Electronics Letters*, Vol. 52 No. 8 pp. 578–580, 2016
- [61] X. L. Bao and M. J. Ammann, “Monofilar Spiral Slot Antenna for Dual-Frequency Dual-Sense Circular Polarization,” *IEEE Transactions on Antennas and Propagation*, vol. 59, no. 8, pp. 3061–3065, 2011.
- [62] Q. Liu, J. Shen, H. Liu, and Y. Liu, “Dual-Band Circularly-Polarized Unidirectional Patch,” *IEEE Transactions on Antennas and Propagation*, vol. 62, no. 12, pp. 6428–6434, 2014.
- [63] X. Bao and M. J. Ammann, “Dual-Frequency Dual-Sense Circularly-Polarized Slot Antenna Fed by Microstrip Line,” *IEEE Transactions on Antennas and Propagation*, vol. 56, no. 3, pp. 645–649, 2008.
- [64] Y. Shao, and Z. Chen, “A Design of Dual-Frequency Dual-Sense Circularly-Polarized Slot Antenna,” *IEEE Transactions on Antennas and Propagation*, vol. 60, no. 11, pp. 4992–4997, 2012.
- [65] S. Zuo, L. Yang, and Z. Zhang, “Dual-Band CP Antenna With a Dual-Ring Cavity for Enhanced Beam width,” *IEEE Antennas and Wireless Propagation Letters*, vol. 14, pp. 867–870, 2015.
- [66] W. Cao, A. Liu, B. Zhang, and T. Yu, “Dual-Band Spiral Patch-Slot Antenna With Omnidirectional CP and Unidirectional CP Properties,” *IEEE Transactions on Antennas and Propagation*, vol. 61, no. 4, pp. 2286–2289, 2013.
- [67] Y. Sung, “Dual-Band Circularly Polarized Pentagonal Slot Antenna,” *IEEE Antennas and Wireless Propagation Letters*, vol. 10, pp. 259–261, 2011.
- [68] J. Lu and C. Liou, “Planar Dual-Band Circular Polarization Monopole Antenna for Wireless Local Area Networks,” *IEEE Antennas and Wireless Propagation Letters*, vol. 14, pp. 478–481, 2015.

- [69] U. Mashayak and V. G. Kasabegoudar, “Dual Band Circularly Polarized Printed Antenna with Branched Microstrip Feed,” *Communications on Applied Electronics (CAE)* , Volume 6 , No.4, December 2016
- [70] S. M. Noghabaei, S. K. A. Rahim, P. J. Soh, M. Abedian, and G. A. E. Vandebosch, “A Dual-Band Circularly-Polarized Patch Antenna with a Novel Asymmetric Slot for WiMAX Application,” *Radio Engineering*, vol. 22, no. 1, pp. 291–295, 2013.
- [71] Y. Chen, Y. Jiao, G. Zhao, F. Zhang, Z. Liao, and Y. Tian, “Dual-Band Dual-Sense Circularly Polarized Slot Antenna With a C-Shaped Grounded Strip,” vol. 10, pp. 915–918, 2011.
- [72] D. Yu, S. Gong, Y. Wan, and W. Chen, “Omnidirectional Dual-Band Dual Circularly Polarized Microstrip Antenna Using Modes,” *IEEE Antennas and Wireless Propagation Letters*, vol. 13, pp. 1104–1107, 2014.
- [73] W. Li, B. Liu, and H. Zhao, “The U-Shaped Structure in Dual-Band Circularly Polarized Slot Antenna Design,” *IEEE Antennas And Wireless Propagation Letters*, vol. 13, pp. 447–450, 2014.
- [74] Y. Cai, K. Li, Y. Yin, and X. Ren, “Dual-Band Circularly Polarized Antenna Combining Slot and Microstrip Modes for GPS With HIS Ground Plane,” *IEEE Antennas And Wireless Propagation Letters*, vol. 14, pp. 1129–1132, 2015.
- [75] C. Wang, M. Shih, and L. Chen, “A Wideband Open-Slot Antenna With Dual-Band Circular Polarization,” *IEEE Antennas And Wireless Propagation Letters*, vol. 14, pp. 1306–1309, 2015.
- [76] C. Wu, C. Lu, J. Shen, and Z. Ye, “A CPW-Fed Slot Antenna with Dual Band and Dual Circular Polarization,” *Proceedings of ISAP2016*, Okinawa, Japan, pp. 810–811, 2016.

- [77] J. Zhang, L. Zhu, N. Liu, and W. Wu, “CP patch antenna with controllable polarisation over dual-frequency bands,” *IET Microwaves, Antennas and Propagation*, vol. 11, pp. 224–231, 2017.
- [78] Yi Liu, Xi Li, Lin Yang and Ying Liu, “A Dual-polarized Dual-band Antenna with Omni-directional Radiation Patterns”, DOI 10.1109/TAP.2017.2708093, *IEEE Transactions on Antennas and Propagation*, pp. 0–3, 2017.
- [79] C. Chen and E. K. N. Yung, “Dual-Band Dual-Sense Circularly-Polarized CPW-Fed Slot Antenna With Two Spiral Slots Loaded,” *IEEE Transactions on Antennas and Propagation*, vol. 57, no. 6, pp. 1829–1833, 2009.
- [80] F. Alizadeh, Changiz Ghobadi, Javad Nourinia, Mahdi Dadashi and Rahim Barzegari “A design of ring-shaped dual-band / multi-band circularly polarized microstrip antenna based on slots mutual coupling,” *International Journal of Microwave and Wireless Technologies*, vol. 1, pp. 1–9, 2015.
- [81] R. Xu, J. Li, and G. Yang, “A Novel Dual-Band Dual-Sense Circularly Polarized Antenna Based on Simple Printed Dipole Structure,” 978-1-5386-3284-0/172017 *IEEE* pp. 173–174, 2017.
- [82] J. Lin, Z. Qian, W. Cao, S. Shi, Q. Wang, and W. Zhong, “A Low-Profile Dual-Band Dual-Mode and Dual-Polarized Antenna Based on AMC,” *IEEE Antennas and Wireless Propagation Letters*, vol. 16, pp. 2473–2476, 2017.
- [83] D.D. Wang, C.Y. Yuan, W.J. Lu and H.B. Zhu, “Conceptual design of a dual band circularly polarised square loop antenna under even mode resonance”, 978-1-5386-1608-6/17/*IEEE*, pp. 6–8, 2017.

- [84] Hu Rack Lee, Hong Kyun Ryu, Sungkyun Lim, and Jong Myung Woo, "A Miniaturized, Dual-Band, Circularly Polarized Microstrip Antenna for Installation Into Satellite Mobile Phones," *IEEE Antennas and Wireless Propagation Letters*, vol. 8, pp. 823–825, 2009.
- [85] Y. Zhang, X. Li, L. Yang, and S. Gong, "Dual-Band Circularly Polarized Annular-Ring Microstrip Antenna for GNSS Applications," *IEEE Antennas and Wireless Propagation Letters*, vol. 12, pp. 615–618, 2013.
- [86] T. Chang, "Dual band CP antenna by adding sleeves to the monopole," *2015 IEEE 4th Asia-Pacific Conf. Antennas Propag.*, pp. 195–196, 2015.
- [87] Y. Hu, B. Hu, and H. Zhang, "A New Compact Dual-Band CP Antenna for GPS and DSRC Applications," *2017 Sixth Asia-Pacific Conf. Antennas Propag.*, pp. 1–3.
- [88] R. Caso, A. Michel, and P. Nepa, "Dual-Band UHF-RFID / WLAN Circularly Polarized Antenna for Portable RFID Readers," *IEEE Trans. Antennas Propag.*, vol. 62, no. 5, pp. 2822–2826, 2014.
- [89] Qiang Liu, Junyu Shen, Jungang Yin, Hongli Liu, and Yuanan Liu, "Compact 0.92/2.45-GHz Dual-Band Directional Circularly Polarized Microstrip Antenna for Handheld RFID Reader Applications," *IEEE Trans. Antennas Propag.*, vol. 63, no. 9, pp. 3849–3856, 2015.
- [90] K. Qian, and X. Tang, "Compact LTCC Dual-Band Circularly Polarized Perturbed Hexagonal Microstrip Antenna", *IEEE Antennas Wirel. Propag. Lett.*, vol. 10, pp. 1212–1215, 2011.
- [91] Xiao-Yu He, Lei Chang, Ling-Lu Chen, "A Multifunction Broad-Beam Antenna with Dual Bands and Dual Circular-Polarizations," *2016 IEEE MTT-S Int. Wirel. Symp.*, no. 36, pp. 1–4.

- [92] F. Samadi, Mohsen. Karamirad, Changiz.Ghobadi, Javad. Nourinia, Rahim. Barzeghari “A Dual Band Circularly Polarized Antenna with Parasitic Element for Gain enhancement,” 2016 8th Int. Symp. Telecommun., pp. 447–451, 2016.
- [93] Q. Wu, H. Wang, C. Yu, X. Zhang, and W. Hong, “L / S-Band Dual-Circularly Polarized Antenna Fed by 3-dB Coupler”, IEEE Antennas Wirel. Propag. Lett., vol. 14, pp. 426–429, 2015.
- [94] S. Zhou, P. Li, and Y. Wang, “A Dual-Band Dual-Sense Circularly polarized square-ring slot antenna,” 2012 Int. Conf. Microw. Millim. Wave Technol., vol. 3, pp. 1–4, 2012.
- [95] M. Matsunaga, “A Compact Dual-Band Circularly Polarized Spiral Antenna,” 2016 Int. Symp. Antennas Propag., pp. 978–979, 2016.
- [96] R. Xu, J.-Y. Li, J. Liu, D.-J. Wei, K. Wei, Y.-X. Qi, and J.-J. Yang “A Very Simple Dual-band Dual-sense Circularly Polarized Square Slot Antenna,” 978-1-5386-7102-3/18/IEEE, pp. 123–124, 2018.
- [97] The-Nan Chang, Chien-Ping Liu, Jyun-Ming Lin, “Dual - Band CP Antenna by Line -Coupling to a Patch and a Ring”, International Journal of Electrical, Electronics And Data Communication, no. 2, pp. 68-71, 2017.
- [98] K. G. Tan, A. W. Reza, M. Subri, and A. Rani, “Design of Stacked Microstrip Dual-band Circular Polarized Antenna,” Radio engineering, vol. 21, no. 3, pp. 875–880, 2012.
- [99] B. Mubarak, S. Ellis, A. Ahmed, and J. J. Kponyo, “A Circularly Polarized Planar Monopole Antenna with Wide AR Bandwidth Using a Novel Radiator/Ground Structure,” Global Journal of Researches in Engineering: F Electrical and Electronics Engineering, vol. 17, no. 3, 2017.

- [100] J. Wu, Y. Yin, Z. Wang, and R. Lian, “Dual-Band Circularly Polarized Antenna with Differential Feeding,” *Progress In Electromagnetics Research C*, vol. 49, no. March, pp. 11–17, 2014.
- [101] Jianjun Wu, Xueshi Ren, Zhaoxing Li, and Yingzeng Yin, “ Modified Square Slot Antennas For Broadband Circular Polarization” , *Progress In Electromagnetics Research C*, Vol. 38, pp 1–14, 2013.
- [102] L. Zhang, S. Gao, Q. Luo and P. R. Young, “Inverted-S Antenna With Wideband Circular Polarization and Wide Axial Ratio Beam width,” *IEEE Transactions on Antennas and Propagation*, vol. 65, no. 4, pp. 1740–1748, 2017.
- [103] K. Hirose, K. Shinozaki and H. Nakano “A Comb-Line Antenna Modified for Wideband Circular Polarization,” *IEEE Antennas and Wireless Propagation Letters*. vol. 14, pp. 1113–1116, 2015.
- [104] Mehrdad Nosrati, and Negar Tavassolian, “Miniaturized Circularly Polarized Square Slot Antenna with Enhanced Axial-Ratio Bandwidth Using an Antipodal Y-strip”, *IEEE Antennas and Wireless Propagation Letters*, vol.16, pp. 817–820, 2017.
- [105] S. Karamzadeh, V. Rafii, M. Kartal, and M. Dibayi, “Circularly Polarized Square Slot Antenna Using Crooked T-Shape Technique ,” *ACES journal*, Vol. 30, No. 3, March 2015.
- [106] T. Mondal, S. Maity, R. Ghatak, S. Ranjan, and B. Chaudhuri, “Design and analysis of a wideband circularly polarised perturbed psi-shaped antenna,” *IET Microwaves, Antennas & Propagation*, vol. 12, no. c, pp. 1582–1586, 2018.
- [107] J. Wei, X. Jiang, and L. Peng, “Ultrawideband and High-Gain Circularly Polarized Antenna with Double-Y-Shape Slot,” *IEEE Antennas and Wireless Propagation Letters*, vol. 16, pp. 1508–1511, 2017.

- [108] R. U. I. Xu, J. Li, and J. I. E. Liu, “A Design of Broadband Circularly Polarized C-Shaped Slot Antenna With Sword-Shaped Radiator and Its Array for L / S-Band Applications,” Digital Object Identifier 10.1109/ ACCESS.2017.2788008, pp. 5891–5896, 2018.
- [109] A. Narbudowicz, Matthias John, Vit Sipal, Xiulong Bao, and Max J. Ammann et al., “Design Method for Wideband Circularly Polarized Slot Antennas,” *IEEE Transactions on Antennas and Propagation*, vol. 63, no. 10, pp. 4271–4279, 2015.
- [110] R. Joseph and T. Fukusako, “Circularly Polarized Broadband Antenna with Circular Slot on Circular Groundplane” “Progress In Electromagnetics Research C, Vol. 26, 205–217, 2012.
- [111] K. Ding, Y. Guo, and C. Gao, “CPW-Fed Wideband Circularly Polarized Printed Monopole Antenna with Open Loop and Asymmetric Ground Plane,” *IEEE Antennas and Wireless Propagation Letters*, vol. 16, pp. 833–836, 2017.
- [112] K. Ding, C. Gao, T. Yu, and D. Qu, “Wideband CP slot antenna with backed FSS reflector,” *IET Microwaves, Antennas & Propagation*, vol. 1, pp. 1–6, 2017.
- [113] Shing-Lung, Steven Yang, Ahmed A. Kishk, and Kai-Fong Lee, “Wideband Circularly Polarized Antenna With L-Shaped Slot,” *IEEE Transactions on Antennas and Propagation*, vol. 56, no. 6, pp. 1780–1783, 2008.
- [114] S. L. S. Yang, K. F. Lee, A. A. Kishk, and K. M. Luk, “Design and Study of Wideband Single Feed Circularly Polarized Microstrip Antennas,” *Progress In Electromagnetics Research*, vol.80, pp. 45–61, 2008.
- [115] H. Huang and B. Wang, “A Simple V-Shaped Slot Antenna with Broadband Circular Polarization,” *Progress In Electromagnetics Research Letters*, vol. 67, no. February, pp. 67–73, 2017.

- [116] Z. Wu, G. M. Wei, X. Li, and L. Yang, "A Single-Layer and Compact Circularly Polarized Wideband Slot Antenna Based on Bent Feed," *Progress In Electromagnetics Research Letters*, vol. 72, pp. 39–44, 2018.
- [117] S. Trinh-van, Y. Yang, K. Lee, and K. C. Hwang, "Broadband Circularly Polarized Slot Antenna Loaded by a Multiple-Circular-Sector Patch," *Sensors*, doi:10.3390/s1805157, 18, 1576; 2018.
- [118] X. L. Bao, M. J. Ammann, and P. Meevov, "Microstrip-Fed Wideband Circularly Polarized Printed Antenna," *IEEE Transactions on Antennas and Propagation*, vol. 58, no. 10, pp. 3150–3156, 2010.
- [119] C. F. Zhou and S. W. Cheung, "A Wideband CP Crossed Slot Antenna Using $1 - \lambda$ Resonant Mode with Single Feeding," *IEEE Transactions on Antennas and Propagation*, vol. 65, no. 8, pp. 4268–4273, 2017.
- [120] J. Chen and J. Row, "Wideband Circularly Polarized Slotted-Patch Antenna with a Reflector," *IEEE Antennas and Wireless Propagation Letters*, vol. 14, pp. 575–578, 2015.
- [121] X. Gao and Z. Shen, "UHF/UWB Tag Antenna of Circular Polarization," *IEEE Transactions on Antennas and Propagation*, vol. 64, no. 9, pp. 3794–3802, 2016.
- [122] N. Ghassemi, K. Wu, and S. Claude, "Compact Coplanar Waveguide Spiral Antenna With Circular Polarization for Wideband Applications," *IEEE Antennas and Wireless Propagation Letters*, vol. 10, pp. 666–669, 2011.
- [123] S. Mohammadi, J. Nourinia, C. Ghobadi, J. Pourahmadazar, and M. Shokri, "Compact Broadband Circularly Polarized Slot Antenna Using Two Linked Elliptical Slots for C-Band Applications," *IEEE Antennas and Wireless Propagation Letters*, vol. 12, pp. 1094–1097, 2013.
- [124] S. Mao and S. Chen, "Time-domain characteristics of ultra-wideband tapered loop antennas," *Electronics Letters*, vol. 42, no. 22, pp. 3–4, 2006.

- [125] S. Mao and J. Yeh, “Ultrawideband Circularly Polarized Spiral Antenna Using Integrated Balun With Application to Time-Domain Target Detection,” *IEEE Transactions on Antennas and Propagation* vol. 57, no. 7, pp. 1914–1920, 2009.
- [126] A. S. A. El-hameed, D. A. Salem, and E. A. Abdallah, “Ultra Wide Band CPW-Fed Circularly Polarized Square Slot Antenna,” *AP-S* 2013, pp. 5–6, 2013.
- [127] R. Kumar, B. Huyart, and J. Cousin, “Dual-Circular Polarized Dumbbell-Shaped Crossed-Dipole Planar Antenna for UWB Application,” *7th European Conference on Antennas and Propagation (EuCAP)*, pp. 1474–1478, 2013.
- [128] M. S. Ellis, Z. Zhao, J. Wu, and X. Ding, “A Novel Simple and Compact Microstrip-Fed Circularly Polarized Wide Slot Antenna with Wide Axial Ratio Bandwidth for C-Band Applications,” *IEEE Transactions on Antennas and Propagation*, vol. 64, no. 4, pp. 1552–1555, 2016.
- [129] K. Hung and Y. Lin, “Novel Broadband Circularly Polarized Cavity-Backed Aperture Antenna With Traveling Wave Excitation,” *IEEE Transactions on Antennas and Propagation*, vol. 58, no. 1, pp. 35–42, 2010.
- [130] Q. Chen, H.-L. Zheng, T. Quan, and X. Li “Broadband Cpw-Fed Circularly Polarized Antenna With Equiangular Tapered-Shaped Feedline For Ultra-Wideband Applications” *Progress In Electromagnetics Research C*, Vol. 26, 83–95, 2012.
- [131] S. Karamzadeh, V. Ra, M. Kartal, and H. Saygin, “Compact UWB CP square slot antenna with two corners connected by a strip line,” *Electronics Letters*, vol. 52, no. 1, pp. 11–12, 2016.

- [132] J. P. Shinde, Raj Kumar, M. D. Uplane , P. N. Shinde “Circularly Polarized Rectangular Slot Antenna with Trapezoidal Tuning Stub for UWB Application,” 978-1-4577-1099-5/11 IEEE, pp. 1–4, 2011.
- [133] Y. Shen and C. L. Law, “A Microstrip-Fed Quasi-Spiral Circularly Polarized Ultra-Wideband Antenna,” AP-S/URSI 2011, pp. 1463–1466, 2011.
- [134] J. Pourahmadazar, S. Member, C. Ghobadi, J. Nourinia, and N. Felegari, “Broadband CPW-Fed Circularly Polarized Square Slot Antenna with Inverted-L Strips for UWB Applications,” IEEE Antennas and Wireless Propagation Letters, vol. 10, pp. 369–372, 2011.
- [135] J. Pourahmadazar and S. Mohammadi, “Compact circularly-polarised slot antenna for UWB applications,” Electronics letters, vol. 47, no. 15, pp. 2–3, 2011.
- [136] H. Tang, K. Wang, R. Wu, and C. Yu, “Compact broadband CP monopole antenna with tilted branch,” Electronics Letters, vol. 52, no. 21, pp. 1739–1740, 2016.
- [137] P. Tendolkar, A. Shah, and A. Jeyakumar, “Study of CPW-Fed Slot Antenna for UWB Application,” International Journal of Innovative Research in Computer and Communication Engineering, pp. 2826–2830, 2015.
- [138] Y. Zhong, G. Yang, J. Mo, and L. Zheng, “Compact Circularly Polarized Archimedean Spiral Antenna for Ultrawideband Communication Applications,” IEEE Antennas and Wireless Propagation Letters , vol. 16, pp. 129–132, 2017.
- [139] J. Wei, X. Jiang, and L. Peng, “Ultra Wideband and High Gain Circularly Polarized Antenna with Double-Y-Shape Slot,” IEEE Antennas and Wireless Propagation Letters vol. 1225, pp. 2–5, 2016.

- [140] Raghupatruni V., Ram Krishna and Raj Kumar, “Design of Temple Shape Slot Antenna for Ultra Wideband Applications” *Progress In Electromagnetics Research B*, Vol. 47, 405–421, 2013.
- [141] M. Shokri, V. Ra, S. Karamzadeh, Z. Amiri, and B. Virdee, “Miniaturised ultra- wideband circularly polarised antenna with modified ground plane,” *Electronics Letters*, vol. 50, no. 24, pp. 6–7, 2014.
- [142] J. Sze, J. Wang, and C. Chang, “Axial-ratio bandwidth enhancement of asymmetric-CPW-fed circularly-polarised square slot antenna,” *Electronics Letters*, vol. 44, no. 18, pp. 3–4, 2008.
- [143] S. Fu, S. Fang, Z. Wang, and X. Li, “Broadband Circularly Polarized Slot Antenna Array Fed by Asymmetric CPW for L-Band Applications,” *IEEE Antennas and Wireless Propagation Letters*, vol. 8, pp. 1014–1016, 2009.
- [144] J. Pourahmadazar and V. Rafii, “Broadband circularly polarised slot antenna array for L- and S-band applications,” vol. 48, no. 10, pp. 9–10, 2012.
- [145] T. Chang, “Wideband circularly polarised antenna using two linked annular slots,” *Electronics Letters*, vol.47, no. 13, pp. 12–13, 2011.
- [146] S. Du and Q. Chu, “A CPW-Fed Broadband Circularly-Polarized Square Slot Antenna with E-Shaped Slits in Ground Plane, Proceedings of the 39th European Microwave Conference”, pp. 225–227, 2009.
- [147] T. Li, F. Zhang, F. Gao, and Y. Guo, “CPW-Fed Circularly Polarized Square Slot Antenna with Enhanced Bandwidth and Reduced Size for Wideband Wireless Applications,” *Progress In Electromagnetics Research C*, vol. 65, no. June, pp. 121–129, 2016.
- [148] J. Jan, C. Pan, K. Chiu, and H. Chen, “Broadband CPW-Fed Circularly-Polarized Slot Antenna With an Open Slot,” *IEEE Transactions on Antennas and Propagation*, vol. 61, no. 3, pp. 1418–1422, 2013.

- [149] S. H. Yeung, K. F. Man and W. S. Chan, “A bandwidth improved circular polarised Slot Antenna using a Slot Composed of Multiple Circular Sectors,” *IEEE Transactions on Antennas and Propagation* vol. 59, no. 8, pp. 3065–3070, 2011.
- [150] R. Xu, J. Liu, and K. Wei, “A Simple Design of Compact Dual - wideband Square Slot Antenna with Dual - sense Circularly Polarized Radiation for WLAN/Wi - Fi Communications,” *IEEE Antennas and Wireless Propagation Letters*, vol. 2, pp. 2–7, 2018.

.....✂.....

Chapter 3

METHODOLOGY

<i>Contents</i>	3.1 <i>Ansys HFSS Simulation Tool</i>
	3.2 <i>Characteristic Mode Analysis Using CST</i>
	3.3 <i>Antenna Fabrication Procedure</i>
	3.4 <i>Antenna Measurement Facilities</i>
	3.5 <i>Experimental Techniques</i>
	3.6 <i>Conclusion</i>

This chapter is a brief overview of simulation tools, fabrication techniques and the experimental methodology adopted to confirm the results. Available facilities utilised to carry out the current research work are also described. Simulation studies were carried out using ANSYS HFSS, which is a software tool based on Finite Element Method. The theoretical analysis of the circularly polarised antennas were carried out using Characteristic Mode Analysis. This analysis method was carried out using a software tool, Computer Simulation Technology (CST) Microwave Studio. The photolithographic method was used for the development of circularly polarised antenna prototypes. The simulation results were confirmed using Vector Network analyzer and Anechoic Chamber. This chapter is concluded by providing a comprehensive account of the experimental set up.

3.1 Ansys HFSS: A tool for antenna simulation

In order to materialise our goals, the support of an efficient simulation software tool is mandatory. There are numerous choices for the selection of tools. It should facilitate the refinement of various dimensions to achieve better results, and parametric analysis as well as the theoretical analysis of the structure should be possible with it. High-frequency products like RF and microwave components, antennas, antenna arrays, IC packages, printed circuit boards speedy interconnects, filters and connectors may be designed and simulated using 3D electromagnetic (EM) simulation software ANSYS HFSS. ANSYS HFSS is widely used to design high-frequency, high-speed electronics found in communications systems, radar systems, advanced driver assistance systems (ADAS), satellites, internet-of-things (IoT) products and other high-speed RF and digital devices [1]. The three-dimensional electromagnetic problems may be accurately solved by using this software. With the help of Finite Element Method (FEM), powerful graphics and adaptive meshing technique, it yields superior performance.

Overview of design and simulation process:

The geometrical design and simulation steps of the antenna are described below.

- 1) Draw the geometrical shape with proper dimensions of the substrate.
- 2) Choose and assign the material to substrate from a list of materials.

- 3) Draw the geometrical shape of the patch with proper dimensions and assign the boundary to patch.
- 4) Create the ground plane and assign boundary.
- 5) Find out the feed location through optimisation.
- 6) Create an air-filled radiation box of suitable volume around the system.
- 7) Create the analysis setup. Fix the solution frequency and then add frequency sweep. The range of frequency sweep and number of frequency points are selected.
- 8) Set up the far-field which will finally validate the model.
- 9) Check results.

In this research work, the antennas were parametrically analysed using the optimization tools integrated with the HFSS package.

3.2 Characteristic Mode Analysis using CST Microwave studio

Antenna engineers met with the challenge of optimizing antenna performance, while integrating multi-band antennas into compact devices. The Characteristic Mode Analysis (CMA) tool is the newly introduced extension to the CST STUDIO SUITE integral equation solver and it is possible to solve the above problems. CMA is a mode of analysis developed to provide a clear understanding of the behaviour of a conducting surface. A set of orthogonal current-modes which are supported on a conducting surface are calculated by CMA. By using

CMA, feed location can be easily sorted out into a particular radiating mode and can tune to the correct resonant frequencies.

The integral equation solver module of CST STUDIO SUITE, facilitates the process of calculating the characteristic modes, calculates the modal significance, eigen values and characteristic angles. Through the analysis of these three entities the circular polarisation behaviour of the antenna may easily be fixed. The far field radiation pattern and surface current distribution coupled with each mode, enable the users to have a clear insight into their device. While developing an antenna with multi-band behaviour, the current modes on the antenna at the desired resonant frequency may easily be calculated with the CMA tool and the geometry may be optimized to increase the coupling to the desired mode [2].

3.3 Antenna fabrication procedure

The step by step procedure of fabrication of antenna prototypes is described below.

3.3.1 Selection of substrate

Material dependant parameters like dielectric constant and loss tangent are highly important. In this piece of research work, single sided and double-sided substrates are selected. Different substrate materials are available. In order to mount the antenna on curved surfaces, flexible substrate materials are used. In high dielectric constant substrates, surface waves will be excited. This also causes spurious radiations in undesired directions. To reduce the propagation delay, substrate with low relative

permittivity and low loss are required. For the dissipation of heat, thermal conductivity should be high. Substrate characteristics that are to be considered are the thickness, isotropic behaviour, homogeneity and dimensional strength. In this work, considering the availability, low cost factor and versatility, FR4 is used as the substrate for the fabrication of the antenna prototypes. [3-4].

3.3.2 Photolithography

The fabrication steps are described one by one and depicted in Figure 3.1.

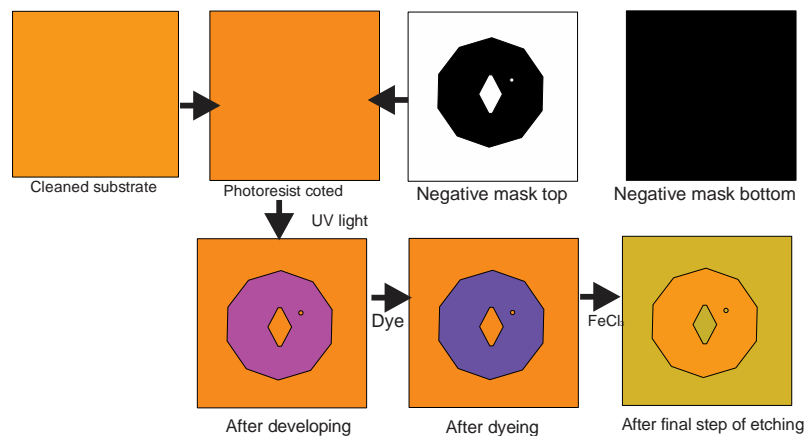


Figure 3.1. Different steps in the prototype fabrication

A double sided copper clad (FR4) substrate piece of suitable thickness, length and width is taken. It is cleaned with a wire gauss with utmost care and dried to get rid of impurities, which may cause discontinuities on the copper traces etched on the substrate, and may adversely affect the performance of the antenna. Any sort of deviation from the etched structure will shift the designed resonant frequency, especially at

high frequencies. A thin layer of negative photo resist diluted with thinner, prepared in the ratio 1:1, is coated on the top surface. The lower side of the substrate, where a thin coating of copper is there, is covered with cello tape. The mask is placed just above the photo resist-coated substrate surface, that is the top layer and exposed to UV light. The developer solution will not wash out the hardened portions. In order to have a clear view of the hardened photo resist portions on the copper coating, the board is then immersed in dye ink solution. Then unnecessary portions of copper are etched off by immersing the etched substrate in Ferric Chloride (FeCl_3) solution. The cello tape fixed on the lower side to protect the ground plane is peeled off and ensured that it remains intact.

3.4 Antenna Measurement Facilities

The antenna measurements are carried out using the antenna research facility which includes Vector Network Analysers (HP8510C, R&S ZVB20, Agilent PNA E8362B), antenna positioner facility and anechoic chamber [5].

3.4.1 Performance network analyzer PNA E8362B

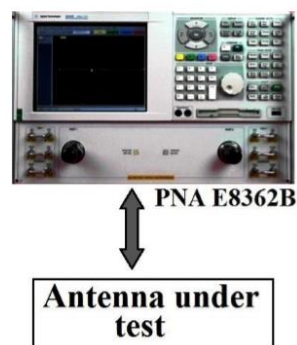


Figure 3.2. E8362B performance Network Analyzer

The Agilent (Keysight Technologies) E8362B PNA (Performance Network Analyzer) has high sweep speed, good dynamic range, a little trace noise and flexible connectivity options. Hence antenna designers and engineers prefer this model of PNA [6].

In this piece of research work, this PNAE 8362B and ZVB20 analysers are used for the measurement of various scattering parameters, far field parameters like axial ratio and radiation patterns.

3.4.2 Anechoic chamber

The anechoic chamber is a large room with prefixed dimensions, which depend on the wavelength of measurements, lined with microwave absorbers affixed on all sides. The side walls, roof and the floor are fixed with these absorbers, to avoid the electromagnetic energy reflections. It provides a zone which is quite and free from all sorts of EM distortions, which is highly essential for antenna measurements. All the antenna measurements are done in this anechoic chamber and this reflections free environment provides error free results. The photograph of the anechoic chamber in which the measurements are carried out is shown in figure 3.3 below.

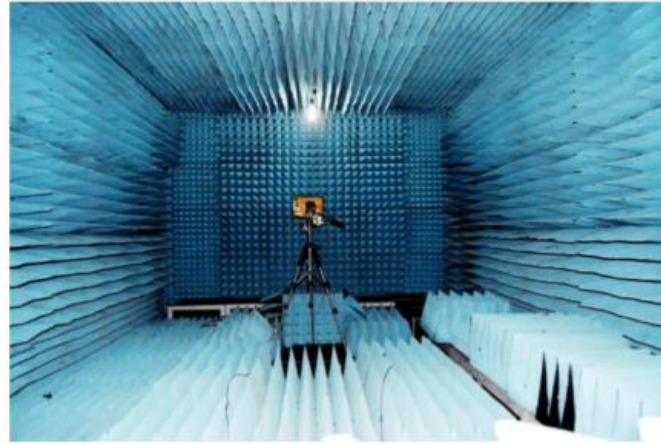


Figure 3.3. Anechoic chamber

High quality carbon black impregnated polyurethane foam having low density are used for making these absorbers. Metallic sheet(aluminium) surrounds the chamber on all the sides to resist external electromagnetic interferences [8].

3.4.3 Hardware and software set up for far field radiation pattern measurement

The set up comprises of a stepper motor-controlled turn table, on which the antenna for study is placed. MATLAB based in-house automation software “Crema Soft” is there for coordination. This is used for calibration, antenna measurements and material characterization of the substrate. The control box communicates with the stepper motor-controlled turn table and Network Analyzer through GPIB.

3.5 Experimental techniques

There is a set of standard experimental techniques for carrying out various measurements of various antenna parameters.

To compensate for the losses incurred with various cables and connectors accompanying the equipment, calibration is to be done. Known standards of open, short and matched loads validate this calibration procedure, which ensures accuracy and precision. Single port calibration Proper phase delay is applied during calibration, to ensure that the reference plane for all measurements is at 0°.

3.5.1 Measurement of S parameters

The S -parameter 'S11' is defined as $-20 \log(|\Gamma|)$. Where 'Γ' is the reflection coefficient [9]. The expression for the S parameter S11 is,

$$|S11| = -20 \log (|\Gamma|) \text{ dB.}$$

The S11/S22 versus frequency is displayed in phase magnitude form and then stored on the computer with the aid of CREMA SOFT. The scattering parameter S21 is the transmission coefficient or the ports isolation parameter.

The difference in frequencies (Δf) corresponding to -10dB points of the return loss curve is taken as the bandwidth or 2:1 VSWR bandwidth of the antenna.

The fractional bandwidth is calculated as $\frac{\Delta f}{f_r}$. When multiplied by 100 it gives the percentage bandwidth. The input impedance corresponding to the resonant frequency can be determined from the Smith Chart displayed on the network analyser.

3.5.2 Radiation pattern

It is the pictorial representation of the radiation properties of an antenna [9]. Normally, two principal plane patterns are identified for directional antennas and three patterns for antennas with Omni-directional patterns. Generally, far-field patterns are measured at a larger distance. The measurement set up is shown in Figure 3.4

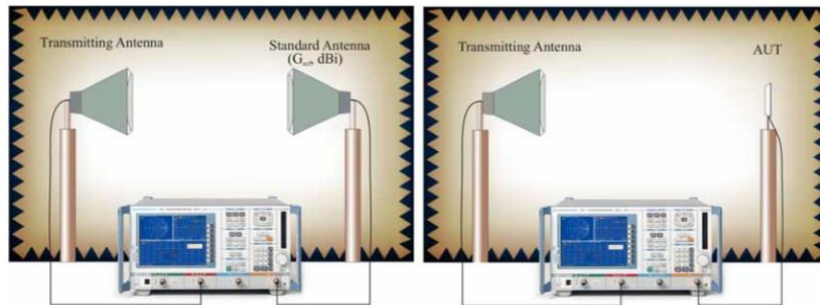


Figure 3.4. Antenna radiation pattern measurement setup

The AUT is treated as receiver placed on the turn table, is placed in the anechoic chamber. The transmitting horn antenna is connected to PNA. The XOZ and YOZ plane radiation patterns are measured in S21/S12 mode. The optimum reception is achieved and then THRU calibration is done. Setting of suitable gate parameters in the time domain, in the network analyser, avoids spurious reflections which may corrupt the measured data [10].

3.5.3 Antenna gain and efficiency

Gain of an antenna may be defined with a reference antenna. When both the antennas are fed with the same input power, it is the ratio of the

radiation intensity in the strongest direction, to the radiation intensity of the reference antenna. Actually, gain of an antenna is a passive characteristic [10].

In an experimental setup identical to that of the radiation pattern measurement, the absolute gain is measured using the gain comparison method [9]. The absolute gain is obtained as follows.

$$G \text{ (dBi)} = G_{\text{ref}} \text{ (dBi)} + |S_{21}|_{\text{AUT}}$$

Antenna efficiency as per IEEE definition is the ratio of the total power radiated by the antenna to the net power accepted by the antenna at its terminals during the radiation process [10]. To measure the efficiency, Wheeler cap method is used [11-12]. The efficiency may be calculated using the following expression:

$$\text{Efficiency, } \eta = \frac{\text{Input resistance without cap} - \text{Input resistance with cap}}{\text{Input resistance without cap}}$$

3.5.4 Polarization

The polarization measurement experimental setup is identical to that of the radiation pattern. The AUT is configured as the transmitter and the wide a band horn as the receiver. The horn is then rotated through 360° and S21 measurement is done. From this, polarisation pattern is plotted.

3.5.5 Axial ratio



Figure 3.5. Axial ratio measurement setup

The experimental set up is similar to that for polarisation measurement. The AUT is stationary. The standard horn placed on the turn table is rotated on its own vertical axis through 360° and noted the maximum and the minimum values of power received at port 2. For a particular frequency, Axial Ratio (AR) = Maximum Power in dB – Minimum Power in dB.

A graph is plotted between the frequency and difference power in dB. From this 3 dB ARBW is calculated. The centre frequency is also noted.

3.5.6 Group Delay

Group delay is defined as the negative derivative of the signal phase with respect to frequency [13 -14]. A signal experiences both amplitude and phase distortions when it passes through a device or medium and the amount of distortion depends on its characteristics. There are several frequency components in an incident waveform. The group delay gives a measure of average time delay of input signal at each frequency. This is a measure of the dispersive nature of the device. The group delay will vary with frequency, if the device has a non-linear phase response. The input signal suffers different delays at various frequencies. As a result, the output waveform will be distorted. The group delay plot is very effective for the analysis of nonlinearity present in the phase. For measurement, two identical antennas placed in far field and oriented face to face, are connected to two ports of the network analyser. Then measured the group delay using delay option. The same is repeated by placing the antennas side by side separated by the same distance.

3.6 Conclusion

Methodology applied for simulation, analysis, fabrication and measurement of antenna characteristics in this piece of research work are discussed in brief. The characteristic mode analysis of the CP antennas using CST is discussed in brief. Theory and measurement procedure of various antenna parameters such as reflection coefficient, radiation pattern gain, efficiency, and axial ratio as well as time domain characteristics such as group delay are explained to evaluate the CP behaviour of the antennas.

References

- [1] Antenna design and simulation – CST, <https://www.cst.com/Applications/>
- [2] W. Sorgel and W. Wiesbeck, “Influence of the Antennas on the Ultra-Wideband Transmission”, *EURASIP Journal on Applied Signal Processing*, pp. 296–305, 2005.
- [3] A. H. Mohammadian, A. Rajkotia, and S. S. Soliman, “Characterization of UWB transmit-receive antenna system,” *IEEE Conf. Ultra Wideband Systems and Technology*, pp. 157–161, 2003.
- [4] Y. Duroc, T. P. Vuong, and S. Tedjini, “A Time/Frequency Model of Ultrawideband Antennas”, *IEEE Transactions on Antennas and Propagation*, vol. 55, no. 8, pp. 2342—2351, 2007.
- [5] J. Kunisch and J. Pamp, “UWB radio channel modelling considerations,” *Proc. International Conference on Electromagnetics in Advanced Applications (ICEAA ’03)*, pp. 277–284, 2003.
- [6] C. E. Baum, E. G. Farr, and D. V. Giri, “Review of Impulse-Radiating Antennas”, *Sensor and Simulation Notes*, Air Force Research Laboratory, USA, 1998.
- [7] J. Liang, Thesis on “Antenna Study and Design for Ultra Wideband Communication Applications” 2006.
- [8] M. Hiebel, *Vector Network Analyser (VNA) Calibration: The Basics*, ROHDE & SCHWARZ.
- [9] C. A. Balanis, *Antenna Theory: Analysis and Design*, Wiley & Sons, 1996.
- [10] H.G. Schantz, “Radiation efficiency of UWB antennas”. *Proceedings of the IEEE UWBST Conference*, 2002.

- [11] W. Sorgel, F. Pivit, and W. Wiesbeck, “Comparison of frequency domain and time domain measurement procedures for ultra-wideband antennas,” Proc. 25th Annual Meeting and Symposium of the Antenna and Measurement Techniques Association (AMTA’03), pp. 72–76, 2003.
- [12] W. Wiesbeck, G. Adamiuk and C. Sturm, “Basic Properties and Design Principles of UWB Antennas”, Proceedings of the IEEE, vol. 97, no. 2, pp. 372- 386, 2009.
- [13] W. Sorgel, S. Knorz and W. Wiesbeck, “Measurement and Evaluation of Ultra Wideband Antennas for Communications”, International ITG Conference on Antennas – INICA, pp. 377- 380, 2003
- [14] T. G. Ma and S. K. Jeng, “Planar Miniature Tapered-Slot-Fed Annular Slot Antennas for Ultra wide-Band Radios’, IEEE Transactions on Antennas and Propagation, vol. 53, no. 3, pp. 1194 - 1202, 2005.

.....✂.....

**SINGLE BAND CIRCULARLY POLARISED
POLYGONAL MICROSTRIP ANTENNAS**

Contents	<i>Introduction to single band circularly polarized microstrip antennas</i>
	<i>4.1 Circularly Polarised Hexagonal Patch Antenna with Polygonal slot</i>
	<i>4.2 Circularly Polarised Dodecagonal Patch Antenna with Polygonal slot</i>
	<i>4.3 Hexagonal Circularly Polarised Patch Antenna with elliptical and circular slots</i>
	<i>4.4 Dodecagonal Circularly Polarised Patch Antenna with elliptical slot</i>
	<i>4.5 Circularly Polarised Decagonal Patch Antenna with Polygonal slot</i>
	<i>4.6 Circularly Polarised Tridecagonal Patch Antenna with Polygonal slot</i>
	<i>4.7 Circularly Polarised Patch Tetra decoganal Patch Antenna with polygonal slot</i>
	<i>4.8 Circularly Polarised Hexadecagonal Patch Antenna with elliptical slot</i>

The design procedure of eight different types of single band circularly polarized microstrip patch antennas with slots are portrayed in this chapter. Slotted structure has been employed to achieve compactness and improvement of the circular polarization characteristics. The design equations derived have been validated with different substrates. Extensive parametric analysis has been carried out to investigate the various antenna characteristics. All the designs have been simulated and verified experimentally. Circular polarization characteristics of one of the antennas is fixed through modal analysis, as a sample case.

Introduction

Microstrip patch antennas are the most preferred geometries for circular polarization characteristics. Microstrip patch CP structures can be of single feed or multiple feed types, which decides the generation of mechanism. The attracting feature of single feed type CP microstrip antenna is its simplicity. There is need to incorporate phase shifters and power dividers. The two orthogonal modes and the 90° phase shift, the essential conditions required for CP generation, need to be internally generated by the proper design of antenna geometry. For linearly polarised communication systems the receiving and transmitting antenna must be aligned to avoid polarisation mismatch, whereas for a system using CP antennas overcome this problem, as orientation of the antennas is not a stringent issue here. This property is especially useful for RFID systems, as detection of the portable tag is ensured regardless of its orientation. The industrial, scientific and medical (ISM) radio bands are reserved internationally for the use of radio frequency (RF) energy for industrial, scientific and medical purposes [1]. 2.4 GHz ISM band has got versatile applications. Several brands of radio control equipment use the 2.4 GHz band range for low power remote control of toys, from gas powered cars to miniature aircraft. Wi-Fi, Bluetooth, cordless phone and a lot of unlicensed gadgets operate in this band and hence very popular. Energy harvesting systems and active RFID systems, the two major systems also operate in this band. Usage of circularly polarized antennas enhance the versatility of 2.4 GHz ISM band. By using a CP antenna with good AR, positioning accuracy is improved. Single band CP patch antennas offer less ARBW. In this chapter, the main concern is to develop

compact single band CP antennas with enhanced ARBW, usable in 2.4 GHz ISM band.

4.1 Circularly Polarised Hexagonal Patch Antenna with Polygonal Slot

A patch antenna may be made a CP antenna by the use of a single probe. This is to excite a quasi-symmetrical shape and to support two degenerated modes [2- 4]. The CP radiation is obtained by these two modes, when they satisfy the conditions such as equal magnitude and phase quadrature between them. They are discerned by detuning the fundamental mode and are polarized in mutually perpendicular linear directions. By tuning the asymmetry of the patch's shape and optimising the probe's exact position with respect to the nature of asymmetry, this is achievable [5]. Polygonal antenna geometry embedded with polygonal slot is selected as the basic structure for all the antennas described in this chapter.

There are several perturbation methods to bring about circular polarized radiation in single feed patch antennas. A few distinct methods include, inserting an elliptical slot at the center of a circular patch [5], using a cross slot embedded on the radiating patch [6], truncating the corners of a square patch and inserting slits of different lengths at the edges of a square patch [7], the combination of two equal right angle slot antennas with equal perpendicular length on the ground plane fed by microstrip line [8], a circular patch with a rectangular slot oriented at 45° [9], two asymmetric orthogonal slits positioned in the center of the patch antenna [1]. There are many shapes suited for the modal degeneration. The

disc shape, which is a direct way to split the radiator fundamental mode, consists a thin slit cut through the center [9]. The feed point was positioned at a location, where two modes at near degenerate frequencies are excited in the vicinity of 2.45 GHz.

4.1.1 Antenna Geometry

Figure 4.1(a) shows the antenna geometry. The antenna is fabricated on a substrate of $\epsilon_r = 4.4$, $\tan\delta = 0.02$ and $h = 1.6\text{mm}$. It consists of regular hexagonal patch as the radiating element, which is fabricated using copper material of thickness 0.035 mm on the top side of the substrate and the copper ground plane is of dimensions $50\text{mm} \times 50\text{mm} \times 0.035\text{mm}$ on the bottom, situated on the center of the patch oriented along the X axis. The dimensions of the hexagonal slot are designated as i) b - the smaller Y axis dimension (top and bottom width), ii) c - the larger Y axis dimension (central width) and iii) d - the larger X axis dimension (height). These dimensions are such that $b < c < d$. The aspect ratio 'k' is defined as ratio of 'd' to 'c' with 'b' constant. As stated earlier, in order to generate circularly polarized waves, the simplest approach is to excite two equal amplitude degenerate orthogonal modes by a single feed point at an estimated location. The simplest way to excite degenerate modes TM_{01} and TM_{10} is to cut a thin slit through the center [9]. In this proposed antenna a hexagonal slot with unequal sides is chosen as the asymmetry or detuning element, in order to radiate circularly polarized waves. The radiation of circularly polarized wave is highly sensitive with respect to the position of the feed location and the dimensions of the central slot.

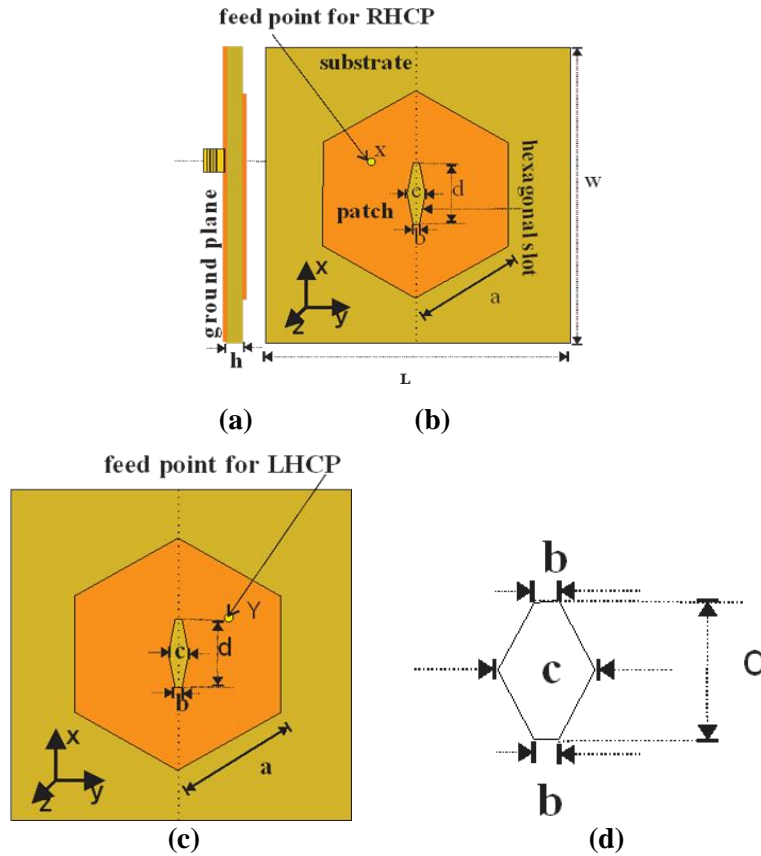


Figure 4.1. Geometry of the proposed antenna. (a) side view (b) Top view of RHCP antenna (c) Top view of LHCP antenna. (d) central irregular hexagonal slot geometry, Guided wavelength $\lambda_g = 0.0604$ m, $a = 17.244\text{mm}$ ($0.285 \lambda_g$), $b=1\text{mm}$ ($0.0166 \lambda_g$), $c = 7\text{mm}$ ($0.116\lambda_g$), $d = 11.4\text{mm}$ ($0.189\lambda_g$), $k = 1.62$, $L = W = 50$ mm ($0.8278 \lambda_g$). X (21mm,19 mm), Y (21mm, 31mm).

The antenna is excited through co - axial probe at the location X to produce Right Handed Circular Polarisation (RHCP) and at the feed location Y to radiate electromagnetic waves with Left Handed Circular Polarisation (LHCP). The co-axial probe feed point for RHCP antenna is the mirror image as that for LHCP antenna with respect to the center of the patch. The

feed location is chosen along the locus of 50 Ω characteristic impedance and is adjusted for good matching. It was proved that with annular shapes, it is possible to enhance the bandwidth because less amount of energy is stored beneath the patch metallization and less quality factor therein [10].

The authors have experimentally demonstrated in [11] that when the patch shape is dodecagonal, gain is slightly less (4.82 dBi /4.67 dBi), ARBW is 5.5 % and when the shape is hexagonal with elliptical and circular slots, the gain is 4.5dBi and ARBW is 5.8% [12]; both designed for the same resonant frequency 2.45GHz. The novelty of the proposed antenna is its shape, percentage area reduction, compactness and the mode of generation of circularly polarized radiation, simplicity in design and easiness of fabrication.

4.1.2 Design equations and the CP mechanism

In order to design the hexagonal patch antenna, the design of the circular patch antenna is considered, as the two antennas are closely related to each other [13]. The side length ‘a’ of the regular hexagon for a resonant frequency of $f_r = 2.687\text{GHz}$ is designed as follows. The dominant mode resonance frequency of a circular patch is given by [13]

$$f_r = \frac{X_{mn} c}{2\pi r_e \sqrt{\epsilon_r}} \quad (1)$$

where f_r is the resonant frequency of the patch, $X_{mn} = 1.8411$ for the dominant mode TM_{11} , c is the velocity of light in free space, ϵ_r the relative permittivity of the substrate, ‘ r_e ’ is the effective radius of the equivalent circular patch and is given by [13]

$$r_e = r \left\{ 1 - \frac{2h}{\pi r \epsilon_r} \left(\ln \frac{\pi r}{2h} + 1.7726 \right) \right\}^{0.5} \quad (2)$$

where ‘r’ is the actual radius of the circular patch and ‘h’ is the height of the substrate. Then by equating the areas of a circle and a regular hexagon, the edge or side length of the regular hexagon ‘a’ may be found out as in [13],

$$\pi r_e^2 = \frac{3\sqrt{3}}{2} a^2 \quad (3)$$

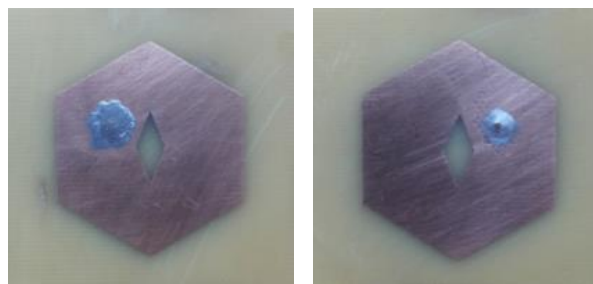
The introduced central slot contributes towards the generation of circularly polarized waves and also to reduce the resonant frequency of the patch. The normalized impedance ratio function corresponding to the degenerated TM_{01} odd mode to TM_{10} even mode is given as [5]

$$\beta_\zeta(\omega) = \frac{\zeta_o(\omega)}{\zeta_e(\omega)} = \frac{1 + jQ\left(\frac{\omega}{\omega_e} - \frac{\omega_e}{\omega}\right)}{1 + jQ\left(\frac{\omega}{\omega_o} - \frac{\omega_o}{\omega}\right)} \quad (4)$$

By proper choice of ω_o and ω_e in the vicinity of ω , phase difference between the components is chosen as 90° and magnitude to be proportional to AR. Here in this work, f_0 is chosen to be 2.45 GHz, f_o and f_e are chosen such that AR is less than 3dB. As the fundamental mode exhibits a zero in the central area, the fields will not be affected significantly. The fundamental mode splits into degenerate orthogonal modes by the proper choice of feed point and asymmetry. For the odd mode, which is oriented towards the slot (X axis), the perturbation is minimum as the top and bottom width of the slot is made narrow enough. If the slot had been a rectangular geometry with width ‘b’ and height ‘d’ and no change in orientation, the odd mode surface current would not have

been affected by this perturbation and the resonant angular frequency would have been approximately that of fundamental resonant frequency [10]. Whereas, for the even mode (oriented about y axis), the surface current is forced to traverse more length around the slot. On account of more electrical length, even mode resonant frequency ω_e is reduced [14].

At this juncture, if a second orthogonal cut is made at the centre, it will enhance the electrical path of the odd mode and results in the reduction of corresponding resonant frequency. Here in this work, instead of making an orthogonal cut, the central width of the hexagonal slot (7mm) is made larger than the top and bottom width (1mm). The same effect of second orthogonal cut is achieved due to this enhancement of central width. Similarly, signal in odd mode also has to traverse more length and therefore resonant frequency is reduced. By selecting appropriate dimensions for the slot, the two degenerate mode frequencies are made nearly equal. Overall dimension of the antenna is reduced.



(a) RHCP antenna (b) LHCP antenna

Figure 4.2. Photographs of the antenna prototypes

The photographs of the proposed antennas are depicted in Figure 4.2. To design the hexagonal patch, design equations are derived based on the

geometry and frequency of operation after computing the guided wavelength λ_g (the wavelength in the dielectric $\lambda_g = \lambda_0/\epsilon_{\text{reff}}$, where λ_0 is the free space wavelength and the effective permittivity of the substrate ϵ_{reff} is computed as 4.106, using the formula [3])

$$\epsilon_{\text{reff}} = \epsilon_r - \frac{c_r \epsilon_r}{2} \left(\frac{2h}{x} + \frac{h^2}{x^2} \right) \quad (5)$$

where $c_r = 0.7$, being a thin substrate, x is the radius of the circumscribed circle - the circle in which the hexagon is inscribed- and h is the height of the substrate. By selecting proper slot dimensions and by choosing exact feed location, the two orthogonal degenerate modes are made nearly equal amplitude with a phase difference of 90° . Thus, the mandatory condition for achieving circular polarization; equal amplitude with a phase difference of 90° for the degenerate modes [15] is achieved. Overall size of the patch antenna is determined by the resonant frequency. The edge of the hexagonal patch is designed for a resonant frequency of 2.69 GHz. Due to the central slot the resonant frequency is reduced to 2.45 GHz and thus the overall dimension is reduced by a factor of 22.5%.

4.1.3 Results and analysis

Using the computed parameters, two antennas, one RHCP and the other LHCP were simulated using Ansoft HFSS 13.0. Antenna prototypes designed with optimized parameters were fabricated on FR4 substrate. Optimum feed point was chosen for the best impedance matching of the antenna. Then experimental analysis was carried out with Network Analyser PNAE 8362B, in anechoic chamber.

4.1.3.1 Measured and simulated $|S_{11}|$ plots

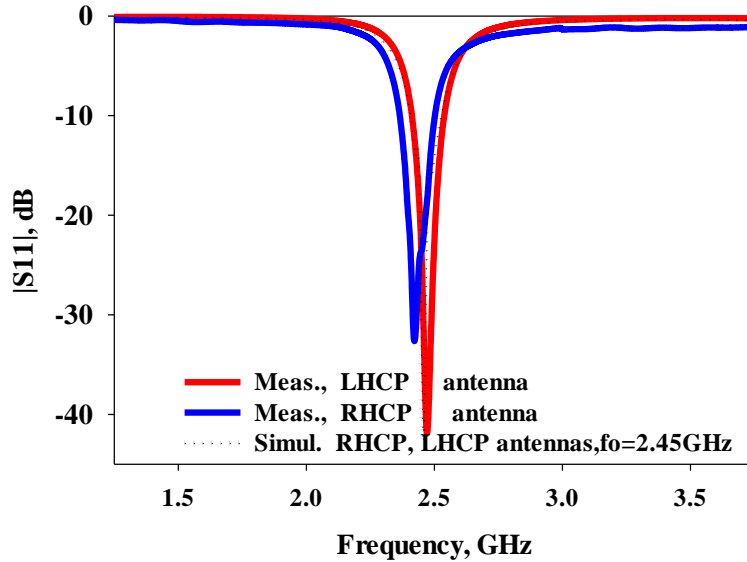


Figure 4.3. $|S_{11}|$ plots of RHCP and LHCP antennas.

The measured $|S_{11}|$ of the proposed antennas are plotted in Figure 4.3. It is noted that the fundamental resonant frequency of the antenna without slot is 2.69 GHz, whereas with slot, the measured return loss is 32 dB at 2.42 GHz and the corresponding 10 dB bandwidth is 130 MHz for the proposed RHCP antenna. The measured return loss is 41.78 dB at 2.44 GHz for LHCP antenna with corresponding 10 dB impedance bandwidth of 128 MHz. The simulated return loss is 42 dB for both the antennas at a resonant frequency of 2.45 GHz. The simulated and measured values are close to each other. Due to fabrication tolerances, the value obtained for the RHCP antenna prototype is less to a small extent.

4.1.3.2 Axial ratio

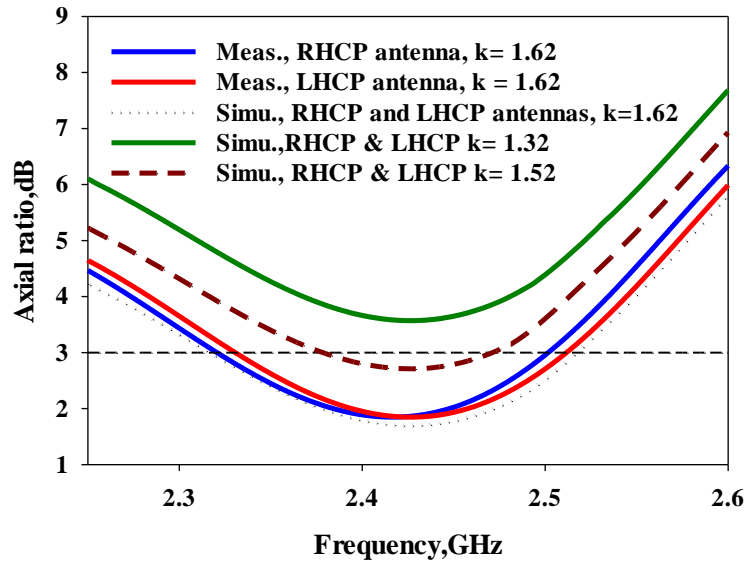


Figure 4.4. Simulated (parametric) and measured axial ratio plots

A parametric study is done by varying the parameter ‘k’, which is the aspect ratio of height ‘d’ to the central width of the central irregular hexagonal slot, keeping ‘b’ constant. It is observed that when the value of k when exceeds 1.5 circularly polarized radiation is exhibited and clear from Figure 4.4. When k = 1.32, it does not exhibit CP and when k = 1.52, AR is just below 3 dB for a small range of frequencies. The realization of circularly polarized radiation is confirmed at k = 1.62, as the necessary criterion of axial ratio < 3 dB is satisfied for a range of frequencies from 2.31 GHz to 2.51 GHz. When k = 1.62, the least simulated value of axial ratio = 1.8212 dB is obtained with the fabricated RHCP antenna prototype and the corresponding axial ratio bandwidth is measured to be 180MHz (7.43%). It is 181.2 MHz for LHCP antenna prototype (7.42%).

4.1.3.3 Radiation patterns

Measured and simulated bore sight radiation patterns of RHCP and LHCP antennas at $f_0 = 2.45$ GHz are depicted in Figure 4.5 and found to be in good agreement with simulated plots. Measured 3 dB beam widths are 80° and 86° for RHCP and LHCP antennas respectively.

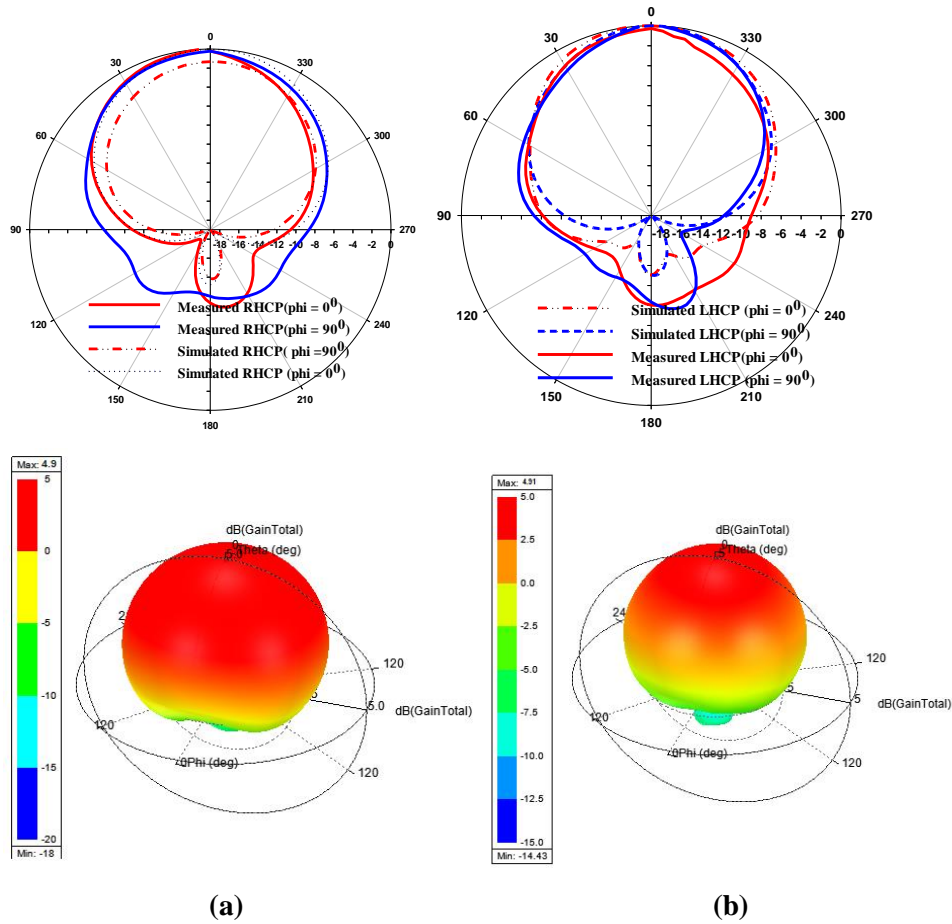


Figure 4.5. Radiation patterns of (a) RHCP antenna (b) LHCP antenna
At a resonant frequency $f_0 = 2.45$ GHz

4.1.3.4 Measurement of gain and efficiency

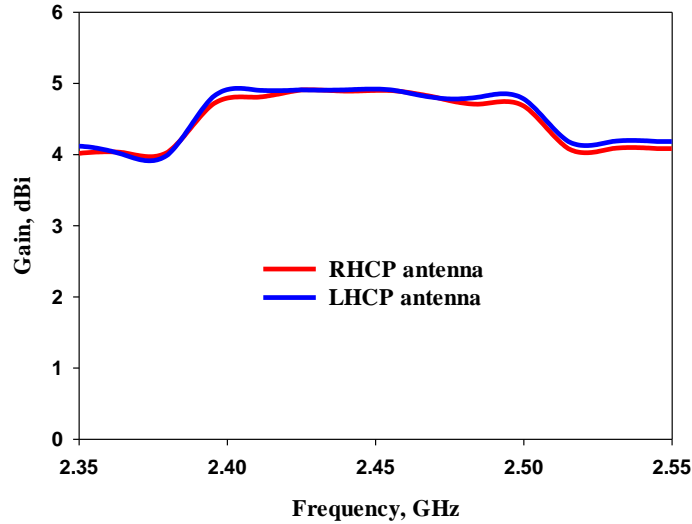


Figure 4.6 Measured gain plots of the antenna prototypes

The gain of the RHCP and LHCP antenna prototypes were measured using gain comparison method. As depicted in the Figure 4.6, RHCP antenna gives a maximum gain of 4.9 dBi at the frequency 2.42 GHz and LHCP antenna, 4.91 dBi at 2.44 GHz. Efficiency of 89.9% was achieved with both antenna prototypes.

4.1.3.5 Surface Current Patterns

The surface current distribution simulated at the centre frequency is plotted in Figures 4.7 and 4.8 for RHCP and LHCP antennas respectively. Surface current distribution at $\varphi = 0^\circ$ is equal in magnitude and opposite in direction to that at $\varphi = 180^\circ$. Similar is the case of surface current distribution at $\varphi = 90^\circ$ and at $\varphi = 270^\circ$. Hence the criterion for circular polarization is satisfied. As the direction of view chosen as +Z-axis, the

direction of rotation of current is clockwise and the sense of polarization is confirmed as left-hand circular polarization (LHCP) for the feed position at Y. Feed position at X confirms right hand circular polarization (RHCP).

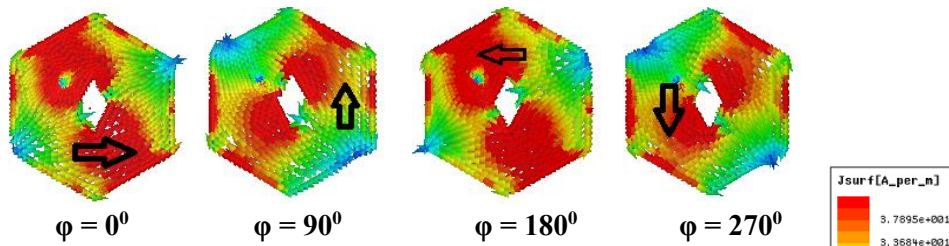


Figure 4.7. Surface current distribution of RHCP antenna

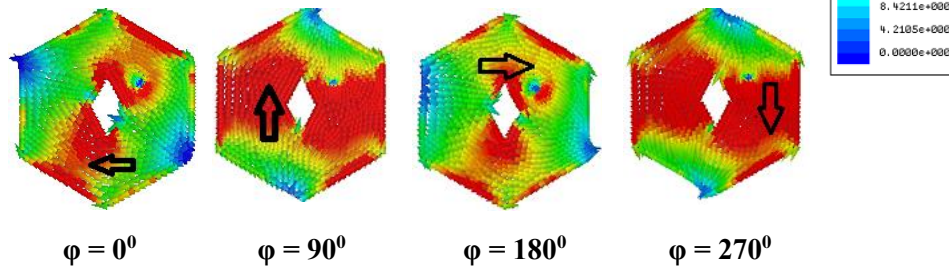


Figure 4.8. Surface current distribution of LHCP antenna

4.1.3.6 Confirmation of the sense of polarization

The sense of direction of polarization of the fabricated antennas under study is tested using helical antennas designed at the measured resonant frequency as per the design methodology in [16] & [17]. The RHCP helical antenna gives more output when tested with RHCP antenna under study and the LHCP helical antenna gives more output when tested with LHCP antenna. Graphs plotted in Figure 4.9 confirm the directions of sense of polarization of the antenna prototypes.

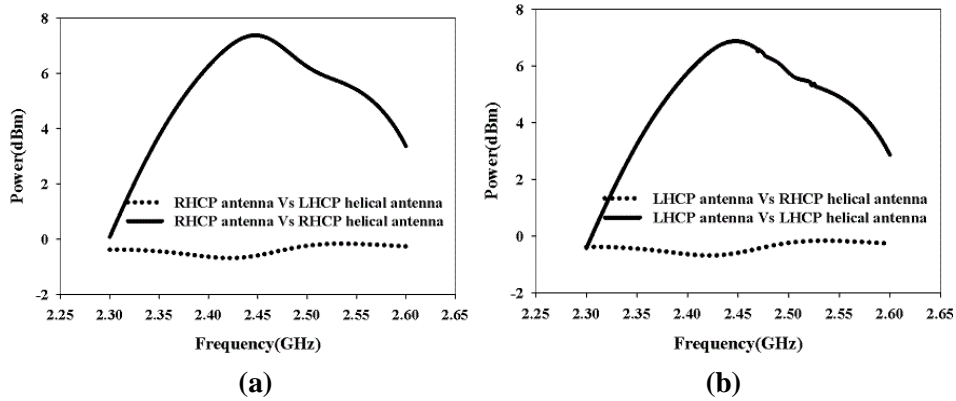


Figure 4.9. Sense of direction of polarisation using helical antennas, when tested (a) RHCP antenna (b) LHCP antenna

4.1.3.7 Confirmation of circular polarisation using Smith Chart

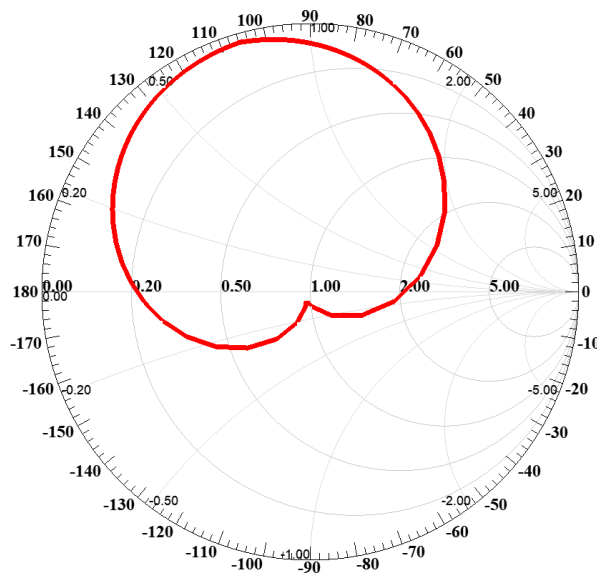


Figure 4.10. Simulated input impedance variation of the RHCP and LHCP antennas

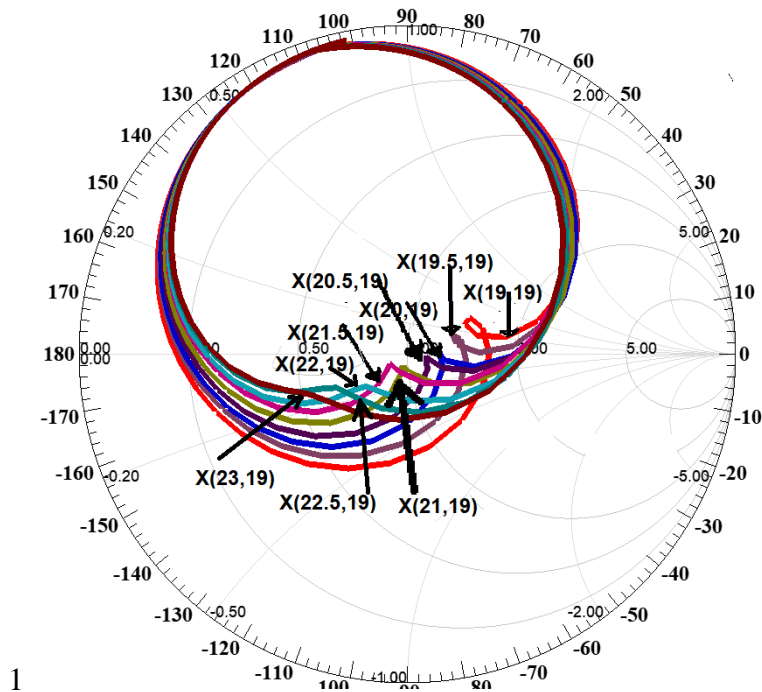


Figure 4.11. Simulated input impedance variation of the RHCP antenna for different feed positions.

The Smith chart representation of impedance plot shown in Figure 4.10 is the exact method to confirm whether the choice of feed position is the suitable one, for good CP radiation. The best minimum axial ratio at a CP resonant frequency is indicated by a dip in the smith chart. That is, two orthogonal modes are excited. The presence of a loop indicates a axial ratio value. In this antenna the feed position X (21, 19) is the best position that offers CP behavior for the RHCP antenna and Y(21, 31) for the LHCP antenna. Here the kink is formed corresponding to the centre frequency 2.45 GHz for both RHCP and LHCP antennas. This confirms the excitation of two resonant degenerate modes of circular polarization and the best CP performance at this frequency 2.45 GHz. Figure 4.11

shows the impedance variation corresponding to the parametric variation of the feed location of RHCP antenna and the corresponding loop formation in the Smith chart. This study justifies the choice of location of the point X (21,19) for Ant.1(RHCP) and Y(21,31) for Ant.2(LHCP). Both antennas are having dimensions $50 \times 50 \times 1.6 \text{mm}^3$. The performance comparison of antenna prototypes with a basic reference circular patch antenna having central elliptical slot [5] and four other circularly polarized antennas in literature [18-21], is done and values are tabulated in Table 4.1. The circular shape of the patch and central elliptical shape of the slot in [5] is modified to get antenna prototypes in this work. Achieved size reduction of 22.5 %, with reference to antenna in [5], is due to increased electrical length on account of shapes of patch and slot. Increased ARBW is due to the choice of feed point and the aspect ratio of the slot. More IBW is due to the choice of feed location and shape of the patch. For the comparison of size reduction, reference antenna [5] only is chosen due to similarity in shape and antennas of [18-21] are chosen for the comparison of other values.

Table 4.1: Performance comparison of various CP antennas

Parameter	[5]	[18]	[19]	[20]	[21]	Ant1	Ant2
Center f req. GHz	2.45	2.40	.924	2.47	2.45	2.42	2.44
Return Loss, dB	19	26	21	26.3	21	32	42
Gain, dBi	3.85	4.3	1.9	6.6	7	4.9	4.91
AR min, dB	-	0.8	0.7	0.77	0.9	1.82	1.815
ABBW, %	1.22	0.47	1.62	0.8	1.43	7.43	7.42
IBW %	5.3	1.9	3.74	2.85	6.5	5.4	5.25
3 dB beam width	-	-	80 ⁰	-	78 ⁰	80 ⁰	79 ⁰
%size reduction	9.5	-	-	-	-	22.5	22.5

4.1.4 Appropriateness of the antennas for RFID reader applications at 2.45GHz

The RHCP antenna prototype offers 10 dB impedance bandwidth of 130 MHz (2.3645 GHz- 2.4965), 3 dB ARBW of 180 MHz (2.32 GHz- 2.50GHz) and a gain of 4.9 dBi. Similarly, the LHCP antenna prototype offers a 10 dB impedance bandwidth of 128MHz (2.5415 GHz- 2.4135 GHz) and 3 dB ARBW of 181.2 MHz (2.3312 GHz – 2.5124 GHz) and a gain of 4.91 dBi. These values are in compliance with standards of parameters for air interface communications for RFID applications at 2.45 GHz [22]. Hence these antennas are well suited for RFID applications.

4.1.5 Analytical Treatment

In this section, analytical aspects of the proposed design method, the polarization behavior of the antenna with respect to the geometry and physical characteristics, are dealt with [5]. The circular polarization behavior of polygonal patch antennas are analysed as a function of geometry and structural characteristics. First of all, the analysis is done based on the traditional equivalent circuit approach [9] and then the mathematical formulation is performed to enforce the polarization characteristics [5].

4.1.5.1 Modal expansion

Microstrip patch antennas, modeled as lossy resonant cavities, are narrow-band radiators. Perfect magnetic walls enclose them and are bounded by perfect electric walls on the upper and lower sides [3]. The cavity field distribution is analysed in terms of eigen-modes. E_z , H_x and H_y are the three non-zero components. According to the Green function

theory, the electrical field, can be expressed by a set of homogeneous Helmholtz equation eigen-functions [3],

$$E_z(r) = j\omega\mu_0 J_0 \sum_{m,n=0}^{\infty} \frac{\Psi_{mn}^*(r)\Psi_{mn}(r_p)S_{mn}(P)}{k^2 - k_{mn}^2} \quad (5)$$

Where k_{mn} is the modal wave-number of the mn mode, S_{mn} , the function related to the geometry of the probe, r_p the position of the probe with respect to the patch and J_0 the feeding current. The wave-number may be modified as [5]

$$k^2 = \epsilon_r (1 - j\delta_{eff}) k_0^2 \quad (6)$$

On account of various antenna losses. The impedance observed from the probe at the location r_p can be written as [5]

$$Z_{in} = \frac{V_{in}}{J_0}$$

$$i.e., Z_{in} = -j\omega\mu_0 t \sum_{m,n=0}^{\infty} \frac{\Psi_{mn}^2(r_p)S_{mn}(P)}{\epsilon_r (1 - j\delta_{eff}) k^2 - k_{mn}^2} \quad (7)$$

$$\text{letting } \omega_{mn} = c \frac{k_{mn}}{\sqrt{\epsilon_r}}$$

$$Z_{in} = \frac{\mu_0 t c^2}{\epsilon_r} \sum_{m,n=0}^{\infty} j\omega \frac{\Psi_{mn}^2(r_p)S_{mn}(P)}{\omega_{mn}^2 - (1 - j\delta_{eff})\omega^2} \quad (8)$$

Then equivalent circuit parameters for mn mode can be written as [5]

$$\alpha_{mn} = \frac{\mu_0 t c^2}{\epsilon_r} \Psi_{mn}^2(r_p) S_{mn}(P)$$

$$R_{mn}^{-1} = \frac{\omega \delta_{eff}}{\alpha_{mn}}$$

$$C_{mn} = \frac{1}{\alpha_{mn}}$$

$$L_{mn} = \frac{\alpha_{mn}}{\omega_{mn}^2}$$

Finally, it is concluded that [5]

$$Z_{in} = \sum_{m,n=0}^{n=\infty} Z_{mn}$$

$$Z_{in} = \sum_{m,n=0}^{m,n=\infty} \frac{1}{R_{mn}^{-1} + j\omega C_{mn} + \frac{1}{j\omega L_{mn}}}$$

This is because the input impedance of the patch is shown to be equivalent to the response of a network consisting of an infinite series of parallel RLC resonators as shown in Figure 4.12.

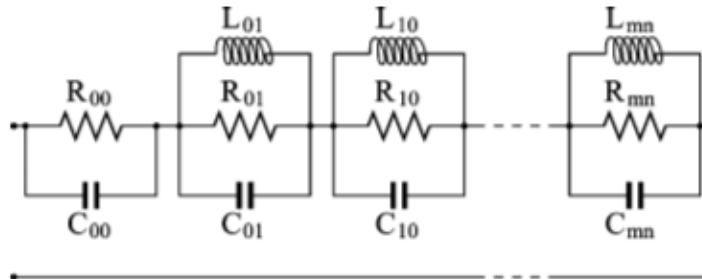


Figure 4.12 Equivalent circuit corresponding to modal expansion of input impedance [5]

Each resonant mn mode is equivalent to a single parallel RLC, except for the fundamental TM_{00} mode, which consists only of static capacitance and relative losses. The modal resistance R_{mn} is theoretically frequency dependent, but can be approximated to be a constant value within the band of interest, due to the narrowness of the mode resonance bandwidth. R_{mn}

represents the sum of the radiation, dielectric and metal losses. The voltage across R_{mn} may be considered to be proportional to the radiated field from the mn mode and $\omega = \frac{1}{\sqrt{LC}}$ the angular frequency of the mn -th mode. The analytical expression of Ψ_{mn} might be very complicated for arbitrary geometries and consequently the circuit parameters. But the equivalent circuit formulation is still valid even if the expressions are not in closed form [5]. For a single TM_{mn} mode its mode impedance may be expressed as [5]

$$Z_{mn}(\omega) = R_{mn} \phi_{mn}(\omega)$$

$$Z_{mn}(\omega) = R_{mn} \frac{1}{1 + jQ_{mn} \left(\frac{\omega}{\omega_{mn}} - \frac{\omega_{mn}}{\omega} \right)}$$

Where $\phi_{mn}(\omega)$ is the normalized frequency response. Though the values of circuit parameters R_{mn} , C_{mn} , L_{mn} dependent on the patch geometries, a generalized approach is described below. Let us consider quasi-symmetrical geometry where a single mode is detuned into two orthogonal and overlapping ones. Concerning the fundamental frequency, the modal expansion can be limited to the first three terms: TM_o , TM_e from the fundamental detuning and TM_∞ , which represents all higher order modes. The corresponding modal impedances are Z_o , Z_e and Z_∞ [5].

$$Z_{in} = Z_o + Z_e + Z_\infty$$

$$Z_{in} = R_o \phi_o(\omega) + R_e \phi_e(\omega) + Z_\infty(\omega)$$

When the detuned modes are combined each other properly the far field CP is obtained. Let us assume that the contribution of all other higher modes is zero, i.e $Z_\infty(\omega)$ is zero and the quality factor Q is

same for the detuned even and odd modes, then the normalized impedance ratio function may be written as [5]

$$\beta(\omega) = \frac{\phi_o(\omega)}{\phi_e(\omega)} = \frac{1 + jQ\left(\frac{\omega}{\omega_e} - \frac{\omega_e}{\omega}\right)}{1 + jQ\left(\frac{\omega}{\omega_o} - \frac{\omega_o}{\omega}\right)}$$

Magnitude of the above yields AR and Phase angle gives phase difference between odd (ω_o) and even (ω_e) modes, which account for CP generation. ω corresponds to center frequency and Q, the quality factor.

4.1.5.2 Orthogonal near- degenerate modes

As illustrated above, orthogonal near degenerate modes are resolved from the analysis of surface current distribution. The simulated surface current distribution on the RHCP antenna in Figure. 4.7 and 4.8 shows that, the CP radiation is the result of the excitation of two orthogonal near-degenerate modes at 2.32 GHz and 2.5 GHz respectively.

Hence frequency corresponding to ω_e is 2.32 GHz and that corresponding to ω_o is 2.5 Hz. From the plot of the impedance ratio function $\beta(\omega)$ in Figure 4.13, it is clear that it is tangent to the imaginary axis and the odd and even modes are in quadrature with ω_c . Hence the critical condition for CP [5] is satisfied.

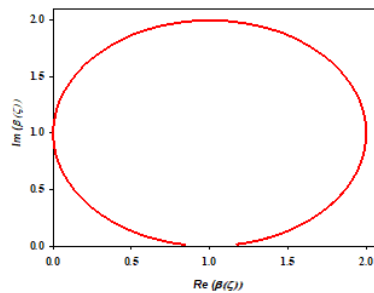


Figure 4.13. Real part Vs Imaginary part plot of Impedance ratio $\beta(\omega)$

From the impedance plots in the Figures, 4.14 and 4.15, it is estimated that the input impedance, Z_{in} is $49.85 - j 3.25$ ohms, corresponding to 2.45 GHz, at the feed position X.

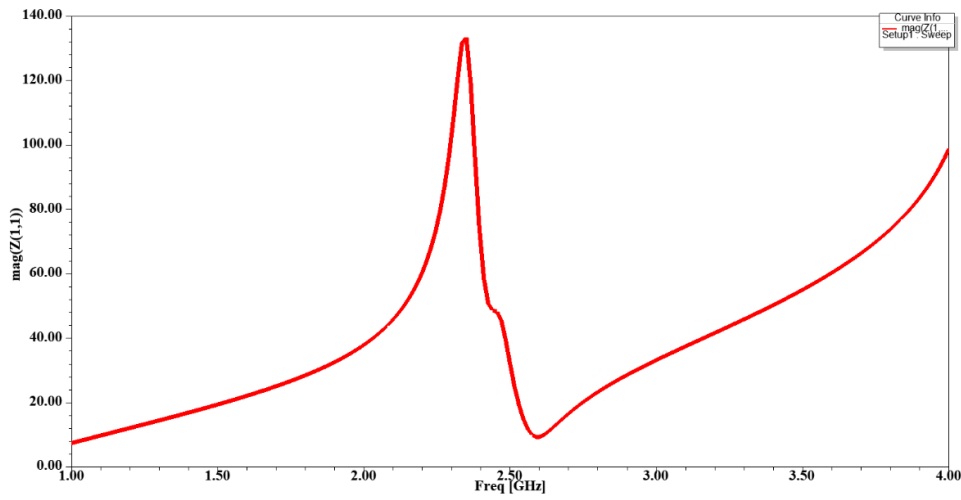


Figure 4.14. Real part of impedance Vs frequency plot

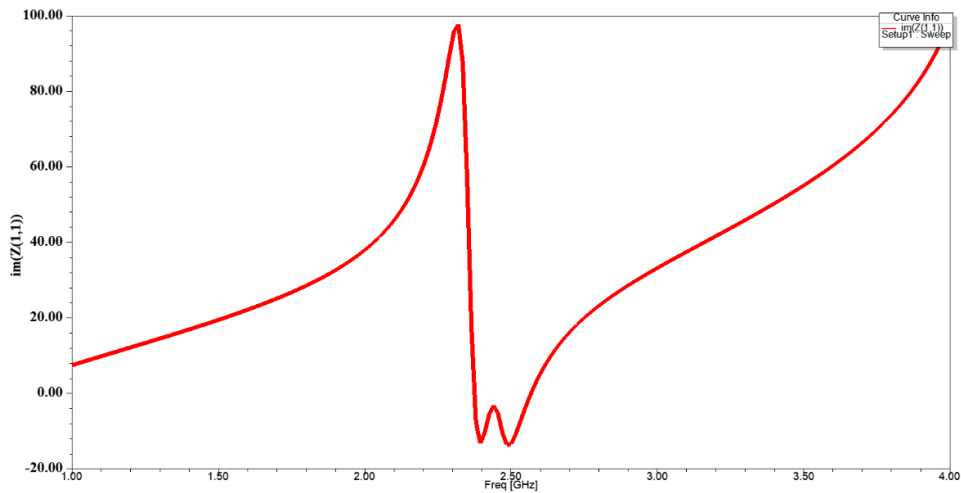


Figure 4.15. Imaginary part of impedance Vs frequency plot

Where the term $-j3.25$ corresponds to the higher order modes dominated by the capacitive reactance. Corresponding modal resistances are obtained as follows [5],

$$R_e = R_N^2 + X_N^2 / R_N + X_N$$

$$R_o = R_N^2 + X_N^2 / R_N - X_N$$

Substituting the values of R_N and X_N from Z_{in} , which is equal to $R_N - jX_N$, the values of modal resistances are obtained as

$$R_e = 46.99 \Omega \text{ and } R_o = 53.55 \Omega.$$

The choice of exact feed position to yield optimal CP characteristics is estimated from the impedance curves corresponding to various feed positions on RHCP antenna, as shown in Figures 4.16 and 4.17 below. For almost all the feed positions, two peaks are visible. This is the zone where the combination of the modes leads to the best CP. The best choice of position X (21, 19) gives one peak to be near to 50 ohms.

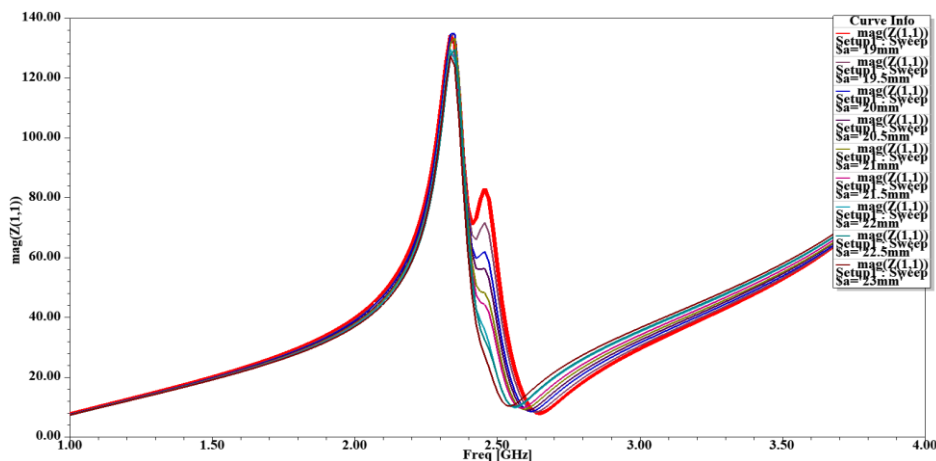


Figure 4.16 Real part of impedance under parametric variation of feed position

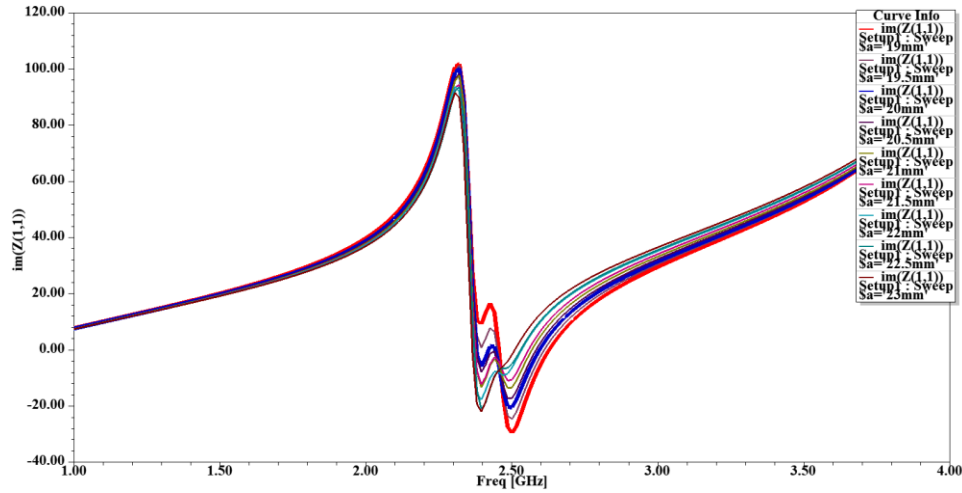


Figure 4.17 Imaginary part of impedance under parametric variation of feed position

To demonstrate the effective advantages of using this analytical method, Figure 4.18 shows the comparison of E_x/E_y obtained from this approach versus the corresponding quantity given by a full-wave simulation, by ANSYS HFSS.

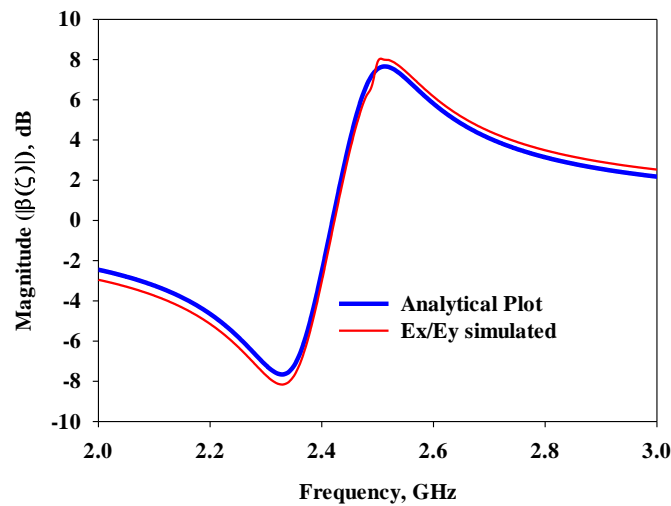


Figure 4.18 Magnitude of Impedance ratio (dB) Vs frequency plot

The first is the modulus of $\beta(\omega)$ plotted in dB form, while the second is the numerically computed ratio. These two plots coincide and as such the method of modal analysis adopted in this piece of work is justified.

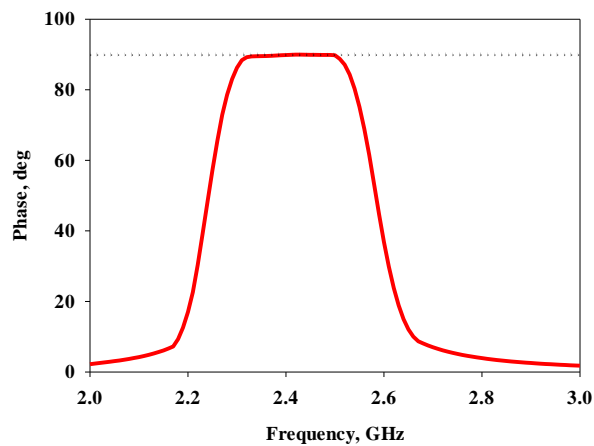


Figure 4.19. Phase angle of $\beta(\omega)$ Vs frequency plot

The phase plot of the impedance ratio function $\beta(\omega)$, is depicted in Figure 4.19. This is plotted in the operating range. The phase value remains to be 90° , in the range from 2.32 GHz to 2.53 GHz and hence ensures the axial ratio band width of 210 MHz for the RHCP antenna, which exactly matches with the simulated value. Hence it is concluded that the analytical treatment applied in this work proves to be exact, as the values obtained through this approach match with simulated and experimental results.

4.2 Circularly Polarized Dodecagonal Patch Antenna with Polygonal Slot

In this work, a novel microstrip patch antenna, 12-sided polygon (dodecagon) shaped patch, with the perturbation technique of embedding a central irregular hexagon shaped slot, for exciting CP radiation designed at the 2.45GHz band is proposed. Good CP bandwidth and compactness is achieved on account of the central slot. The structure exhibits good impedance matching, gain and circularly polarized radiation characteristics over the entire operating band.

4.2.1 Antenna geometry

The proposed antenna is designed on FR4 substrate of size 50mm×50mm×1.6mm, with dielectric constant 4.4, thickness 1.6mm and $\tan\delta = 0.02$. By introducing some asymmetry in the structure, the resonant frequencies of two degenerate modes can be made slightly different from each other with equal amplitude and a phase difference of 90° between them, for producing CP. The novelty in this work is the selection of shape for the patch and the method of introducing asymmetry by means of the irregular hexagonal slot as depicted in Figure 4.20 (d). The slot is positioned in the center of the patch and oriented along the X axis. The dimensions of the slot are chosen such that $b < c < d$. The parameter 'k' is defined as the ratio, 'd' to 'c' with 'b' constant. The choice of dimensions of the slot and the feed position ensure the splitting of the fundamental mode into degenerate modes and phase quadrature between them. The radiation of circularly polarized wave is highly sensitive with respect to the position of the feed point and the dimensions of the central slot [5]. The antenna is excited through the co-axial probe at the location 'X' to produce Right Handed Circular Polarization

(RHCP) and at the feed location 'Y' to radiate electromagnetic waves with Left Handed Circular Polarization (LHCP). The feed point for RHCP antenna is the mirror image as that of the LHCP antenna with respect to the center of the patch, chosen along the locus of 50Ω characteristic impedance and is adjusted for the best matching.

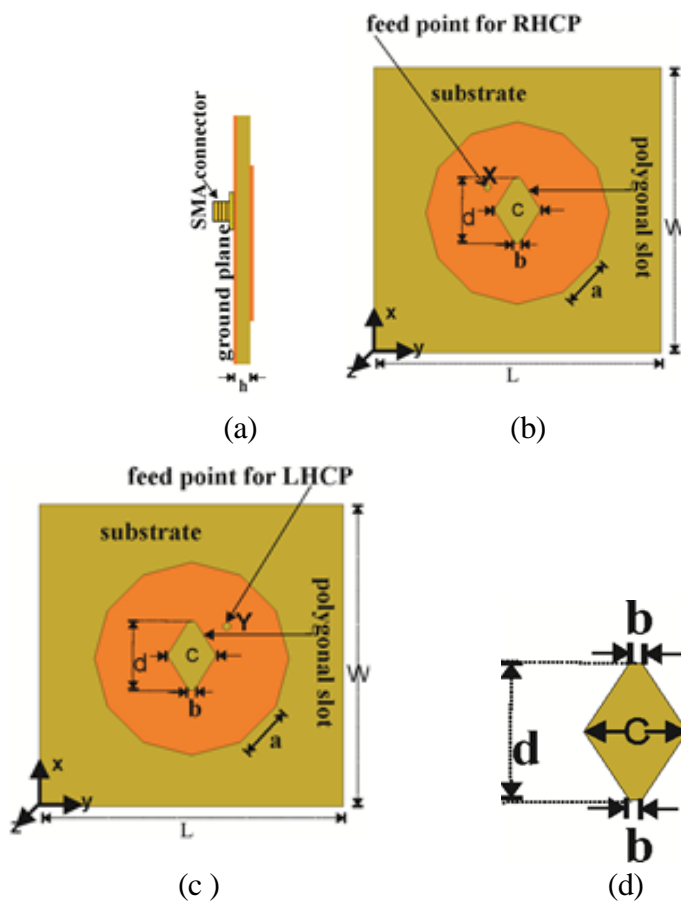


Figure 4.20. Geometry of the proposed antenna. (a) Side view, (b) Top view of the RHCP antenna, (c) Top view of the LHCP antenna and (d) the Central slot geometry. Guided wavelength $\lambda_g = 0.0604$ m, $a = 8.28\text{mm}$ ($0.137\lambda_g$), $b = 1\text{mm}$ ($0.0166\lambda_g$), $c = 8\text{mm}$ $d = 11.4\text{mm}$ $k = 1.425$, $L = W = 50$ mm ($0.8278\lambda_g$), X (29 mm, 19.8 mm), Y (29 mm, 30.2mm).

4.2.2 Design equations

In order to design the dodecagonal patch antenna, the design of the circular patch antenna is considered first, as it is closely related to the proposed structure [13]. The side length ‘a’ of the regular dodecagon for a resonant frequency of $f_r = 2.77$ GHz is computed as follows. The dominant mode resonance frequency of a circular patch is given by [13] as,

$$f_r = \frac{X_{mn} c}{2\pi r_e \sqrt{\epsilon_r}} \quad (9)$$

where ‘ f_r ’ is the resonant frequency of the patch, $X_{mn} = 1.8412$ for the dominant mode TM_{11} , ‘ r_e ’ the effective radius of the equivalent circular patch [13],

$$r_e = r \left\{ 1 - \frac{2h}{\pi r \epsilon_r} \left(\ln \frac{\pi r}{2h} + 1.7726 \right) \right\}^{0.5} \quad (10)$$

where ‘r’ is the radius of the circular patch and ‘h’ the height of the substrate.

The edge of the regular dodecagon ‘a’ may be found out [13] as,

$$a = r_e \sqrt{\frac{\pi}{11.196}} \quad (11)$$

By selecting appropriate dimensions for the slot, the two degenerate mode frequencies are made nearly equal. The central slot, thus introduces annular effect and thereby enhanced bandwidth. Though the edge of the dodecagonal patch is designed for a resonant frequency of 2.77GHz, due to the presence of the central slot, the resonant frequency is reduced to 2.45 GHz and hence an area reduction of 21.17% is achieved.

4.2.3 Results and discussion

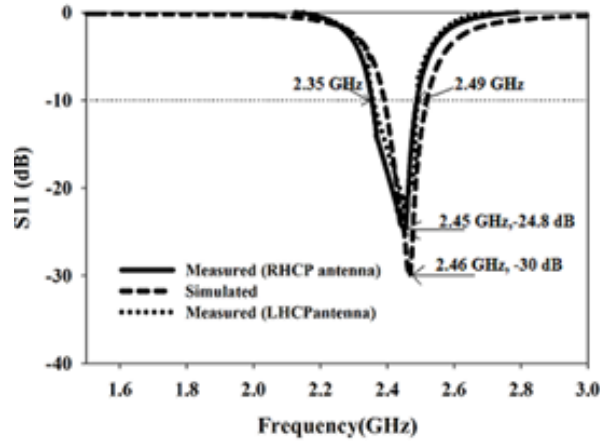


Figure 4.21. $|S_{11}|$ versus frequency plots at $f_0 = 2.45\text{GHz}$

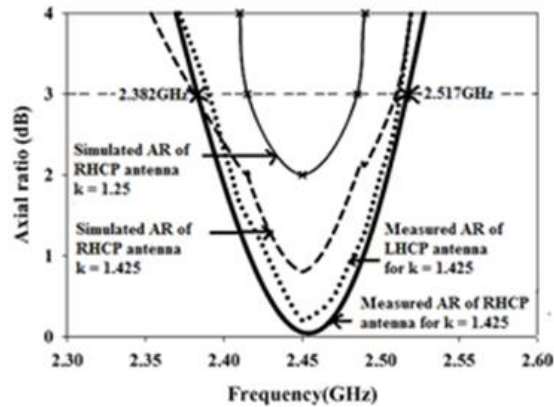


Figure 4.22. Axial ratio versus frequency plot

Using the computed parameters, the structure is simulated using Ansys HFSS13.0. The simulation graphs of return loss, axial ratio and surface current pattern are plotted. Antenna prototypes are fabricated on an FR4 substrate with optimized parameters and the antenna measurements are done using the ZVB20 Network Analyzer. The measured and simulated $|S_{11}|$ characteristics of the RHCP antenna are compared in

Figure 4.21. It is noted that the fundamental resonant frequency of the antenna without slot is 2.77 GHz. At the same time, with slot, the simulated resonant frequency is 2.46 GHz and the experimental result is 2.45 GHz. Simulation studies have been carried out to understand the variation of axial ratio with 'k' and depicted in Figure 4.22. It is observed that when the value of $k \geq 1.25$, axial ratio becomes less than 3dB and thus one criterion for CP radiation is satisfied. $k = 1.425$ gives good results.

The proposed antenna is designed on an FR4 substrate of size $50 \text{ mm} \times 50 \text{ mm} \times 1.6 \text{ mm}$, with dielectric constant 4.4, thickness 1.6 mm and $\tan \delta = 0.02$.



Figure 4.23. Photographs of the antenna prototypes (a) RHCP antenna (b) LHCP antenna

The antenna is excited through the co - axial probe at the location 'X', to produce RHCP and at the feed location 'Y', to produce LHCP. The feed point for RHCP antenna is the mirror image as that of the LHCP antenna with respect to the center of the patch, chosen along the locus of 50Ω characteristic impedance and is adjusted for the best matching.

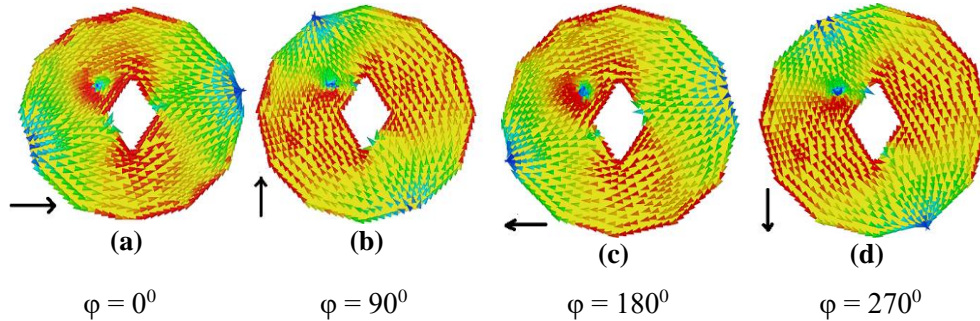


Figure 4.24. Simulated surface current distribution of the RHCP antenna at four different values of the excitation phase angle φ .

The surface current distributions simulated for RHCP antenna at the center frequency of 2.45 GHz are plotted in Figure 4.24. Surface current distribution at the excitation phase angle $\varphi = 0^\circ$ is equal in magnitude and opposite in direction to that at $\varphi = 180^\circ$. Same is the case of surface current distribution at $\varphi = 90^\circ$ and $\varphi = 270^\circ$. It is true for both the antennas and hence the criterion for CP is satisfied. As the direction of view chosen as +Z-axis, the direction of rotation of current is anticlockwise and the sense of polarization is confirmed as left handed circular polarization for the feed position Y. The direction of rotation of current is clockwise and the sense of polarization is confirmed as right handed circular polarization for the feed position X. The sense of polarization is also tested and verified using helical antennas designed at the measured resonant frequency 2.45 GHz as per the design methodology [16,17]. Figure 4.25 depicts, corresponding received power plots. The simulated Smith chart depicted in Figure 4.26 indicates a dip marked at the center frequency 2.45 GHz corresponding to RHCP and LHCP antennas. Hence the excitation of two orthogonal degenerate

modes in both the antennas is confirmed, justifying the circularly polarized radiation [16].

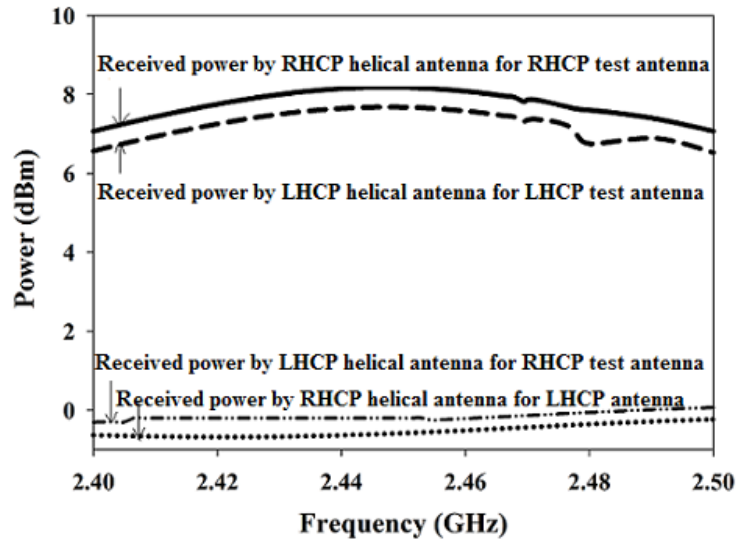


Figure 4.25. Plots of received power by RHCP and LHCP helical antennas

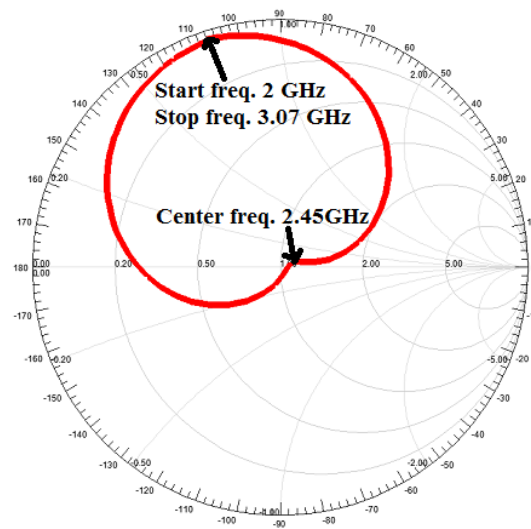


Figure 4.26. Simulated Smith chart of the RHCP and LHCP antennas

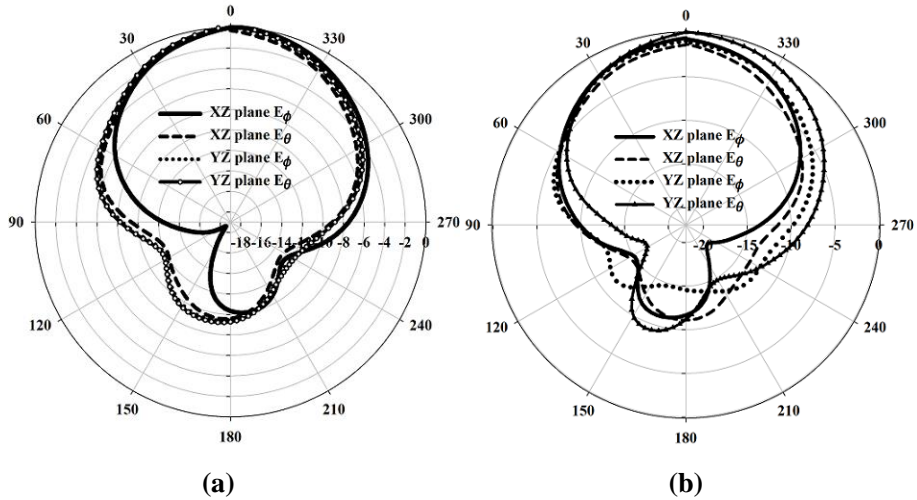


Figure 4.27. Measured radiation pattern plots of (a) RHCP antenna (b) LHCP antenna

The measured boresight radiation patterns of RHCP and LHCP antennas in the XZ and YZ planes at $\phi = 0^\circ$ and 90° are plotted in Figure 4.27. The patterns are almost identical. The gain is measured using gain-comparison method and depicted in Figure 4.28. Both antenna prototypes yielded an efficiency of 87.5%.

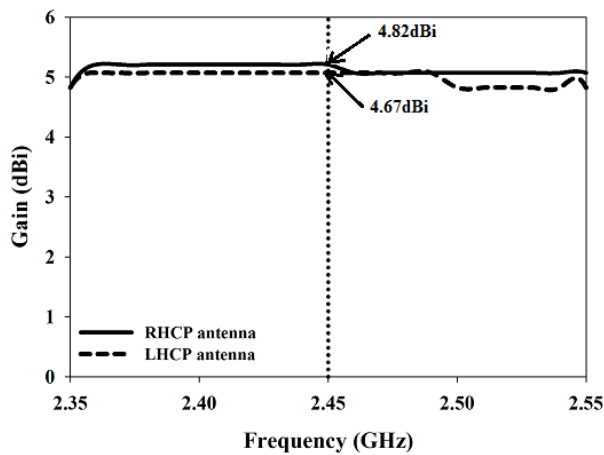


Figure 4.28. Measured gain plot of the proposed antennas

The measured values of the proposed RHCP and LHCP antennas are compared to the circular patch antenna [5] and tabulated in Table 4.2. Theoretical values of the following antenna parameters for the proposed antennas are computed and compared with the optimized values [17, 2] and are tabulated in Table 4.3. Design equations are validated with different substrates having different thicknesses and tabulated in Table 4.4. Here the theoretical value of the resonant frequency is computed based on 14.81% increase in electrical length due to the central slot on the patch antennas.

Table 4.2. Comparison of measured values of the proposed antennas with the circular patch [5]

Parameter	Circular patch antenna with elliptical slot [5]	Proposed RHCP antenna	Proposed LHCP antenna
Center frequency	2.45 GHz	2.45 GHz	2.45 GHz
Return loss	19 dB	24.8dB	22dB
Gain	3.85dBi	4.82 dBi	4.67 dBi
Minimum axial ratio	0 dB	0.06 dB	0.2 dB
Axial ratio bandwidth	30 MHz (1.22%)	135MHz (5.5%)	135MHz (5.5%)
10dB impedance bandwidth	130 MHz (5.3%)	140 MHz (5.7%)	140 Hz (5.7%)
3 dB Beam width	-	85 ^o	88 ^o
Area reduction	9.5%	21.17%	21.17%

Table 4.3. Comparison of theoretical and optimized values of the proposed antennas.

Parameter	Theoretical value	Optimised value of the RHCP antenna	Optimised value of the LHCP antenna
Resonant frequency	2.42GHz	2.45 GHz	2.45 GHz
Input impedance	57 Ω	56.1 Ω	58.6 Ω
Return loss	23.68 dB	24.8 dB	22 dB
Minimum axial ratio	0.2567 dB	0.22 dB	0.23 dB

Table 4.4. Validation of different substrates and comparison with simulation

Substrate	No. of sides of polygon	ϵ_r	h (mm)	a (mm)	k	Computed values			Simulated values				
						Fr GHz	Zin Ω	Ar min, dB	Fr GHz	Zin Ω	RL, dB	Ar min, dB	
FR4	10	4.4	1.6	8.28	1.425	2.42	57	23.68	0.26	2.45	58.6	22	0.23
Rogers RO4003	10	3.38	1.57	8.28	1.425	2.41	55	20.0	0.24	2.42	55.5	21	0.25
Rogers RO3006	10	6.15	1.25	8.28	1.425	2.43	58	25	0.25	2.44	58.9	24	0.24
Rogers 6010LM	10	10.2	0.635	8.28	1.425	2.40	56	21.15	0.23	2.41	57	22	0.23

A single feed circularly polarized irregular hexagonal slotted regular dodecagonal patch antenna has been designed, simulated and experimentally investigated. The structure is novel due to the choice of dodecagon shape for the patch and the central hexagonal slot perturbation method. The antennas cover RFID band with a center frequency of 2.45GHz, with broadside radiation characteristics. The measured 10dB impedance and 3dB axial ratio bandwidths confirm the usefulness of the structures to industrial, scientific and medical (ISM) bands in handheld RFID reader applications.

4.3 Hexagonal Circularly Polarized Patch Antenna with elliptical and circular slots

4.3.1 Antenna Geometry

The proposed antenna geometry consists of regular hexagonal patch with a central elliptical slot and two circular slots; one on the right side and the other on the left side of the elliptical slot. It is fabricated on an

FR4 substrate with a dielectric constant 4.4, thickness 1.6 mm and a $\tan \delta = 0.02$. As depicted in Figure 4.29, the elliptical slot is situated on the centre of the patch oriented along the X axis. The dimensions of the elliptical slot are designated as b the major radius (base radius), the secondary radius c and the aspect ratio k the ratio of c to b . The radius of the circular slot r_a is chosen to be 3mm.

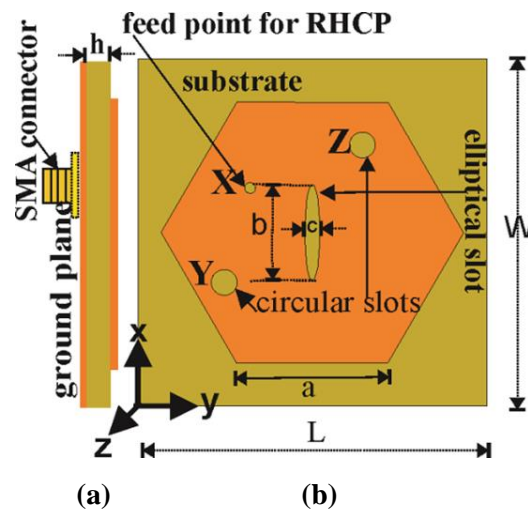


Figure 4.29. Geometry of the proposed antenna. (a) side view and (b) Top view, $a = 17.52\text{mm}$, $b = 11.2\text{mm}$, $c = 0.84\text{mm}$, $k = 0.15$, $L = W = 40.4\text{mm}$, guide wavelength $\lambda_g = 0.0606\text{ m}$, $\epsilon_{\text{reff}} = 4.087$, $X(25.4\text{mm}, 13\text{mm})$, $r_a = 3\text{mm}$, $Y(14.4\text{mm}, 10\text{ mm}, 1.6\text{mm})$ $Z(30.4\text{mm}, 26\text{mm}, 1.6\text{mm})$

In this structure, elliptical and the circular slots are chosen as the detuning elements to split the fundamental TM_{11} mode to two orthogonal modes TM_{01} and TM_{10} [5]. The dimensions of the elliptical and circular slots are so crucial, as it affects the radiation of circularly polarized waves. The antenna is excited through co-axial probes at the feed location

X to give circularly polarized electromagnetic radiation in the clockwise direction, i.e., Right Handed Circular Polarization (RHCP). The feed point is chosen along the locus of 50Ω characteristic impedance and is adjusted for good matching. The photograph of the proposed antenna is depicted in Figure 4.30.



Figure 4.30. Photograph of the antenna prototype

4.3.2 Design equations

As the circular and hexagonal shapes are closely related to each other, the design of a circular patch is considered for the design of a hexagonal patch antenna [13]. Then by equating the areas of a circle and a regular hexagon, the edge or side length of the regular hexagon a may be found [13] out as,

$$a = r_e \sqrt{\frac{2\pi}{3\sqrt{3}}} \quad (12)$$

By the proper selection of the feed point, the dominant mode is detuned into two equal amplitude orthogonal degenerate modes,

orthogonal even mode TM_e and orthogonal odd mode TM_o , without considering the higher order modes. By introducing the asymmetry, the resonant frequencies of two degenerate modes are made nearly equal. By introducing the asymmetry due to the central elliptical slot and the two circular slots, the dominant mode of the patch is detuned into two orthogonal degenerate modes, the odd mode and the even mode. The odd mode is oriented about the X axis and the even mode is oriented about the Y axis. The odd mode suffers minimum perturbation due to the elliptical slot. The edge of the hexagonal patch is designed for a resonant frequency of 2.63 GHz. Due to the elliptical and circular slots the resonant frequency is reduced to 2.45 GHz and thus the overall dimension is reduced by a factor of 18.10%.

To design the hexagonal patch, design equations are derived based on the geometry and the frequency of operation, after computing the guide wavelength λ_g , that is the wavelength in the dielectric is given by,

$$\lambda_g = \frac{\lambda_0}{\sqrt{\epsilon_{\text{reff}}}} \quad (13)$$

where λ_0 is the free space wavelength at 2.45 GHz and the effective permittivity of the substrate ϵ_{reff} is computed as 4.106, using the formula in [3] as,

$$\epsilon_{\text{reff}} = \epsilon_r - \frac{C_r \epsilon_r}{2} \left(\frac{2h}{x} + \frac{h^2}{x^2} \right) \quad (14)$$

where $C_r = 0.7$, being a thin substrate, x is the radius of the circumscribed circle (the circle in which the hexagon is inscribed) and h is the height of the substrate.

4.3. 3 Results and Discussion

|S11| characteristics

Using the computed parameters, the antenna was simulated using Ansys HFSS 13.0 and tested using ZVB20 vector network analyzer. Optimum feed point was chosen for the best impedance matching of the antenna. The measured and simulated |S11| characteristics of the proposed antenna at the co-axial feed point X are plotted in Figure 4.31. The fundamental resonant frequency of the antenna without slots is 2.63 GHz, whereas with slot, the simulated resonant frequency is 2.45 GHz.

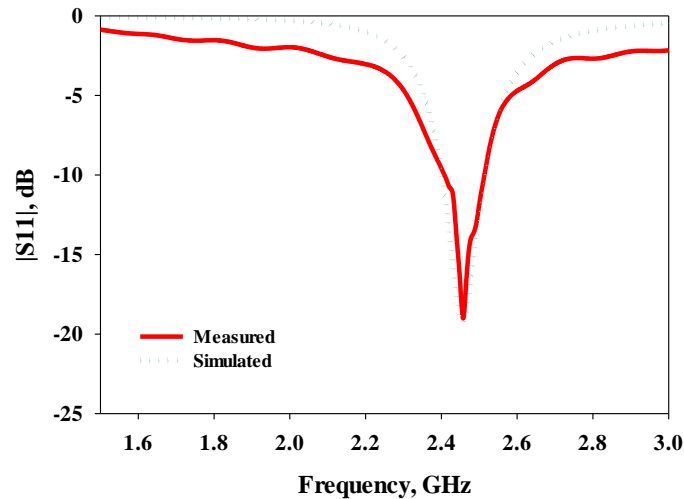


Figure 4.31. |S11| versus frequency plot of at $f_0 = 2.45\text{GHz}$

Axial ratio

The axial ratio is the magnitude of the normalized impedance ratio. Simulation results show that for various values of aspect ratio k (the ratio of secondary radius to base radius), the value of minimum axial ratio varies. It is observed that when k exceeds 0.08, axial ratio becomes less

than 3 dB and hence circular polarization is exhibited. The CP radiation at $k = 0.15$ is confirmed from the simulated axial ratio graphs shown in Figure 4.32, where the necessary criterion for CP, the axial ratio < 3 dB, is satisfied.

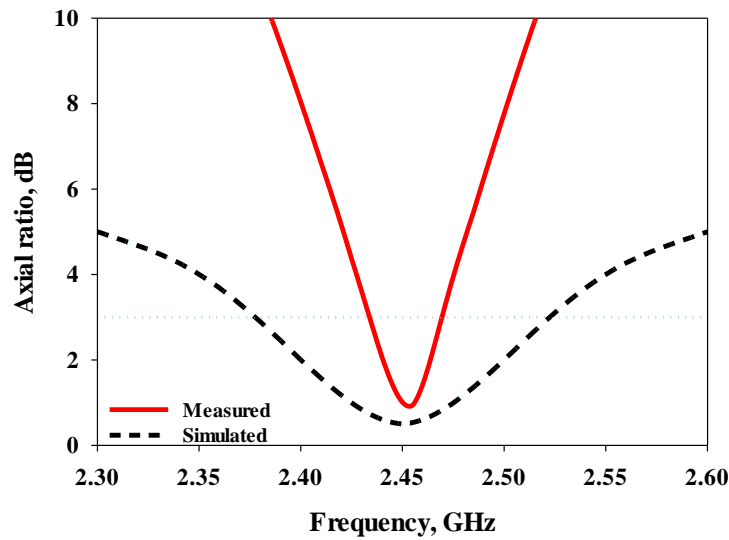


Figure 4.32. Axial ratio plot of the proposed structure

Surface current distribution

The surface current distribution simulated at the center frequency of 2.45 GHz is plotted in Figure 4.33. Surface current distribution at $\varphi = 0^\circ$ is equal in magnitude and opposite in direction to that at $\varphi = 180^\circ$. Same is the case of surface current distribution at $\varphi = 90^\circ$ and $\varphi = 270^\circ$ and hence the criterion for CP is satisfied. The direction of rotation of current is clockwise in the +Z axis and the sense of polarization is confirmed as right handed circular polarization.

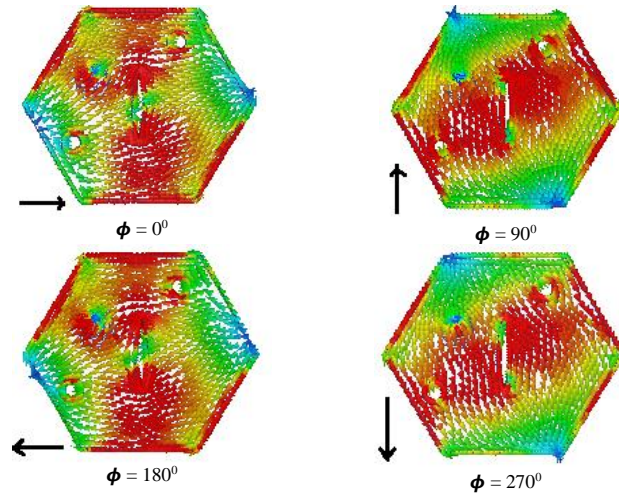


Figure 4.33. Surface current distribution

Radiation pattern

The measured radiation patterns of the proposed antenna in XZ and YZ planes for $\phi = 0^\circ$ and 90° are plotted in Figure 4.34. The pattern gives a 3 dB beam width of 80° .

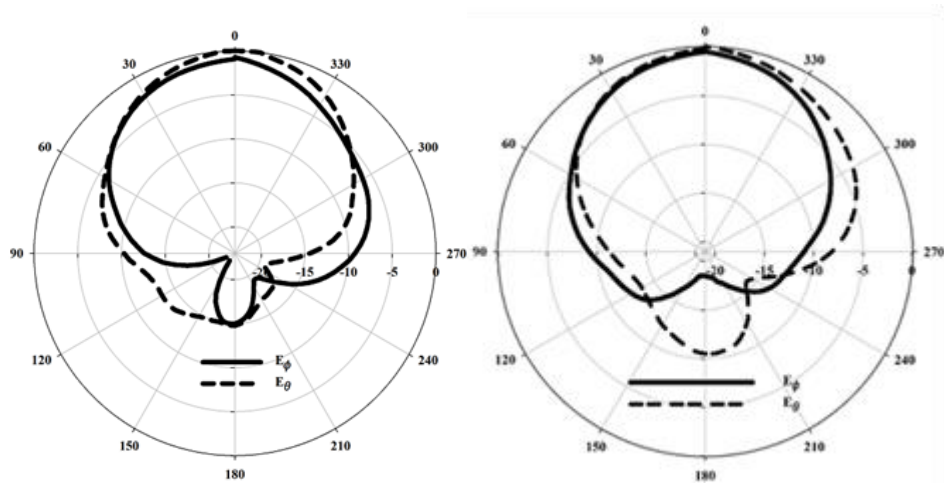


Figure 4.34. Radiation pattern of the antenna in (a) XZ plane (b) YZ plane

Gain and efficiency

The gain of the antenna is measured using gain comparison method and the measured value is 4.5 dBi at 2.45 GHz. The efficiency is measured to be 86%.

Smith chart

The simulated Smith chart is depicted in Figure 4.35. The dip in it corresponds to the center frequency 2.45 GHz, indicates the excitation of two orthogonal degenerate modes, justifying the circularly polarized radiation.

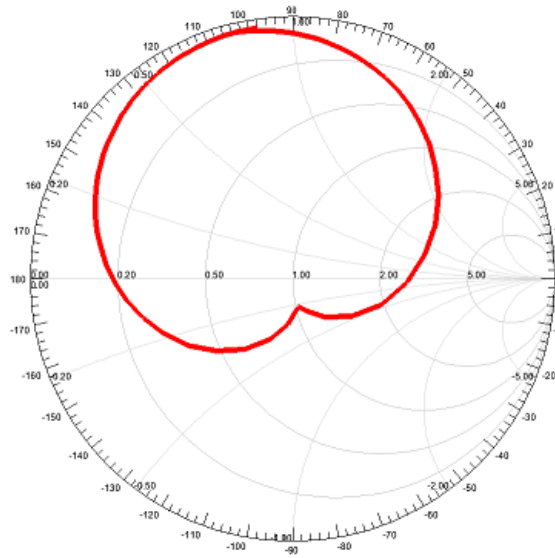


Figure 4.35. Smith chart

The measured values of the antenna are compared with the circular patch antenna with elliptical slot [5] and tabulated in Table 4.5.

Table 4.5. Comparison of measured values

Parameter	Circular patch antenna with elliptical slot [5]	Proposed antenna
Center frequency	2.45 GHz	2.45GHz
Return loss	19 dB	19dB
Gain	3.85dBi	4.5 dBi
Minimum axial ratio	0 dB	0.5dB
Axial ratio bandwidth	30 MHz (1.22%)	143 MHz(5.8%)
10dB impedance bandwidth	130 MHz (5.3%)	100MHz(4.08 %)
3 dB beamwidth	-	80°
Area reduction	9.5%	18.06 %

A novel design of a single feed circularly polarized hexagonal patch antenna has been designed, simulated and experimentally investigated. The elliptical and circular slots perturbation method yields better circular polarization characteristics. The experimental results confirm that it is suitable for RFID applications in the 2.45 GHz band.

4.4 Dodecagonal Circularly Polarised Patch Antenna with elliptical slot

4.4.1 Antenna Geometry

The proposed antenna geometry consists of regular dodecagonal patch with an elliptical slot fabricated on FR4 substrate which has a dielectric constant 4.4 , thickness 1.6 mm and a $\tan \delta=0.02$. As depicted in Figure 4.36, the elliptical slot is situated on the center of the patch oriented along the X axis. The dimensions of the elliptical slot are

designated as 'b' the major radius (base radius) and the ratio k, which is the aspect ratio of secondary radius 'c' to base radius.

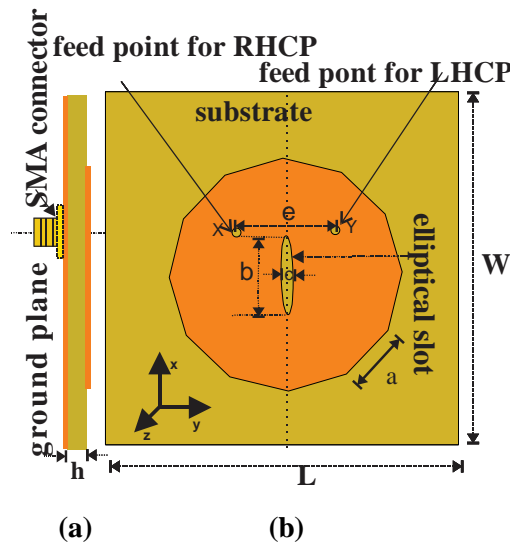


Figure 4.36. Geometry of the proposed antenna. (a) side view and (b) top view $a = 8.54\text{mm}$, $b = 11.2\text{mm}$, $c = 0.84\text{mm}$, $k = 0.15$, $e = 14\text{mm}$, $L = 50\text{mm}$, $W = 50\text{mm}$, $X (19.25\text{mm}, 18\text{mm})$, $Y (19.25\text{mm}, 32\text{mm})$.

In this work an elliptical slot is chosen as the detuning element to split fundamental TM_{11} mode to two orthogonal modes TM_{01} and TM_{10} . The structure of the ellipse is found to be suitable to split the fundamental mode. Figure 4.36(a) depicts the side view of the antenna and Figure 4.36(b) depicts the top view of the antenna. The antenna is excited through co-axial probes at the feed location X to give circularly polarized electromagnetic radiation in the clockwise direction, i.e, RHCP and at the feed location Y to radiate electromagnetic waves with opposite sense of polarization, i.e, LHCP. The co-axial probe feed point for RHCP antenna is the mirror image as that for LHCP antenna with respect to the centre of

the patch. The feed point is chosen along the locus of 50Ω characteristic impedance and is adjusted for good matching. Hence the feed point location not only determines the matching but also the circularly polarized radiation condition.

In order to design the dodecagonal patch antenna, the design of the circular patch antenna is considered, as the two antennas are closely related to each other [13]. By equating the areas, the edge of the regular hexagon 'a' may be found out from

$$11.196 a^2 = \pi r_e^2 \quad (15)$$

Where 'a' is the side length of the regular dodecagon and r_e is the effective radius of the circular patch. The central elliptical slot has two effects. One is the reduction of resonant frequency due to its behavior as a slot and thereby increasing the electrical length and the other one is its behavior as the detuning element to split the TM_{11} mode. By selecting proper slot dimensions and feed location, the two degenerate modes can be made to be equal in amplitude and a phase difference of 90° , result in a circular polarized radiation [5].

Thus, the perturbation produced by the elliptical slot gives rise to mode degeneration. As it increases the electrical length, the resonant frequency is reduced. Actually, the edge of the dodecagonal patch is designed for a resonant frequency of 2.687 GHz. Due to the central slot the resonant frequency is reduced to 2.4168 GHz and thus the overall dimension is reduced by a factor of 10%. The design values are, guide wavelength $\lambda_g = 0.0606$ m, diagonal length of the patch = $0.54 \lambda_g$, edge

$a = 0.14 \lambda_g$, $\epsilon_{\text{eff}} = 4.087$, base radius = $0.092 \lambda_g$, secondary radius = $0.0138 \lambda_g$, substrate length $L = \text{width}$ and $W = 50\text{mm}$.

4.4.2 Results and discussion

Using the computed parameters, the antenna was simulated using Ansoft HFSS 13.0, then tested using ZVB20 vector network analyser. Optimum feed point was chosen for the best impedance matching of the antenna.

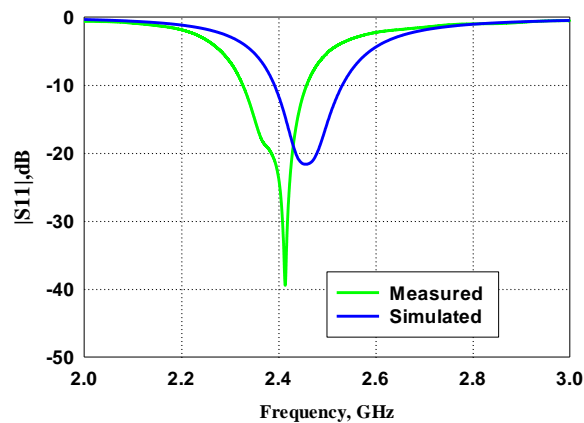


Figure 4.37. |S11| characteristics

The measured and simulated |S11| characteristics of the proposed antennas at the co-axial feed point X are plotted in Figure 4.37. The fundamental resonant frequency of the antenna without slot is 2.687 GHz, whereas with slot the simulated resonant frequency is 2.45 GHz. The measured return loss is -39dB and 10dB impedance bandwidth is 5.4% (130 MHz) at 2.4168 GHz. Due to manufacturing tolerances, slight deviation is there between simulated and experimental results.

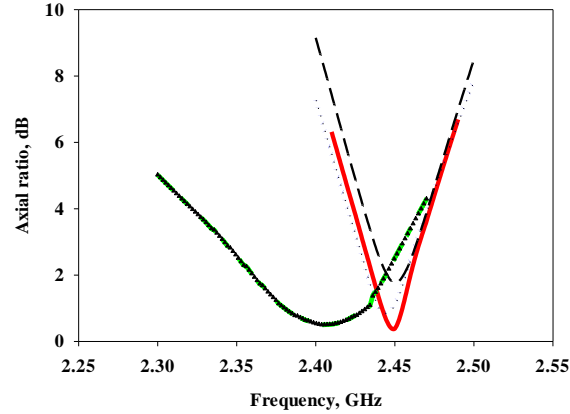


Figure 4.38. Axial ratio versus frequency plots for different values of k .

A parametric study is conducted by varying the parameter k . It is observed that when k exceeds 0.08 circular polarization radiation is exhibited. The achievement of CP radiation at $k = 0.15$ is confirmed from the simulated axial ratio graphs shown in Figure 4.38, where the necessary criterion of axial ratio < 3 dB is satisfied. For $k = 0.15$, the least simulated value of axial ratio = 0.38 dB is achieved and the measured value of axial ratio is 0.5dB (116 MHz- 5% ARBW).

Gain measured using gain comparison method is 4.58 dBi. Antenna efficiency is measured to be 88%. Area reduction is 16%.

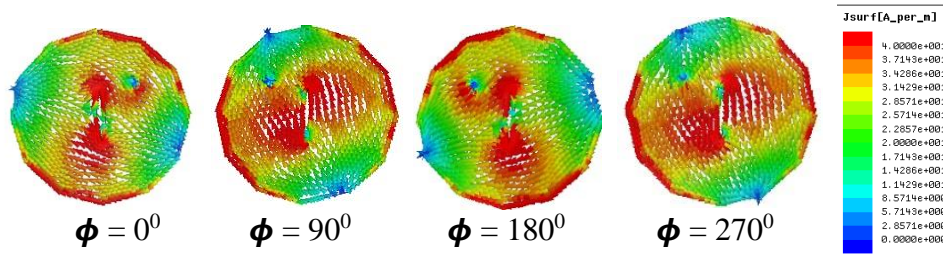


Figure 4.39. Surface current distribution of RHCP antenna

The surface current distribution of RHCP antenna simulated at the center frequency 2.45 GHz is plotted in Figure 4.39. Surface current distribution at 0° is equal in magnitude and opposite to that at 180° . Similar is the case at 90° and 270° . Surface current distribution of the LHCP antenna exhibits the same nature.

Radiation pattern

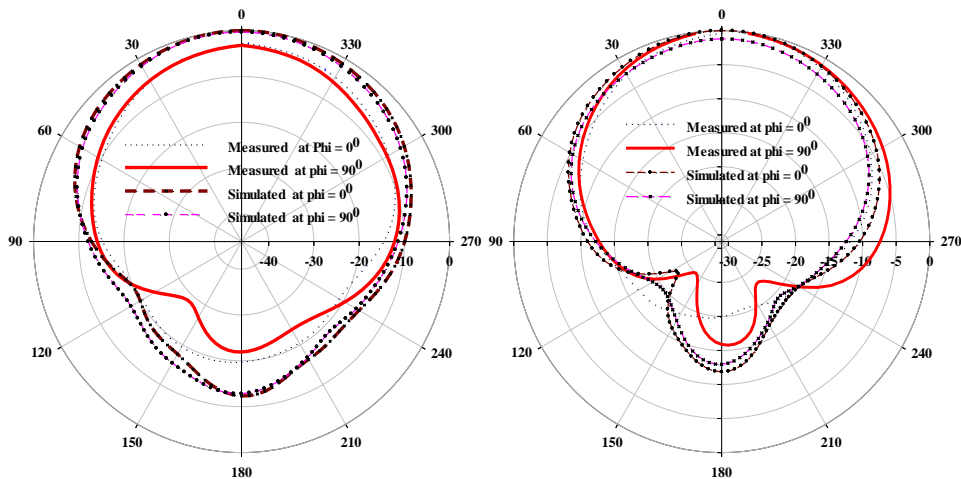


Figure 4.40. Radiation pattern of (a) RHCP antenna (b) LHCP antenna

The sensitivity to fabrication tolerance is also studied [2]. As the uncertainties due to the manufacturing tolerance are known a priori, change in resonant frequency due to a change of 0.01% in ‘a’ is 0.01%, neglecting the effect of tolerance in the nonuniformity of substrate thickness and variations in ϵ_r .

A novel design of a single feed circularly polarized elliptical slotted regular dodecagonal patch antenna has been designed, simulated and experimentally investigated. The central elliptical slot perturbation

method and the choice of dodecagon shape for the patch yields better circular polarization characteristics. Experimental results confirm its appropriateness for RFID applications in the 2.45 GHz band.

4.5 Circularly Polarized Decagonal Patch Antenna with Polygonal slot

4.5.1 Antenna geometry

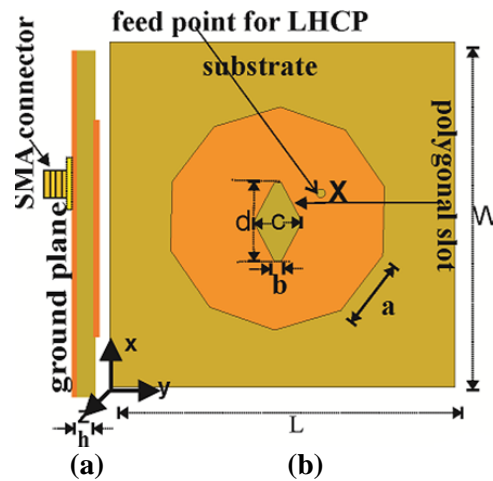


Figure 4.41. Geometry of the proposed antenna. (a) side view (b) top view of LHCP antenna, Guided wavelength $\lambda_g = 0.0604$ m, $a = 10$ mm ($0.166 \lambda_g$) $b = 1$ mm ($0.0166 \lambda_g$), $c = 7$ mm ($0.116 \lambda_g$), $d = 11.4$ mm ($0.189 \lambda_g$), $k = 1.62$, $L = W = 50$ mm ($0.8278 \lambda_g$) and $X(21\text{mm}, 19\text{mm})$.

This antenna structure as depicted in Figure 4.41, is a decagonal microstrip patch antenna with a central irregular hexagonal slot which is used to serve purpose of perturbation. The dimensions of the patch, slots and the feed point location are extremely important and are optimized for good performance. It exhibits good circular polarization radiation characteristics. The photograph of the developed antenna prototype is depicted in Figure 4.42.

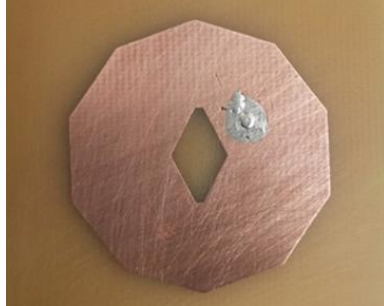


Figure 4.42. Photograph of the antenna prototype

As the circular patch and hexagonal patch are closely related to each other, the design of a circular patch is considered for the design of a decagonal patch antenna [13]. Then by equating the areas of a circle and a regular decagon, the edge or side length of the regular decagon a may be found [13] out as,

$$a = 0.408 r_c \quad (16)$$

By the proper selection of the feed point, the dominant mode is detuned into two equal amplitude orthogonal degenerate modes, orthogonal even mode TM_e and orthogonal odd mode TM_o , without considering the higher order modes. By introducing the asymmetry, the resonant frequencies of two degenerate modes are made nearly equal.

The normalized impedance ratio of the detuned modes is a complex number, which has a magnitude part and phase part. The phase part corresponds to the phase difference of the CP field components, while the magnitude is proportional to the axial ratio. The angle is designed to be 90° and the magnitude to be less than 3 dB. Thus, the criterion for circular polarization is satisfied. By selecting appropriate dimensions for the slot, the two degenerate mode frequencies are made nearly equal.

The edge of the hexagonal patch is designed for a resonant frequency of 2.73 GHz. Due to the slot the resonant frequency is reduced to 2.4386 GHz and thus the overall dimension is reduced by a factor of 21%.

To design the decagonal patch, design equations are derived based on the geometry and the frequency of operation after computing the guide wavelength λ_g , which is the wavelength in the dielectric.

4.5.2 Results and discussion

|S₁₁| characteristics

Using the computed parameters, the antenna was simulated using Ansys HFSS 13.0 and tested using ZVB20 vector network analyzer. Optimum feed point was chosen for the best impedance matching of the antenna. The measured and simulated reflection characteristics of the proposed antenna at the co-axial feed point X are plotted in Figure 3. The fundamental resonant frequency of the antenna without slots is 2.73 GHz, whereas with slot the simulated resonant frequency is 2.4386 GHz.

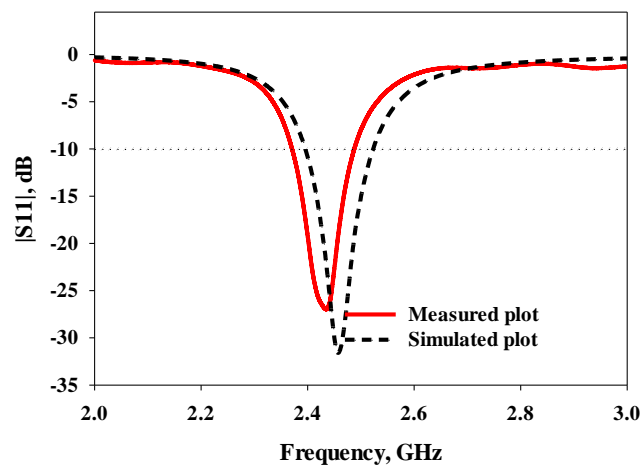


Figure 4.43. |S₁₁| versus frequency characteristics

Axial ratio

A parametric study is done by varying the parameter ‘k’, the aspect ratio. The realization of circularly polarized radiation is confirmed at $k = 1.62$, as the necessary criterion of axial ratio < 3 dB is satisfied and depicted in Figure 4. When $k = 1.62$, the least simulated value of axial ratio = 0.3428 dB is obtained with the fabricated prototype and the corresponding axial ratio bandwidth is calculated to be 62.18 MHz (2.58%) as plotted in Figure 4.44.

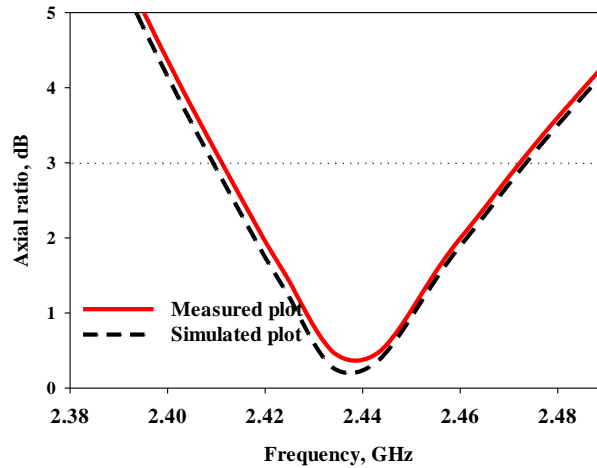


Figure 4.44. Axial ratio plot

Surface current distribution

The surface current distribution simulated at the center frequency of 2.45 GHz is plotted in Figure 4.45. Surface current distribution at $\varphi = 0^\circ$ is equal in magnitude and opposite in direction to that at $\varphi = 180^\circ$. Same is the case of surface current distribution at $\varphi = 90^\circ$ and $\varphi = 270^\circ$ and hence the criterion for CP is satisfied. The direction of rotation of current

is anticlockwise in the +Z axis and the sense of polarization is confirmed as left handed circular polarization.

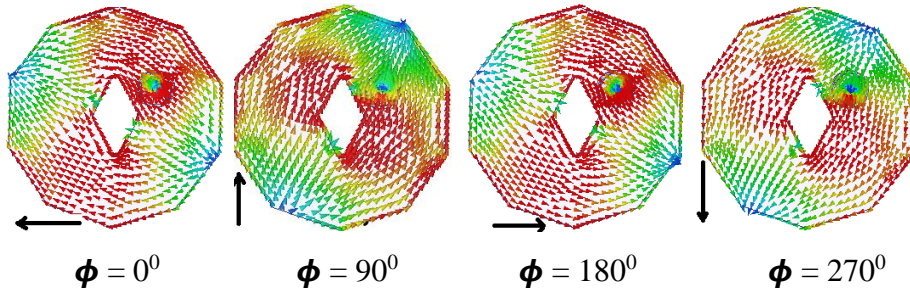


Figure 4.45. Surface current distribution of the proposed antenna

Radiation pattern

The measured radiation patterns of the proposed antenna in XZ and YZ planes for $\phi = 0^\circ$ and 90° are plotted in Figure 4.46. The pattern gives a 3 dB beam width of 88° .

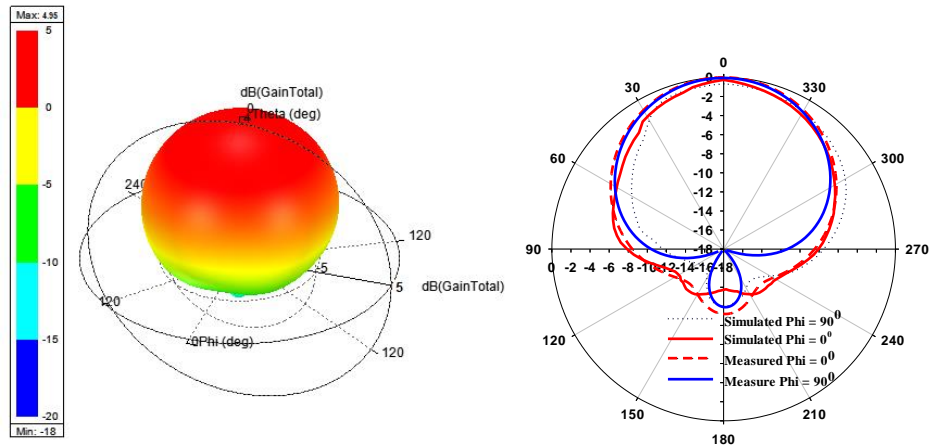


Figure 4.46. Radiation pattern of the antenna

Gain and efficiency

The gain of the antenna is measured using gain comparison method and the measured value is 4.95 dBi at 2.4386GHz and the efficiency is measured to be 84%.

Smith chart

The simulated Smith chart is depicted in Figure 4.47. The kink in the plot corresponds to the center frequency 2.45 GHz, indicates the excitation of two orthogonal degenerate modes, justifying the circularly polarized radiation.

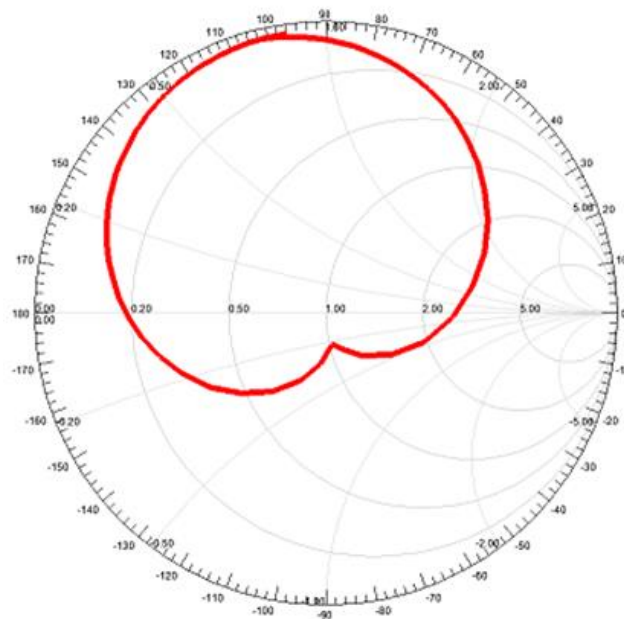


Figure 4.47. Smith chart

The measured values of the antenna are compared with the circular patch antenna with elliptical slot [5] and tabulated in Table 4.6.

Table 4.6. Comparison of measured values

Parameter	Circular patch antenna with elliptical slot [5]	Proposed antenna
Center frequency	2.45 GHz	2.4386GHz
Return loss	19 dB	27.12dB
Gain	3.85dBi	4.95 dBi
Minimum axial ratio	-	0.3428dB
Axial ratio bandwidth	30 MHz (1.22%)	62.18MHz (2.58%)
10dB impedance bandwidth	130 MHz (5.3%)	116.6MHz(5 %)
3 dB beamwidth	-	88°
Area reduction	9.5%	21 %

4.6 Circularly Polarised Tridecagonal Patch Antenna

4.6.1 Antenna geometry

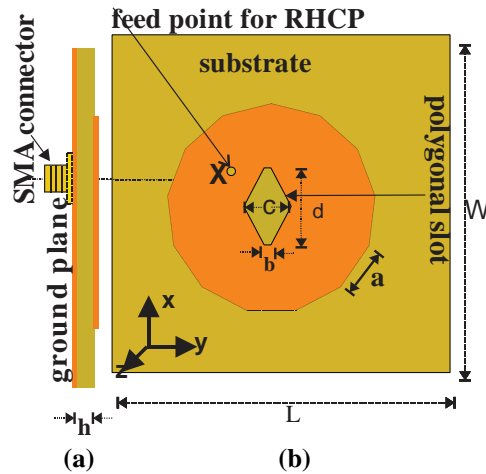


Figure 4.48. Geometry of the proposed antenna. (a) side view (b) top view of LHCP antenna, Guided wavelength $\lambda_g = 0.0604$ m, $a = 7.607$ mm $b=1$ mm($0.0166 \lambda_g$), $c = 7$ mm ($0.116\lambda_g$), $d = 11.4$ mm($0.189\lambda_g$), $k = 1.62$, $L = W = 50$ mm($0.8278 \lambda_g$) and $X(21$ mm, 19 mm).

The antenna geometry is depicted in Figure 4.48. The dimensions of the hexagonal slot are designated as i) b - the smaller Y axis dimension (top and bottom width), ii) c - the larger Y axis dimension (central width) and iii) d - the larger X axis dimension (height). These dimensions are such that $b < c < d$. The ratio 'k' is defined as ratio of 'd' to 'c' with 'b' constant. In order to generate circularly polarized waves, the simplest approach is to excite two equal amplitude degenerate orthogonal modes by a single feed point at an estimated location. In this structure, the central hexagonal slot is chosen as the detuning elements to split the fundamental TM_{11} mode to two orthogonal modes TM_{01} and TM_{10} [5]. The dimensions of the central slot are so crucial that it affects the radiation of circularly polarized waves. The antenna is excited through co-axial probes at the feed location X to give circularly polarized electromagnetic radiation in the clockwise direction, i.e., LHCP. The feed point is chosen along the locus of 50Ω characteristic impedance and is adjusted for good matching. The photograph of the proposed antenna is depicted in Figure 4.49



Figure 4.49. Photograph of the antenna prototype

4.6.2 Design equations

As the circular patch and hexagonal patch are closely related to each other, the design of a circular patch is considered for the design of a decagonal patch antenna. Then by equating the areas of a circle and a regular decagon, the edge or side length of the regular decagon a may be found out as [13],

$$a=0.488 re \quad (17)$$

The edge of the hexagonal patch is designed for a resonant frequency of 2.73 GHz. Due to the slot the resonant frequency is reduced to 2.4876 GHz and thus the overall dimension is reduced by a factor of 26.33%.

4.6.3 Results and discussion

|S11| characteristics

Using the computed parameters, the antenna was simulated using Ansys HFSS 13.0 and tested using Agilent E8362B precision network analyzer. Optimum feed point was chosen for the best impedance matching of the antenna. The measured and simulated reflection characteristics of the proposed antenna at the co-axial feed point X are plotted in Figure 4.50. The fundamental resonant frequency of the antenna without slots is 2.73 GHz, whereas with slot the simulated resonant frequency is 2.4876 GHz.

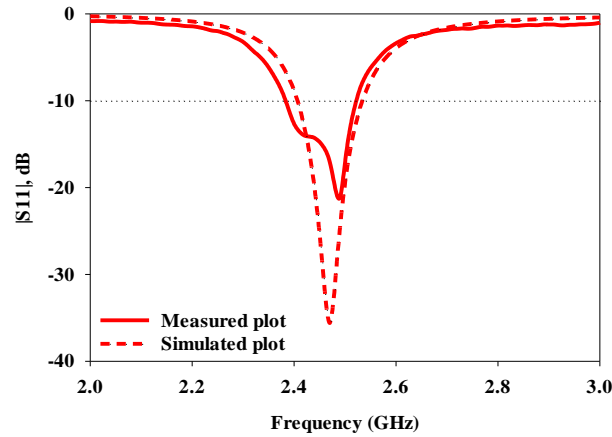


Figure 4.50. $|S_{11}|$ versus frequency plot of the proposed structure

Axial ratio

A parametric study is done by varying the parameter ‘k’, the aspect ratio. The realization of circularly polarized radiation is confirmed at $k = 1.62$, as the necessary criterion of axial ratio < 3 dB is satisfied and depicted in Figure 4.51. When $k = 1.62$, the least simulated value of axial ratio = 0.3428 dB is obtained with the fabricated prototype and the corresponding axial ratio bandwidth is calculated to be 62.18 MHz (2.58%).

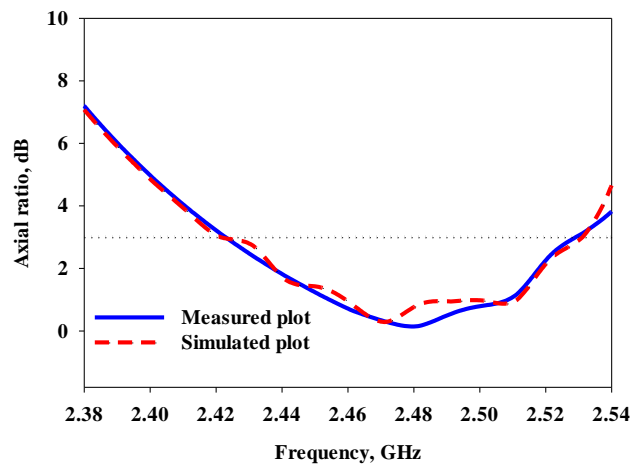


Figure 4.51. Axial ratio plot

Surface current distribution

The surface current distribution simulated at the center frequency of 2.45 GHz is plotted in Figure 4.52. Surface current distribution at $\varphi = 0^\circ$ is equal in magnitude and opposite in direction to that at $\varphi = 180^\circ$. Same is the case of surface current distribution at $\varphi = 90^\circ$ and $\varphi = 270^\circ$ and hence the criterion for CP is satisfied. The direction of rotation of current is clockwise in the +Z axis and the sense of polarization is confirmed as right handed circular polarization.

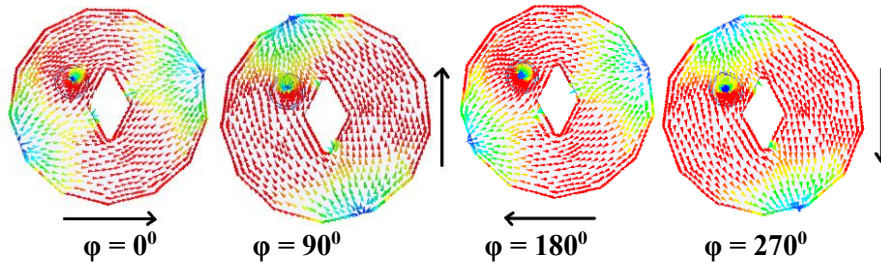


Figure 4.52. Surface current distribution

Radiation pattern

The measured radiation patterns of the proposed antenna in XZ and YZ planes for $\varphi = 0^\circ$ and 90° are plotted in Figure 4.53. The pattern gives a 3dB beam width of 90° .

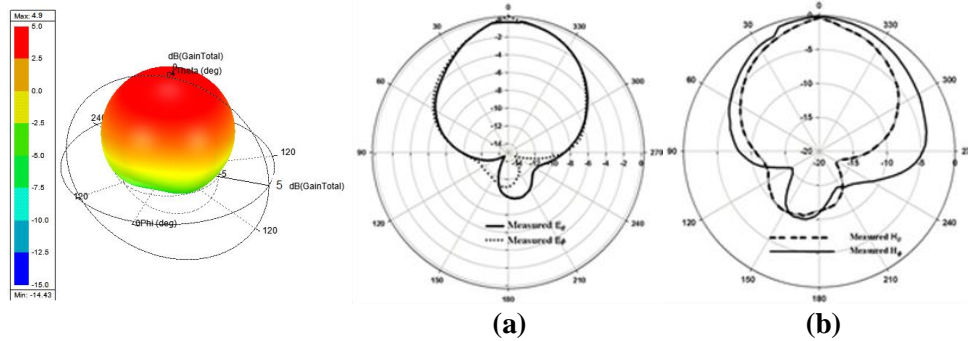


Figure 4.53. Radiation pattern of the antenna in (a) XZ and (b) YZ planes

Gain and efficiency

The gain of the antenna is measured using gain comparison method and the measured value is 4.98 dBi at 2.4876GHz and the measured efficiency is 89%.

The measured values of the antenna are compared with the circular patch antenna with elliptical slot [5] and tabulated in Table 4.7.

Table 4.7. Comparison of measured values

Parameter	Circular patch antenna [9]	Proposed antenna
Center frequency	2.45 GHz	2.4876GHz
Return loss	19 dB	21.3857dB
Gain	3.85dBi	4.98 dBi
Axial ratio(min)	-	0.15dB
Axialratio bandwidth	30 MHz (1.22%)	108MHz (4.35%)
10dBimpedance bandwidth	130 MHz 5.3%	140MHz 5.65 %
3 dB beamwidth	-	90 ^o
Area reduction	9.5%	26.33 %

4.7 Circularly Polarised tetra decogonal patch antenna

4.7.1 Antenna geometry

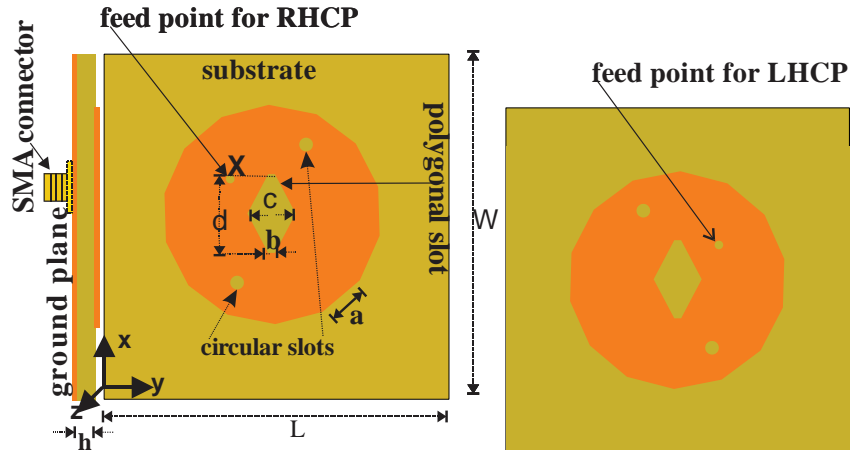


Figure 4.54. Geometry of the proposed antenna. (a) side view (b) top view of RHCP antenna, (c) LHCP antenna, Guided wavelength $\lambda_g = 0.0604$ m, $a = 7.607$ mm $b=1\text{mm}(0.0166\lambda_g)$, $c = 7\text{mm}$ ($0.116\lambda_g$), $d=11.4\text{mm}(0.189\lambda_g)$, $L=W=50\text{mm}(0.8278 \lambda_g)$, $X(21\text{mm},19 \text{ mm})$, $Y(21\text{mm},31\text{mm})$, RHCP antenna co-ordinates of circular slots((15,30),(35,20)) and LHCP antenna((15,20), (35,30)) and the radius of circle 1mm.

The dimensions of the hexagonal slot are designated as i) b - the smaller Y axis dimension (top and bottom width), ii) c - the larger Y axis dimension (central width) and iii) d – the larger X axis dimension(height).

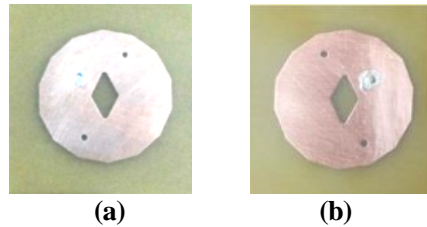


Figure 4.55. Photographs of the antenna prototypes (a) RHCP (b) LHCP

The photographs of the proposed antennas are depicted in Figure 4.55. The dimensions are such that $b < c < d$. The ratio 'k' is defined as ratio of 'd' to 'c' with 'b' constant.

4.7.2 Design

The design of the circular patch antenna is considered for designing the tetra decagonal patch antenna, as the two antennas are closely related to each other [5]. The side length 'a' of the regular tetra decagon for a resonant frequency of $f_r = 2.7\text{GHz}$ is designed as follows. The dominant mode resonance frequency of a circular patch is given by [13]

$$f_r = \frac{X_{mn} c}{2\pi r_e \sqrt{\epsilon_r}} \quad (18)$$

where f_r is the resonant frequency of the patch , $X_{mn} = 1.8411$ for the dominant mode TM_{11} , c is the velocity of light in free space, ϵ_r the relative permittivity of the substrate, 're' is the effective radius of the equivalent circular patch.

Then by equating the areas of a circle and a regular tetra decagon, the edge or side length of the regular tetra decagon 'a' may be found out as in [5],

$$a = 0.4525 r_e \quad (19)$$

Due to the hexagonal and circular slots the resonant frequency is reduced to 2.45 GHz and thus the overall dimension is reduced by 26.54%.

4.7.3 Results and discussion

|S₁₁| characteristics

Using the computed parameters, the antenna was simulated using Ansys HFSS13.0 and tested using Agilent E8362B precision network analyzer. The measured reflection characteristics of the proposed antennas at the co-axial feed point are plotted in Figure 4.56. The fundamental resonant frequency of the antenna without slots is 2.7 GHz, whereas with slot the simulated resonant frequency is 2.4541 GHz for RHCP antenna and 2.46 GHz for LHCP antenna.

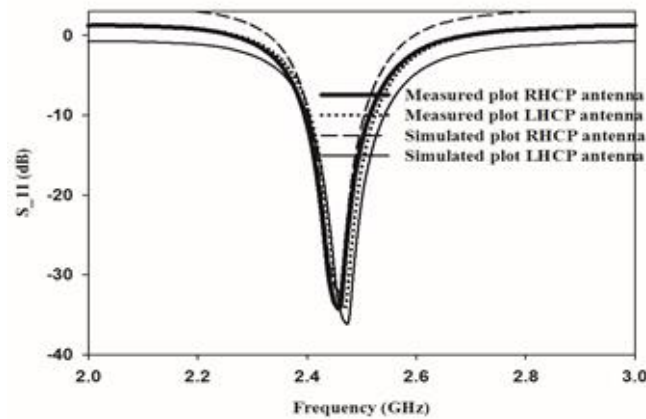


Figure 4.56 |S₁₁| versus frequency plots of the proposed structures

Axial ratio

A parametric study is done by varying the parameter 'k'. The realization of circularly polarized radiation is confirmed at $k = 1.62$, as the necessary criterion of axial ratio < 3 dB is satisfied and depicted in Figure 4.57.

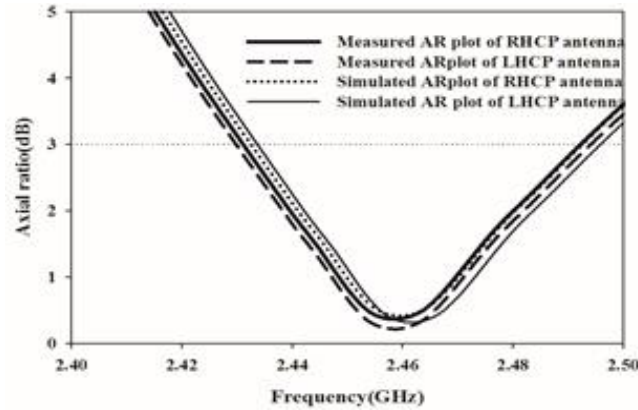


Figure 4.57. Axial ratio versus frequency plots

When $k = 1.62$, the least value of axial ratio 0.35 dB and 0.215 dB is obtained with the fabricated RHCP and LHCP prototypes respectively.

Surface current distribution

The simulated surface current distribution is plotted in Fig. 6.

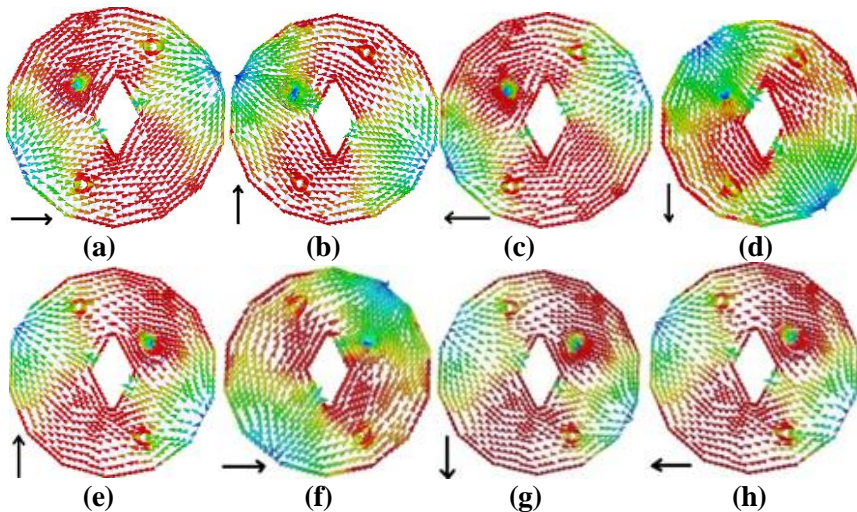


Figure 4.58. Surface current distribution (a) to (d) RHCP, (e) to (h) LHCP. (a) & (e) $\varphi = 0^\circ$, (b) & (f) $\varphi = 90^\circ$, (c) & (g) $\varphi = 180^\circ$ and (d) & (h) $\varphi = 270^\circ$.

At $\varphi = 0^\circ$ it is equal in magnitude and opposite in direction to that at $\varphi = 180^\circ$. Same is the case at $\varphi = 90^\circ$ and $\varphi = 270^\circ$ and hence the criterion for

CP is satisfied. The direction of rotation is clockwise in the +Z axis and the sense of polarization is right handed and anticlockwise for left handed.

Radiation pattern

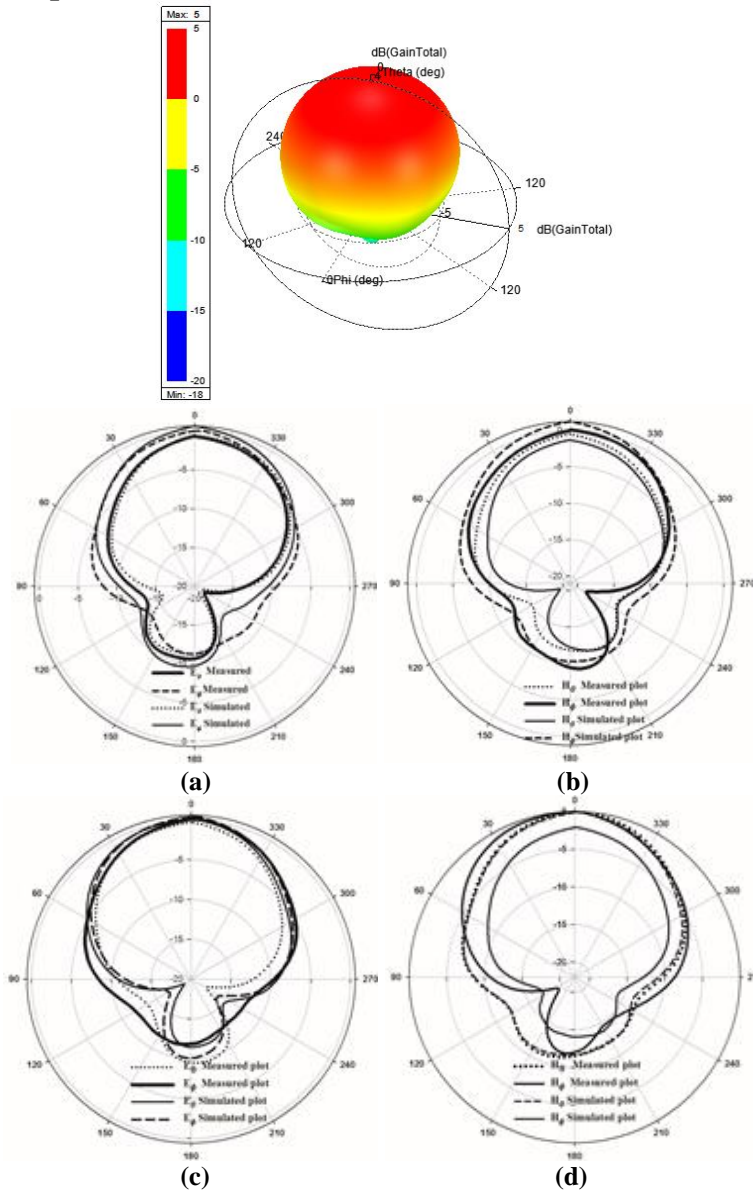


Figure 4.59. Radiation pattern of the RHCP antenna in (a) XZ (b) YZ planes & LHCP antenna in (c) XZ and (d) YZ planes.

Gain and efficiency

The gain of the antennas is measured using the gain comparison method and the measured value is 5 dBi at 2.45GHz for both antenna prototypes and efficiency is measured to be 88%. The measured and simulated boresight radiation pattern diagrams are depicted in Figure 4.59.

The measured values of the antennas are tabulated in Table 4.8.

Table 4.8. Comparison of measured values

Parameter	RHCP antenna	LHCP antenna
Center frequency	2.4541 GHz	2.46GHz
Return loss	34.264 dB	34dB
Gain	5.1dBi	5.1 dBi
Axial ratio(min)	0.35dB	0.215dB
Axialratio bandwidth	61 MHz (2.5%)	61MHz (2.5%)
10dBimpedance bandwidth	116 MHz 4.73%	116MHz 4.73 %
3 dB beamwidth	82 ⁰	81.5 ⁰
Area reduction	26.54%	26.54 %

4.8 Circularly Polarised Hexadecagonal Patch Antenna

4.8.1 Antenna geometry

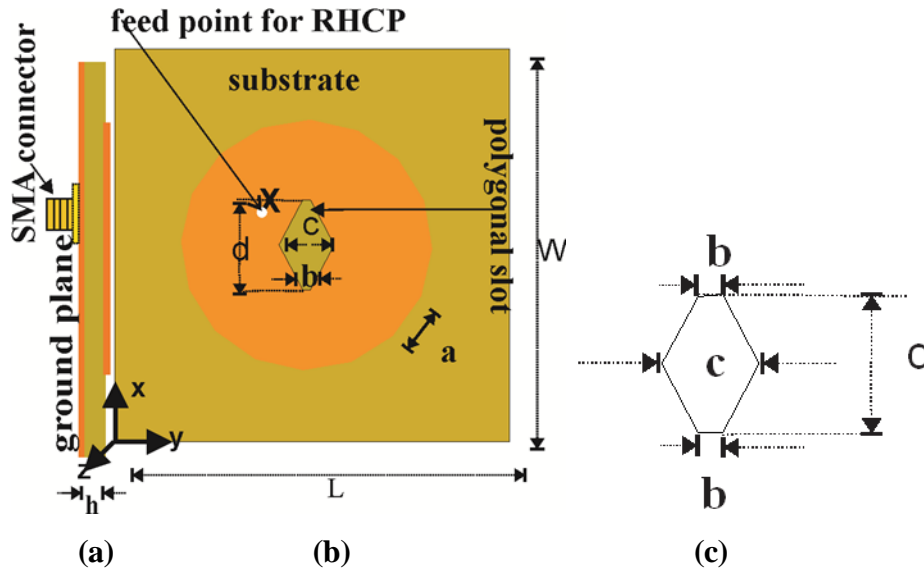


Figure 4.60. Geometry of the proposed antenna. (a) side view (b) top view of LHCP antenna, Guided wavelength $\lambda_g = 0.0604$ m, $a = 6.2$ mm, $b = 1$ mm ($0.0166 \lambda_g$), $c = 7$ mm ($0.116 \lambda_g$), $d = 11.4$ mm ($0.189 \lambda_g$), $k = 1.62$, $L = W = 50$ mm ($0.8278 \lambda_g$) and X (21mm, 19 mm).

The antenna geometry is depicted in Figure 4.60. It is fabricated on an FR4 substrate ($\epsilon_r = 4.4$, $\tan \delta = 0.02$ and $h = 1.6$ mm). Dimensions of the hexagonal slot are designated as i) b - the smaller Y axis dimension (top and bottom width), ii) c - the larger Y axis dimension (central width) and iii) d - the larger X axis dimension (height). These dimensions are such that $b < c < d$. The ratio ' k ' is defined as the ratio of ' d ' to ' c ' with ' b ' constant. The dimensions of the central slot are so crucial that they affect the radiation of circularly polarized waves. The antenna is excited through co-axial probes at the feed location X to give circularly polarized electromagnetic

radiation in the clockwise direction, i.e., Right Handed Circular Polarization (RHCP). The feed point is chosen along the locus of 50Ω characteristic impedance and is adjusted for good matching. The photograph of the proposed antenna is depicted in Figure 4.61. The edge of the hexagonal patch is designed for a resonant frequency of 2.7 GHz. Due to the slot, the resonant frequency is reduced to 2.41 GHz and thus the overall dimension is reduced by a factor of 25.27%.

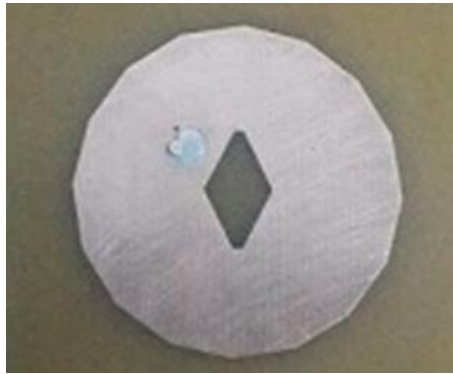


Figure 4.61. Photograph of the antenna prototype

4.8.2 Design equations

As the circular patch and hexa decagonal patch are closely related to each other, the design of a circular patch is considered for the design of a hexa decagonal patch antenna. Then by equating the areas of a circle and a regular hexa decagon, the edge or side length of the regular hexa decagon a may be found out as [13],

$$a = 0.395r_e \quad (20)$$

The constant in the above equation varies for different number of sides.

4.8.3 Results and discussions

|S₁₁| characteristics

Using the computed parameters, the antenna was simulated using Ansys HFSS 13.0 and tested using Agilent E8362B precision network analyzer. Optimum feed point was chosen for the best impedance matching of the antenna. The measured and simulated reflection characteristics of the proposed antenna at the co-axial feed point X are plotted in Figure 3. The fundamental resonant frequency of the antenna without slots is 2.7 GHz, whereas with slot the simulated resonant frequency is 2.41 GHz.

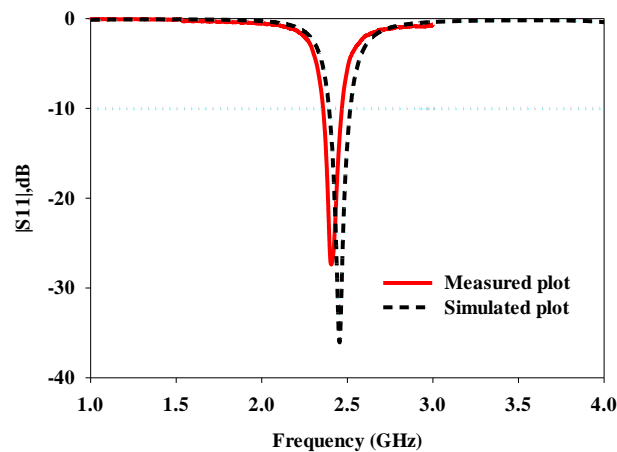


Figure 4.62 |S₁₁| versus frequency plot

Axial ratio

A parametric study is done by varying the parameter 'k', the aspect ratio. The realization of circularly polarized radiation is confirmed at $k = 1.62$, as the necessary criterion of axial ratio < 3 dB is satisfied and depicted in Figure 4.63. When $k = 1.62$, the least value of axial ratio = 1.3428 dB is obtained with the fabricated prototype and the corresponding axial ratio bandwidth is calculated to be 72.18 MHz (3%).

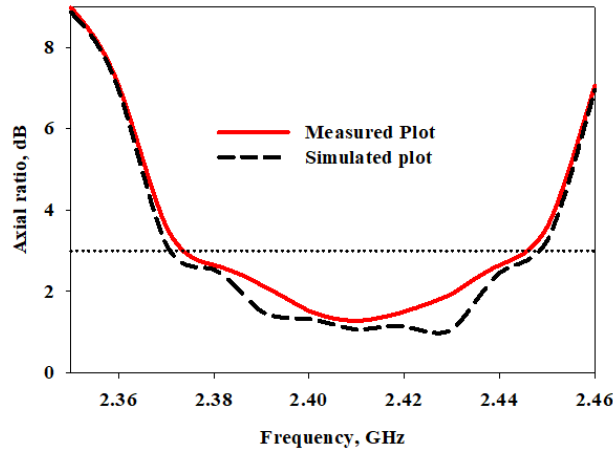


Figure 4.63. Axial ratio plot

Surface current distribution

The surface current distribution simulated at the center frequency of 2.4GHz is plotted in Figure 4.64. Surface current distribution at $\varphi = 0^\circ$ is equal in magnitude and opposite in direction to that at $\varphi = 180^\circ$. Same is the case of surface current distribution at $\varphi = 90^\circ$ and $\varphi = 270^\circ$ and hence the criterion for CP is satisfied. The direction of rotation of current is clockwise in the +Z axis and the sense of polarization is confirmed as right handed circular polarization.

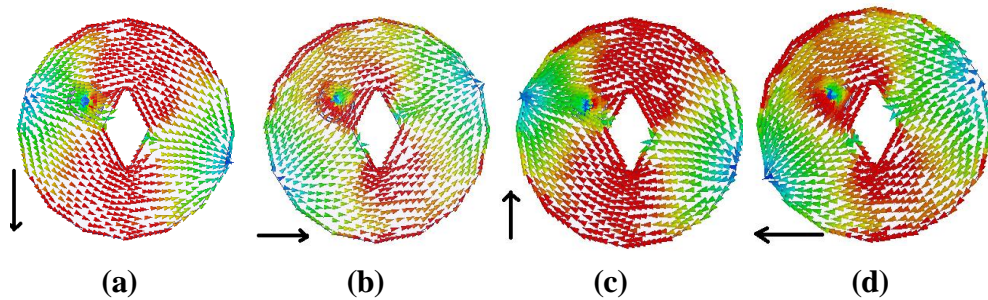


Figure 4.64 Surface current distribution at (a) $\varphi = 0^\circ$, (b) $\varphi = 90^\circ$, (c) $\varphi = 180^\circ$ and (d) $\varphi = 270^\circ$.

Radiation pattern

The measured radiation patterns of the proposed antenna in XZ and YZ planes for $\varphi = 0^0$ and 90^0 are plotted in Figure 4.65. The pattern gives a 3dB beam width of 90^0 .

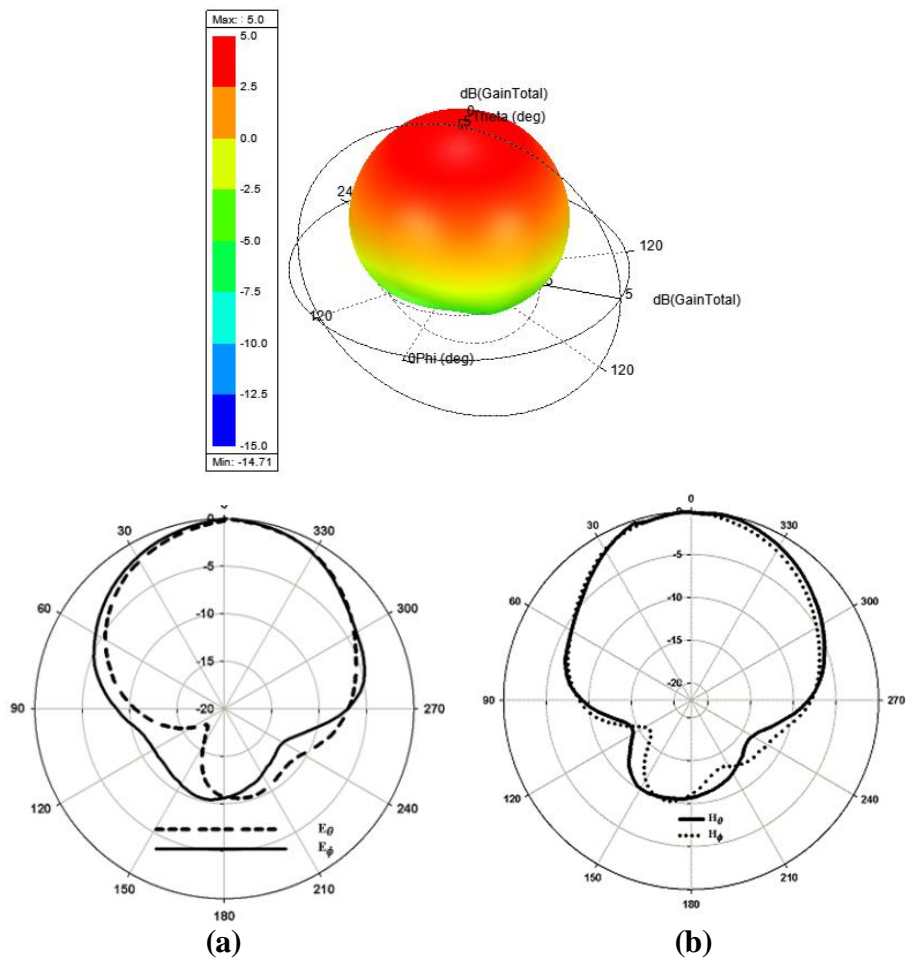


Figure 4.65. Measure radiation pattern of the antenna in (a) XZ and (b) YZ planes

Gain and efficiency

The gain of the antenna is measured using gain comparison method and the measured value is 5.09 dBi at 2.41 GHz, and the efficiency is measured to be 89%

The measured values of the antenna are compared with the circular patch antenna with elliptical slot [5] and tabulated in Table 4.9.

Table 4.9. Comparison of measured values

Parameter	Circular patch antenna with elliptical slot [5]	Proposed antenna
Center frequency	2.45 GHz	2.41GHz
Return loss	19 dB	27.1644dB
Gain	3.85dBi	5.09 dBi
Axial ratio(min)	-	1.27dB
Axialratio bandwidth	30 MHz (1.22%)	72.18MHz (3%)
10dBimpedance bandwidth	130 MHz 5.3%	116MHz (4.85 %)
3 dB beamwidth	-	90 ⁰
Area reduction	9.5%	25.27 %

Summary of the chapter

Compared the performance of eight different single band circularly polarized polygonal patch antennas which have been designed and developed as illustrated in this chapter with the reference antenna mentioned in [5] and depicted in the Table 4.10 below.

Table 4.10. Comparison of performance of single band CP antennas

Parameter	[5]	AntI*	AntII*	AntIII*	AntIV*	AntV*	AntVI*	AntVII*	AntVIII*
Centre frequency GHz	2.45	2.42	2.45	2.45	2.42	2.44	2.48	2.45	2.41
Return loss dB	19	32	24.8	19	39	27.12dB	21.3857	34.264	27.164
Gain dBi	3.85	4.9	4.82	4.5	4.6	4.95	4.98	5.1	5.09
Min.AR	-	1.82	0.06	0.50	0.38	0.3428	0.15	0.35	1.27
ARBW MHz, % w.r.t centre freq.	30	180	135	143	116	62.18	108	61	72.18
IBW MHz	130	130	140	100	130	116.6	140	116	116
3dB beam width	-	80 ⁰	88 ⁰	80 ⁰	81 ⁰	88 ⁰	90 ⁰	80 ⁰	90 ⁰
Area reduction	9.5%	21.17%	22.5%	18.06 %	10%	21 %	26.33 %	26.54%	25.27 %

* AntI – Hexagonal patch with polygonal slot (Section 4.1)

AntII – Dodecagonal patch with polygonal slot (Section 4.2)

AntIII -Hexagonal patch with elliptical and circular slots (Section 4.3)

AntIV- Dodecagonal patch with elliptical slot (Section 4.4)

AntV- Decagonal patch with polygonal slot (Section 4.5)

Ant VI- Tridecagonal patch with polygonal slot (Section 4.6)

AntVII- Tetradecagonal patch with polygonal slot (Section 4.7)

AntVIII- Hexadecagonal patch with polygonal slot (Section 4.8)

The single band circularly polarized patch antennas have been analyzed in this chapter. The key inferences derived from the studies can be summarized as below.

The polygonal or elliptical shaped patches with central can be conveniently used to produce circular polarisation.

Circularly polarized radiation at the fundamental frequency is produced by the merging of near degenerate TM_{01} and TM_{10} modes. The shape and dimensions of the central slot has good dependence on CP. Reduction in patch size through slot dimensions maintains the fundamental frequency within the concerned frequency band. Null current positions occur at certain locations on the patch. The location of feed point has got an effect on CP characteristics. Design equations developed are found to hold good for different substrates.

References

- [1] Horng-Dean Chen, Shang-Huang Kuo, Chow-Yen Desmond Sim, and Ching-Han Tsai “Coupling-Feed Circularly Polarized RFID Tag Antenna Mountable on Metallic Surface”, IEEE Transactions On Antennas And Propagation, Vol. 60, No. 5, May 2012.
- [2] K. Carver and J. Mink, “Microstrip antenna technology,” IEEE Trans. Antennas Propag., vol. 29, no. 1, pp. 2–24, 1981.
- [3] R. Garg,” Microstrip Antenna Design Handbook”, Boston, MA: Artech House, 2001.
- [4] B. Kim, B.Pan, S. Nikolaou, Y.-S.Kim, J. Papapolymerou, and M. M. Tentzeris, “Anovel single-Feed circular microstrip antenna with reconfigurable polarization capability,” IEEE Trans. Antennas Propag., vol. 56, no. 3, pp. 630–638, 2008.

- [5] Maddio Stefano, Alessandro Cidronali Gianfranco Manes, “A New Design Method for Single-Feed Circular Polarization Microstrip Antenna With an Arbitrary Impedance Matching Condition”, IEEE Transactions on Antennas and Propagation, Vol.59 , No.2, pp 379-389, 2011.
- [6] Row J.S. and C.Y.Ai, “Compact design of single feed circularly polarized microstrip antenna”, Electronics Letters, Vol.40, No.18, pp 1093–1094, 2004.
- [7] Chen W.S., C.K Wu.and K.L.Wong, “Novel compact circularly polarized square microstrip antenna”, IEEE Transactions on Antennas and Propagation, Vol.49, No.3,pp 340– 342, 2001
- [8] Pomsathit A., C. Benjangkprasert, N.Anantrasirichail, V. Chutchavong, and T. Wakabayashi, “Circularly Polarized Right Angle Slot Antennas for WLAN of IEEE 802.11b/g”, International Symposium on Communications and Information Technologies ISCIT 2008, Lao, pp 4650, 2008.
- [9] Barbero J., H. Lazo, F. Municio, and M. TeDeCe, “ Model for the patch radiator with a perturbation to achieve circular polarization”, IEE Colloquium on Recent Developments in Microstrip Antennas, London, , pp 6/1 - 6/4., Feb 1993
- [10] A. Bhattacharyya and L. Shafai, A wider band microstrip antenna for circular polarization, IEEE Transactions on Antennas and Propagation, Vol. 36, No. 2, pp 157–163, 1988.
- [11] Prakash K.C, S.Mathew, R.Anitha, P.V. Vinesh, M.P.Jayakrishnan, P.Mohanan, K. Vasudevan, Circularly polarized dodecagonal Patch Antenna with Polygonal slot for RFID Applications Progress in electromagnetic Research, vol.61, 9-15, 2016.
- [12] Prakash K.C, Vinesh P.V, Jayakrishnan. M.P, Dinesh. R, Mohammad Ameen, Vasudevan K, Hexagonal Circularly Polarized Patch Antenna for RFID Applications, Int. Journal. Cybernetics and Informatics, vol. 5, no. 2, pp. 173–182, 2016

- [13] Kushwaha Nagendra and Raj Kumar, “Design Of Slotted Ground Hexagonal Microstrip Patch Antenna And Gain Improvement With FSS Screen”, *Progress In Electromagnetics Research B*, Vol. 51, pp 177–199, 2013.
- [14] K.C. Prakash, S.Mathew, R. Anitha, P. V. Vinesh, M.P. Jayakrishnan, P. Mohanan, and K Vasudevan, “Circularly Polarized Dodecagonal Patch Antenna with Polygonal Slot for RFID Applications”, *Progress In Electromagnetics Research C*, Vol. 61, 9–15, 2016
- [15] Mathur V., Manisha Gupta, “Comparison of Performance Characteristics of Rectangular , Square and Hexagonal Microstrip Patch Antennas”, *Proceedings of 3rd International Conference on Reliability, Infocom Technologies and Optimization (ICRITO) (Trends and Future Directions)*, Noida ,India, October2014
- [16] Steven (Shichang) Gao, Qi Luo and Fuguo Zhu,” *Circularly Polarized Antenna*” , John Wiley & Sons Ltd, United Kingdom, 2014.
- [17] Balanis C. A., “*Antenna theory: Analysis and design*, second edition” , John Wiley & Sons Inc, New Delhi,2007.
- [18] Nasimuddin, X. Qing, and Z. N. Chen, “Compact asymmetric-slit microstrip antennas for circular polarization,” *IEEE Trans. Antennas Propag.*, vol. 59, no. 1, pp. 285–288, 2011.
- [19] Y.-F. Lin, H.-M. Chen, S.-C. Pan, Y.-C. Kao, and C.-Y. Lin, “Adjustable axial ratio of single-layer circularly polarised patch antenna for portable RFID reader,” *Electron. Lett.*, vol. 45, no. 6, p. 290, 2009.
- [20] D. L. Nguyen, K. S. Paulson, and N. G. Riley, “Reducedsized circularly polarised square microstrip antenna for 2.45 GHz RFID applications,” *IET Microwaves, Antennas and Propag.*, vol. 6, no. 1, p. 94, 2012.

- [21] Z.-Y. Zhang and K.-L. Wu, “A Circularly Polarized Table- like Air Patch Antenna with Four Grounded Metal Legs,”IEEE Antennas Wirel. Propag. Lett., vol. 1225, no. c, pp.1–1, 2016.
- [22] www.understandrfidstandards.com › 2-45-ghz-air-interface-standards

.....❧.....

**DUAL BAND CIRCULARLY POLARISED
MICROSTRIP ANTENNA**

Contents	<i>Introduction to dual band circularly polarized microstrip antennas</i>
	<i>5.1 Introduction to dual band Circularly Polarised slot Antenna for wireless applications</i>
	<i>5.2 Antenna geometry</i>
	<i>5.3 Measurement and Simulation results</i>
	<i>5.4 Study of surface current and electric field patterns</i>
	<i>5.5 A detailed study of antenna evolution</i>
	<i>5.6 Characteristic mode analysis of the antenna</i>
	<i>5.7 Chapter Summary</i>

The design procedure of a dual band circularly polarized microstrip patch antenna with asymmetric structure is portrayed in this chapter. Slotted structure has been employed to achieve compactness and improvement of the circular polarization characteristics. Extensive parametric analysis has been carried out to investigate various antenna characteristics. The design has been simulated and verified experimentally. Circular polarization characteristics of the antenna is confirmed through characteristic mode analysis. Through the theory of Characteristic Modes, two significant physical quantities, the characteristic currents and the characteristic eigenvalues, are solved. A clear physical insight into the electromagnetic properties of an object is possible through these quantities [1-2]. Here in this work, Characteristic mode analysis is done through the evaluation of characteristic angle and modal significance using simulation software CST [3].

Introduction

As described in the previous chapter, CP radiation may be obtained from patch antennas, if the two orthogonal modes TM₀₁ and TM₁₀ are excited with a 90° phase difference. However, these basic CP patch antennas have very narrow bandwidth. In order to enhance the AR bandwidth of CP patch antennas, various methods are adopted. It is possible to enhance the CP bandwidth by using a modified slot shape, rather than single rectangular slot or crossed slot on a patch antenna [4]. Wide slot CP antennas have many advantages like wide bandwidth, low profile and easy integration with monolithic microwave-integrated circuits [5-7]. Considering the advantages of wide slot circularly polarized antennas, research is going on in this area and many research works have been reported in literature. The excitation of two orthogonal modes with equal amplitude and in-phase quadrature - essential conditions for the generation of circular polarization - are achieved by introducing some perturbations which may be either symmetric or asymmetric into the slot antenna [8] – [21].

Numerous broadband circularly polarized slot antennas have been developed, which have wide impedance and axial-ratio bandwidths by choosing different design methods on patch and ground structures. Literature shows that CP patch antennas with compact size have only small bandwidths. Multi feed stacked patches yield more ARBW but have the disadvantages like higher profile and more complex configuration. CP crossed dipoles are structurally simple but have only moderate CP bandwidth. But CP slot antennas can achieve more AR bandwidth.

Usually these wide slot antennas generate polarization with opposite sense (i.e. RHCP and LHCP) in the front and rear directions. Miniaturised CP antennas yielded less bandwidth. Hence researchers highly concentrate to design wide slot CP antennas which yield high band widths. WS CP antennas tend to occupy larger areas and possess wider CP bands.

Usually in CP patch antennas, in the ground plane, energy cannot be radiated. It is not possible to get two orthogonal electric field components for the generation of CP. The tangential component of the electric field gets attenuated and only normal component is radiated in the ground plane. When the dimensions of the ground plane being made larger than the patch, this effect gets predominated. But the ground plane dimension is minimised, in WS CP antennas. For single feed CP antennas, the relation of dimensions between patch and the ground plane need to be either unity or near to unity. But, when the structure of the ground becomes slotted one, it allows both orthogonal components to be radiated in the ground plane. The radiation pattern of an omnidirectional antenna is in such a way that, it has a having non-directional nature in a given plane of the antenna and a directional pattern in the plane orthogonal to it. Omnidirectional Circularly Polarised Antennas have several applications including Global Navigation Satellite Systems (GNSS), RFID, TT&C modules and WLAN [22]. OCPAs used in GPS applications have enough sky coverage, irrespective of antenna orientation and easy manufacture procedure and low cost besides other advantages of CP antennas [22].

Wide slot CP antenna provide omni directional radiation pattern and such highly beneficial in many areas as stated above. Hence by the

introduction of slots and stubs both in the patch and ground structures with controlled dimensions, ARBW of the omnidirectional CP antennas may also be controlled.

5.1 A Printed Dual band Circularly Polarized Slot Antenna for Wireless Applications

Printed, dual band circularly polarized antenna is presented. Dual band CP antenna1 (DBCPA1) and dual band CP antenna2 (DBCPA2), having the same design but opposite orientations and radiating with opposite senses of circular polarisation are fabricated. Antenna elements include stubs and slots of different shapes both on the top radiating patch and on the bottom ground plane. Significant impedance bandwidth (IBW) and 3 dB axial ratio bandwidth (ARBW) were spanned over two bands for both the antenna prototypes.

5.2 Antenna Geometry

FR4 substrate material with a size of $30 \times 33.5 \times 0.8 \text{ mm}^3$ is selected for the antenna design, which has $\epsilon_r = 4.4$, loss and tangent factor of 0.02 . $\epsilon_{\text{reff}} = (\epsilon_r + 1)/2$. The geometries for compact dual-band CP antennas are depicted in Figures 5.1- 5.2. Figure 5.1a shows the top view of the DBCPA1, wherein the bottom ground plane seen through the substrate is also shown. Figure 5.1b shows the side view of the antenna. Figure 5.1c shows the geometry of DBCPA2, which is the exact mirror image of DBCPA1 in both planes. Figure 5.1d shows the side view of this antenna. Antenna geometry of DBCPA1 is given in Figure 5.2. Figure 5.2a the top feed structure and Figure 5.2b the bottom ground structure. The labels with corresponding dimensions are given in Table 1.

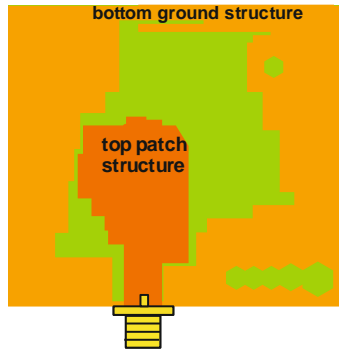


Figure 5.1a: DBCPA1 top view

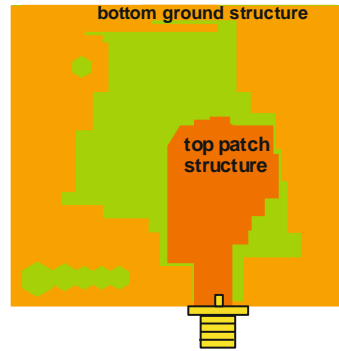


Figure 5.1c: DBCPA2 top view



Figure 5.1b: DBCPA1 side view



Figure 5.1d: DBCPA2 side view



Figure 5.2a: DBCPA1 top feed structure

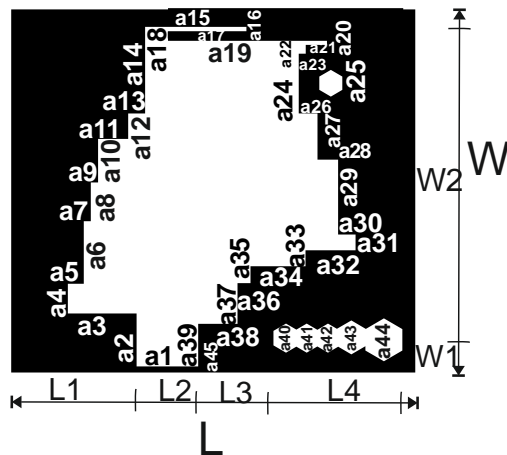


Figure 5.2b: Bottom ground structure

Table 5.1: DBCPA1 labels and dimensions

Label	Value (mm)	Label	Value (mm)	Label	Value (mm)	Label	Value (mm)	Label	Value (mm)
a1	5.10	a16	0.36	a31	1.30	b2	6.20	b17	1.58
a2	4.37	a17	6.50	a32	4.15	b3	1.58	b18	0.57
a3	5.70	a18	0.75	a33	1.32	b4	1.40	b19	1.37
a4	2.46	a19	13.18	a34	4.56	b5	0.35	b20	2.42
a5	1.32	a20	0.33	a35	1.40	b6	1.42	b21	11.71
a6	5.17	a21	1.75	a36	1.10	b7	1.30	b22	2.58
a7	0.58	a22	0.73	a37	3.36	b8	1.78	b23	4.32
a8	3.20	a23	0.59	a38	3.26	b9	1.38	L1	10.40
a9	0.60	a24	4.93	a39	3.52	b10	4.45	L2	5.10
a10	3.60	a25	1.10	a40	2.40	b11	0.50	L3	6.24
a11	2.50	a26	1.55	a41	2.40	b12	2.84	L4	10.69
a12	2.10	a27	3.82	a42	2.40	b13	3.97	W1	2.70
a13	1.40	a28	1.71	a43	2.80	b14	0.73	W2	25.86
a14	7.16	a29	6.18	a44	3.50	b15	2.03	L	33.50
a15	8.40	a30	1.45	b1	3.80	b16	0.31	W	30.00

Feedline has a width of 3.8mm. One of the attractions of this antenna is to give wider bandwidth. The dimensions of bottom ground plane and slot embedded on it determine antenna characteristics [22]. The structures of majority of the antennas in literature are symmetric. This work is an investigation to get better results with asymmetric design strategy.

The impedance matching is achieved by adjusting dimensions and position of the feed line and ground plane. It is readily seen from the return loss characteristics and axial ratio characteristics that the antenna gives circular polarized radiation characteristics in two bands.

Formation of dual band is attributed to peculiarity of the structure, which is described in the 15th stage of evolution of the antenna.

5.3 Measurement and simulation results

5.3.1 Measurement of |S₁₁| and Axial Ratio

The experimental analysis was carried out using Agilent Vector Network Analyser PNAE 8362B. The measured |S₁₁| characteristics and its simulated values in respect of DBCPA1 and DBCPA2 are plotted in Figure 5.3. These plots match each other. Axial ratios measurements of DBCPA1 and DBCPA2 along with simulated values are shown in Figure 5.4. DBCPA1 offered IBW of 4.72 GHz (2.63–7.35 GHz, 94.6%), corresponding ARBW of 2.12GHz (3.62–5.74 GHz, 45.3%) in Band I, IBW of 0.98 GHz(7.86 – 8.84 GHz, 117.4%) corresponding ARBW of 1.82 GHz (7.06 – 8.88 GHz, 22.84 %) in Band II. DBCPA2 offered IBW of 4.79 GHz (2.58–7.37 GHz, 96.28 %), corresponding ARBW of 2.31 GHz (3.57–5.88 GHz, 48.9%) in Band I, IBW of 1.11 GHz (7.78 – 8.89 GHz,133.17 %) corresponding ARBW of 1.69 GHz (7.04 – 8.73 GHz, 21.43%) in Band II. The minimum axial ratios measured are 1.3 dB in Band I and 0.9 dB in Band II. The formation of two bands and the corresponding axial ratio bands are the result of peculiarities of the structure, such that for a wide range of frequencies there exist numerous modes, some are horizontal and some are vertical. There exists phase quadrature between them with equal amplitude. It will be proved in the characteristic mode analysis section.

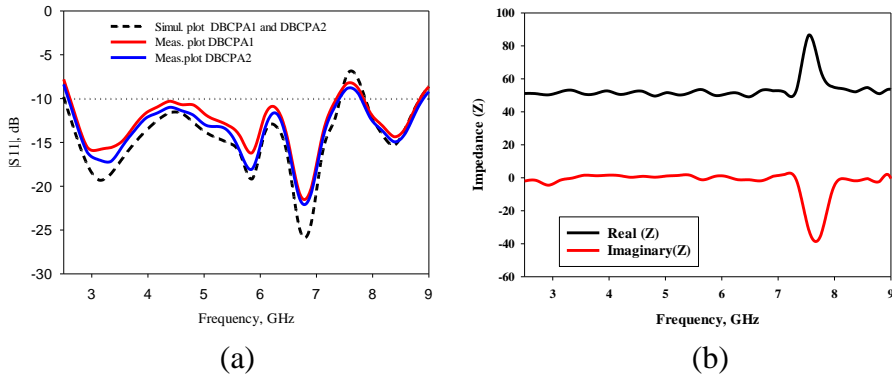


Figure 5.3: (a) Simulated and measured $|S_{11}|$ plots of antennas
(b) Impedance curve of DBCPA1

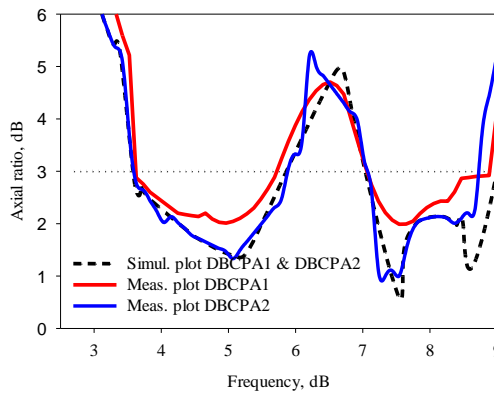


Figure 5.4: Axial ratio plots of DBCPA1 and DBCPA2

5.3.2 Measurement of Gain and Efficiency

Average gain values are measured to be 3.09dBi and 3.2dBi for DBCPA1 and DBCPA2 respectively, in the operating frequency band pertaining to band I. Whereas in band II these values got diminished and the obtained values are 1.51dBi and 1.63dBi for DBCPA1 and DBCPA2 respectively. Peak gain values obtained were 4.0dBi for DBCPA1 and

4.1dBi for DBCPA2 at 6.25 GHz. Gain plots of these antennas are shown in Figure 5.5. The measured antenna efficiency plots are depicted in Figure 5.6. Peak values are observed as 95.94% at 3.4GHz for DBCPA1 and 96.09% at 3.4GHz for DBCPA2 respectively.

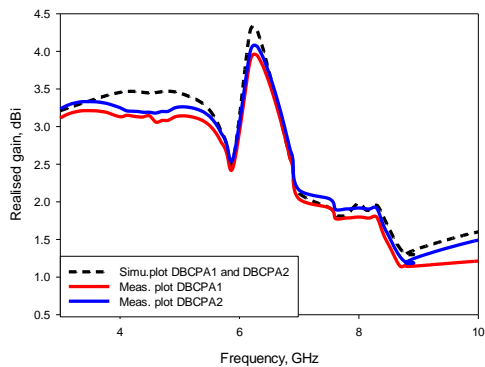


Figure 5.5. Gain plots

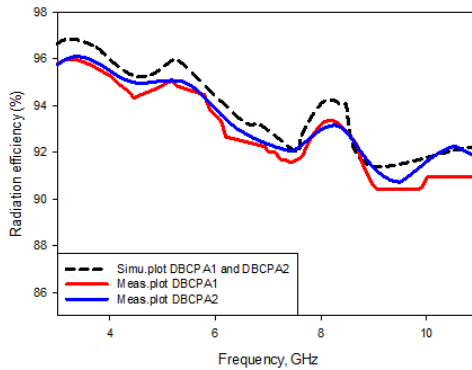
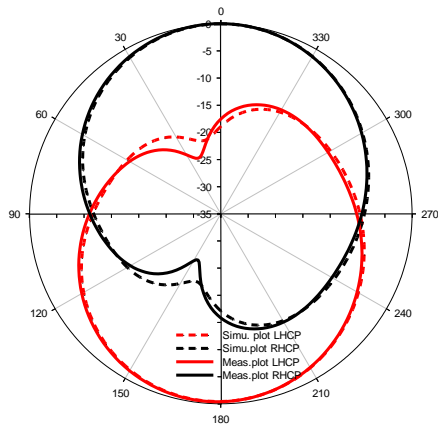


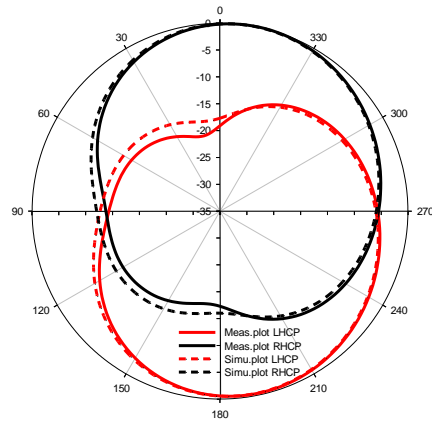
Figure 5.6. % radiation efficiency plots

5.3.3 Radiation pattern

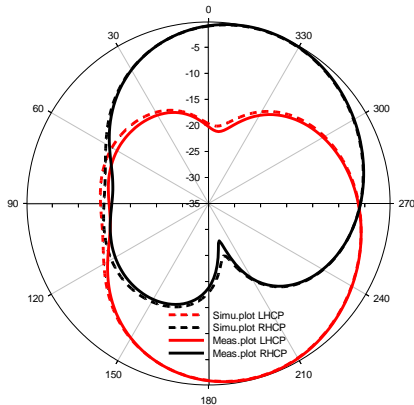
The simulated and measured far-field normalized radiation patterns of DBCPA1 and DBCPA2 in both XZ-plane and YZ-plane at frequencies 4.3GHz, 5.5 GHz and 8.3 GHz are plotted in Figure 5.7 and Figure 5.8 respectively. It is observed that the co-polarization is RHCP for DBCPA1 and LHCP for DBCPA2, whereas the cross-polarisation is LHCP for DBCPA1 and RHCP in the case of DBCPA2. The antenna has a wide half-power beam width at each measured frequency. More than 20dB isolation was observed between corresponding RHCP and LHCP patterns of both DBCPA1 and DBCPA2, for almost all frequencies in two bands.



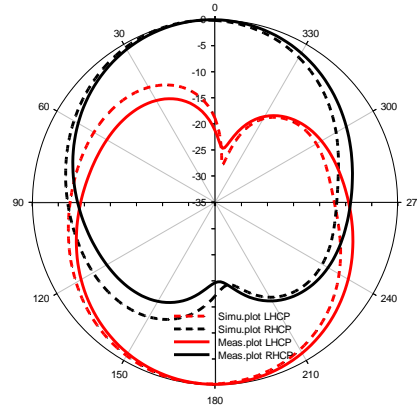
a. At 4.3 GHz, XOZ plane



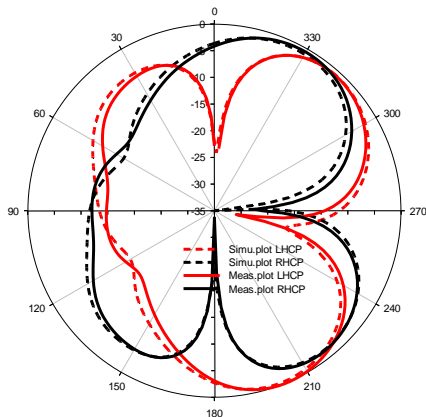
b. At 4.3 GHz, YOZ plane



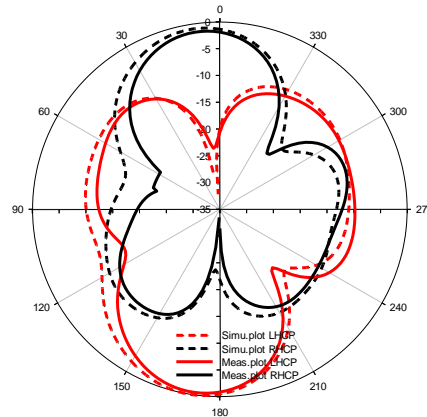
c. At 5.5 GHz, XOZ plane



d. At 5.5 GHz, YOZ plane

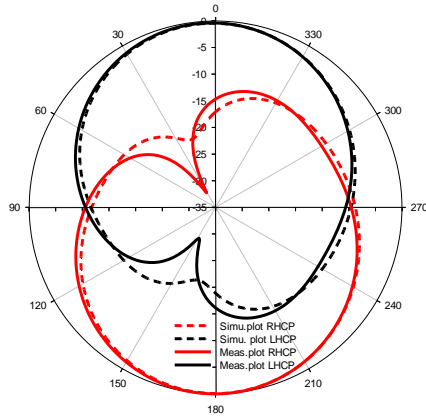


e. At 8.3 GHz, XOZ plane

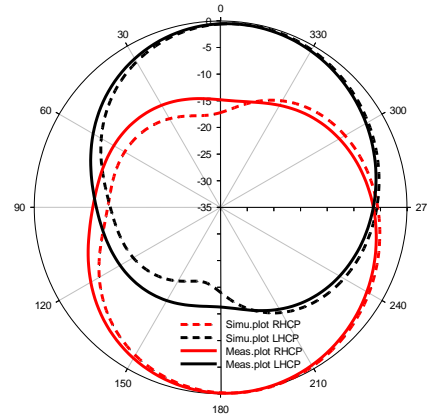


f. At 8.3 GHz, YOZ plane

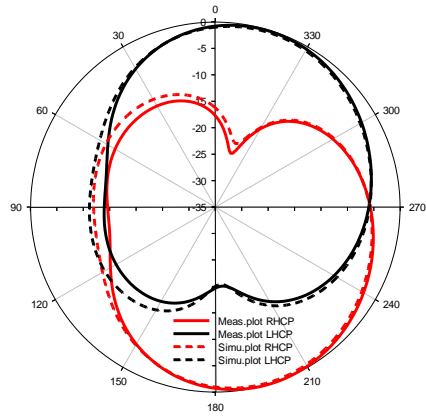
Figure 5.7. Normalised radiation pattern of DBCPA1 in two bands



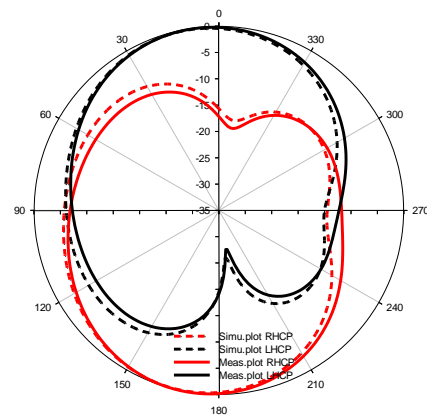
a. At 4.3 GHz, XOZ plane



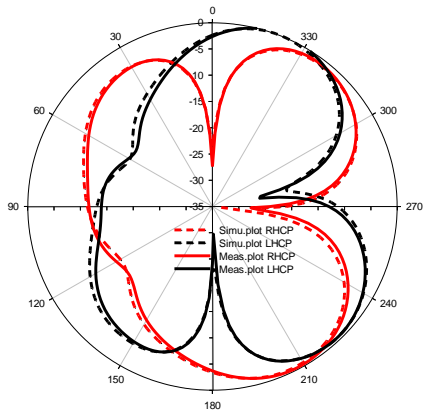
b. At 4.3 GHz, YOZ plane



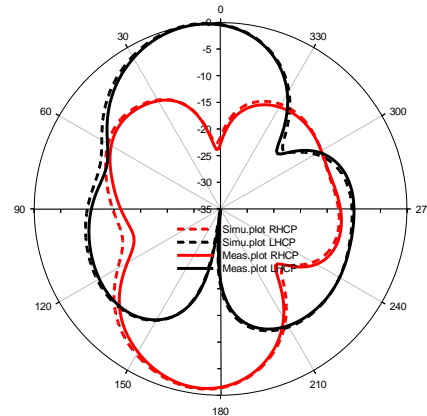
c. At 5.5 GHz, XOZ plane



d. At 5.5 GHz, YOZ plane



e. At 8.3 GHz, XOZ plane



f. At 8.3 GHz, YOZ plane

Figure 5.8. Normalised radiation pattern of DBCPA2 in two bands

5.4 Study of surface current and electric field patterns

1. Surface current pattern on DBCPA1

Each element of the antenna structure has a contribution towards IBW and radiation with circular polarisation at different frequencies. Initially, the location of feed was fixed with utmost care for maximum impedance match. The simulated time varying surface current on the proposed antenna DBCPA1 at regular time phases from 0° to 270° , with an interval of 90° at 4.3 GHz (band I) are depicted in Figure 5.9, at 5.5 GHz (band I) are shown in Figure 5.10 and at 8.3 GHz (band II) are shown in Figure 5.11 respectively.

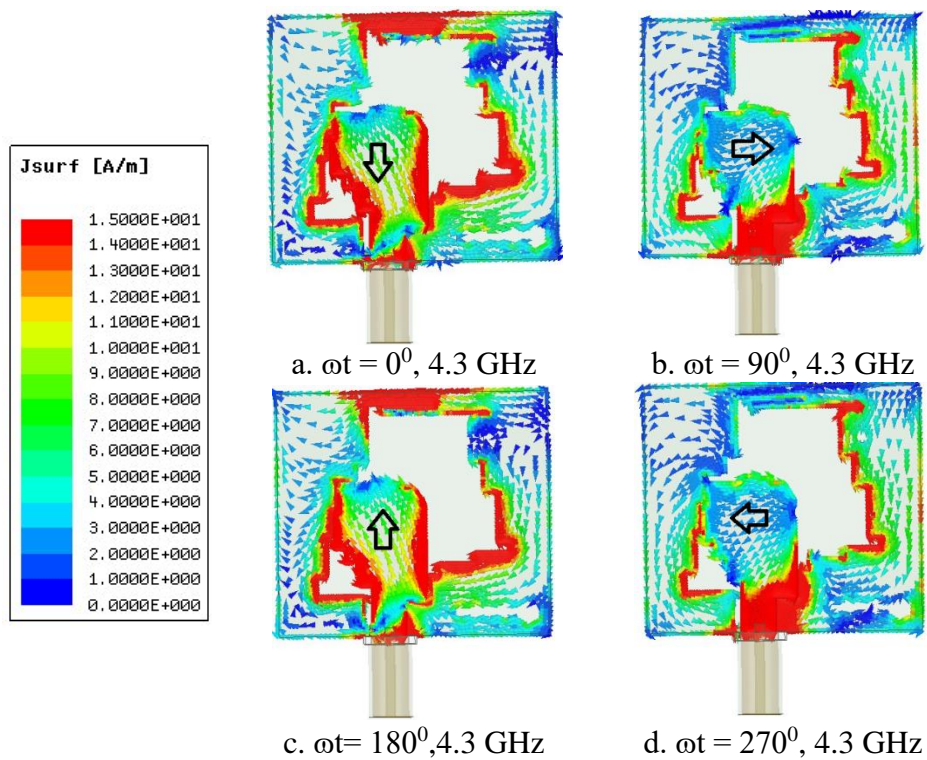


Figure 5.9. Surface current pattern on DBCPA1 at 4.3 GHz (band I)

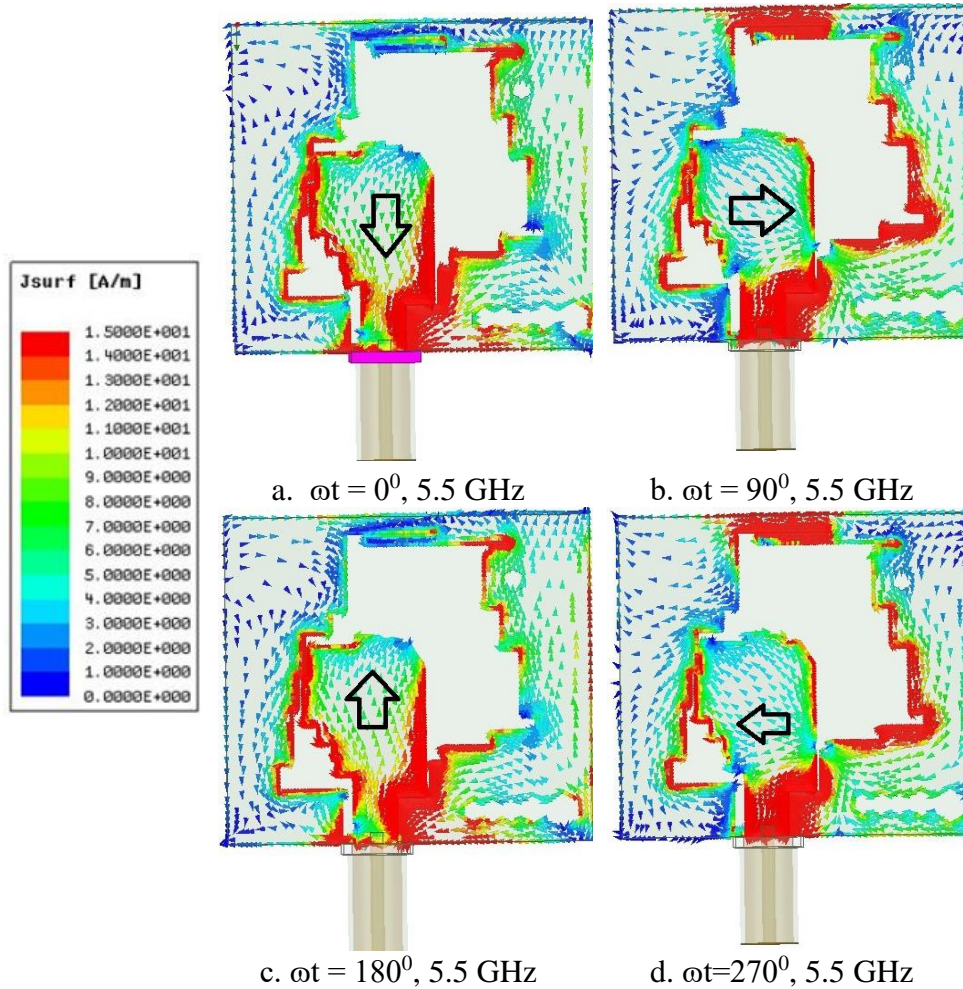


Figure 5.10. Surface current pattern on DBCPA1 at 5.5 GHz (band I)

It can be seen that the surface current distributions at 0° and 180° are equal in magnitude and opposite in direction. Similarly the direction of orientation of surface current vector at 90° phase and 270° phase are equal in magnitude and opposite in direction. This fact is true for all the three resonant frequencies plotted.

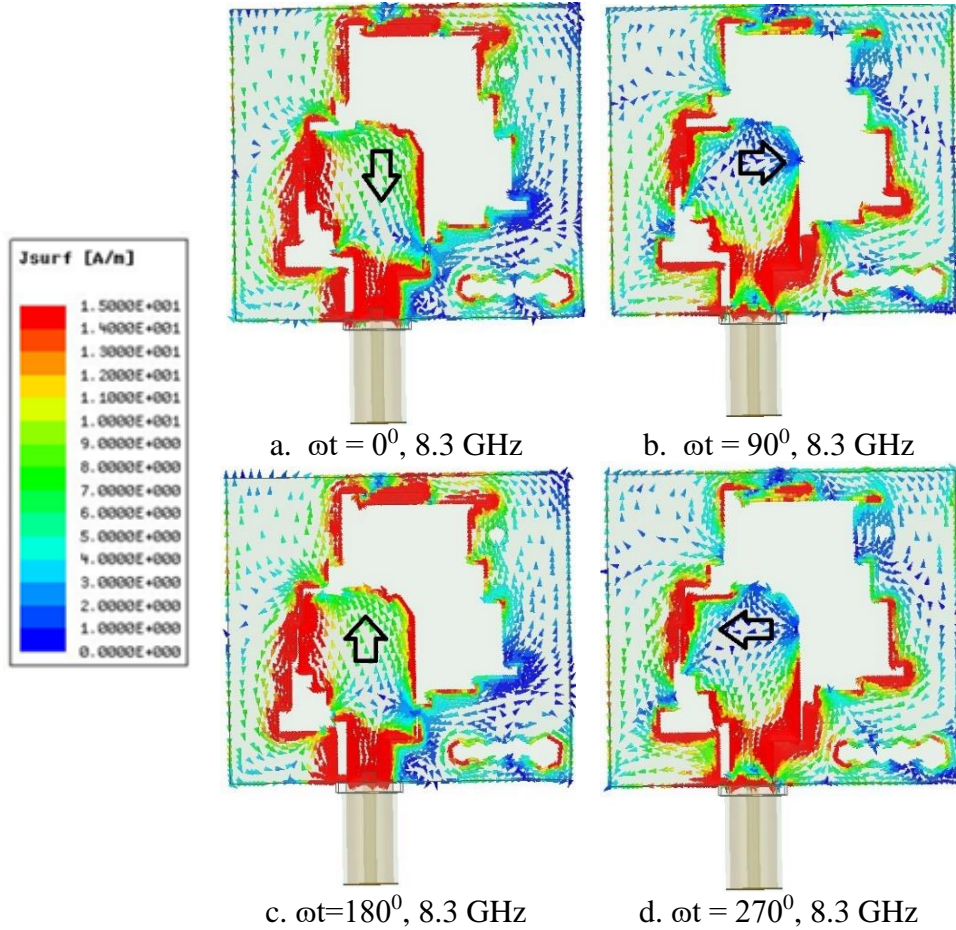


Figure 5.11. Surface current pattern on DBCPA1 at 8.3 GHz (band II)

On the feed structure of DBCPA1, at 0° phase, the surface current flows downwards and at 90° phase, the surface current flows towards right. Similarly, the surface current flows upwards at 180° phase and flows toward left at 270° at all the three frequencies plotted. Hence the surface current flows counterclockwise in the viewer's perspective. Hence, the inference is that DBCPA1 is RHCP in the +Z direction, in both the bands.

2. Electric field pattern on DBCPA1

The electric field behaviour of DBCPA1 is also studied and shown in Figures 5.12 – 5.14. The purpose of this study is to analyse the behavior of the wide slot on the ground plane and its asymmetric structure.

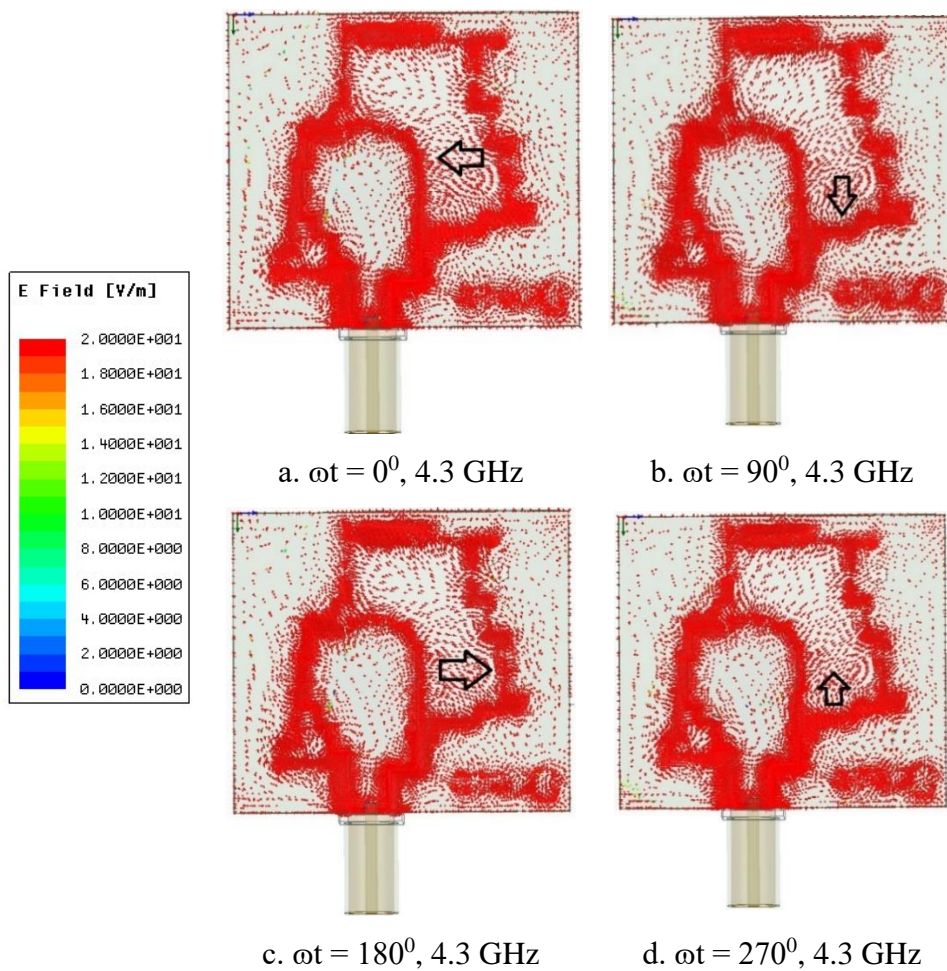


Figure 5.12. Electric field pattern on DBCPA1 at 4.3 GHz (band I)

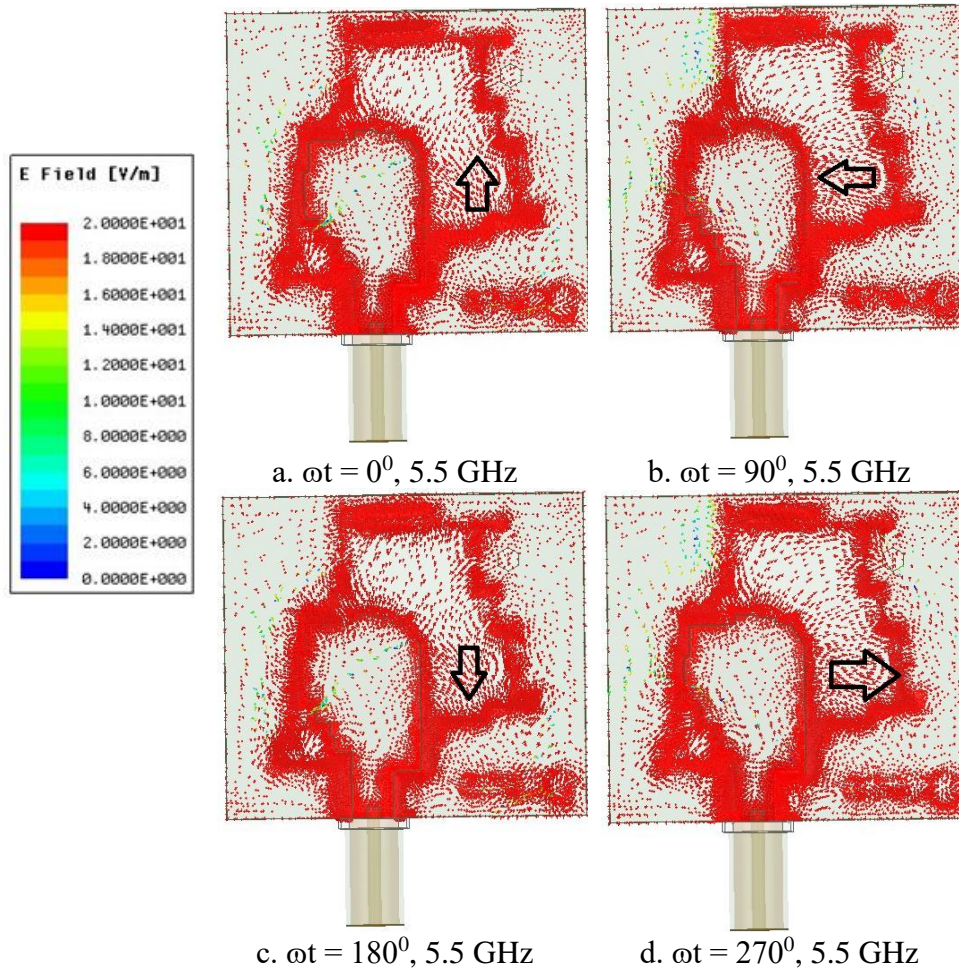


Figure 5.13. Electric field pattern on DBCPA1 at 5.5 GHz (band I)

From the observation of the electric field vector in the ground plane of the antenna, it is understood that at 0° phase, the direction of electric field vector is towards left and at 90° phase it flows downwards. Similarly, the direction of the electric field vector is towards right at 180° phase and flows upwards at 270° when plotted for 4.3 GHz, as depicted in Figure 5.12a – 5.12c. Whereas, when the electric field is plotted for 5.5

GHz, at 00° phase, the direction of electric field vector is upwards and at 90° phase it flows towards left. Similarly, the direction of the electric field vector is downwards at 180° phase and flows towards right at 270° , as shown in Figure 5.13a-5.13c. Both these resonant frequencies belong to the band I.

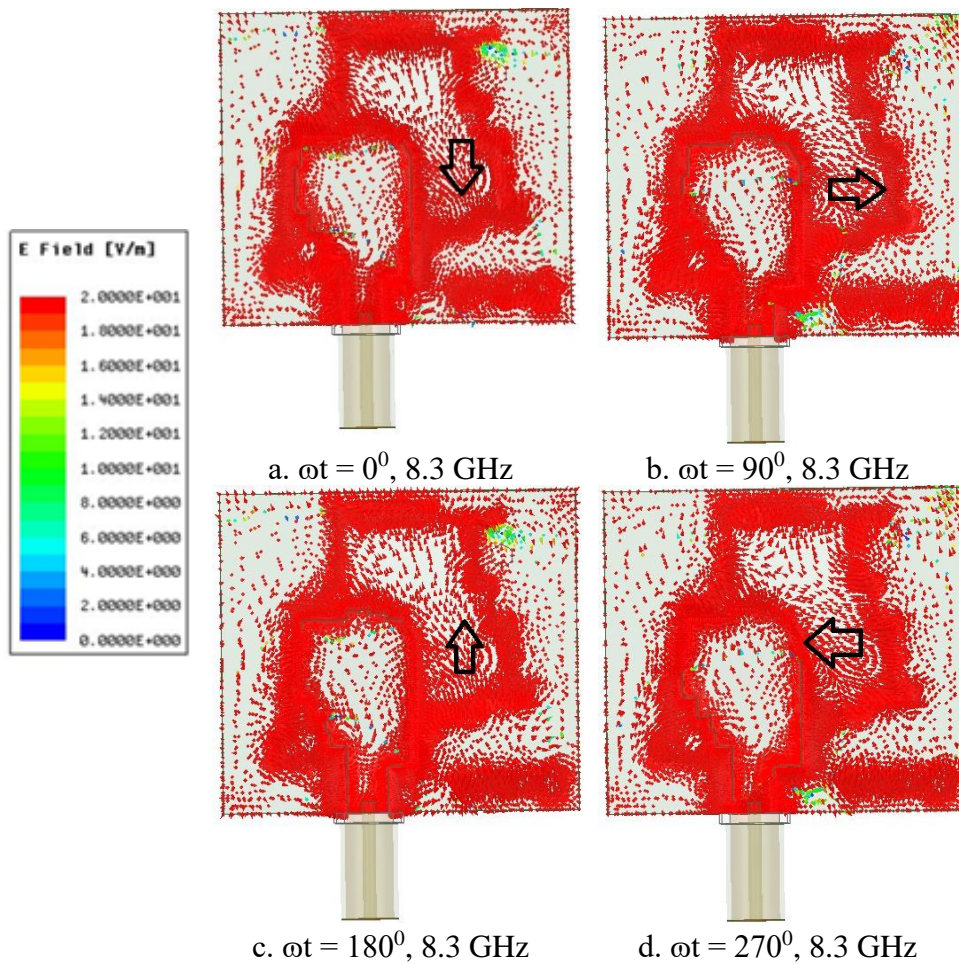


Figure 5.14. Electric field pattern on DBCPA1 at 8.3 GHz (band II)

The electric field pattern is also plotted for 8.3 GHz, which belongs to the second band (band II). At 0° phase, the direction of electric field vector is downwards and at 90° phase it flows towards right. Similarly, the direction of the electric field vector is upwards at 180° phase and flows towards left at 270° , as shown in Figure 14a-14c. The study of the direction of electric fields at various time phases as illustrated above, at all the three resonant frequencies, the direction of rotation is counter clockwise with respect to the -Z direction. Hence, DBCPA1 is RHCP in the +Z direction, and LHCP in the -Z direction in both the bands.

Surface current pattern on DBCPA2

The simulated time varying surface current on DBCPA2 from 0° to 270° , with an interval of 90° at 4.3 GHz (band I) are depicted in Figure 5.15, at 5.5 GHz (band I) are shown in Figure 5.16 and at 8.3 GHz (band II) are shown in Figure 5.17 respectively.

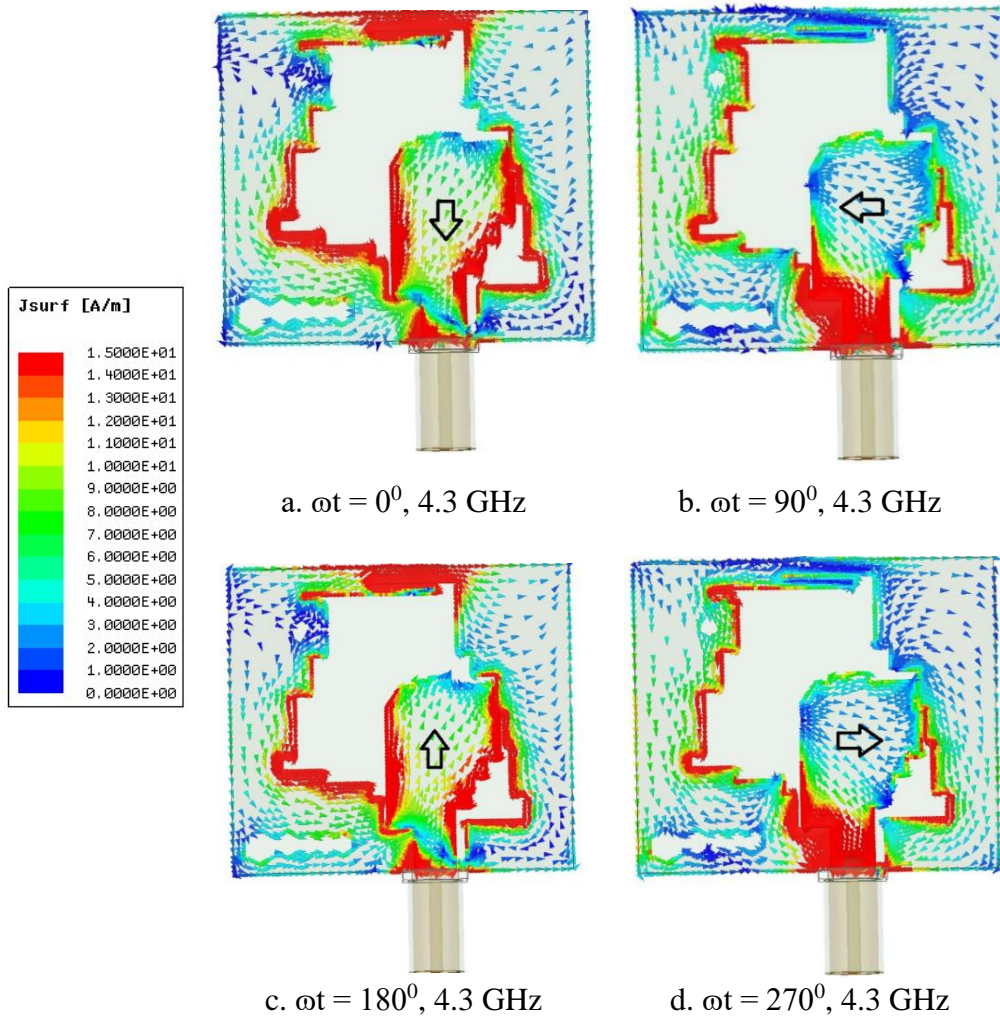


Figure 5.15. Surface current pattern on DBCPA2 at 4.3 GHz (band I)

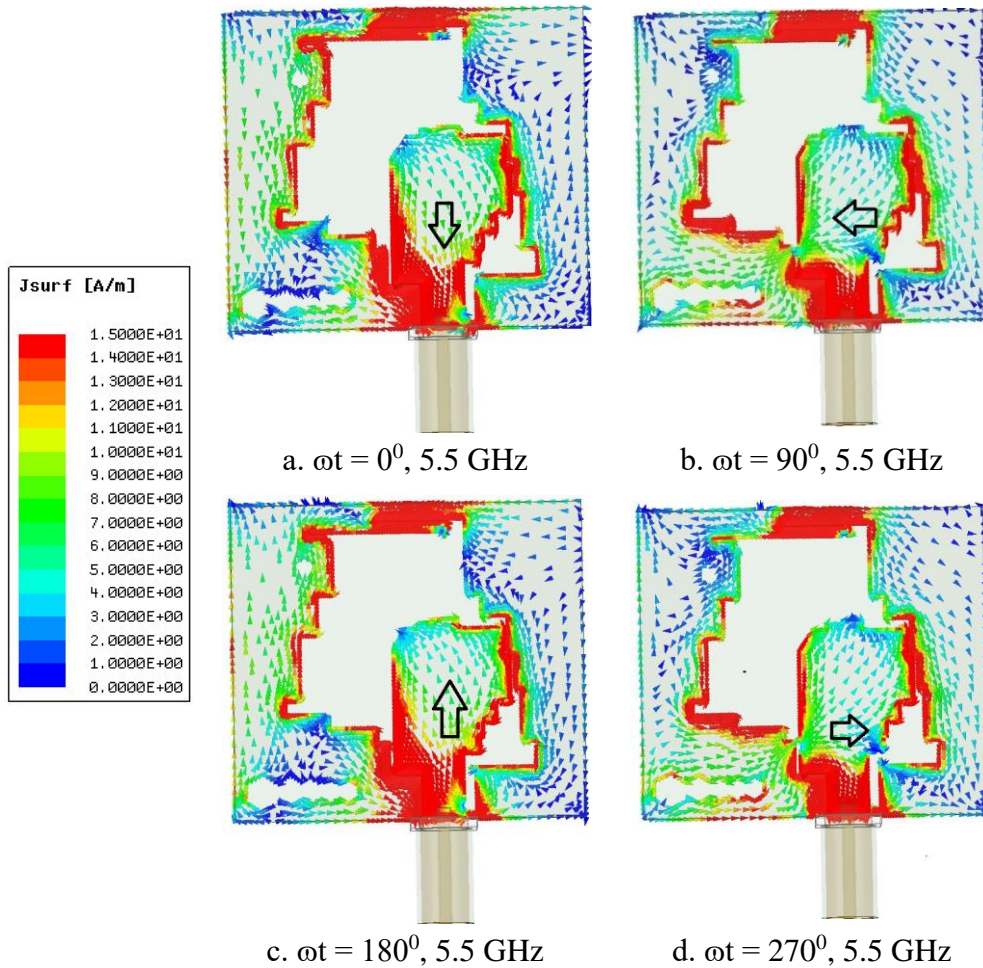


Figure 5.16. Surface current pattern on DBCPA2 at 5.5 GHz (band I)

It can be seen that the surface current distributions at 0° and 180° are equal in magnitude and opposite in phase to that at 90° and 270° at all the three resonant frequencies plotted. At 4.3 GHz and at 5.5 GHz, on the feed structure of DBCPA2, at 0° phase, the surface current flows downwards and at 90° phase, the surface current flows towards left.

Similarly, the surface current flows upwards at 180° phase and flows toward right at 270° .

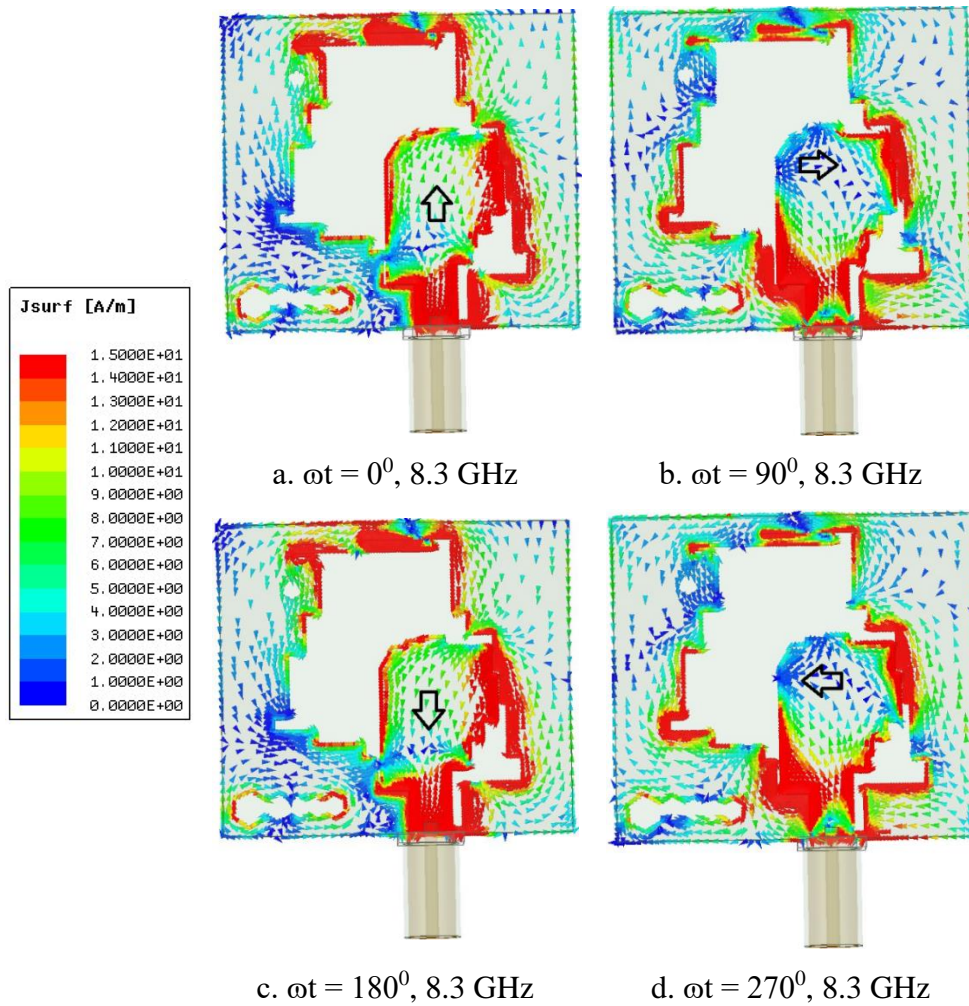


Figure 5.17. Surface current pattern on DBCPA2 at 8.3 GHz (band II)

When the frequency is 8.3 GHz, at 0° phase, the surface current flows upwards and at 90° phase, it flows towards right. At 180° phase it flows downwards and at 270° phase, it flows towards left. Hence the

surface current flows clockwise as far as the viewer is concerned. So, DBCPA2 is LHCP in the +Z direction, in both the bands.

1. Electric field pattern on DBCPA2

The electric field behaviour of DBCPA2 is also studied and shown in Figures 5.18-5.20. The purpose of this study is to analyse the behavior of the wide slot on the ground plane and its asymmetric structure.

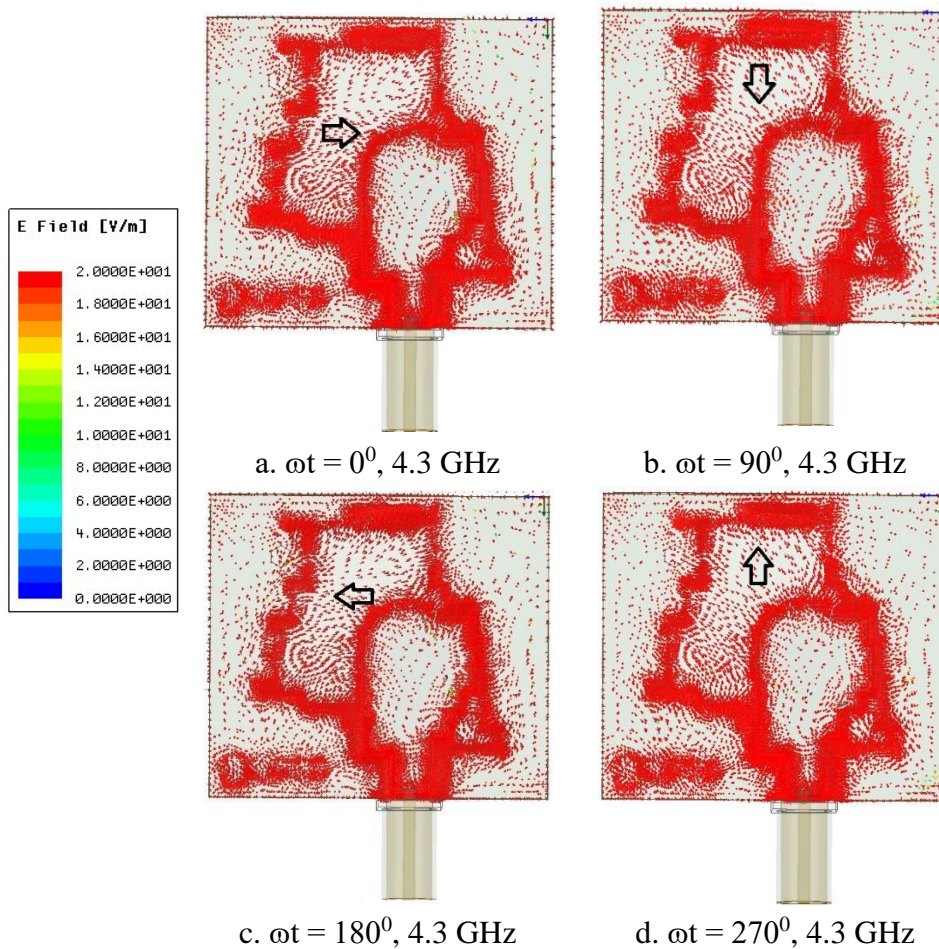


Figure 5.18. Electric field pattern on DBCPA2 at 4.3 GHz (band I)

From the observation of the electric field vector, in the ground plane of the antenna at 4.3 GHz, it is understood that at 0° phase, the direction of electric field vector is towards right and at 90° phase it flows downwards. Similarly, the direction of the electric field vector is towards left at 180° phase and flows upwards at 270° when plotted for 4.3 GHz, as depicted in Figure 5.18a–5.18d.

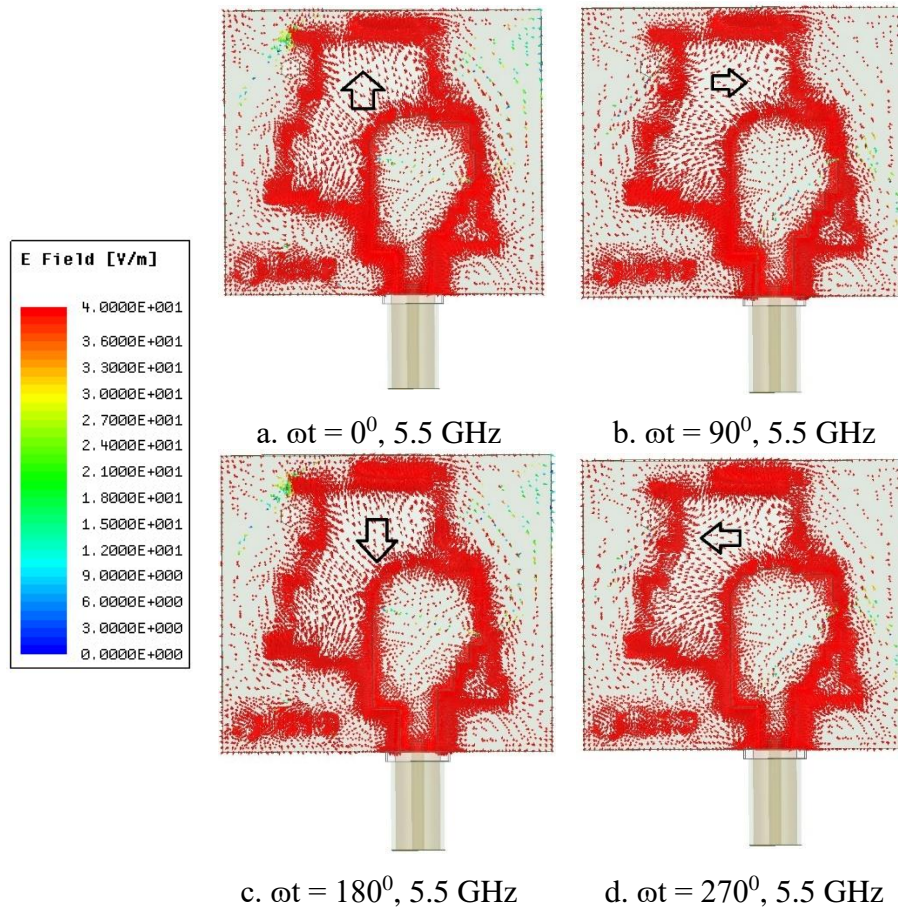


Figure 5.19. Electric field pattern on DBCPA2 at 5.5 GHz (band I)

Whereas, when the electric field is plotted for 5.5 GHz, at 0° phase, the direction of electric field vector is upwards and at 90° phase it flows towards right. Similarly, the direction of the electric field vector is downwards at 180° phase and flows towards left at 270° , as shown in Figure 5.19a-5.19c. Both these resonant frequencies belong to the band I.

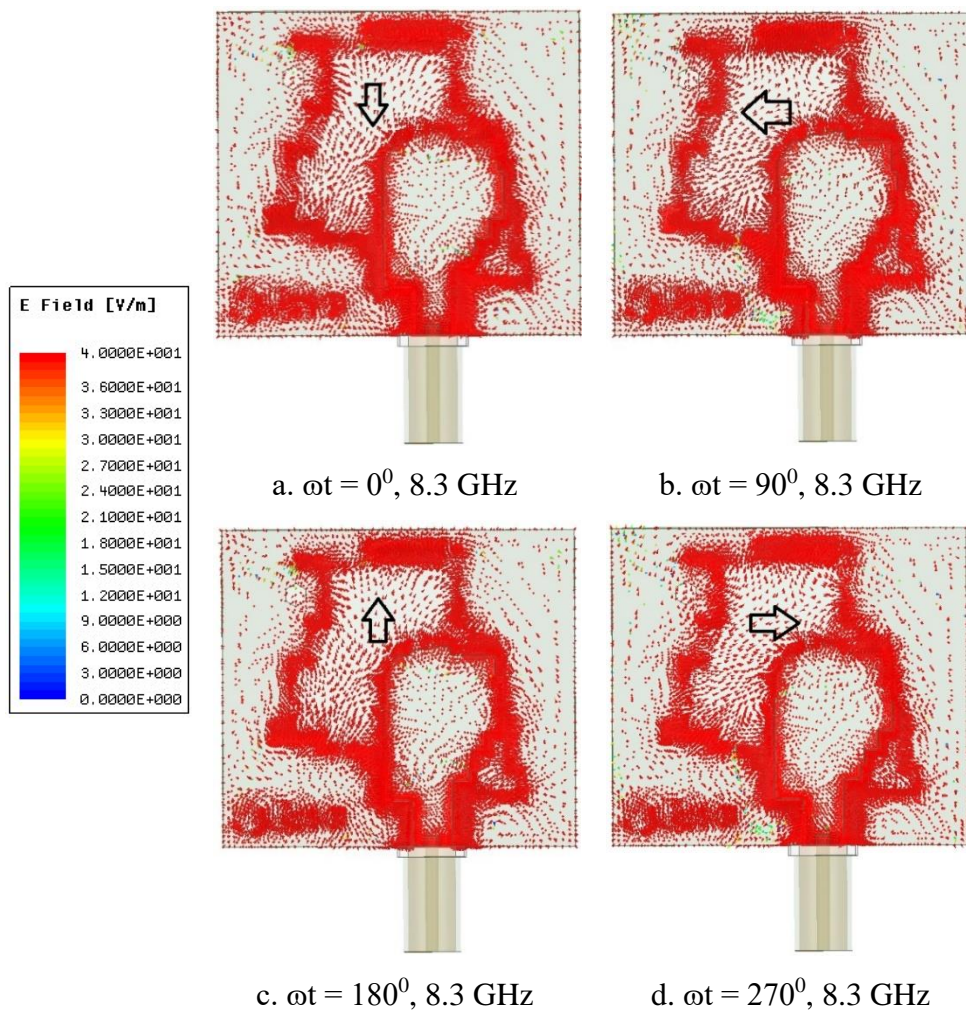


Figure 5.20. Electric field pattern on DBCPA2 at 8.3 GHz (band II)

The electric field pattern is also plotted for 8.3 GHz, which belongs to the second band (band II). At 0° phase, the direction of electric field vector is downwards and at 90° phase it flows towards left. Similarly, the direction of the electric field vector is upwards at 180° phase and flows towards right at 270° , as shown in Figure 5.20a-5.20c. The study of the direction of electric fields at various time phases as illustrated above, at all the three resonant frequencies, the direction of rotation is clockwise with respect to the -Z direction. So, DBCPA2 is LHCP in the +Z direction and RHCP in the -Z direction in both the bands.

5.5 Evolution of the antenna DBCPA1

Stage 1:

It is essential to analyse the circular polarization behavior of the antenna by studying the evolution. It is derived from a rectangular FR4 substrate of dimensions $33.5 \times 33.0 \times 0.8$ mm³. The lower ground plane has the same dimensions. A rectangular copper strip having dimensions 18.17×3.8 mm² is situated on the lower edge of the top surface of the substrate at 11.68 mm away from the origin along Y- direction. From Figure 5.21, it is quite clear that, |S11| is very poor here. However, the axial ratio is below 3 dB from 6.76 GHz to 7 GHz with a minimum value of 1.1 dB at 6.88 GHz. Surface current pattern shows the current on the current is of zero amplitude and that along the feed line is $\lambda/4$.

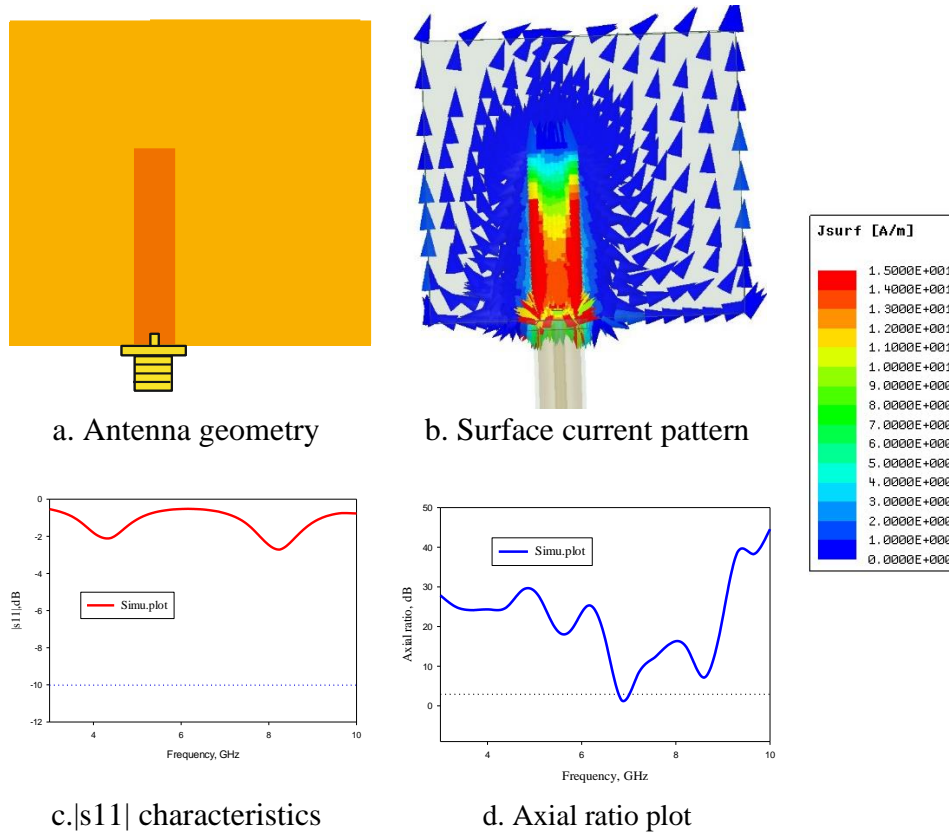


Figure 5.21. Antenna evolution, stage 1.

Stage 2

In the second stage of antenna evolution, a wide rectangular slot of dimensions $23.85 \times 23.38 \text{ mm}^2$ is made on the ground plane of DBCPA1. Corresponding surface current pattern, reflection characteristics and axial ratio plots are depicted in Figure 22. Proceeded with this sort of antenna design technique because slot antennas provide good circular polarization characteristics. By introducing the slot, overall matching is improved. In the lower edge of the characteristics, at 3 GHz, return loss attained a value of -8dB. Axial ratio is well above 3dB.

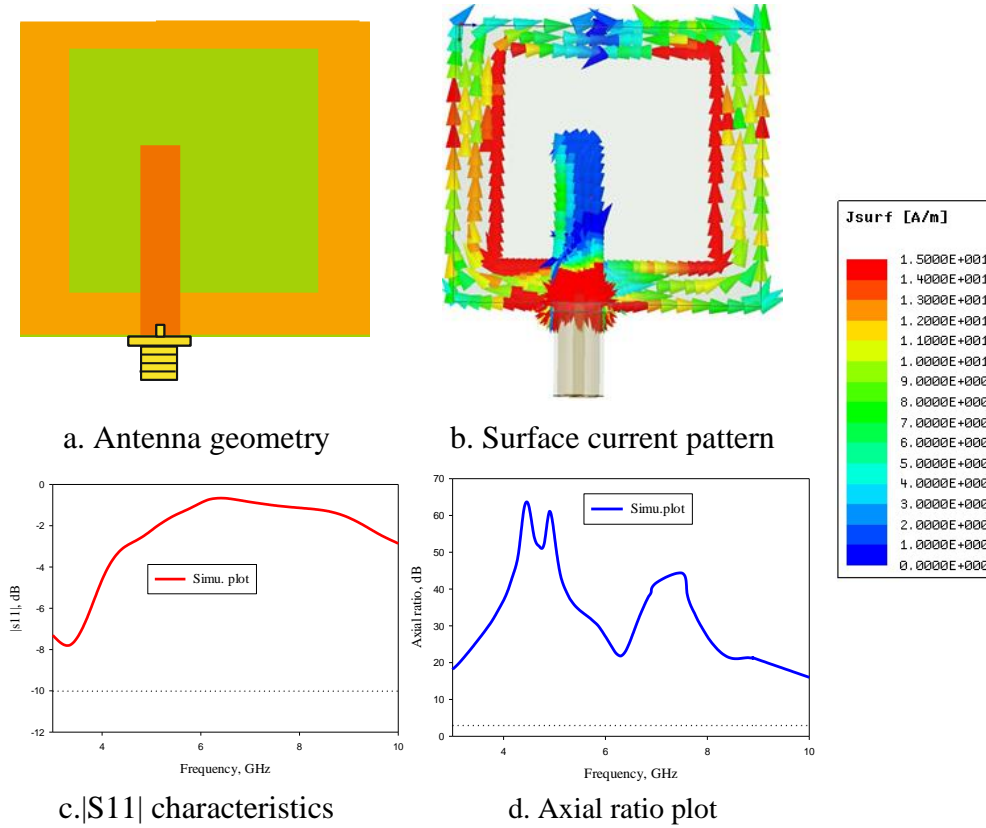


Figure 5.22. Antenna evolution, stage 2.

Stage 3

In the third stage of antenna evolution, three rectangular copper strips are attached to the feed structure. One copper strip of dimensions $13.77 \times 2.56 \text{ mm}^2$ is attached to the right side of the feed structure. Another of dimensions $3.6 \times 0.6 \text{ mm}^2$ to the top side and third one of dimensions $2.02 \times 0.6 \text{ mm}^2$ above that. A small triangular strip of dimensions is removed from the top right corner of the attached right metal strip. As seen from the surface current distribution pattern plotted at 3 GHz shown in

Figure 5.23, improvement is there in axial ratio above 9 GHz. This contribution is made by the newly attached strips of varied dimensions.

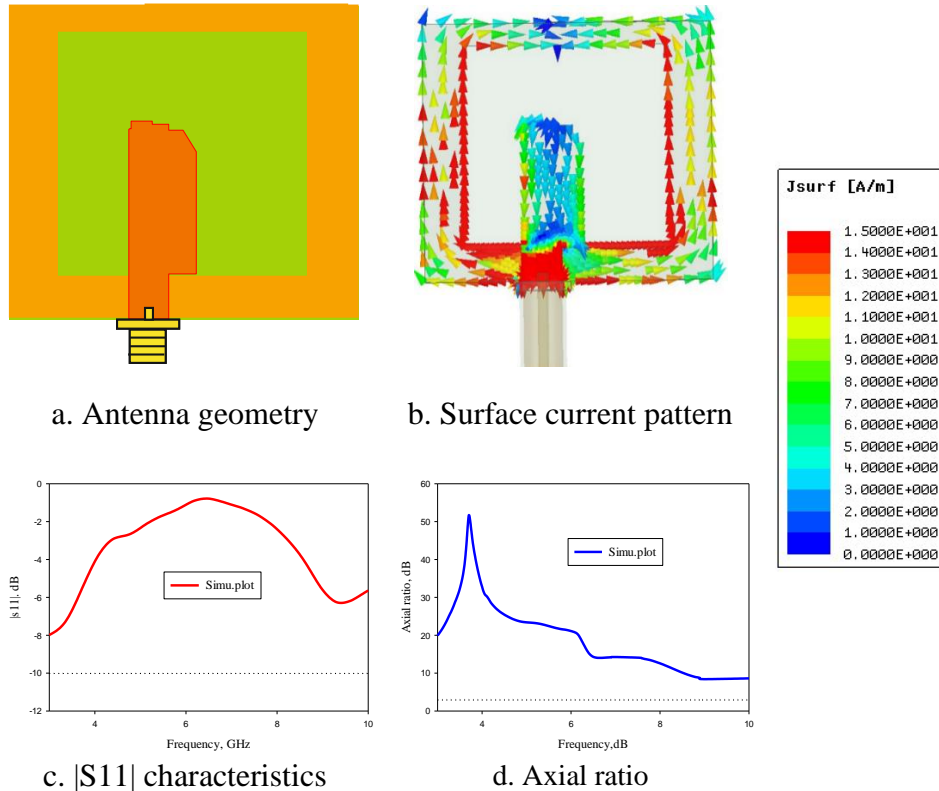


Figure 5.23. Antenna evolution stage 3.

Stage 4

In the fourth stage of evolution of the antenna a metal strip of dimensions $2.84 \times 4.07 \text{ mm}^2$ is attached to the left side of the antenna. As depicted Figure 5.24, no improvement is there in impedance matching; but there is improvement in axial ratio. It falls below 3dB from 6.3 GHz to 6.9 GHz and 7.6 GHz to 9.7 GHz. While plotting the surface current pattern at 8.8 GHz, equal vertical and horizontal currents are readily seen. This contribute to axial ratio less than 3 dB at this frequency.

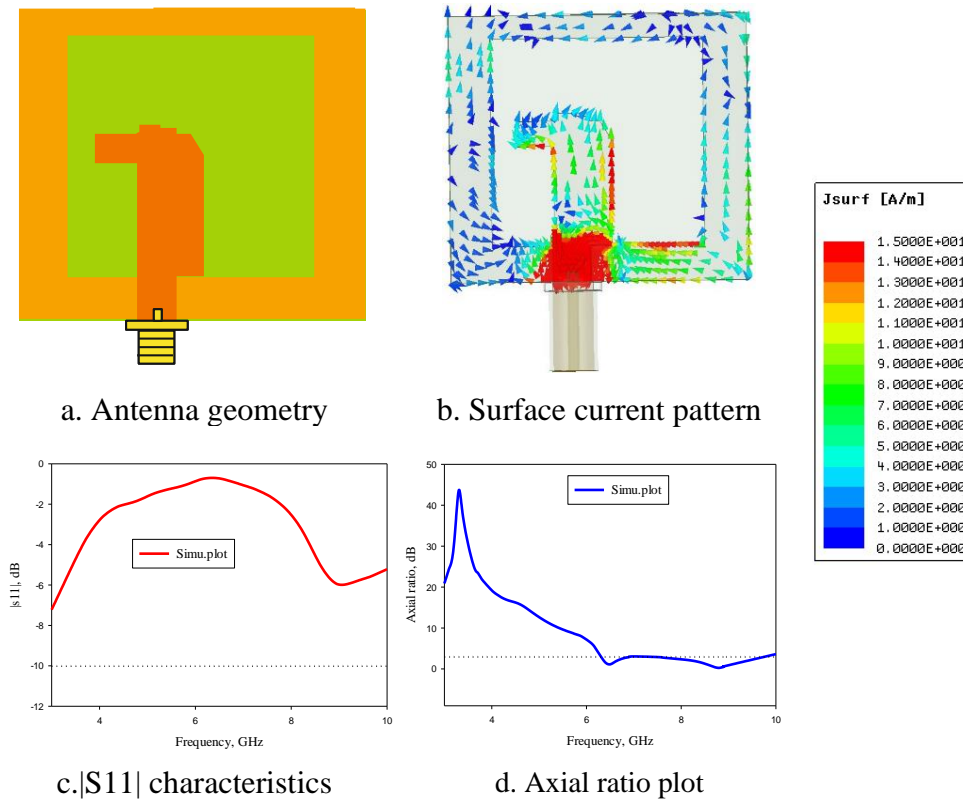


Figure 5.24. Antenna evolution, stage 4.

Stage 5

In the fifth stage of evolution of the antenna, two copper strips; one of dimensions $4.45 \times 4.67 \text{ mm}^2$ and then other of dimensions $1.78 \times 3.29 \text{ mm}^2$ are attached to the left side of the feed structure, just below the previously attached strips in the fourth stage. As shown in Figure 5.25, still no further improvement in impedance matching. The lower value of axial ratio seen in the previous stage being collapsed. It rises up above the 3dB limit. However, this addition is preserved for the sake of final stage improvements in axial ratio and other result.

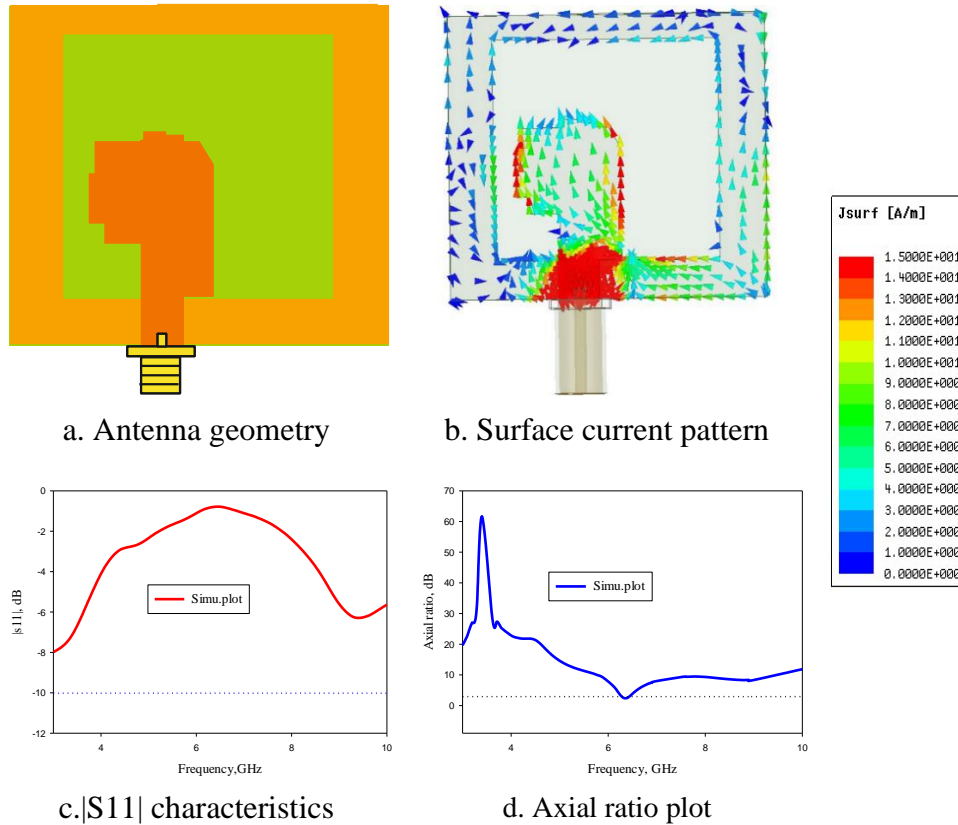


Figure 5.25. Antenna evolution, stage 5.

Stage 6

In the sixth stage of evolution of the antenna, as in the previous stage, no enhancement in return loss characteristics. Two more metallic strips were attached below to the previously added strips; one having the dimensions of $1.4 \times 1.58 \text{ mm}^2$ and the other of $1.42 \times 1.93 \text{ mm}^2$. These added strips have no contribution to the improvement of return loss characteristics and axial ratio. Rather, the contribution will be clear in the later stages. Hence these strips are kept intact. From the surface current

pattern plot at 8.8 GHz, vertical components do not balance the horizontal components. As such the axial ratio is well above 3 dB.

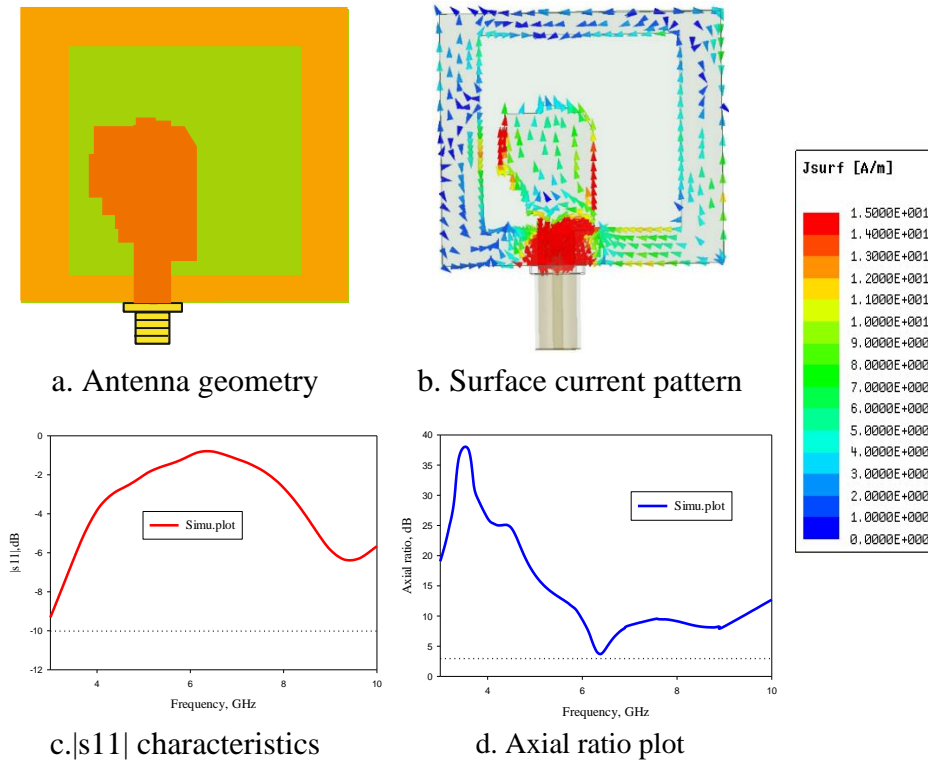


Figure 5.26. Antenna evolution, stage 6.

Stage 7

In the seventh stage of evolution, a rectangular slot was introduced just beneath the feed line. This slot is much wider than the width of the top feed line. Due to the introduction of this slot matching is improved both in the lower and upper ends of the entire band, as shown in the Figure 5.27.

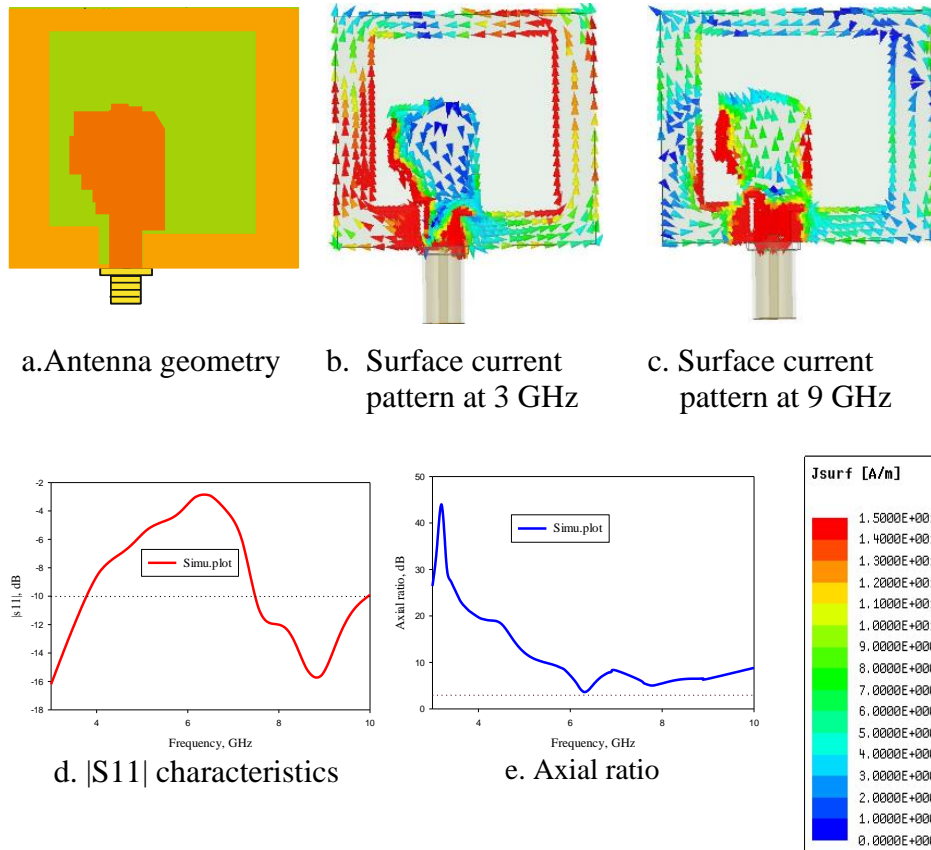


Figure 5.27. Antenna evolution, stage 7.

Matching in the lower side is contributed by peripheral edges of wide slot on the ground, newly introduced slot on the ground and left edge of the top feedline structure. Unfortunately, the axial ratio value is still large. From the surface current pattern plotted at 3 GHz, equal vertical and horizontal currents are not seen. Hence it does not exhibit any circular polarization features. At 9 GHz, matching is provided by right and left edges of the top feed structure and lower and left edges of

wide slot ground plane and newly introduced slot on the ground plane. No circular polarization characteristics at 3 GHz and 9 GHz.

Stage 8

In the eighth stage of evolution, a rectangular strip having dimension of was added at the top right corner of the ground slot and also a small slot of dimension $1.16 \times 1.9 \text{ mm}^2$ was introduced at the top border of the ground plane.

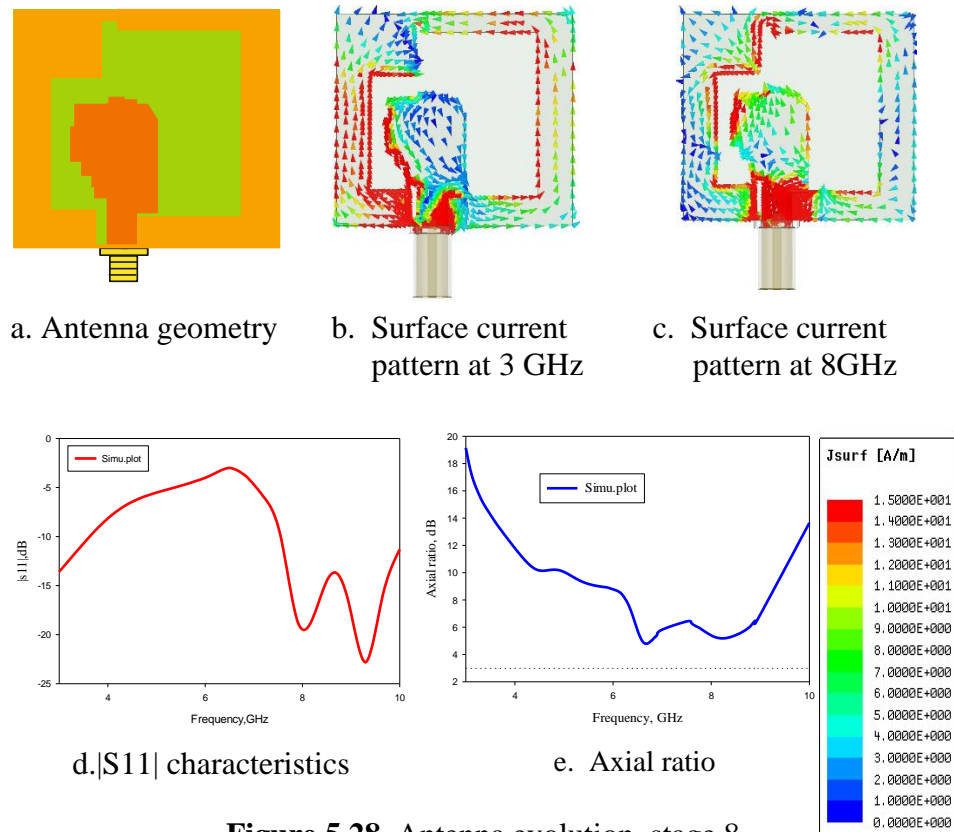


Figure 5.28. Antenna evolution, stage 8.

Figure 5.28 shows that there is sufficient impedance matching in the bands 2.6 GHz to 3.6 GHz and 7.5 GHz to 10.6 GHz. At 3GHz, surface current vector concentrates more on the left border of the ground plane and along the border edges except the vertical edge of the newly introduced rectangular strip. Surface current vector concentrates along the edges of the top feed structure. At 8 GHz, there is minimum current intensity over the right border of the ground plane. But more impedance matching from 7.5 GHz to 10.6 GHz. However, the axial ratio is above 3dB and no circular polarization characteristics so far.

Stage 9

In the ninth stage of evolution, a rectangular strip of dimensions $2.1 \times 5 \text{ mm}^2$ was added just below the added strip of the previous stage. Figure 5.29d reveals that there is not that much improvement in the impedance bandwidth. The lower and upper portions of the reflection characteristics remain more or less the same. Whereas the axial ratio curve falls below 3 dB from 6.58 to 6.76 GHz. This fact is made more clear by the surface current patterns plotted at 3 GHz and 6.7 GHz as seen in Figure 5.29. At 6.7 GHz, vertical and horizontal surface currents are counter balanced as they are equal in magnitude and opposite in direction. This fact can be well established using field pattern diagram in the ground plane wide slot. At 8.3 GHz, the axial ratio is just above 3dB.

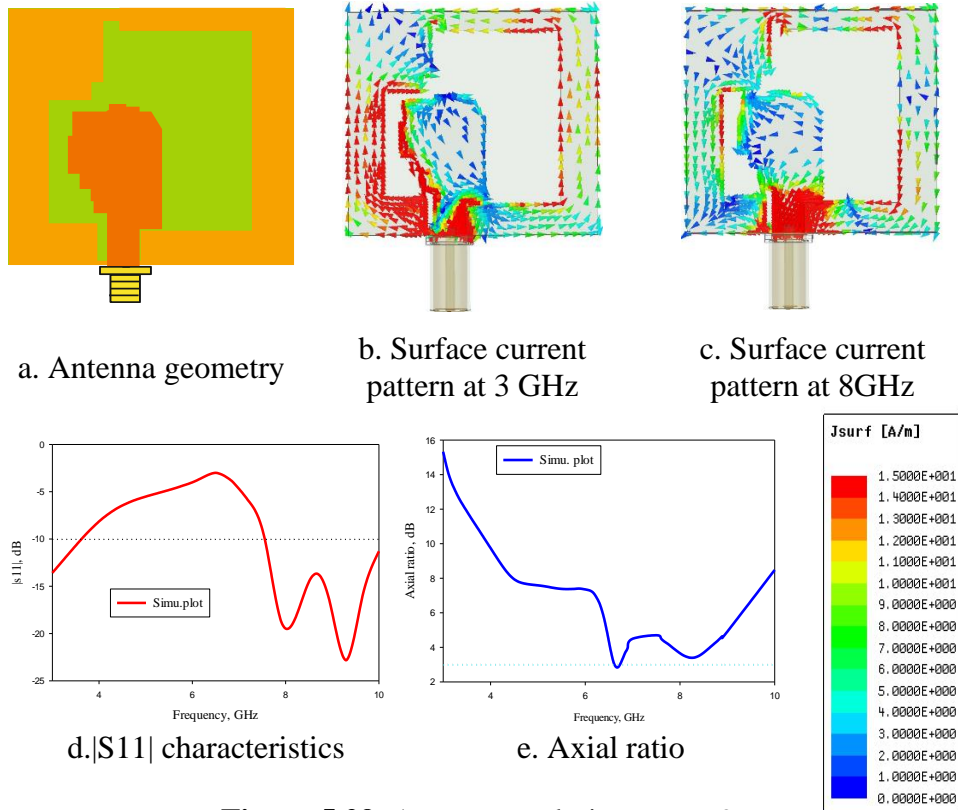


Figure 5.29. Antenna evolution, stage 9.

Stage 10

In the tenth stage of evolution, a vertical strip of dimensions $3.6 \times 0.6 \text{ mm}^2$ was added to the left side of the ground plane just beneath the previously added strip. Also another strip of dimensions $6.75 \times 2 \text{ mm}^2$ was added just to the left of this strip. Matching decreased at 3 GHz and got improved between 7.8 GHz to 10.6 GHz. Surface current patterns plotted at 6.4 GHz and 8.3 GHz as shown in the Figure 5.30, justify the axial ratio below 3 dB from 6.2 GHz to 6.76 GHz and from 7.37 GHz to 8.73 GHz.

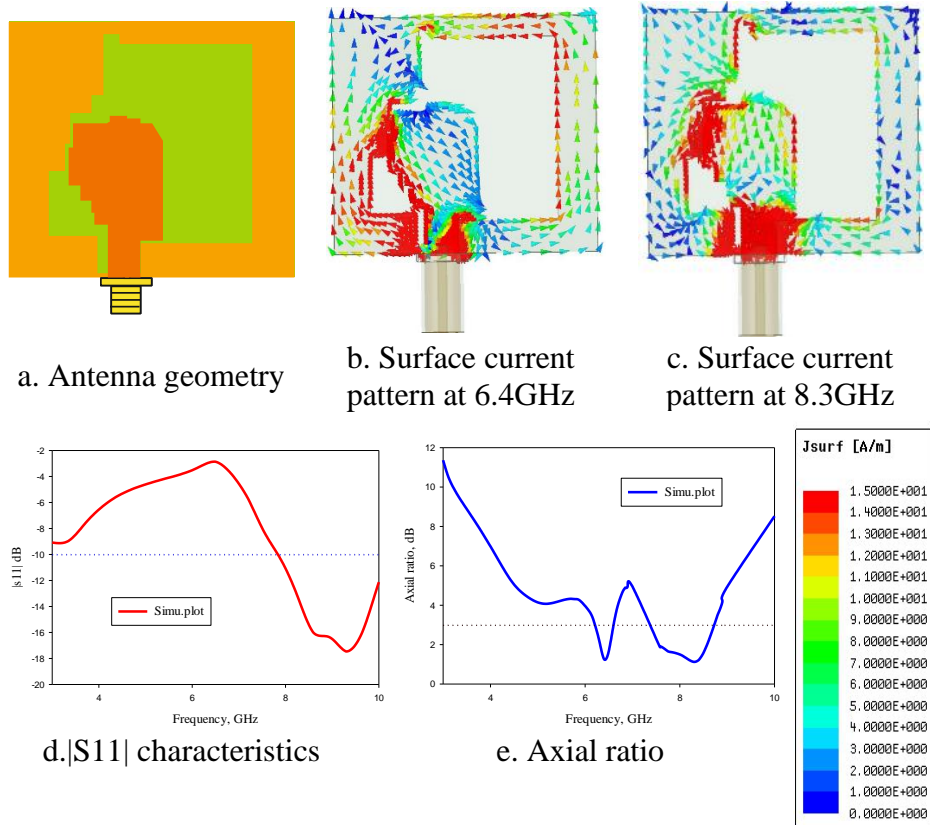


Figure 5.30. Antenna evolution, stage 10

Stage 11

In the eleventh stage of evolution, a vertical strip of dimensions $5.16 \times 1.32 \text{ mm}^2$ was added to the left side of the ground plane just beneath the previously added strip. As shown in Figure 5.31d, matching slightly improved at 3 GHz and enhanced between 7.6GHz to 10.4 GHz. Surface current patterns plotted at 6.5 GHz and 8.3 GHz as shown in the Figure 5.31, justify the axial ratio below 3 dB from 6.2 GHz to 6.76 GHz and from 7.5 GHz to 8.2 GHz. These curves indicate that the addition of the rectangular strip in this stage has no considerable changes in the

performance. It can be seen that at the end of the antenna development the combined effect of all the elements cannot be neglected.

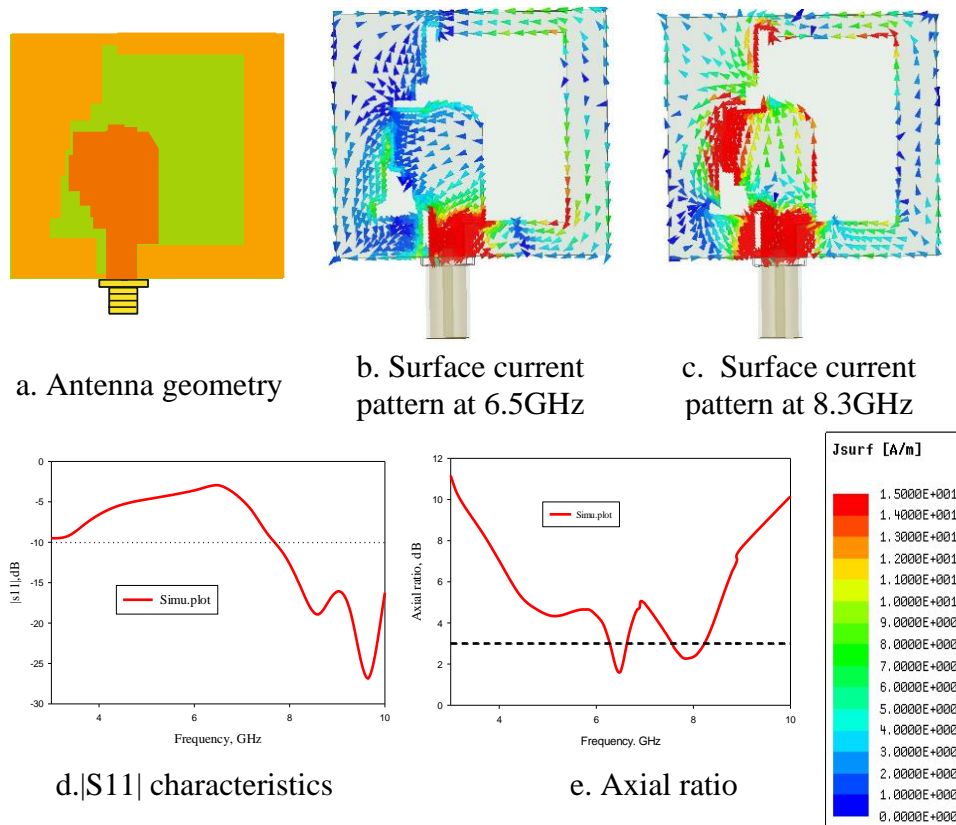


Figure 5.31. Antenna evolution, stage 11

Stage 12

In the twelfth stage of evolution, a rectangular strip of dimensions $6 \times 1.4 \text{ mm}^2$, was added at the top left portion of the ground plane. As shown in Figure 5.32, the improvements in return loss characteristics and axial ratio curve are not considerable. No significant changes are observed in surface current patterns plotted at 6.5 GHz and 8 GHz. Still this newly attached portion is kept intact for a better contribution.

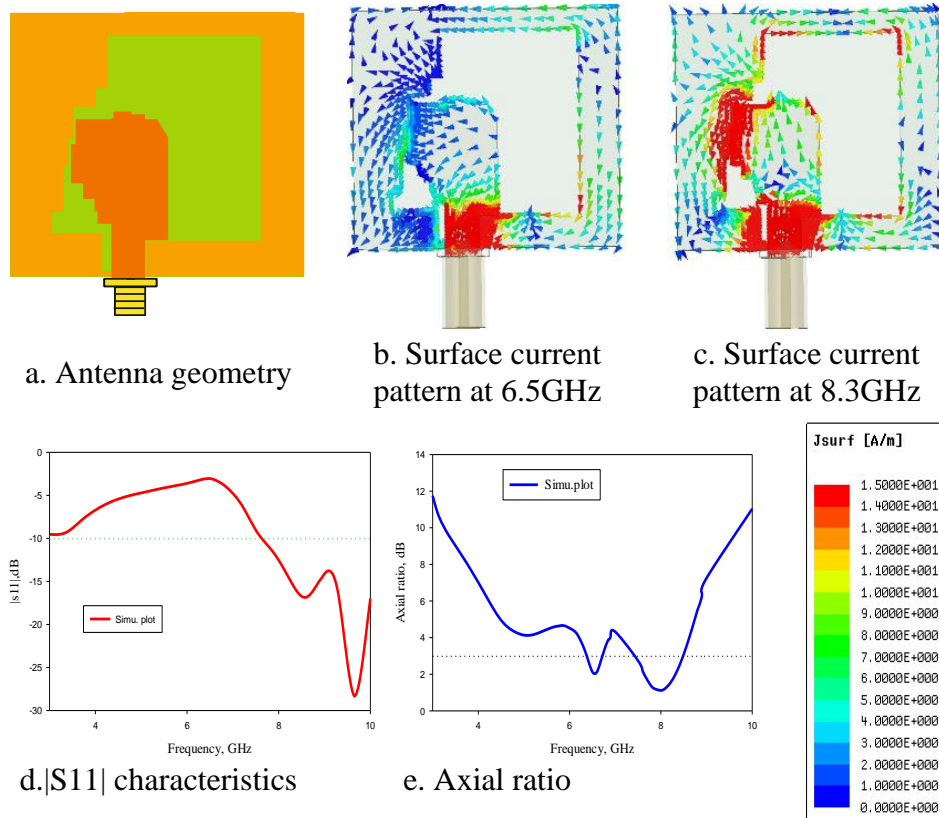


Figure 5.32. Antenna evolution, stage 12

Stage 13

In the thirteenth stage of evolution, two rectangular slots; one of dimensions $1.16 \times 1.9 \text{ mm}^2$ (slot1) and another of dimensions $0.38 \times 6.5 \text{ mm}^2$ (slot2) were added at the top border of the ground plane. Large current densities are observed around the newly introduced horizontal slot2. As shown in Figure 5.33, slight improvements in IBW is observed. Lower edge of the band shifted to 7.6 GHz. 3 dB axial ratio bandwidth ranges from 5.75 GHz to 6 GHz with a minimum value of 1.3 dB at 5.9 GHz and 7.53 GHz to 8.44 GHz, with a minimum value of 1.54 dB at 8 GHz. Surface current patterns are plotted at 3 GHz, 5.9 GHz and at 8 GHz.

Feeble current density is observed over the structure at 5.9 GHz except at some portions. However, the horizontal and vertical orientations justify the axial ratio value below 3 dB, at 5.9 GHz. Whereas intense current densities observed equal in vertical and horizontal directions at 8GHz. Hence 3 dB axial ratio bandwidth is more centered around 8 GHz.

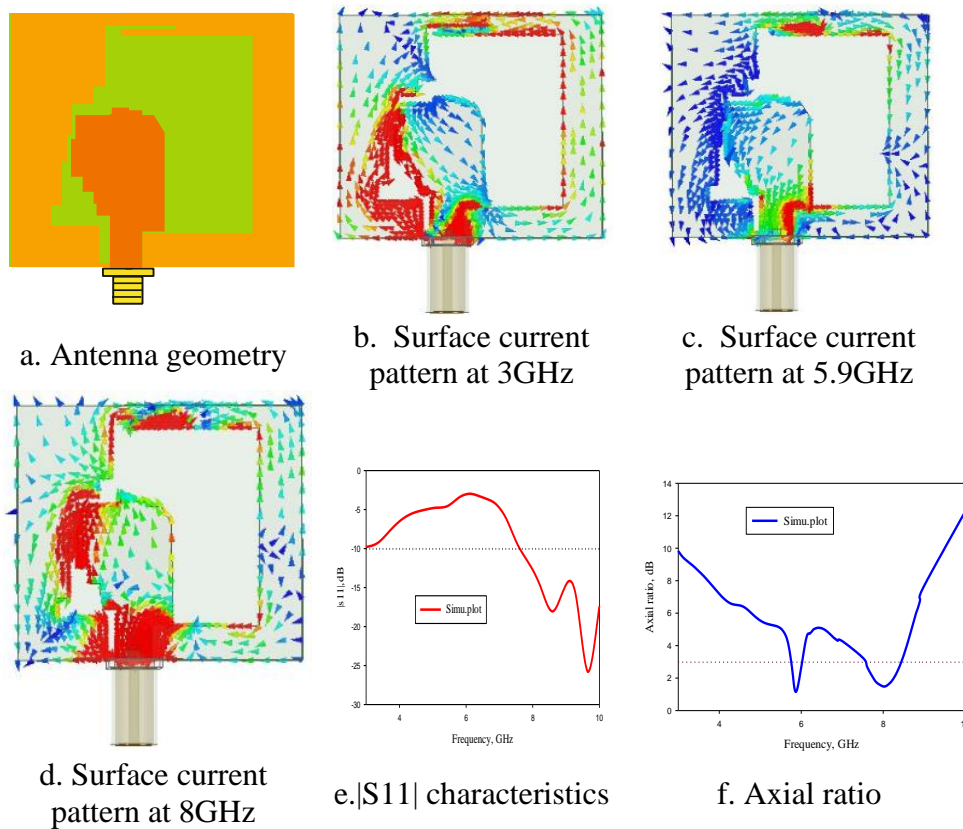


Figure 5.33. Antenna evolution, stage 13

Stage 14

In the fourteenth stage of evolution, a rectangular strip of dimensions $3.36 \times 9.79 \text{ mm}^2$ was introduced at the bottom right corner of the existing border ground plane. AS in Figure 5.34, noticeable improvements

in reflection characteristics as well as axial ratio curve are observed. Surface current patterns are plotted at 3 GHz, 5.5 GHz and at 7 GHz. At 3 GHz, horizontal current density is more than the vertical one. Whereas at other frequencies horizontal current densities counter balance vertical current densities all over the structure. Contribution of the newly introduced strip is at higher frequencies. Horizontal surface currents have large intensities at higher frequencies as seen in the figure. As such 3dB axial ratio bandwidth has been improved and ranges from 4.7 GHz to 5.7 GHz and 6.75 GHz to 7.4 GHz.

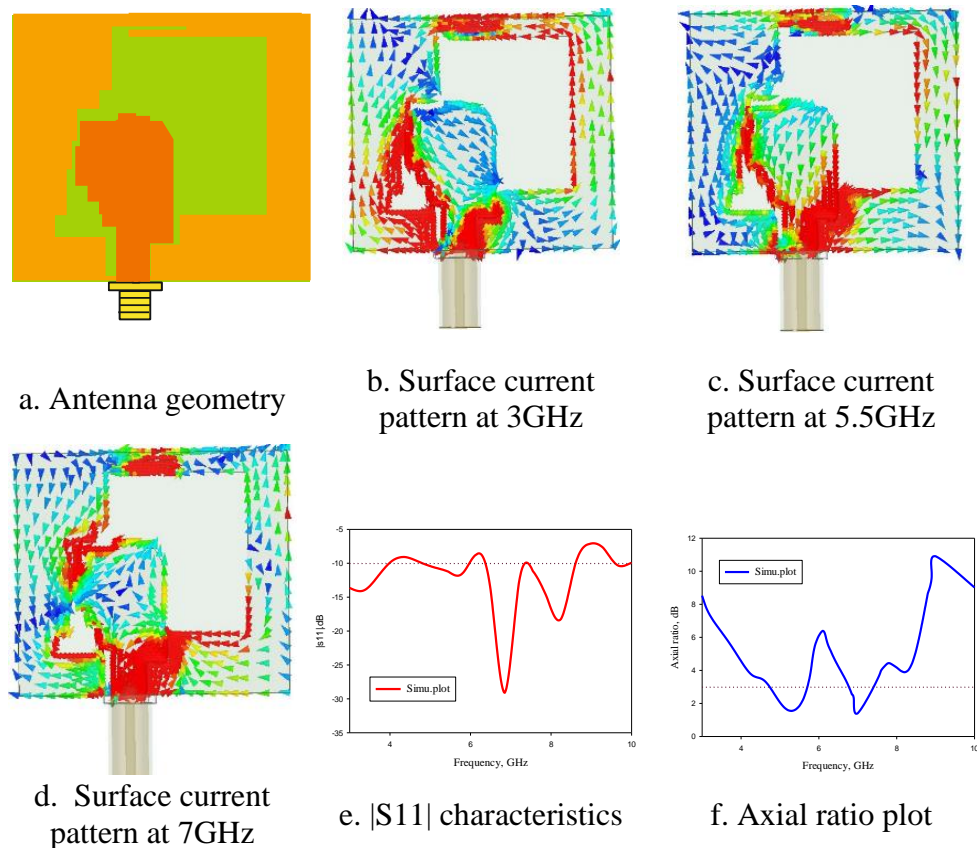


Figure 5.34. Antenna evolution, stage 14

Stage 15

In the fifteenth stage of evolution, a rectangular strip of dimensions $1.28 \times 8.65 \text{ mm}^2$ was added at the right bottom corner portion of the ground plane. As depicted in Figure 5.35, there is a drastic improvement in the return loss characteristics.

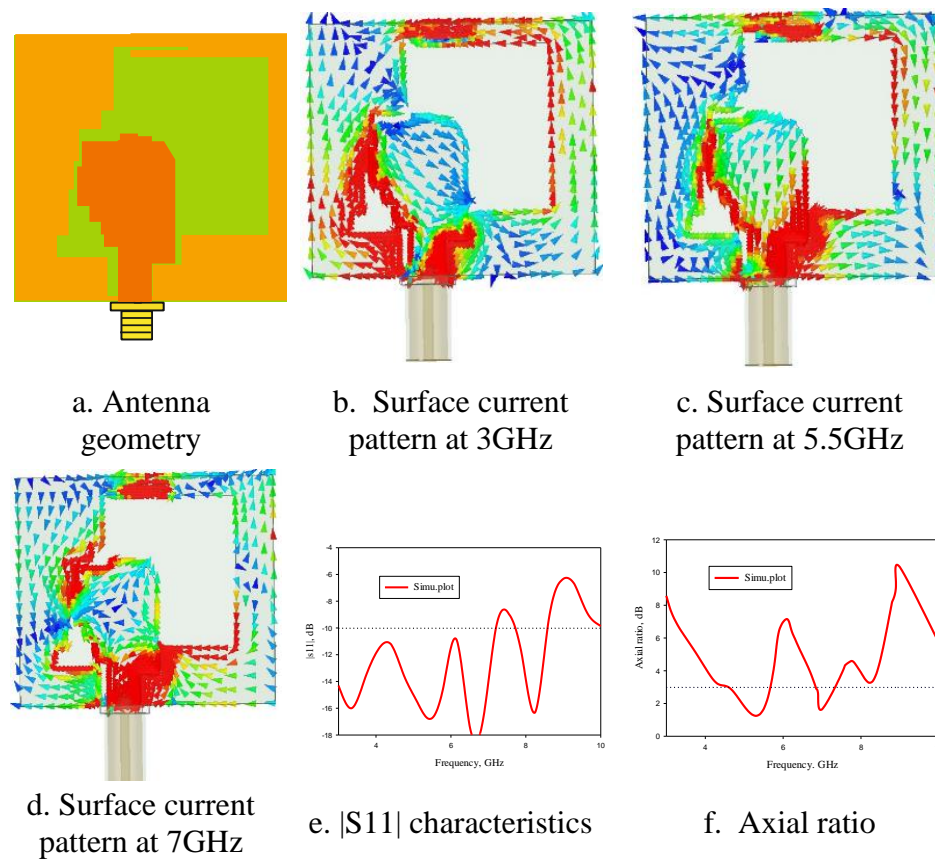


Figure 5.35. Antenna evolution, stage 15

Antenna has a good impedance matching in the band from 3 – 7.2 GHz and from 7.66 to 8.57 GHz. Also, there are two 3 dB axial ratio

bands. One band is from 4.6 GHz to 5.66 GHz and the other is from 6.81 GHz to 7.31 GHz. Surface current patterns are plotted in Figures 5.35b - 5.35d. It can be seen that the introduced rectangular strip improves both reflection and circular polarisation characteristics of the antenna.

Stage 16

In the sixteenth stage of evolution, three rectangular strips were added to the ground structure. One strip of dimensions $0.73 \times 4.13 \text{ mm}^2$ at the top right corner, another of dimensions $4.93 \times 4.71 \text{ mm}^2$ just below that and a third one of dimensions $1.32 \times 4.15 \text{ mm}^2$ at the bottom right corner. By doing so bandwidths, both impedance and axial ratio are improved as in Figure 5.36. Here two bands are seen in the impedance bandwidth diagram. One band is from 3 GHz to 7.18 GHz and another is from 7.71 GHz to 8.79 GHz. The bands are slightly modified. Resonant frequencies in the first band are 3GHz, 5.8GHz and 6.5GHz. Resonant frequency in the second band is 8.2 GHz. Width of the first band slightly reduced by 0.02 GHz and that of the second band is increased by 0.17 GHz. 3 dB axial ratio bands are 4.13 GHz to 5.98 GHz in band1 and 6.63 GHz to 7.36 GHz in band2.

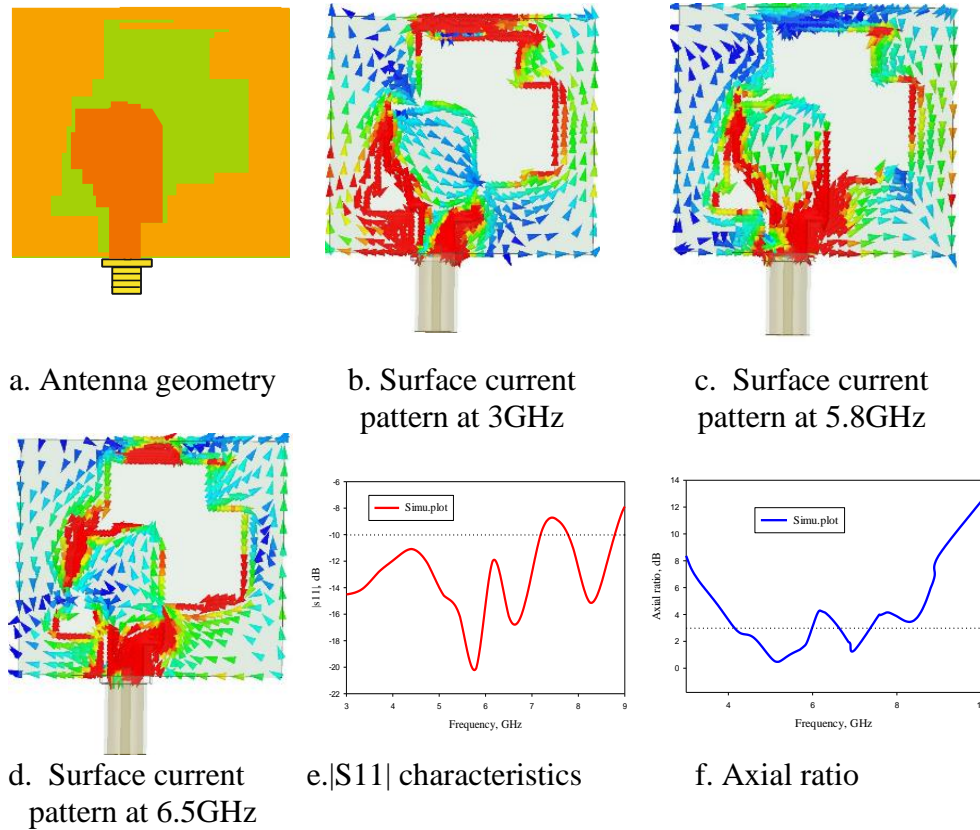


Figure 5.36. Antenna evolution, stage 16

Stage 17

In the seventeenth stage of evolution, one rectangular strip of dimensions $3.8 \times 3.16 \text{ mm}^2$ was added at right border of the bottom ground plane, just below the top strip added in the previous stage. As depicted in Figure 5.37, changes are seen in the $|S_{11}|$ and axial ratio curves as seen. First band is seen from 3 GHz to 7.25 GHz and the second band is seen from 7.75 GHz to 8.75 GHz. Impedance bandwidth of the first band is increased by 0.07 GHz and that of the second band is the same as in the previous stage. The surface current distribution diagram

shows that the newly introduced strip has an effect in the lower band. The 3 dB axial ratio band is from 4 GHz to 6 GHz in band1 and 6.73 GHz to 8.4 GHz in band 2. Hence 3 dB ARBW improvement of 0.33 GHz can be seen in band 1 and 0.94 GHz can be seen in band2, when compared to the structure in the just previous stage of evolution.

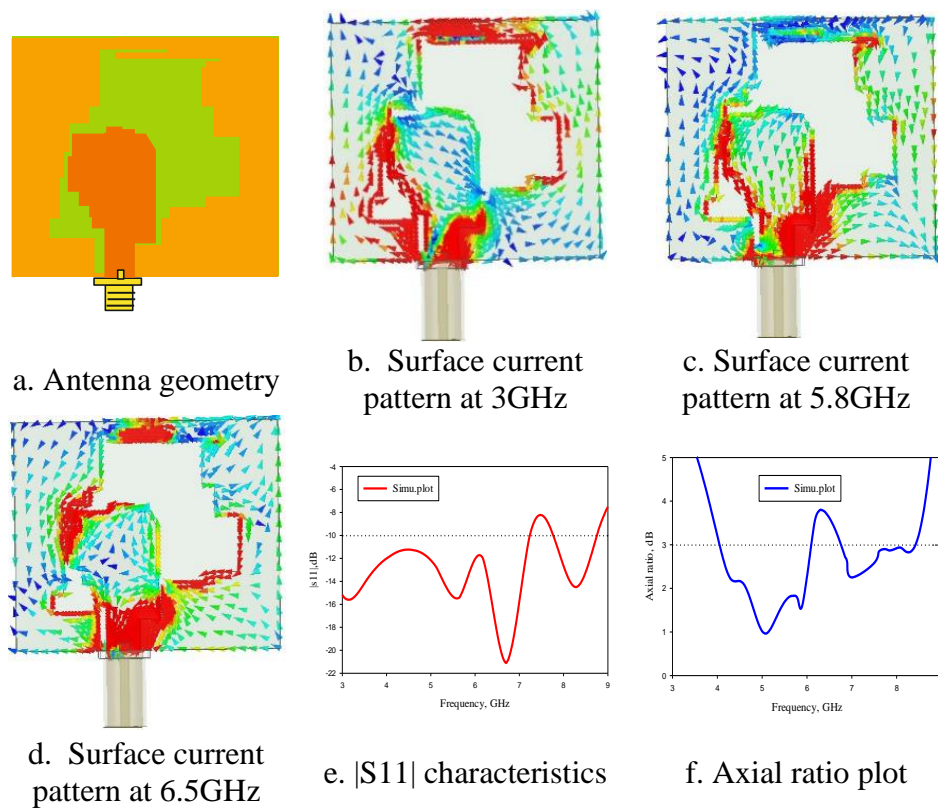


Figure 5.37. Antenna evolution, stage 17

Stage 18

In the eighteenth stage of evolution, a small vertical rectangular strip of dimensions $6.18 \times 1.45 \text{ mm}^2$ was added to the right border of the ground plane. Changes are seen in return loss and axial ratio curves as

seen in the Figure 5.38. First band is seen from 2.5 GHz to 7.31 GHz and the second band is seen from 7.7 GHz to 8.77 GHz. Impedance bandwidth of the first band is increased by 0.06 GHz and that of the second band is increased by 0.07GHz compared to that in the previous stage. The surface current distribution diagram shows that the newly introduced strip has a good contribution to widen the bandwidths, both IBW and ARBW. The 3 dB axial ratio band is from 3.91 GHz to 6.05 GHz in band1 and 7.04 GHz to 8.54 GHz in band 2. Hence 3 dB ARBW improvement of 0.14 GHz can be seen in band 1 and a decrease of 0.17 GHz can be seen in band2, when compared to the structure in the just previous stage of evolution.

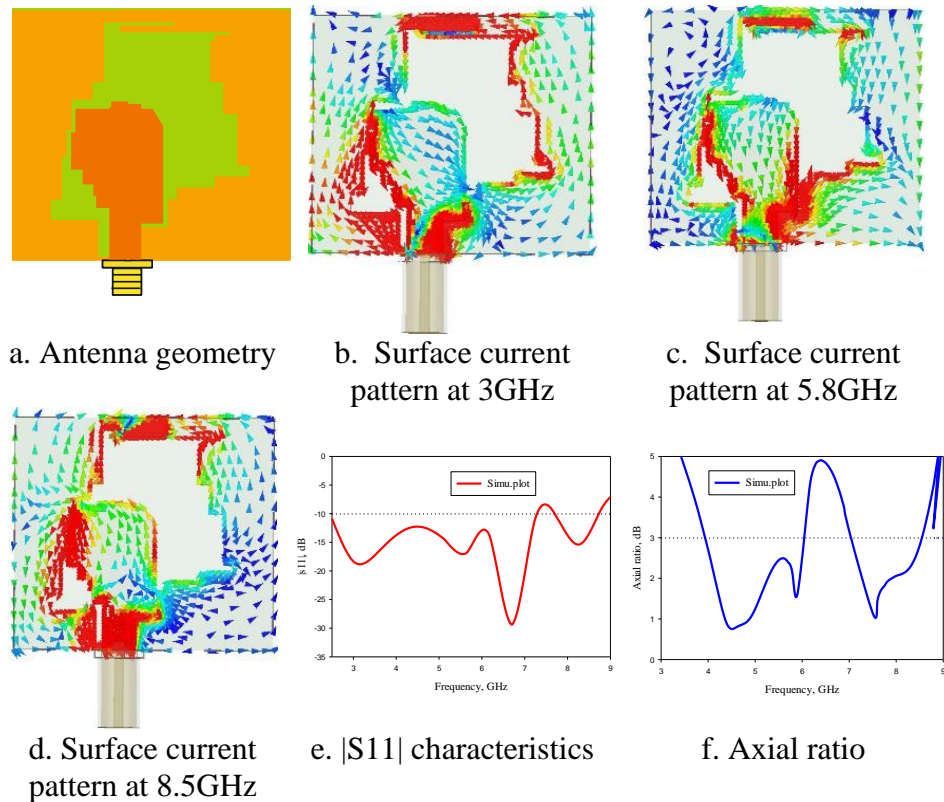


Figure 5.38. Antenna evolution, stage 18

Stage 19

In the nineteenth stage of evolution, five hexagonal slots were introduced at the bottom right corner of the ground plane. Three slots with equal dimensions (side length 1.2mm), one with side length 1.38mm and largest slot with side length 1.73mm. Changes are seen in $|S_{11}|$ and axial ratio curves as seen in the Figure 5.39.

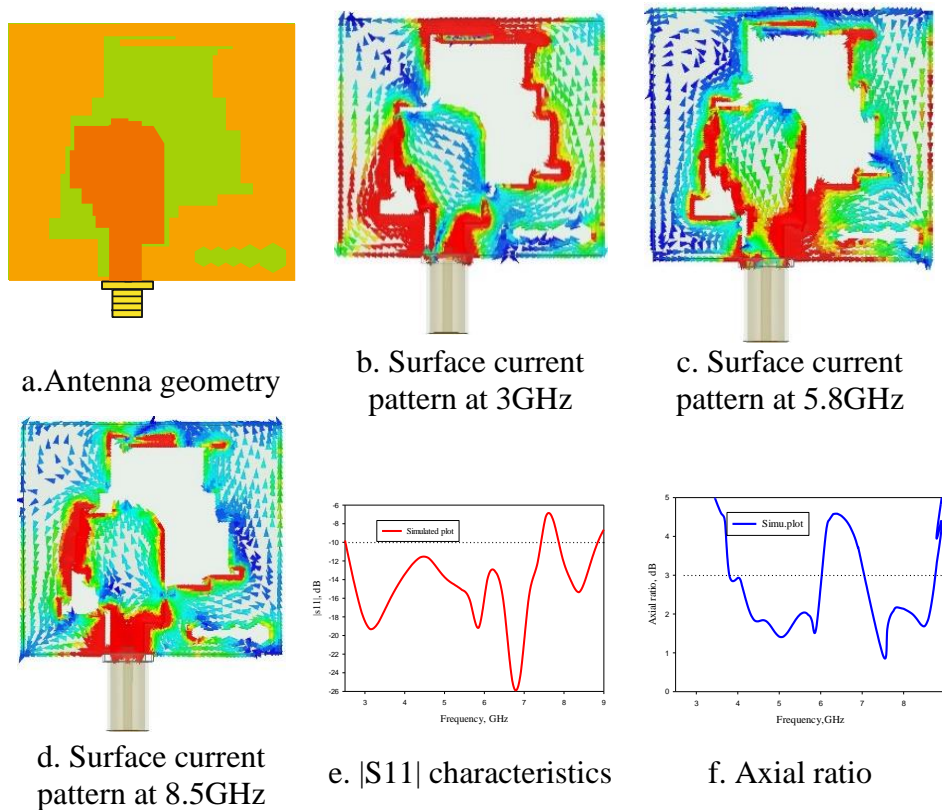


Figure 5.39. Antenna evolution, stage 19

First band is seen from 2.5 GHz to 7.40 GHz and the second band is seen from 7.86 GHz to 8.86 GHz. Impedance bandwidth of the first

band is increased by 0.09 GHz and that of the second band is decreased by 0.07GHz compared to that in the previous stage. The surface current distribution diagram shows that the newly introduced slots have good contribution to widen the bandwidths, both IBW and ARBW. The 3 dB axial ratio band is from 3.79 GHz to 6.05 GHz in band1 and 7.0 GHz to 8.8 GHz in band 2. Hence 3 dB ARBW improvement of 0.12 GHz can be seen in band 1 and an increase of 0.26 GHz can be seen in band2, when compared to the structure in the just previous stage of evolution.

Stage 20

In the twentieth stage of evolution, one hexagonal slot with side length of 1.1 mm was introduced at the top right portion of the ground plane. As depicted in Figure 5.40, changes are observed in the axial ratio curves. First band is seen from 2.5 GHz to 7.40 GHz and the second band is seen from 7.86 GHz to 8.86 GHz. Impedance bandwidth of both bands remains unchanged compared to that in the previous stage. The surface current distribution diagram shows that the newly introduced slots have good contribution to widen the ARBW. The 3 dB axial ratio band is from 3.5 GHz to 5.9 GHz in band1 and 7.0 GHz to 9 GHz in band 2. Hence 3 dB ARBW improvement of 0.14 GHz can be seen in band 1 and an increase of 0.2 GHz can be seen in band2, when compared to the structure in the just previous stage of evolution.

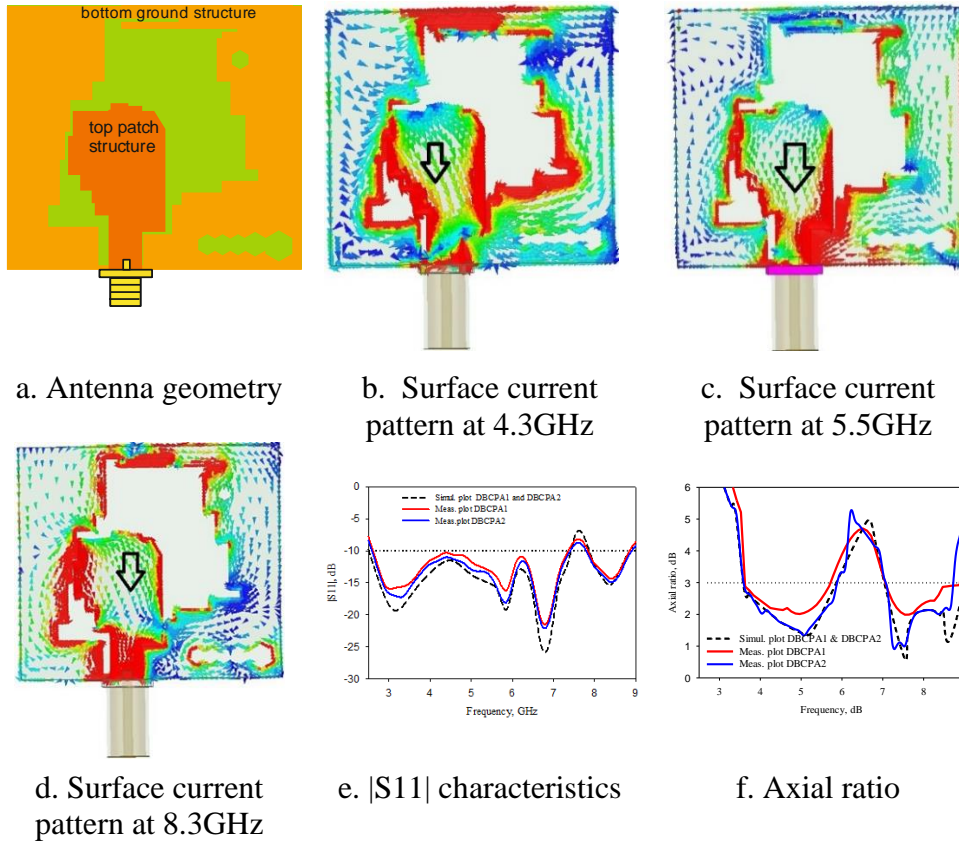


Figure 5.40. Antenna evolution, stage 20.

5.6 Characteristic Mode Analysis of the antenna DBCPA1

The characteristic mode analysis of the antenna helps us to have a clear understanding of the theory behind the CP performance of the antenna [23-30]. This enables us to explore new design strategies for improved performance. In this method of analysis, two quantities are used to describe the performance. They are Characteristic Angle (CA) and Modal Significance (MS); both are described in terms of the eigen value (λ). They are defined as follows

Characteristic Angle (CA) , $\alpha = 1800 - \tan^{-1}(\lambda)$

$$\text{Modal Significance MS} = \frac{1}{|1+j\lambda|}$$

The characteristic angle is the phase angle between a characteristic current and the associated characteristic field. Hence, a mode is at resonance When the characteristic angle of a mode is nearly 1800, it is inferred that this mode is at resonance. The modal significance value of a mode describes its contribution to the total radiation when a source or excitation is applied. When the characteristic angle value difference between two resonant modes is 900 and their MS values are equal; then those modes are said to contribute for CP performance. These are modes are said to be orthogonal modes.

Characteristic mode analysis is carried out for the antenna over a wide range of frequencies; from 2.5GHz to 14GHz. Through this analysis, many characteristics modes have been extracted which account for circular polarization behavior of the antenna in the afore said two bands.

5.6.1 Characteristic modes evaluated with a sorting frequency 2.5 GHz

Using the CMA tool, an integral part of CST, initially characteristic modes at the sorting frequency 2.5 GHz are extracted and eight modes are obtained. Characteristic angle values, modal significance values and eigen values corresponding to these modes are depicted in Figure 5.41, Figure 5.42 and Figure 5.43 respectively. Resonant frequencies corresponding to each mode was sorted out at the characteristic angle value 1800, modal significance value 1 and the eigen value 0. The modes thus sorted out are

depicted in the Table 2 and Table 3. Out of the obtained eight modes, all modes except mode 3 are seen to be significant and contribute for circular polarization behavior of the antenna in two bands as stated earlier. This is clarified later in this chapter. Mode 3 seems to be of no significance because neither the characteristic angle becomes 180° nor the modal significance value becomes 1; during the entire frequency range under consideration. Also, the eigen value seems to be greater than 0 for this particular Mode 3, in the operating frequency range.

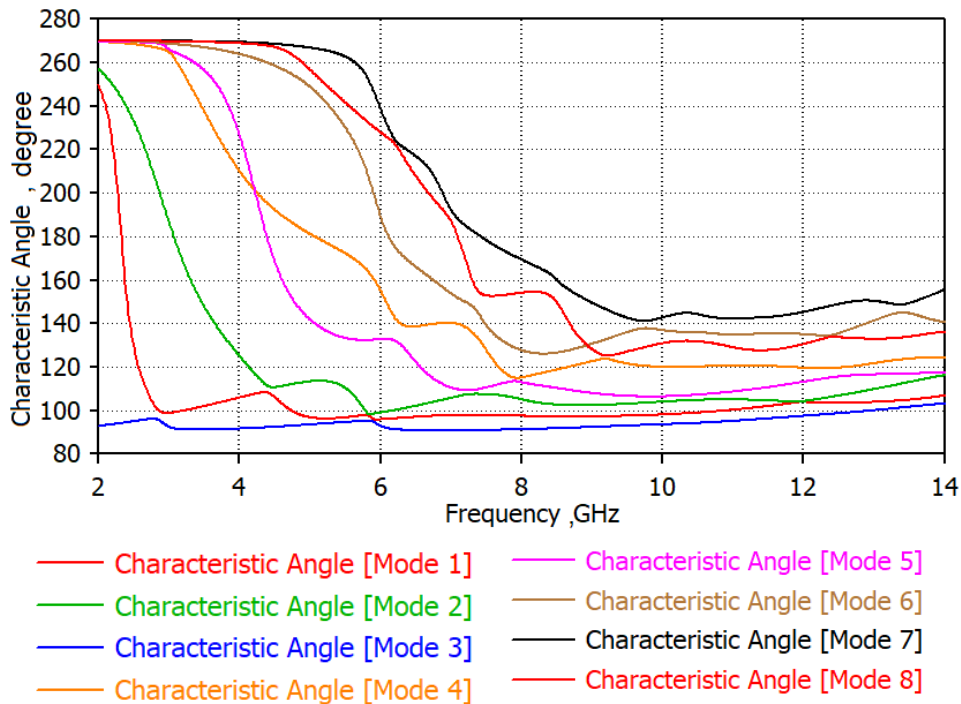


Figure 5.41. Characteristic angles corresponding to eight different modes, sorting frequency 2.5 GHz

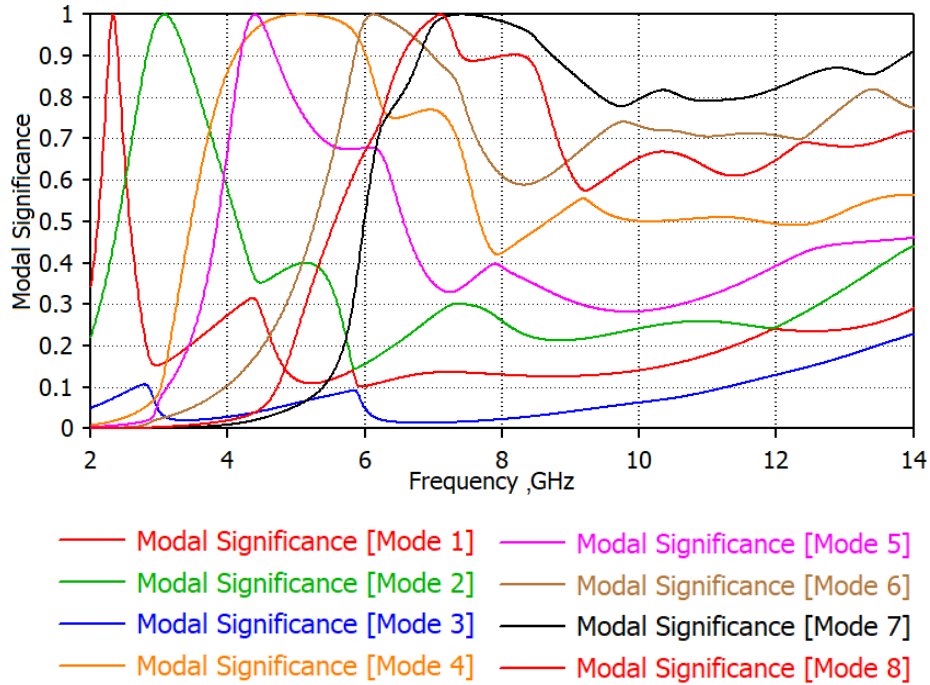


Figure 5.42. Modal significance values corresponding to eight different modes, sorting frequency 2.5 GHz

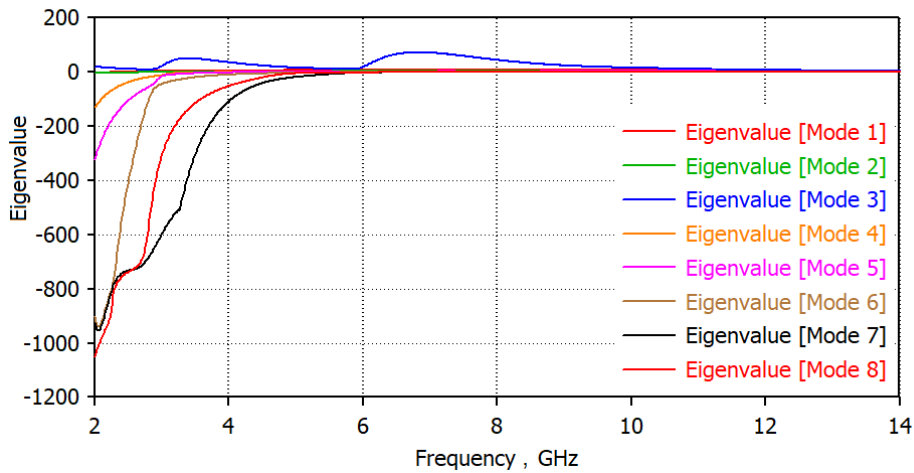


Figure 5.43. Eigen values corresponding to eight different modes, sorting frequency 2.5 GHz

Table 5.2. Significant characteristic modes

Characteristic Mode	Characteristic angle, degrees	Frequency, GHz
Mode 1	180	2.32
Mode 2	180	3.08
Mode 3	Not significant	Not significant
Mode 4	180	5.07
Mode 5	180	4.40
Mode 6	180	6.13
Mode 7	180	7.43
Mode 8	180	7.10

Table 5.3. Significant characteristic modes corresponding to MS value 1

Characteristic Mode	Modal significance value	Frequency, GHz
Mode 1	1	2.32
Mode 2	1	3.08
Mode 3	Not significant	Not significant
Mode 4	1	5.07
Mode 5	1	4.40
Mode 6	1	6.13
Mode 7	1	7.43
Mode 8	1	7.10

5.6.1.1 Orthogonal modes at 2.984 GHz

In order to resolve the horizontal and vertical modes which are involved in generating CP characteristics at certain resonant frequencies; the characteristic angle diagrams at these frequencies are evaluated and

results are obtained corresponding to 90° phase difference between them. It is found that at a sorting frequency of 2.984 GHz, the two modal frequencies are 2.32 GHz and 3.08 GHz. The phase difference between them is 90.020°. These two modes show a modal significance value of 0.61 at 2.516 GHz [28].

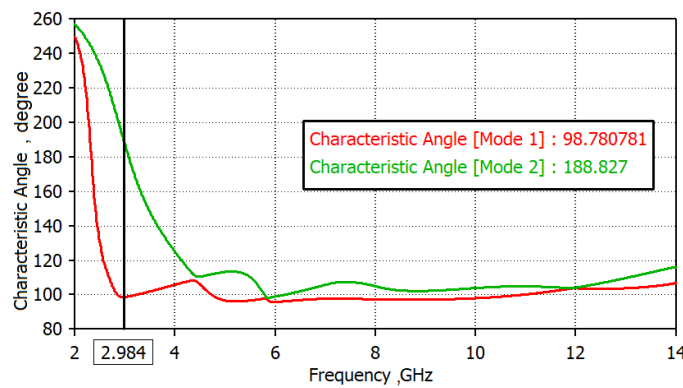


Figure 5.44. Characteristic angles corresponding to Mode1 and Mode2 (orthogonal modes) at the frequency 2.984 GHz.

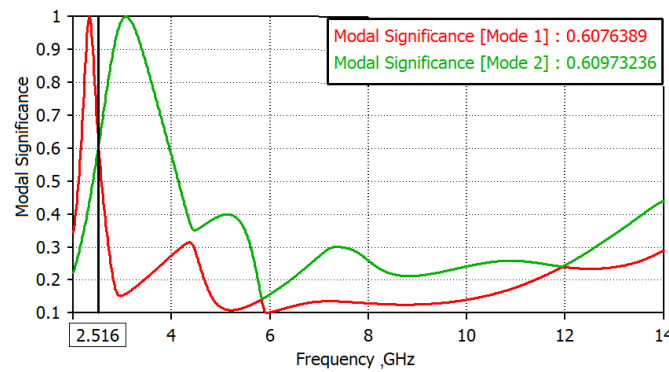


Figure 5.45. Modal significance values corresponding to Mode1 and Mode2

5.6.1.2 Orthogonal modes at 3.512 GHz

The characteristic modes at the resonant frequency 3.512 GHz is resolved out. The resolved modes are mode2, 3.08 GHz and mode4 5.07 GHz. These modes correspond to a phase difference of 90° at the resonant frequency 3.512 GHz. These modes are having the same value of modal significance 0.72 at the frequency 3.74 GHz, as depicted in Figure 5.46- 5.47.

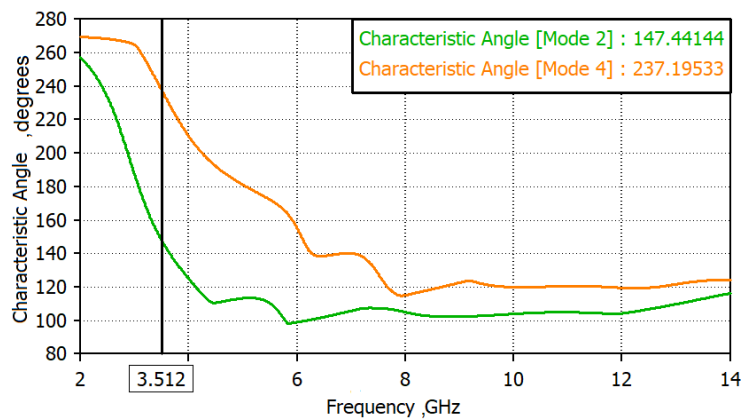


Figure 5.46. Characteristic angles corresponding to Mode1 and Mode2 (orthogonal modes) at the frequency 2.984 GHz.

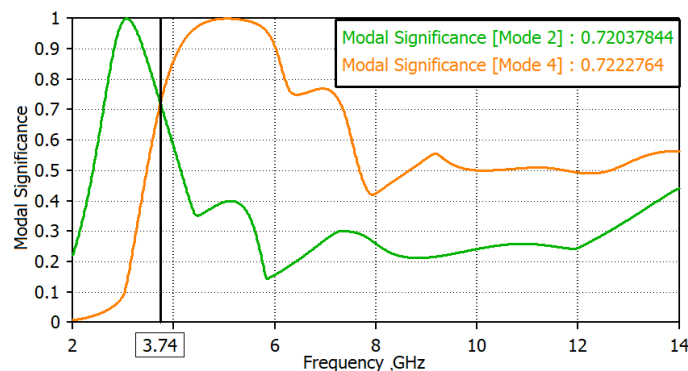


Figure 5.47. Modal significance values corresponding to Mode1 and Mode2

5.6.1.3 Orthogonal modes at 4.16 GHz

The horizontal and vertical modes corresponding to the resonant frequency 4.16 GHz are resolved out. At 4.16 GHz, two modes, mode2 (3.08 GHz) and mode5(4.4GHz) exhibit a phase difference of 89.050 and there exists the same modal significance value of 0.6 at the frequency 3.944 GHz as seen in Figure 5.48-5.49

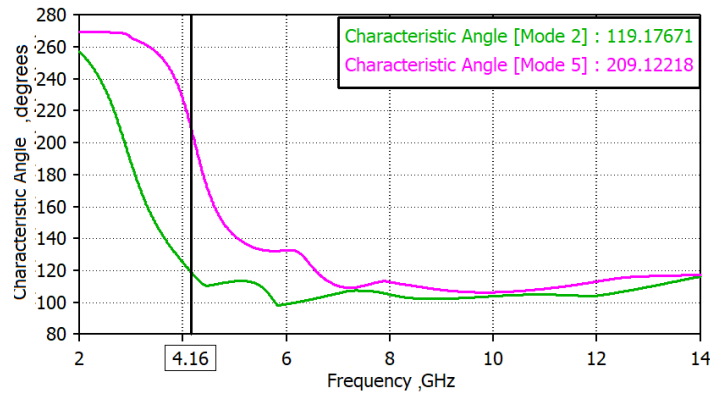


Figure 5.48. Characteristic angles corresponding to Mode2 and Mode5 (orthogonal modes) at the frequency 4.16 GHz.

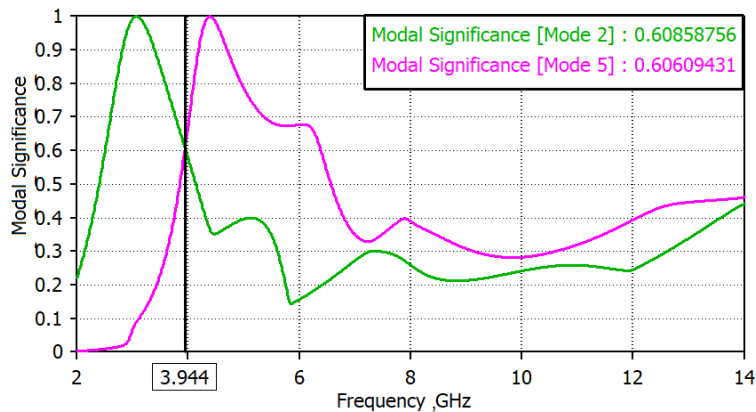


Figure 5.49. Modal significance values corresponding to Mode2 and Mode5

5.6.2 Characteristic modes evaluated with a sorting frequency 8.7 GHz

The characteristic modes at a sorting frequency of 8.7 GHz are extracted and seven modes are obtained. Characteristic angle values, modal significance values and eigen values corresponding to these modes are depicted in Figure 5.50, Figure 5.51 and Figure 5.52 respectively. Resonant frequencies corresponding to each mode was sorted out at the characteristic angle value 1800, modal significance value 1 and the eigen value 0. The modes thus sorted out are depicted in the Table 5.4 and Table5. 5.

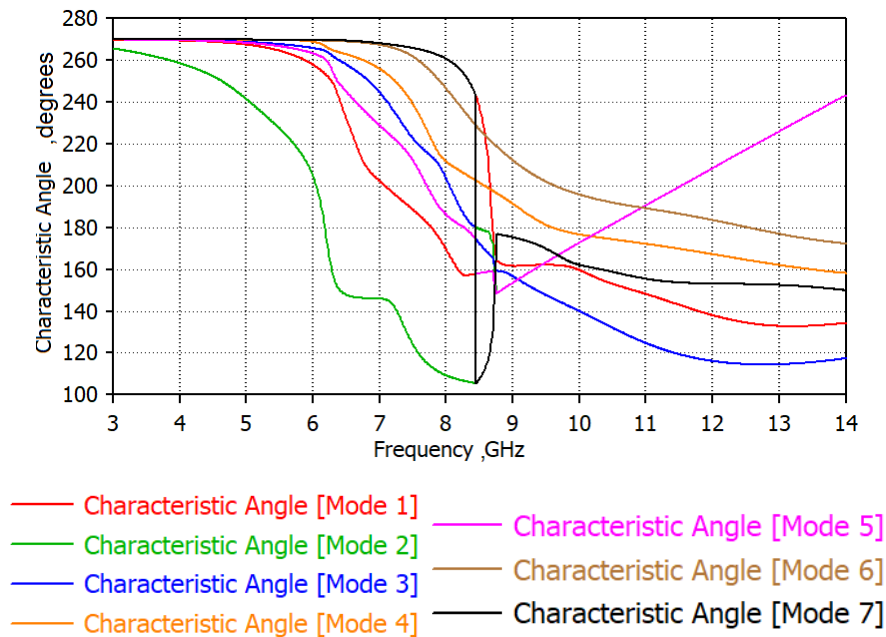


Figure 5.50. Characteristic angles corresponding to seven different modes, sorting frequency 8.7 GHz

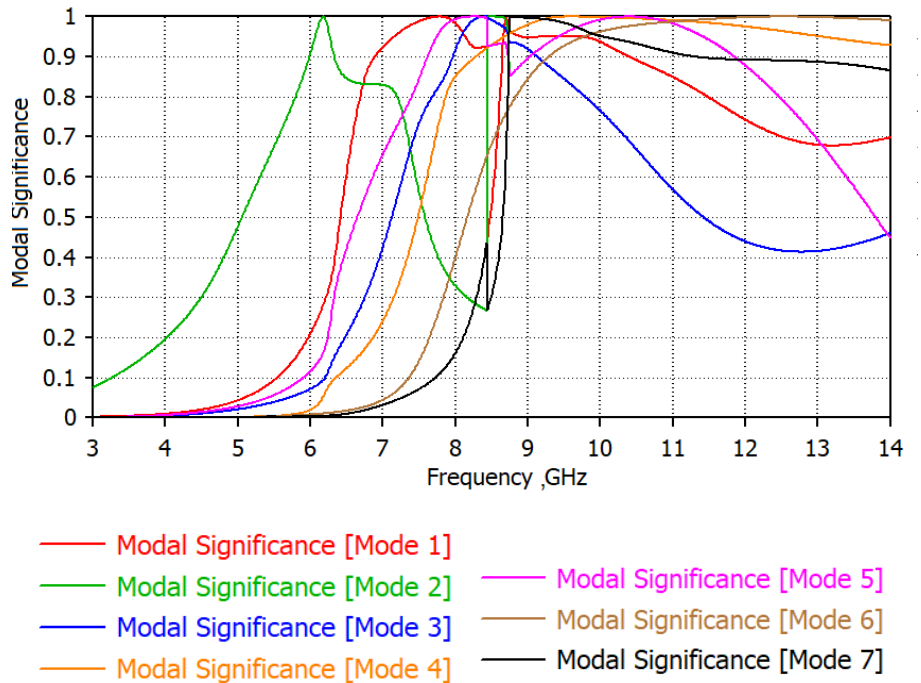


Figure 5.51. Modal significance value plots corresponding to seven different modes, sorting frequency 8.7 GHz

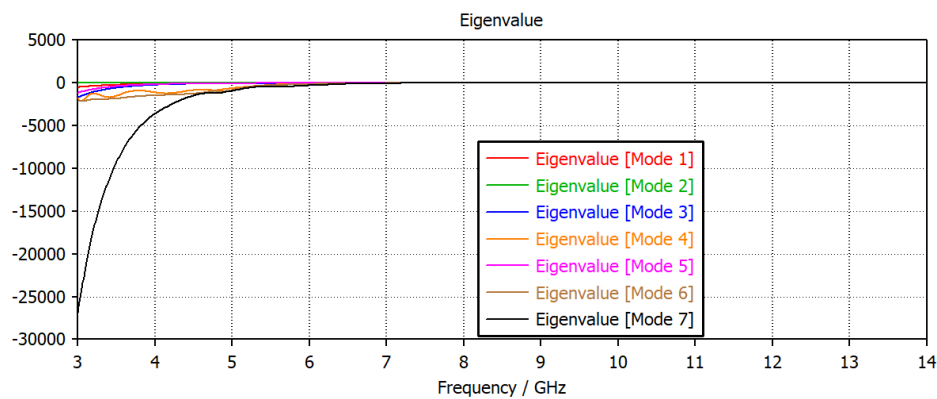


Figure 5.52. Eigen value plots corresponding to seven different modes, sorting frequency 8.7 GHz

Table 5.4. Significant characteristic modes, corresponding to sorting frequency 8.7 GHz

Characteristic Mode	Characteristic angle, degrees	Frequency, GHz
Mode 1	180	7.8, 8.69
Mode 2	180	6.18, 8.445, 10.34
Mode 3	180	8.41
Mode 4	180	9.61
Mode 5	180	8.275, 10.369
Mode 6	180	12.537
Mode 7	180	8.439

Table 5.5. Significant characteristic modes, corresponding to sorting frequency 8.7 GHz

Characteristic Mode	Modal significance	Frequency, GHz
Mode 1	1	7.8, 8.69
Mode 2	1	6.18, 8.445, 10.34
Mode 3	1	8.41
Mode 4	1	9.61
Mode 5	1	8.275, 10.369
Mode 6	1	12.537
Mode 7	1	8.439

5.6.2.1 Orthogonal modes at 6.179 GHz

The modes that contribute for circular polarization corresponding to the resonant frequency 6.18 GHz are resolved out. At 6.18 GHz, two modes, mode2 (6.18 GHz) and mode5 (8.275 GHz) exhibit a phase difference of 89.50 and the two modes, mode2(6.18 GHz) and mode7(8.45 GHz) exhibit a phase difference of 89.840 between them, as depicted in Figures 5.53-5.54.

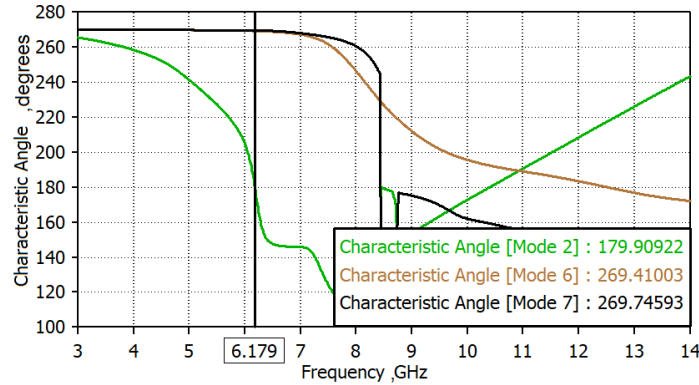


Figure 5.53. Characteristic angles corresponding to Mode2, Mode6 and Mode7 (orthogonal modes) at the frequency 6.179 GHz.

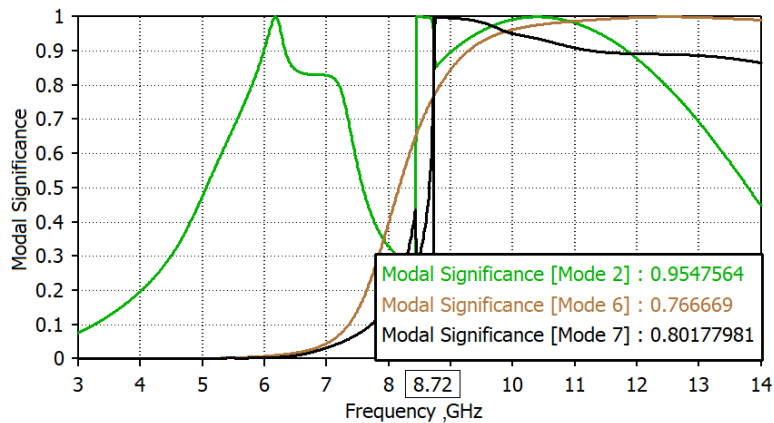


Figure 5.54. Modal significance values corresponding to Mode2, Mode6 and Mode7

5.6.2.2 Orthogonal modes at 6.234 GHz

The modes that contribute for circular polarization corresponding to the resonant frequency 6.234 GHz are resolved out. At 6.234 GHz, two modes, mode2 (6.18 GHz) and mode5 (12.54 GHz) exhibit a phase difference of 90.4 between them. Also there exists a modal significance

value of 0.75 between these characteristic modes at a resonant frequency of 7.27 GHz. Another interesting fact is that these two modes correspond to the same modal significance value of 0.85 at a resonant frequency of 8.764 GHz., as depicted in Figures 5.55 – 5.57.

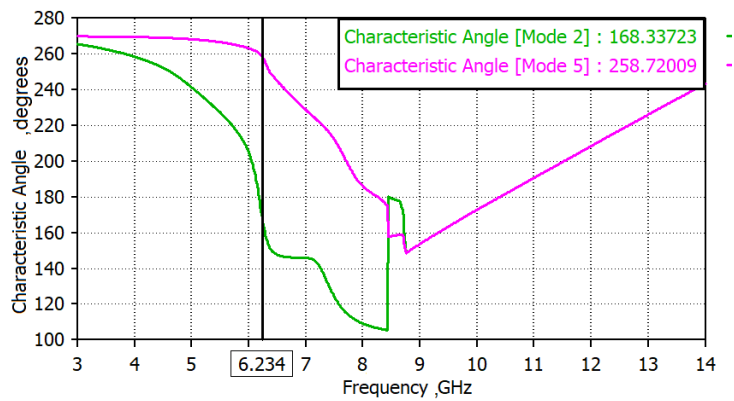


Figure 5.55. Characteristic angles corresponding to Mode2, and Mode5 (orthogonal modes) at the frequency 6.234 GHz.

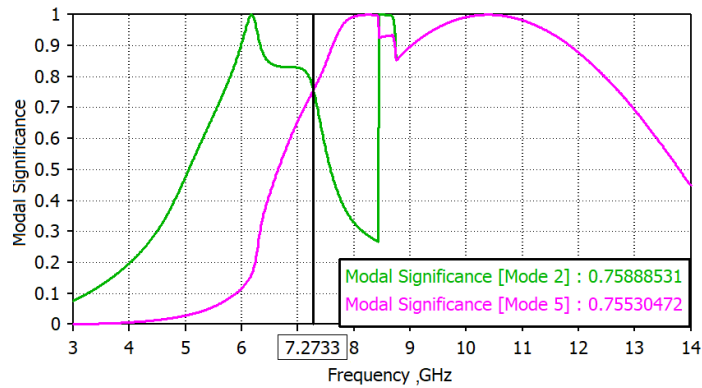


Figure 5.56. Modal significance values corresponding to Mode2 and Mode5

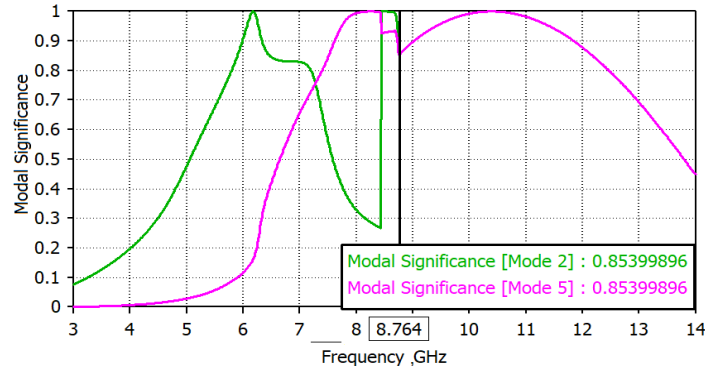


Figure 5.57. Modal significance values corresponding to Mode 2 and Mode 5, at 8.764 GHz.

5.6.2.3 Orthogonal modes at 6.19 GHz

The orthogonal modes that contribute for circular polarization corresponding to the resonant frequency 6.19 GHz are resolved out. At 6.19 GHz, two modes, mode 2 (6.18 GHz) and mode 4 (9.61 GHz) exhibit a phase difference of 89.09 between them. Also there exists a modal significance value of 0.53 between these characteristic modes at a resonant frequency of 7.532 GHz. Another interesting fact is that these two modes correspond to the same modal significance value of 0.9 at a resonant frequency of 8.445 GHz and the same modal significance value of 0.95 at 8.72 GHz, as depicted in Figures 5.58- 5.61

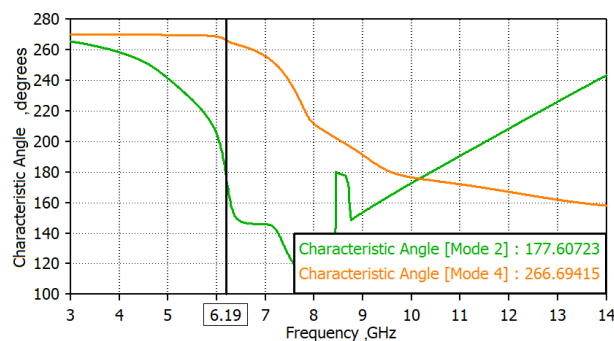


Figure 5.58. Characteristic angles corresponding to Mode 2, and Mode 4

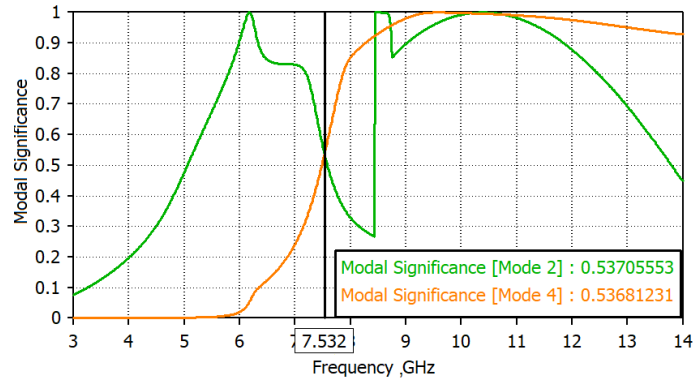


Figure 5.59. Modal significance values corresponding to Mode 2 and Mode4

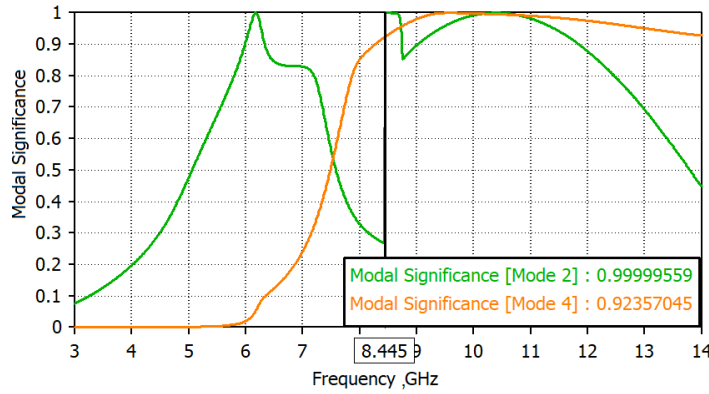


Figure 5.60. Modal significance values corresponding to Mode 2 and Mode4, at 8.445 GHz

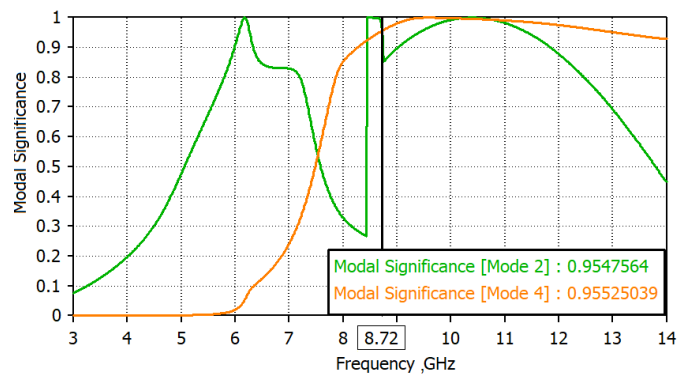


Figure 5.61. Modal significance values corresponding to Mode 2 and Mode4, at 8.72 GHz

5.6.2.4 Orthogonal modes at 8.082 GHz

The orthogonal modes that contribute for circular polarization corresponding to the resonant frequency 8.082 GHz are resolved out. At 8.082 GHz, two modes, mode2 (6.18 GHz) and mode3 (8.41 GHz) exhibit a phase difference of 89.720 between them. Also there exists a same modal significance value of 0.66 between these characteristic modes at a resonant frequency of 7.38 GHz. Another interesting fact is that these two modes correspond to the same modal significance value of 0.99 at a resonant frequency of 8.445 GHz and the same modal significance value of 0.95 at 8.72 GHz. These are depicted in Figures 5.62-5.65.

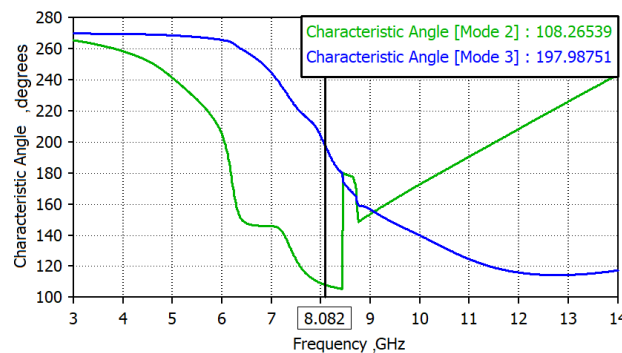


Figure 5.62. Characteristic angles corresponding to Mode2, and Mode3

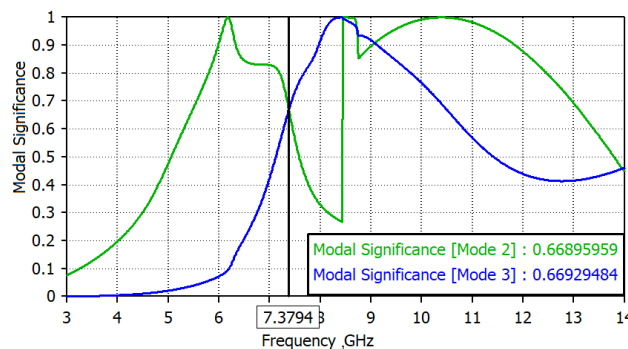


Figure 5.63. Modal significance value corresponding to Mode2, and Mode3

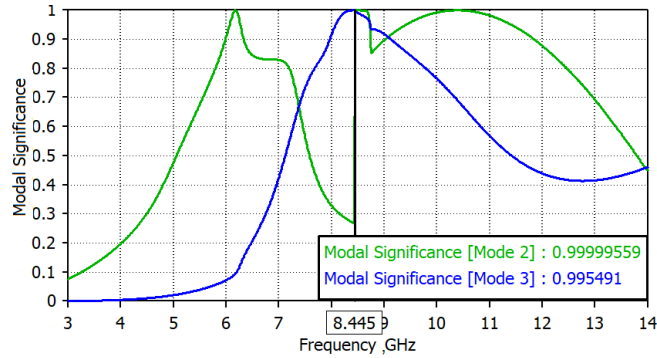


Figure 5.64. Modal significance value corresponding to Mode 2 and Mode3

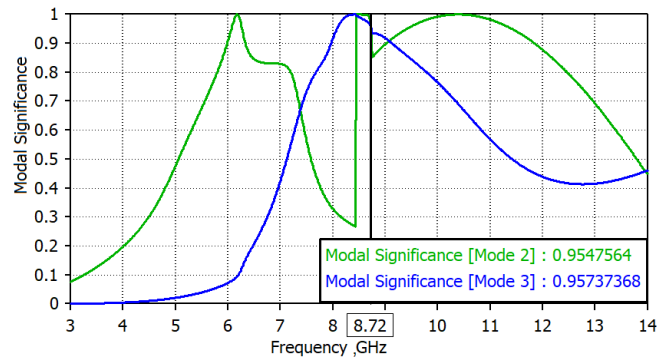


Figure 5.65. Modal significance value corresponding to Mode 2 and Mode3

Photographs of the fabricated antenna prototypes are provided in Figure 5.66 below.

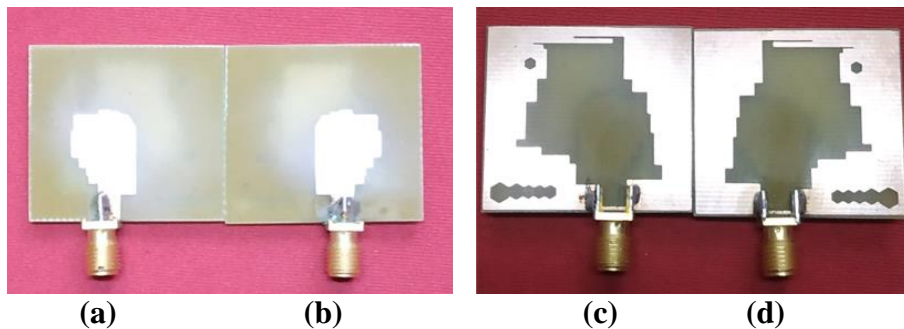


Figure 5.66. (a) DBCPA1 top view (b) DBCPA2 top view (c) DBCPA2 bottom view (d) DBCPA1 bottom view

Chapter summary

The dual band circularly polarized patch antennas are investigated here in this chapter. Major findings are given below.

Placement of asymmetric slots and strips on feed structure and ground structure give rise to improved impedance and axial ratio bandwidths. Formation of two bands and circular polarization characteristics is better established through antenna evolution study using ANSYS HFSS simulation software. Analysis using characteristic mode theory yielded orthogonal modes at various frequencies in two bands. It is a good tool for the analytical study of circular polarization.

References

- [1] Miers, Z. *Systematic Antenna Design Using the Theory of Characteristic Modes*, Lund University, Sweden, 2016.
- [2] Y. Chen et al., “Characteristic Mode Design of Wide Band Circularly Polarized Patch Antenna Consisting of H-Shaped Unit Cells,” *IEEE Trans. Antennas Propag.*, vol. 63, no. 5, pp. 25292–25299, 2007.
- [3] <https://www.cst.com>
- [4] J. Sze, Z. Chen, and C. Chang, “Broadband CPW fed Circularly Polarised square Slot Antenna With Lightning-Shaped Feedline and Inverted-L Grounded Strips,” vol. 58, no. 3, pp. 973–977, 2010.
- [5] K. L. Wong, C. C. Huang, and W. S. Chen, “Printed ring slot antenna for circular polarization,” *IEEE Trans. Antennas Propag.*, vol. 50, pp. 75–77, Jan. 2002.

- [6] J.S. Row, “The design of a squarer-ring slot antenna for circular polarization,” *IEEE Trans. Antennas Propag.*, vol. 53, pp. 1967–1972, Jun. 2005.
- [7] J. Y. Sze, C. I. G. Hsu, M. H. Ho, Y. H. Ou, and M. T. Wu, “Design of circularly polarized annular-ring slot antennas fed by a double-bent microstrip line,” *IEEE Trans. Antennas Propag.*, vol. 55, pp. 3134–3139, Nov. 2007.
- [8] J. Y. Sze and S.-P. Pan, “Design of CPW-fed circularly polarized slot antenna with a miniature configuration,” *IEEE Trans. Antennas Propag.*, vol. 10, pp. 1465–1468, Jan. 2011.
- [9] K. L. Wong, J. Y. Wu, and C. K. Wu, “A circularly polarized patch loaded square-slot antenna,” *Microw.Opt. Technol. Lett.*, vol. 23, pp. 363–365, Dec. 1999.
- [10] J. Y. Sze, K. L. Wong, and C. C. Huang, “Coplanar waveguide-fed square slot antenna for broad band circularly polarized radiation,” *IEEE Trans. Antennas Propag.*, vol.51, no.8, pp.2141–2144, Aug.2003.
- [11] C. C. Chou, K. H. Lin, and H. L. Su, “Broadband circularly polarised cross-patch-loaded square slot antenna,” *Electron Lett.*, vol. 43, pp. 485–486, Apr. 2007.
- [12] J.Y.Sze and Y.H.Ou, “Compact CPW-fed square aperture CP antenna for GPS and INMARSAT applications,” *Microw. Opt. Technol. Lett.*, vol. 49, no. 2, pp. 427–430, Feb. 2007.
- [13] J. Y. Sze and C. C. Chang, “Circularly polarized square slot antenna with a pair of inverted-L grounded strips,” *IEEE Antennas Wireless Propag. Lett.*, vol. 7, pp. 149–151, 2008.
- [14] J.S.Row and S.W.Wu, “Circularly- polarized wide slot antenna loaded with a parasitic patch,” *IEEE Trans.Antennas Propag.*, vol.56,no.9, pp. 2826–2832, Sep. 2008.

- [15] T. Y. Han, Y. Y. Chu, L. Y. Tseng, and J. S. Row, "Unidirectional circularly-polarized slot antennas with broadband operation," *IEEE Trans. Antennas Propag.*, vol. 56, no. 6, pp. 1777–1780, Jun. 2008.
- [16] J. Y. Sze, J. C. Wang, and C. C. Chang, "Axial-ratio-bandwidth enhancement of asymmetric-CPW-fed circularly-polarised square slot antenna," *Electron Lett.*, vol. 44, pp. 1048–1049, Aug. 2008.
- [17] K. L. Wong, C. C. Huang, and W. S. Chen, "Printed ring slot antenna for circular polarization," *IEEE Trans. Antennas Propag.*, vol. 50, no. 1, pp. 75–77, Jan. 2002.
- [18] J. Y. Sze, C.-I. G. Hsu, M. H. Ho, Y. H. Ou, and M. T. Wu, "Design of circularly polarized annular-ring slot antennas fed by a double-bent microstrip line," *IEEE Trans. Antennas Propag.*, vol. 55, no. 11, pp. 3134–3139, Nov. 2007.
- [19] J. Pourahmadazar, C. Ghobadi, J. Nourinia, N. Felegari, and H. Shirzad, "Broadband CPW-fed circularly polarized square slot antenna with inverted-L strips for UWB applications," *IEEE AWPL*, vol. 10, April 2011.
- [20] J. Y. Sze, K. L. Wong, and C. C. Huang, "Coplanar waveguide-fed square slot antenna for broadband circularly polarised radiation," *IEEE Trans. Antennas Propag.*, vol. 51, pp. 2141–2144, August 2003.
- [21] J. Y. Sze and Y. H. Ou, "Compact CPW-fed square aperture CP antenna for GPS and INMARSAT applications," *Microw. Opt. Technol. Lett.*, vol. 49, no. 2, pp. 427–430, February 2007.
- [22] Narbudowicz, A. Z.: *Advanced Circularly Polarised Microstrip Patch Antennas*. Doctoral Thesis. Dublin Institute of Technology, 2013.
- [23] G. Shaker, S. Safavi-Naeini, and N. Sangary, "Modern Antenna Design Using Mode Analysis Techniques," 2015.

- [24] F. H. Lin and Z. N. Chen, “Probe-Fed Broadband Low-Profile Metasurface Antennas using Characteristic Mode Analysis,” no. October, 2017.
- [25] Y. Chen and C. F. Wang, “Synthesis of reactively controlled antenna arrays using characteristic modes and de algorithm,” *IEEE Antennas Wirel. Propag. Lett.*, vol. 11, no. 2, pp. 385–388, 2012.
- [26] C. J. Reddy, “Theory of Characteristic Modes for wideband Antenna Design,” pp. 1–2, 2016.
- [27] M. Poordaraee, H. Oraizi, S. Khajevandi, and F. Hodjat-kashani, “Systematic Octopus-Shape Antenna Design with Circular Polarization by Characteristic Mode Theory,” no. March, pp. 1–6, 2018.
- [28] Yikai Chen, and Chao-Fu Wang, “ Characteristic-Mode-Based Improvement of Circularly Polarized U-Slot and E-Shaped Patch Antennas”, *IEEE Antennas And Wireless Propagation Letters*, Vol.11, 2012
- [29] C. S. Technology, “CMA Analysis of Compact Broadband Planar Antenna.”
- [30] M. M. Elsewe and D. Chatterjee, “Characteristic mode analysis of excitation feed probes in microstrip patch antennas,” 2016 *IEEE Antennas Propag. Soc. Int. Symp. APSURSI 2016 - Proc.*, pp. 33–34, 2016.



**ULTRA WIDE BAND CIRCULARLY POLARISED
MICROSTRIP ANTENNAS**

Contents	<i>Introduction to Ultrawide band circularly polarized microstrip antennas</i>
	<i>6.1 A Compact UWB Circularly Polarized Hexagonal Slot Antenna for Wireless Applications</i>
	<i>6.2 A Compact UWB Circularly Polarized Penta Decagonal Slot Antenna for Wireless Applications</i>
	<i>6.3 Circularly Polarised UWB Antenna for RF Energy Harvesting Applications</i>
	<i>6.4 Printed Circularly Polarised Asymmetric Ultra-wideband Antenna</i>
	<i>6.5 Chapter Summary</i>

The design and development techniques of four different types of ultrawide band circularly polarized microstrip patch antennas are described in this chapter. Slot antennas, where instead of introducing a single polygonal slot or multiple slots on a patch antenna, a modified slot shape can be used to improve the CP bandwidth of patch antennas [1]. Broadband circularly polarized antennas have begun to replace narrowband circularly polarized elements such as microstrip patches [2]. Due to the bidirectional radiation characteristics and lower quality factors, slot antennas have larger bandwidth than microstrip antennas. Accordingly, slot antennas with perturbations are good candidates for broadband CP antennas. Slot antennas are complementary structures to the microstrip antennas by Babinet's Principle. Hence for CP operations, the perturbation technologies applied to slot antennas are good enough to design broadband CP antennas than patch antennas [3,4].

Introduction

Nowadays, researchers highly concentrate on designing wideband CP antennas with varied features to fulfill the requirements of wireless communication systems. Growing interest is observed in accommodating several operating frequencies in a single antenna which provide high IBW and ARBW. UWB electromagnetic pulses of nanosecond duration are very useful in communication field and widely explored for military and biotechnological applications.

Slot antennas with large radiating aperture yield wider bandwidth without increasing the size and thickness. The ground plane size and placement of the slot on the ground plane affect the antenna's behaviour, to a great extent [3]. The conventional design strategies adopted in most of the reported works in literature [5–15], rely on symmetric antenna design technique, where ARBW values obtained do not cover the UWB spectrum to a good extent, with structures of comparable dimensions. Even though 100% ARBW was obtained with spiral and travelling wave structures [2], dimensions of such structures are more than double, compared to the proposed antenna in this work. This work is an investigation to adopt asymmetric design strategy, towards obtaining a compact structure that provides maximum percentage CP band coverage of the UWB spectrum.

Four different ultrawide band antennas each has a wide axial ratio bandwidth are presented in this chapter. All of them have a wide slot ground and lacks symmetric geometrical structure. The structures described in this chapter offer better features in terms of dimensions,

impedance and axial ratio bandwidths and CP band coverage of UWB spectrum compared to the existing antennas described in literature.

6.1 A Compact UWB Circularly Polarized Hexagonal Slot Antenna for Wireless Applications

This antenna has a simple structure and experimentally proved that it has an IBW of 125.97% and an AR BW of 56.31%.

6.1.1 Antenna Design

The geometry of the proposed CPW fed, UWB, CP hexagonal slot antenna is illustrated in Figure 6.1. FR4 substrate ($\epsilon_r = 4.4$, height = 1.6 mm) is used. The feed line is united with three metal strips which control the radiation characteristics. This assembly is positioned on the left side of the structure inside the hexagonal slot. The overall size is 25×25 mm². The side length of the hexagonal slot also affects the CP performance of the antenna. The 12.75mm \times 3mm size of the feed line corresponds to a characteristic impedance of 50 Ω . The CPW gap size is 0.3mm. The structure offers an increased CPBW and improved IBW, because the effective length of the radiation element is increased in a compact size. The optimized dimensions of the antenna structure are given in Figure 6.1. All parameters have been optimised using finite-element methods by commercial HFSS software (Version .13). The photograph of fabricated, antenna prototype is given in Figure 6.2.

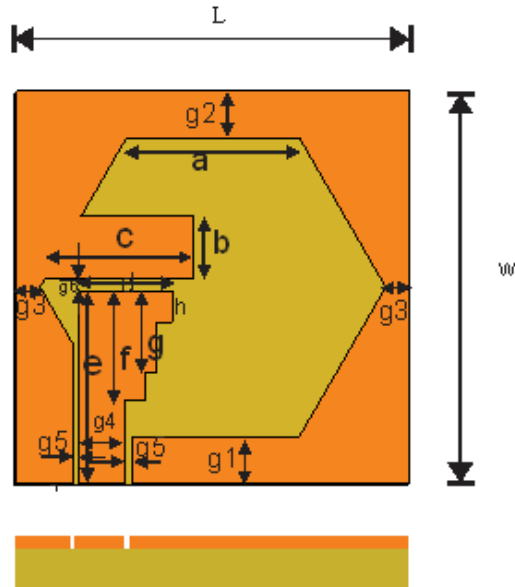


Figure 6.1. Antenna geometry. $L = W = 25\text{mm}$. $a = 17.244\text{ mm}$, $b = 4\text{ mm}$, $c = 9.25\text{ mm}$, $d = 6\text{ mm}$, $e = 12.25\text{ mm}$, $f = 7\text{ mm}$ its corresponding width = 1.25mm , $g = 5.75\text{mm}$ and its width = 0.75 mm , $h = 2\text{mm}$ and its width = 1.75 mm , $g1 = g3 = 0.3\text{mm}$, $g2 = 4\text{mm}$, $g4 = 3\text{ mm}$, $g5 = 0.4\text{mm}$, and $g6 = 0.75\text{mm}$.



Figure 6.2. Photograph of the fabricated prototype

6.1.2 Results And Discussion

The characteristics of the antenna prototype were studied in the anechoic chamber using the Agilent Precision Network Analyser E8362B. The return loss response (S11) and the 3 dB ARBW of the CPHSA are displayed in Figure 6.3 and Figure 6.4 respectively.

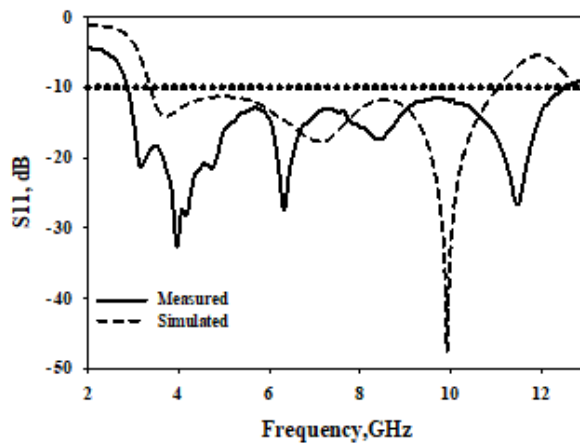


Figure 6.3. $|S_{11}|$ characteristics

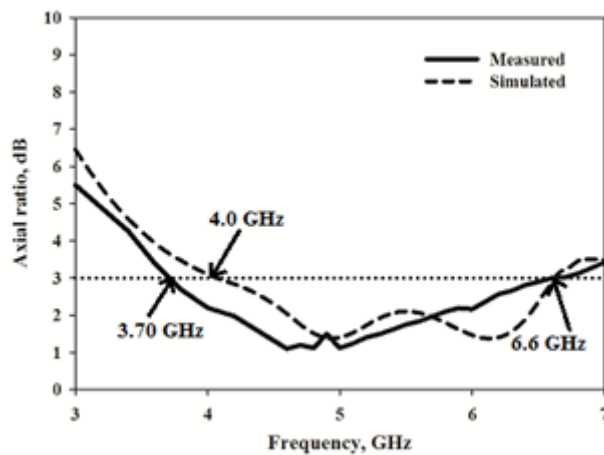


Figure 6.4. Measured and simulated axial ratio

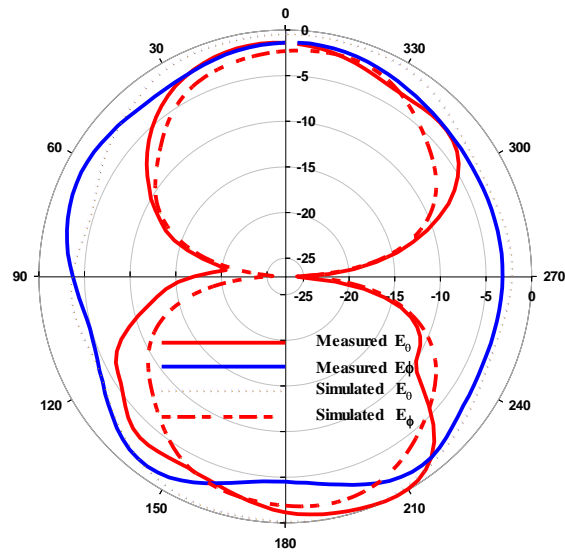


Figure 6.5. Radiation pattern in the XoZ plane at 3.93 GHz

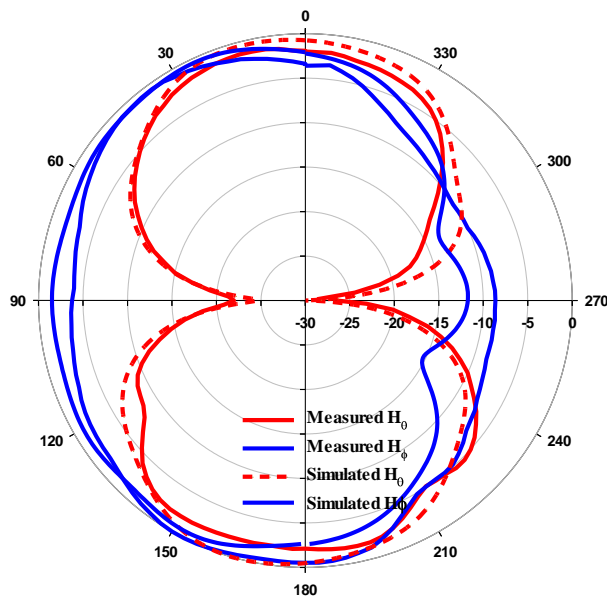


Figure 6.6 Radiation pattern in the YoZ plane at 3.93 GHz

The return loss response curve shows that the 10 dB IBW ranges from 2.85 GHz to 12.55 GHz and the 3 dB ARBW ranges from 3.70GHz to 6.60 GHz. The strip line metal strip assembly significantly increases IBW.

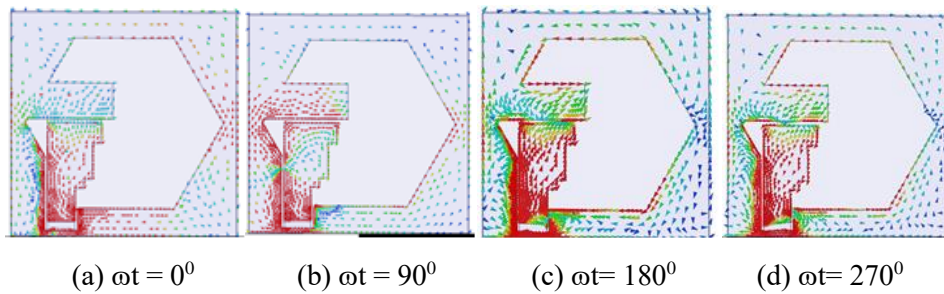


Figure 6.7. Simulated surface current pattern at 3.93GHz.

The stub protruded on the left side of the ground-plane significantly enhances the ARBW [8]. CP performance is obtained by two electric field vectors, which are equal in magnitude, but 90° out of phase. The horizontal component is introduced by the horizontal stub and horizontal stub and vertical component is produced by slot radiator. CP is obtained nearly around 5 GHz. The introduction of feedline metal strip assembly improves impedance and broadband CP characteristics.

The radiation patterns of the developed antenna prototypes are shown in Figure 6.5 and Figure 6.6., which are measured at two different frequencies: The measured results tally with simulation results. The antenna radiates with LHCP in + Z direction, whereas with RHCP in-Z. direction. The peak gain is measured to be 2.5 dBi and is achieved within the AR band.

The simulated surface current distributions of the antenna are shown in Figure 6.7, plotted at 3.93 GHz. Observation is that, the surface current distributions plotted at the time phases of 180° and 270° have same magnitudes but opposite direction with that of the patterns plotted at 0° and 90° respectively. This shows that the proposed antenna is right-hand circular polarized (RHCP) in the -Z direction. There is good agreement between the simulated and experimental results.

Measurement results show that impedance bandwidth is 125.97 %, with respect to the center frequency and percentage AR bandwidth is 56.3.. It is demonstrated that by adding three short stubs to the feed line, contribute to improve CP performance. In addition to its simple structure, the proposed antenna provides enhanced AR bandwidth and CP operation. The performance comparison of the antenna with other similar works in the literature is shown in the Table 6.1

Table 6.1. Comparison with similar works in literature

Reference	Size mm ³	10dB IBW, % relative to the center frequency	3dB 3 dBARBW , % relative to the center frequency
[16]	$80 \times 66 \times 0.5$	3000 – 8000, 88%	3200- 6100, 54%
[17]	$60 \times 60 \times 0.8$	2023-3421, 51.4 %	2075- 3415,48.8 %
[18]	$25 \times 25 \times 0.8$	2985–11232, 116%	5012–7382, 38.24%
[19]	$60 \times 60 \times 0.7$	1600–3055, 51.4 %	2300–3030, 48.8%
[20]	$60 \times 60 \times 0.8$	2674–13 124, 132 %	4995–6945, 33.89%
[21]	$70 \times 70 \times 1.6$	1604–2450, 39.6 %	1840–2080, 12.4 %
[22]	$60 \times 60 \times 0.76$	1772–2591, 30 %	1880–2560, 35%
[23]	$25 \times 25 \times 0.8$	2760–14 820, 137.2 %	4270–6130, 35.7%

[8]	25 x 25 x 1.6	3500 - 9250, 90.2 %	4600 - 6900, 40 %
This work	25x25x1.6	2850-12550, 125.97%	3700 -6600 56.31 %

6.2 A Compact UWB Circularly Polarized Penta Decagonal Slot Antenna for Wireless Applications

The proposed antenna consists of a Penta decagonal (polygon with 15 sides) slot. Broadband CP operation is realized through simple steps.

6.2.1 Antenna Design

The geometry of the proposed UWB, CP pentadecagonal slot antenna is illustrated in Figure 6.8. Being CPW feed structure the ground plane is also printed on the top side of the substrate. The feed line is united with three metal strips which control the radiation characteristics. This assembly is positioned on the right side of the structure inside the penta decagonal slot. The overall size is $25 \times 25 \text{ mm}^2$. The variation in the side length of the pentadecagon affects the CP performance. The structure offers an increased CPBW and improved IBW. The optimized dimensions of the antenna structure are given in Figure 6.8. All dimensions are optimised using finite-element methods by commercial ANSYS HFSS. Photograph of the fabricated antenna prototype is given in Figure 6.9.

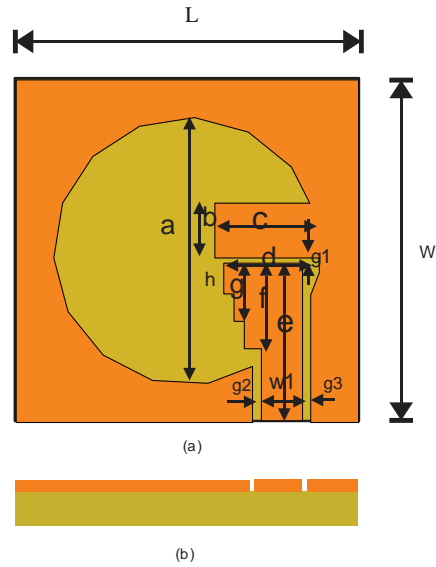


Figure 6.8. Antenna geometry. (a) Top view (b) Cross sectional view.

$L = W = 25\text{mm}$. $a = 3.615\text{ mm}$, $b = 4\text{ mm}$,
 $c = 9.25\text{ mm}$, $d = 5.75\text{ mm}$, $e = 12.25\text{ mm}$,
 $f = 6.25\text{ mm}$ its corresponding width = 1.25mm ,
 $g = 5.25\text{mm}$ and its width = 0.75 mm , $h = 2.25\text{mm}$
 and its width = 1.75 mm , $g1 = .5\text{ mm}$,
 $g2 = g3 = 0.3\text{mm}$.



Figure 6.9. Photograph of the antenna prototype

6.2.2 Results and discussion

The characteristics of the antenna prototype were studied using the Agilent Precision Network Analyser E8362B. The return loss response (S11) and the axial ratio response of the CPPDSA are depicted in Figure 6.10 and Figure 6.11 respectively.

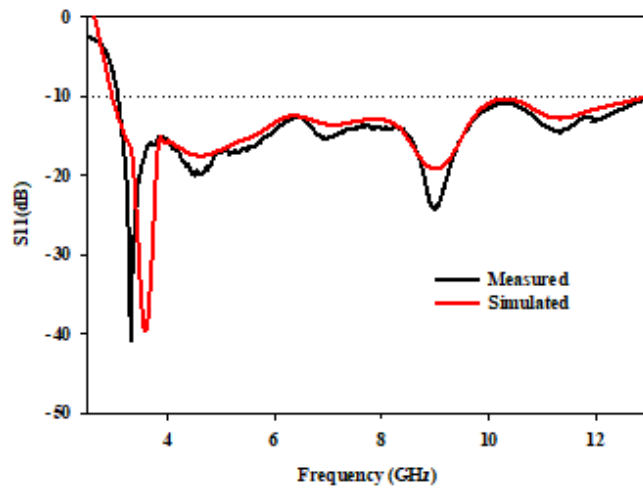


Figure 6.10. Measured and simulated plots of S11

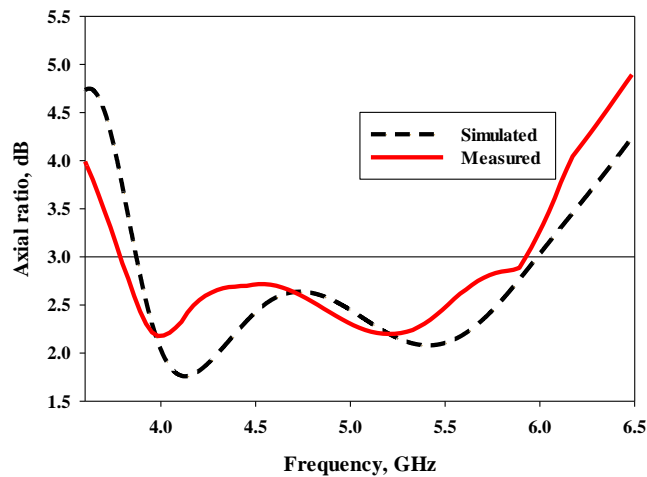


Figure 6.11. Measured and simulated plots of axial ratio

The return loss response curve shows that the 10 dB IBW ranges from 3GHz to 13 GHz and from the axial ratio it is clear that 3 dB ARBW ranges from 3.67GHz to 5.57 GHz. The strip line metal strip assembly significantly increases IBW.

The stub extended on the right side of the ground-plane increases the ARBW. The horizontal stub and the pentadecagonal slot radiator together produce CP performance.

The measured along with simulation radiation patterns of the fabricated antenna prototype are shown in Figure 6.12 (a) to 6.12(d). These are the normalized radiation patterns of the proposed antenna at $\phi = 0^\circ$, $\phi = 45^\circ$, $\phi = 90^\circ$ and $\phi = 135^\circ$ planes respectively, at 4.5 GHz frequency.

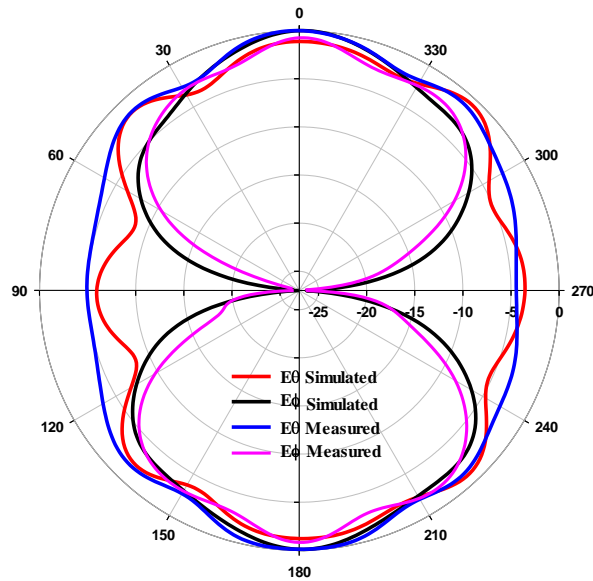


Figure 6.12(a). Radiation pattern at $\phi = 0^\circ$, 4.5 GHz

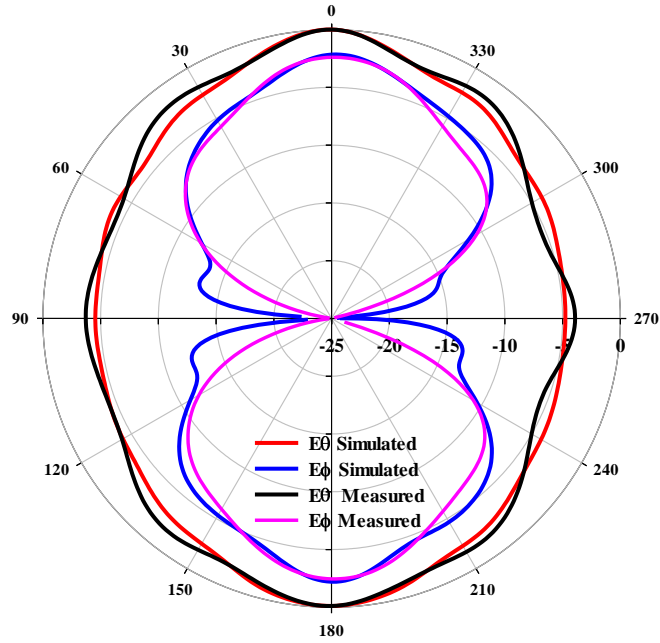


Figure 6.12(b). Radiation pattern at $\phi = 45^0$ 4.5 GHz

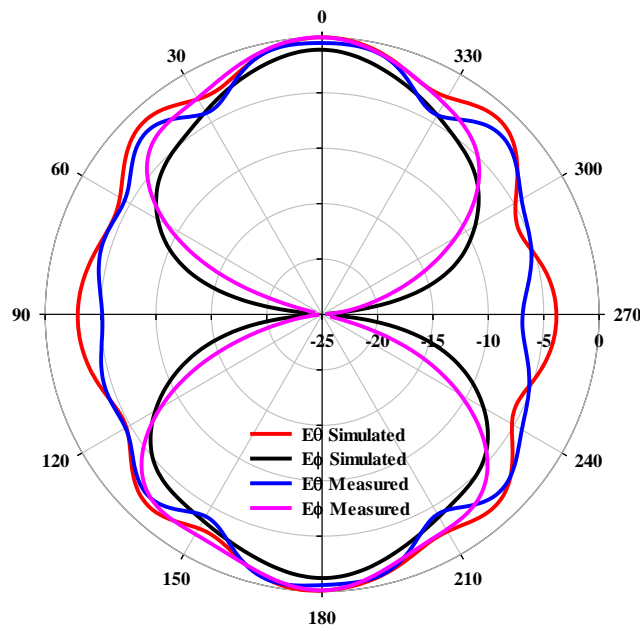


Figure 6.12(c). Radiation pattern at $\phi = 90^0$, 4.5 GHz

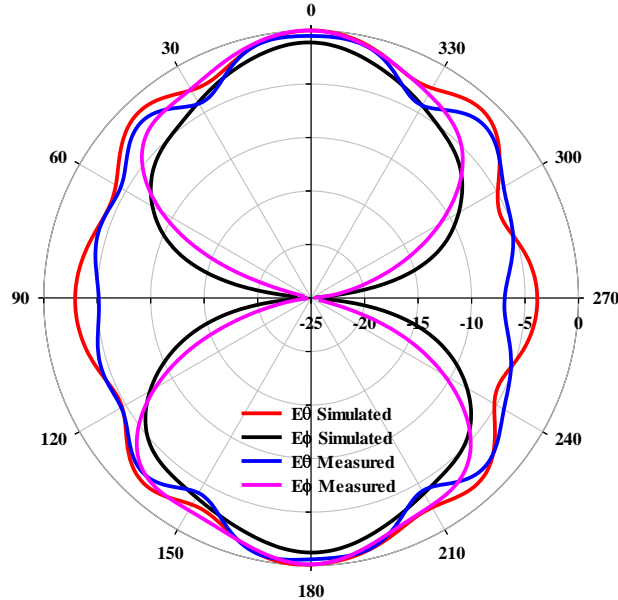


Figure 6.12(d) Radiation pattern at $\phi = 135^\circ$, 4.5 GHz

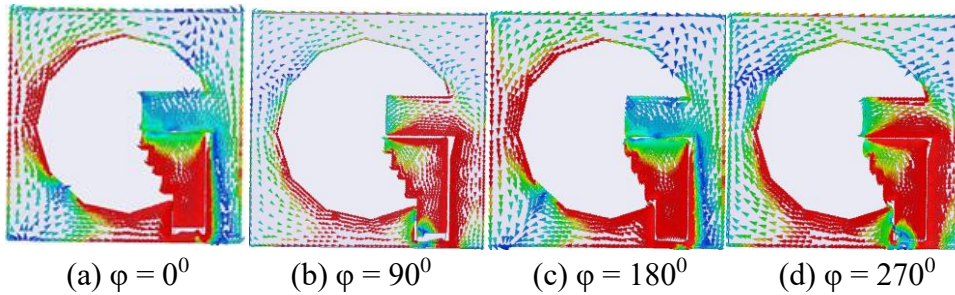


Figure 6.13. Simulated surface current pattern at 4.5 GHz

The surface current distributions of the antenna are shown in Figure 6.13 plotted at 4.5 GHz. It is observed that the surface current distributions in 180° and 270° are equal in magnitude and opposite in phase to 0° and 90° . Hence the antenna is RHCP in the $-z$ -direction.

This work demonstrates a novel and simple compact CP penta decagonal slot antenna. Measurement results show 10 dB impedance band of 3.0-13.0GHz, with a bandwidth of 125. % with respect to the centre

frequency 8 GHz and a CP band of 3.67 GHz – 5.75 GHz, with 3dB axial ratio bandwidth of 56.1% with respect to centre frequency of 4.71 GHz.

6.3 Circularly Polarised UWB Antenna

Circularly polarised, ultra-wide band (UWB), microstrip line fed antenna having asymmetric slotted structure is presented in this work. Two antennas are proposed. Antenna1(A1) radiates with Right Handed Circular Polarisation (RHCP) and Antenna2(A2) with Left Handed Circular Polarisation. The geometrical structure consists of uneven combination of stubs and slots both on the ground plane and the feed element. The geometries are fixed through parametric variations.

6.3.1 Antenna Geometry and Design

The FR4 substrate with a dielectric constant of 4.4 and size of $25 \times 25 \times 1.6 \text{ mm}^3$ is chosen for antenna fabrication. The geometry of the proposed antenna1 (A1) is depicted in Figure 6.14. Another antenna antenna2 (A2) is also proposed, which is the exact mirror image of A1 in both planes and having identical characteristics, whose geometry is shown in Figure 6.15. The geometrical structures show the top patch plane and bottom ground plane of A1 (seen through top plane) with dimensions labelled.

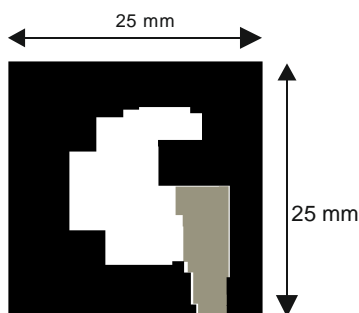


Figure 6.14. Geometry of A1

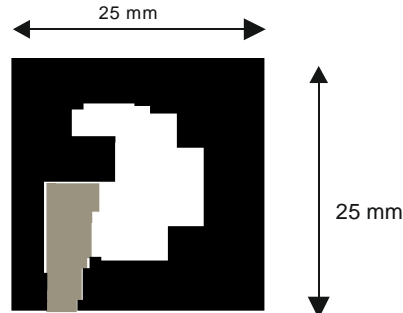


Figure 6.15. Geometry of A2

6.3.2 Study of simulated surface current

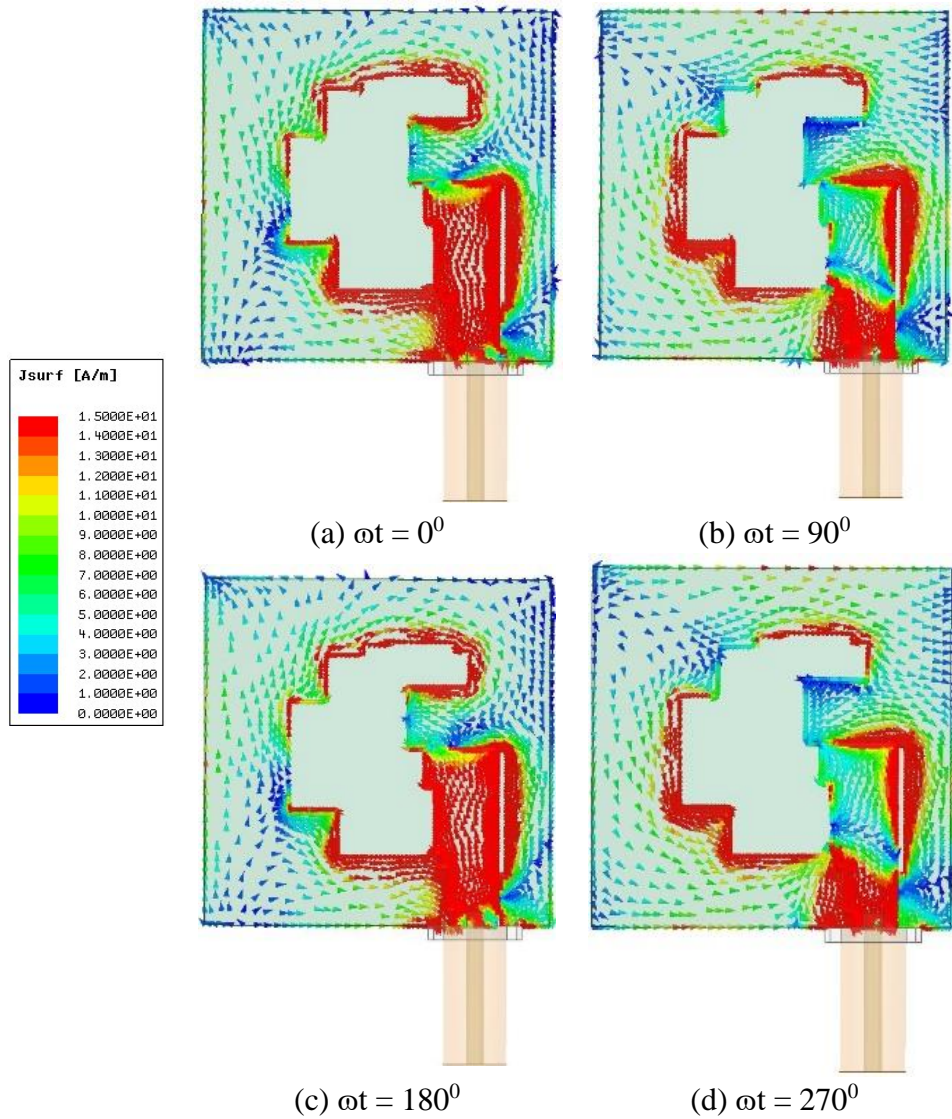


Figure 6.16. Surface current pattern on the proposed antenna A1 at 6 GHz

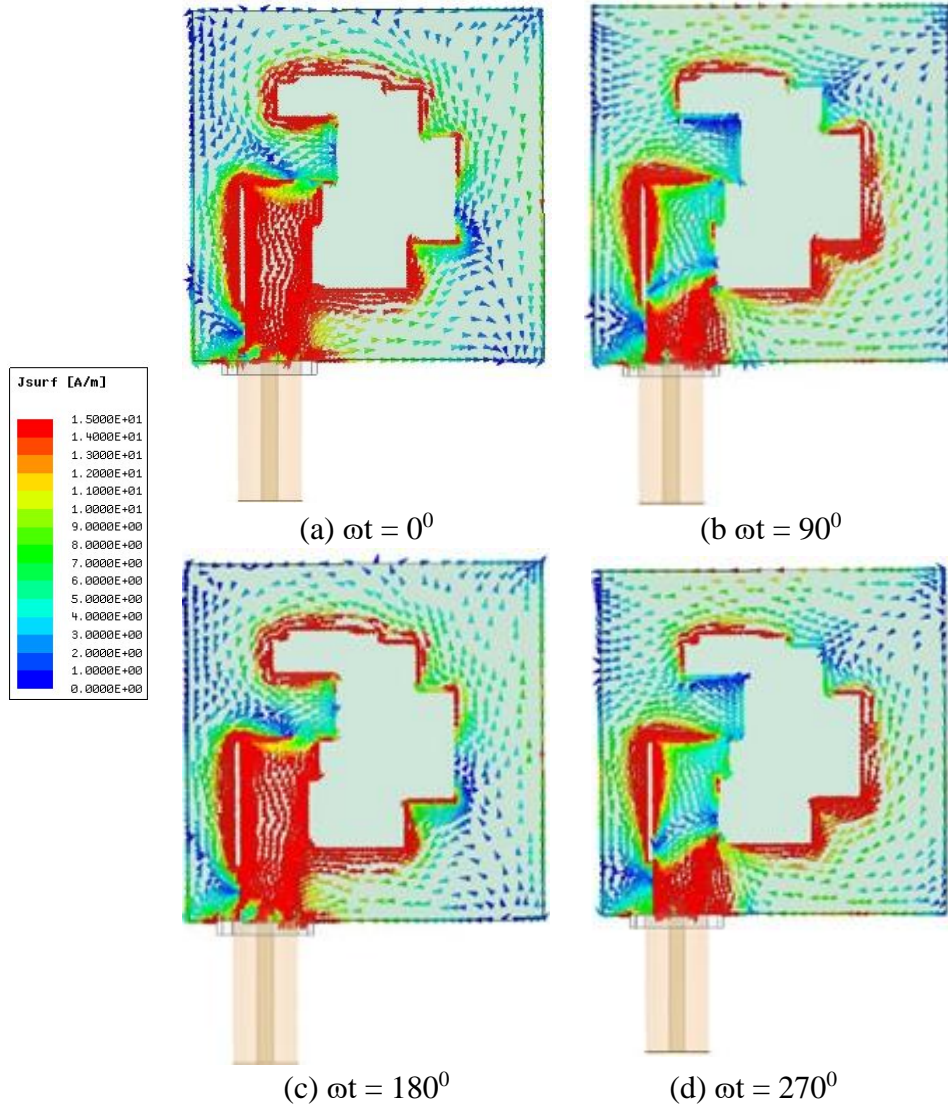


Figure 6.17 Surface current pattern on the proposed antenna A2 at 6 GHz

For a clear understanding of the circularly polarized radiation mechanism, the simulated time-varying surface current distributions of the proposed antenna A1 at regular time phases from 0° to 270° , with an

interval of 90° are depicted in Figure 6.16 at 6 GHz. It is observed that the surface current distributions at 0° and 180° are equal in magnitude and opposite in phase, just same as that at 90° and 270° . On the feed structure of A1, at 0° time phase, the surface current flows right, and at 90° time phase, the surface current flows downwards. Similarly, the surface current flows towards left at 180° time phase and flows upwards at 270° time phase. This shows that the surface current flows anticlockwise with respect to the viewer and as such proposed antenna A1 is Right-hand circularly polarized (RHCP) in the +Z direction. The electric field behaviour of A1 is also studied. From the study of electric field vector in the ground plane of the antenna it is inferred that, proposed antenna A1 is Left hand circularly polarized (LHCP) in the -Z direction. The simulated time-varying surface current distributions of the proposed antenna A2 at regular time phases from 0° to 270° , with an interval of 90° are depicted in Figure 6.17 at 6 GHz. The electric field behaviour of A2 is also studied. From the study it is understood that the radiation behaviour of the proposed antenna A2 is just inverse of A1. Hence A2 radiates with LHCP in the +Z direction and with RHCP in -Z direction.

6.3.3 Measured results and discussion

6.3.3.1 Measurement of S11 and axial ratio

The fabricated prototypes A1 and A2 were experimentally analysed using Agilent Vector Network Analyser PNAE 8362B, in the anechoic chamber. S11 measurements of A1 and A2 are plotted along with the simulation values in Figure 6.18. Also, it is observed that there is close resemblance between measured and simulated results. Axial ratios of the

antennas A1 and A2 were measured using the special setup in the anechoic chamber. These measurements along with simulated values are plotted as depicted in Figure 6.19. The measurement results show better impedance bandwidth (IBW) and ≤ 3 dB axial ratio bandwidth (ARBW). A1 offered IBW of 8.1 GHz (3.1 –11.26 GHz, 114.12 %), ARBW of 3.1 GHz (8.2-5.1 GHz, 46.6%). A2 offered IBW of 8.13 GHz (3.17–11.3 GHz, 112.3%), ARBW of 3.3 GHz (5.0-8.3 GHz, 49.6%). This constitutes a coverage of over 44 % of the UWB spectrum (3.1–10.6 GHz).

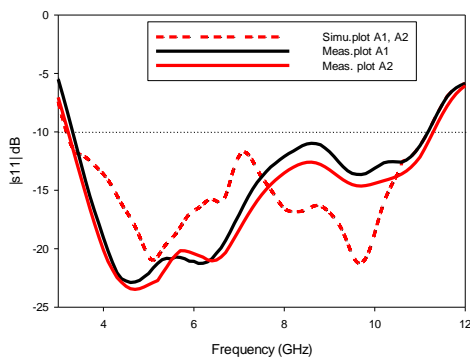


Figure 6.18. S11 Plots

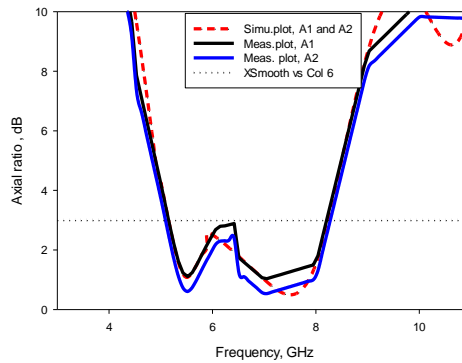


Figure 6.19. axial ratio plots

6.3.3.2 Measurement of gain and efficiency

Gain measurement using the gain comparison method yielded average gain values of 3.48 dBi and 3.5 dBi for A1 & A2 respectively, in the operating frequency band. Peak gain values obtained were 4.19 dBi for A1 and 4.15 dBi for A2 at 5.9 GHz, and efficiency is 85% for A1,A2.

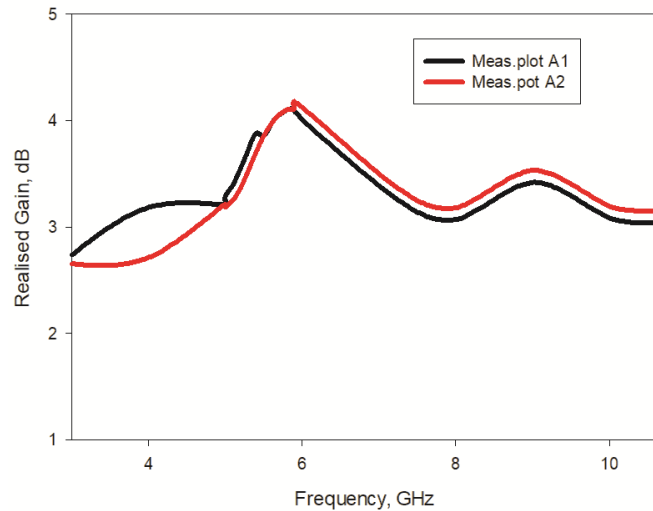


Figure 6.20. Measured realised gain plots of A1 and A2

6.3.3.3 Measurement of radiation pattern

The simulated and measured far-field normalized radiation patterns of A1 in YZ and XZ planes at a resonant frequency of 6 GHz are plotted in Figure 6.21. It is observed that the co polarization is RHCP for A1 and LHCP for A2. Whereas the cross polarisation is LHCP for A1 and RHCP in the case of A2. The antenna has a wide half-power beam width at each measured frequency. The cross polarisation level is lower than 20 dB. More than 20 dB isolation was observed between corresponding RHCP and LHCP patterns of both A1 and A2. Moreover, the radiation patterns of the antenna are stable and symmetrical in both XZ and YZ planes.

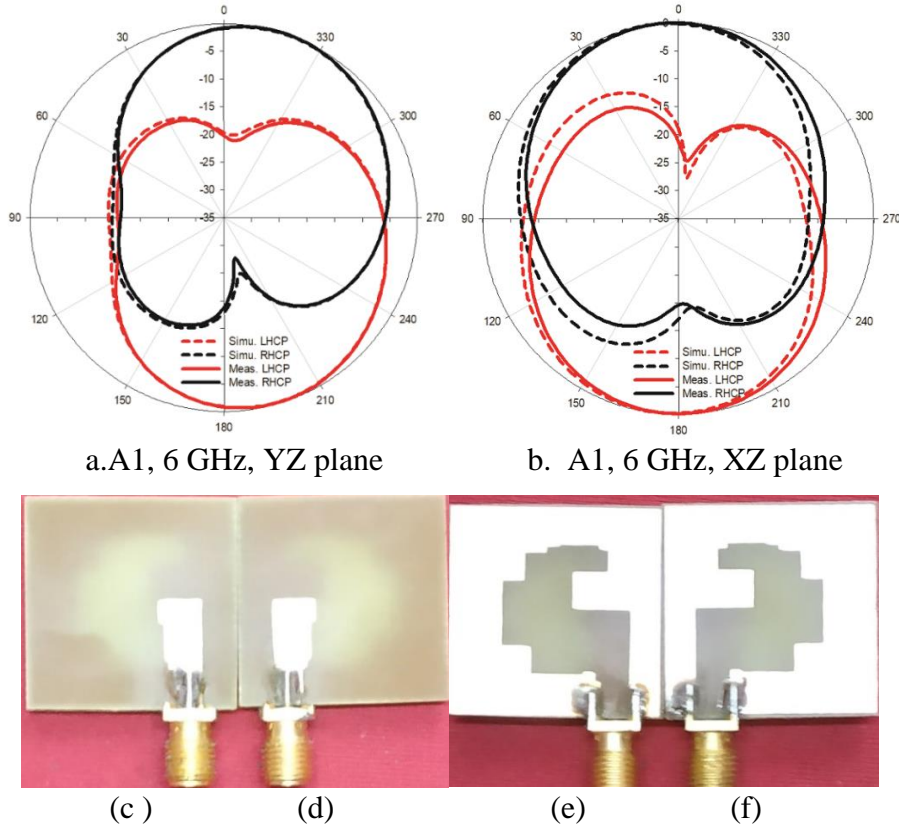


Figure 6.21. Normalised radiation patterns of A1 at 6 GHz (a) YZ plane (b) XZ plane (c) Photograph of A1 top view (d) Photograph of A2 top view (e) Photograph of A2 bottom view (f) Photograph of A1 bottom view

These antennas offered omnidirectional patterns, highly suitable for UWB communication. All measured results match very closely with the simulations.

6.4 Printed Circularly Polarised Asymmetric Ultra-wideband Antenna

Printed, circularly polarised, microstrip line fed antenna having asymmetric slotted structure is presented. Two antennas, antenna 1 (A1)

and antenna 2 (A2), having the same design but radiating with opposite senses of circular polarisation are fabricated. The geometrical structure consists of uneven combination of elements fixed through parametric variations. The proposed design is validated through simulations and experimental investigations.

6.4.1 Antenna geometry and design

The geometry of the proposed antenna, antenna1 (A1) is depicted in Figure 6.22. Another antenna, antenna2 (A2) is also proposed, which is the exact mirror image of A1 in both planes and having identical characteristics, whose geometry is shown in Figure 6.23. Figure 6.24 shows the geometrical structure of the top patch plane and bottom ground plane of A1 (seen through top plane) with dimensions labelled. These labels with corresponding dimensions are given in Table 6.2.

Design Steps

The design process of the proposed antenna A1 is explained through the evolution, comprising of five intermediate structures as shown in Figure 6.25. Antenna 1a, which is the initial structure, has a microstrip line fed radiator having width of 3.72 mm, on the top plane of the substrate. Two copper strips, one attached perpendicularly on the tip and another attached vertically on the right side of this microstrip feed line, forms the radiating element. The off-center feeding structure yield wide bandwidth [8]. Hence the feeding structure is not centered about the top plane of the substrate but shifted slightly towards the left. A rectangular strip ($23.6 \times 21.1 \text{ mm}^2$) is removed from the ground plane to form a wide slot Simulation studies were carried out using ANSYS HFSS. Simulated

reflection coefficient and axial ratio graphs of the antennas (antenna 1a to antenna 1e) are depicted in Figure 6.26 and Figure 6.27 respectively. These graphs are self-narrative of the progress in IBW and ARBW. However, antenna 1a has the least impedance matching and is lacking in CP characteristics. When a triangular portion is removed and two small copper strips are added to the upper portion of the feed line structure antenna 1b is obtained. Now the matching has improved in the lower frequency region but still lacks in CP characteristics, as the axial ratio is well above the 3dB limit. A small triangular cut removed from the top and five copper strips of different dimensions attached to the left of the feed line, antenna 1c is evolved. Now the matching is better than that of its predecessor but no improvement in the CP performance is observed, which is found to rather deteriorate. Antenna 1d is a modified version of antenna 1c, with the addition of four slots. One reverse 'L' slot on the top right corner of the border ground, two rectangular slots just beneath the feed line structure and another inverted 'L' slot on the feed line structure as in Figure 6.24. Now significant improvements are found in reflection coefficient and ARBW, in the upper frequency region. Design was further improved towards reaching the goal. Two sets each of six strips having different dimensions were added along the right and left portions of the ground. One strip was added along the top portion of the ground. Two inverted 'L' slots were added to the top left corner of the ground. IBW and ARBW drastically improved. Finally, the proposed antenna structure, A1 was attained by introducing six hexagonal slots of different dimensions on the bottom right corner of the ground border. This provides full band coverage of UWB and a significant percentage

coverage in ARBW. Thus the role of each element of the antenna at different frequencies in yielding good CP characteristics with good matching in the entire UWB spectrum was confirmed.



Figure 6.22. Structure of the proposed antenna1 (A1)



Figure 6.23. Structure of the proposed antenna2 (A2)

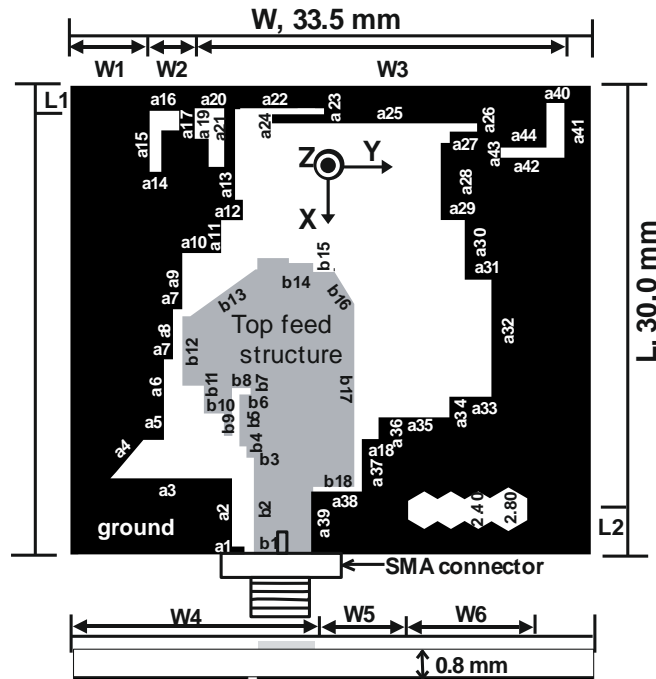


Figure 6.24. Geometrical structure of antenna 1 (A1) with dimensions labelled

Table 6.2. Dimensions of proposed antenna prototypes A1 and A2

Label	Value (mm)	Label	Value (mm)	Label	Value (mm)	Label	Value (mm)	Label	Value (mm)
a1	00.80	a15	03.90	a29	1.55	a43	00.65	b13	05.16
a2	04.37	a16	01.90	a30	03.82	a44	02.95	b14	04.97
a3	07.83	a17	01.25	a31	01.71	b1	03.72	b15	00.57
a4	03.27	a18	01.00	a32	07.48	b2	06.20	b16	02.41
a5	01.32	a19	01.96	a33	02.70	b3	00.48	b17	11.71
a6	05.17	a20	01.90	a34	01.32	b4	00.45	b18	02.58
a7	00.58	a21	03.75	a35	04.56	b5	03.33	W1	05.10
a8	03.20	a22	05.73	a36	01.40	b6	00.72	W2	02.90
a9	03.60	a23	03.35	a37	03.36	b7	00.41	W3	23.80
a10	02.50	a24	00.57	a38	03.27	b8	01.20	W4	15.50
a11	02.10	a25	13.12	a39	04.02	b9	03.06	W5	06.24
a12	01.40	a26	00.53	a40	01.15	b10	01.30	W6	07.67
a13	05.80	a27	01.75	a41	03.50	b11	01.38	L1	01.60
a14	00.75	a28	05.63	a42	04.10	b12	04.45	L2	02.90

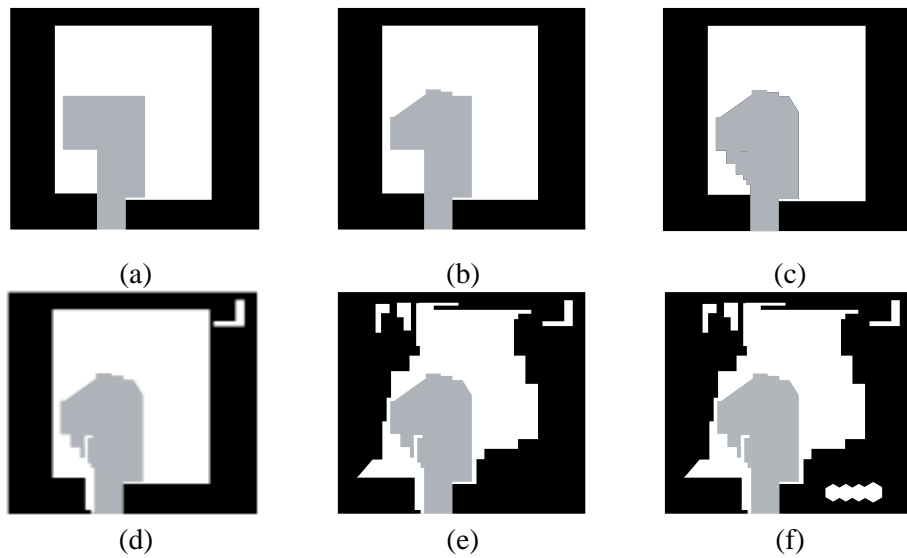


Figure 6.25. Evolution of proposed A1 (a) antenna1a, (b) antenna1b, (c) antenna1c, (d) antenna1d, (e) antenna1e and (f) proposed A1

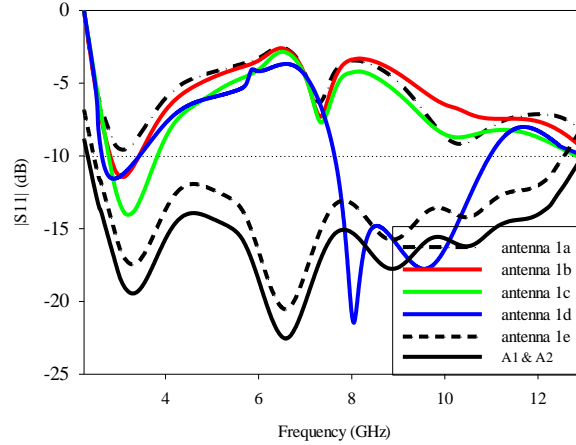


Figure 6.26. Simulated $|S_{11}|$ plots of antennas

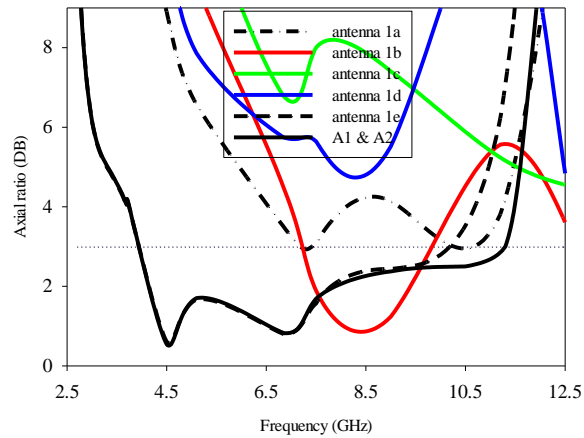


Figure 6.27. Simulated AR plots

6.4.2 Study of surface current and electric field patterns

The contribution towards the ARBW by the hexagonal slots on A1 is better understood from the surface current pattern over A1 and its predecessor antenna 1e, which differ only in terms of these slots, at 11.2 GHz and $\omega t = 0^\circ$ as shown in Figure 6.28. The distribution of surface current vector around these slots gives rise to horizontal and vertical components of electric field equal in magnitude and differ in phase by

90°. Similarly, each element of the structure contributes at different frequencies to enhance IBW and ARBW. Location of the feed was carefully optimized to obtain a good impedance match.

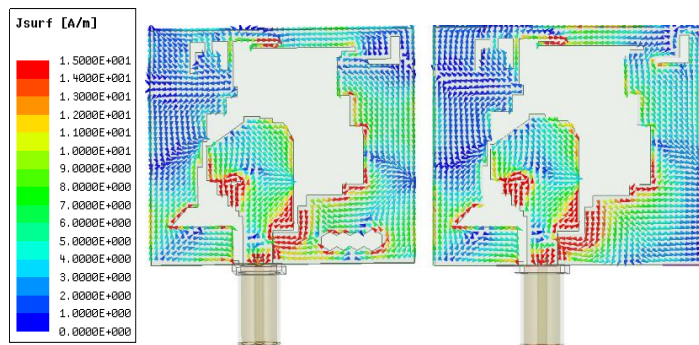


Figure 28. Surface current at $\omega t = 0^\circ$, 11.2 GHz on (a) A1 and (b) antenna 1e

For a better understanding of the circularly polarized radiation mechanism, the simulated time-varying surface current distributions of the proposed antenna A1 at regular time phases from 0° to 270° , with an interval of 90° are depicted in Figure 6.29 at 6.85 GHz. It is observed that the surface current distributions at 0° and 180° are equal in magnitude and opposite in phase to that at 90° and 270° . On the feed structure of A1, at 0° phase, the surface current flows right, and at 90° phase the surface current flows downwards. Similarly, the surface current flows towards left at 180° phase and flows upwards at 270° . This shows that the surface current flows anticlockwise with respect to the viewer and as such proposed antenna A1 is Right-hand circularly polarized (RHCP) in the +Z direction. The electric field behaviour of A1 is also studied and shown in Figure 6.30. From the study of electric field vector in the ground plane of the antenna it is inferred that, the proposed antenna A1 is Left hand circularly polarized (LHCP) in the -Z direction. The simulated time-

varying surface current distributions of the proposed antenna A2 at regular time phases from 0° to 270° , with an interval of 90° are depicted in Figure 6.31, at 6.85 GHz. The electric field behaviour of A2 is also studied and shown in Figure 6.32. From the studies, it is understood that A2 radiates with LHCP in the +Z direction and with RHCP in the -Z direction.

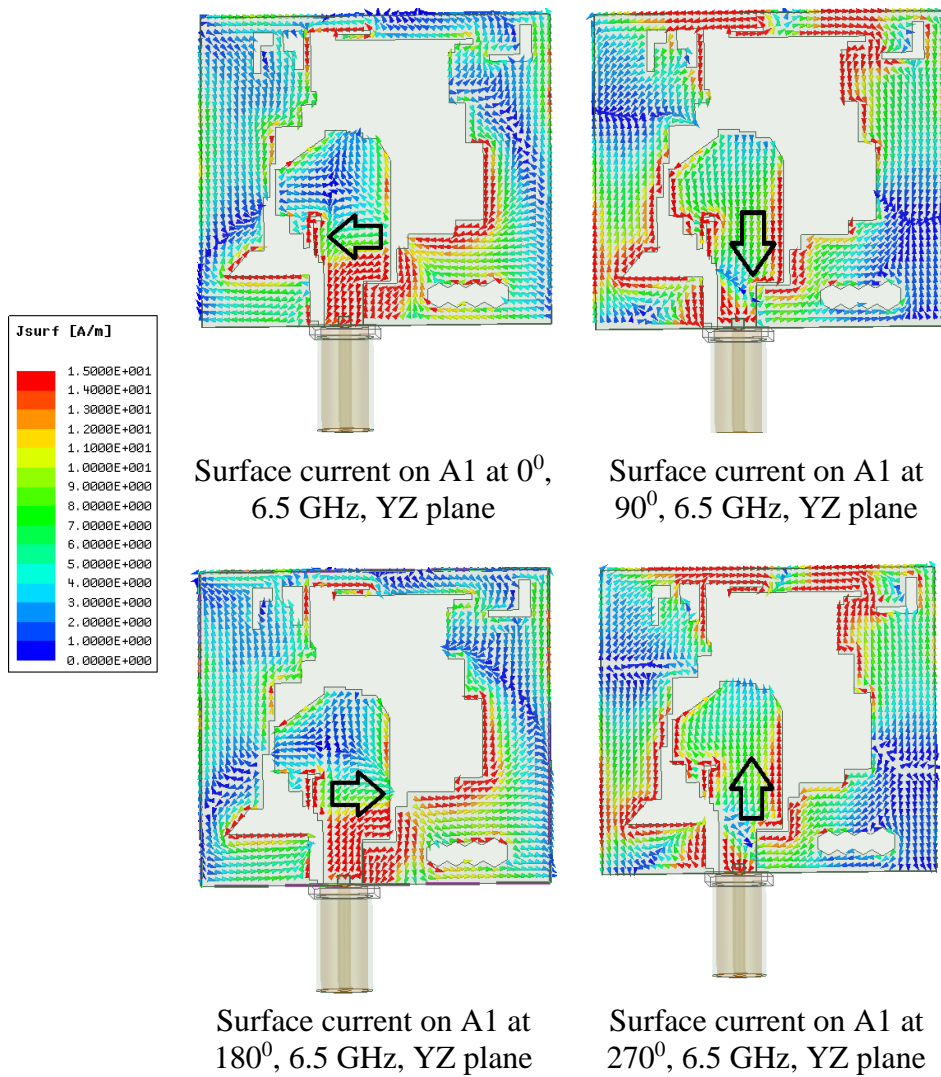


Figure 6.29. Surface current pattern on the proposed antenna A1

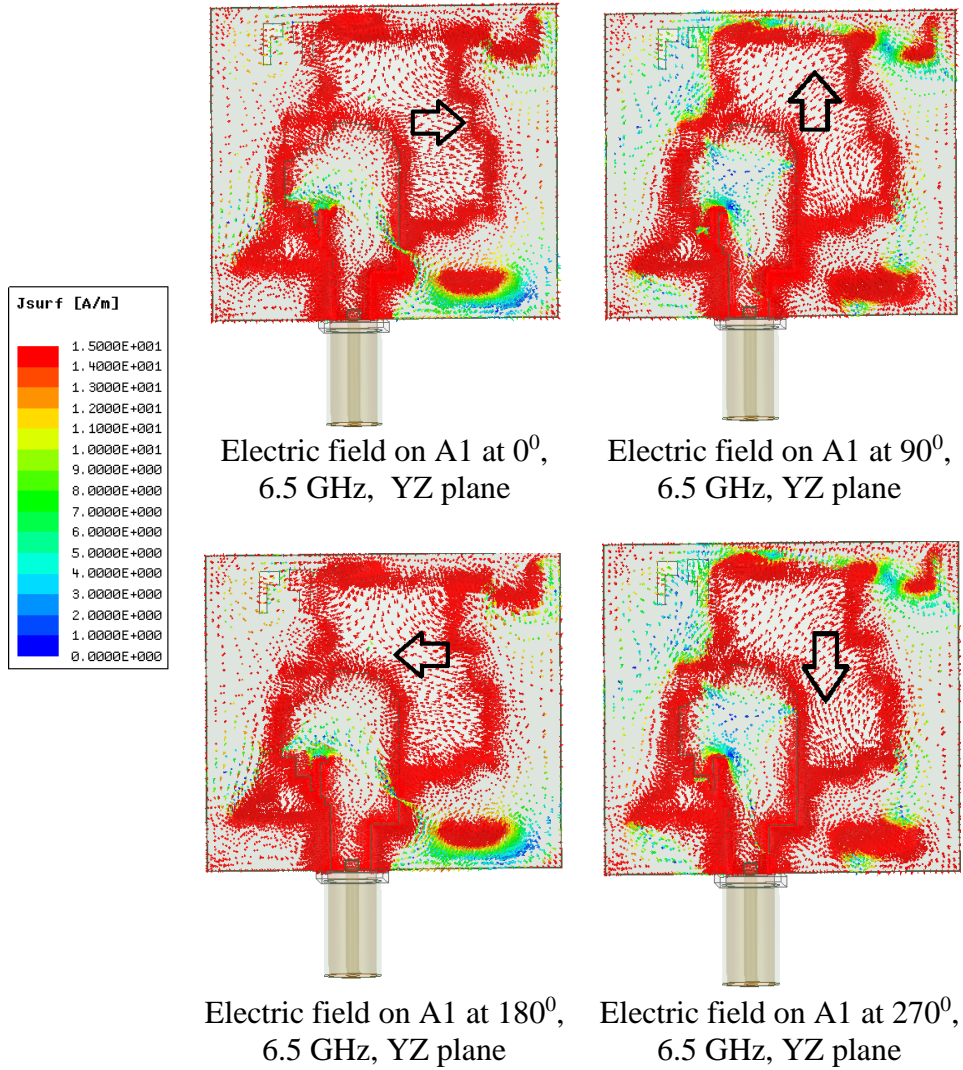


Figure 6.30. Electric field pattern on the proposed antenna A1

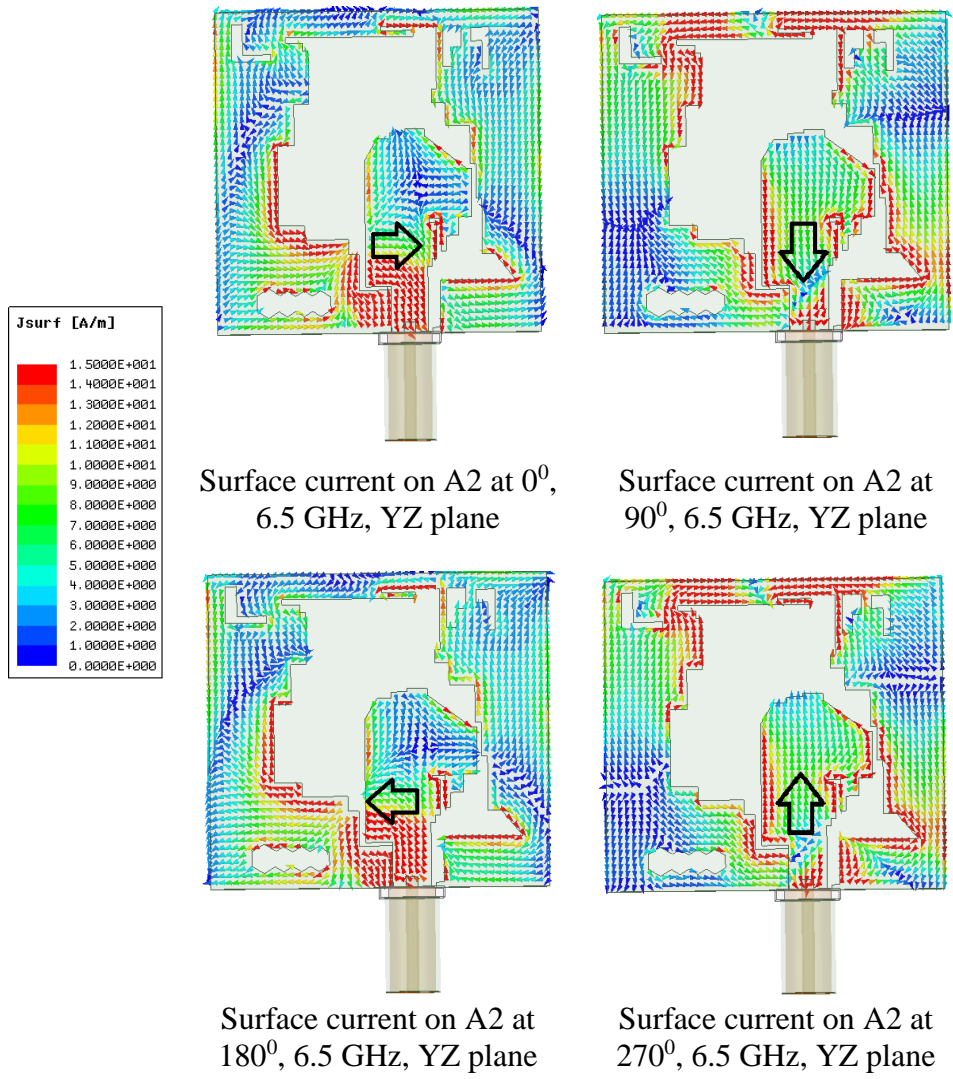


Figure 6.31. Surface current pattern on the proposed antenna A2

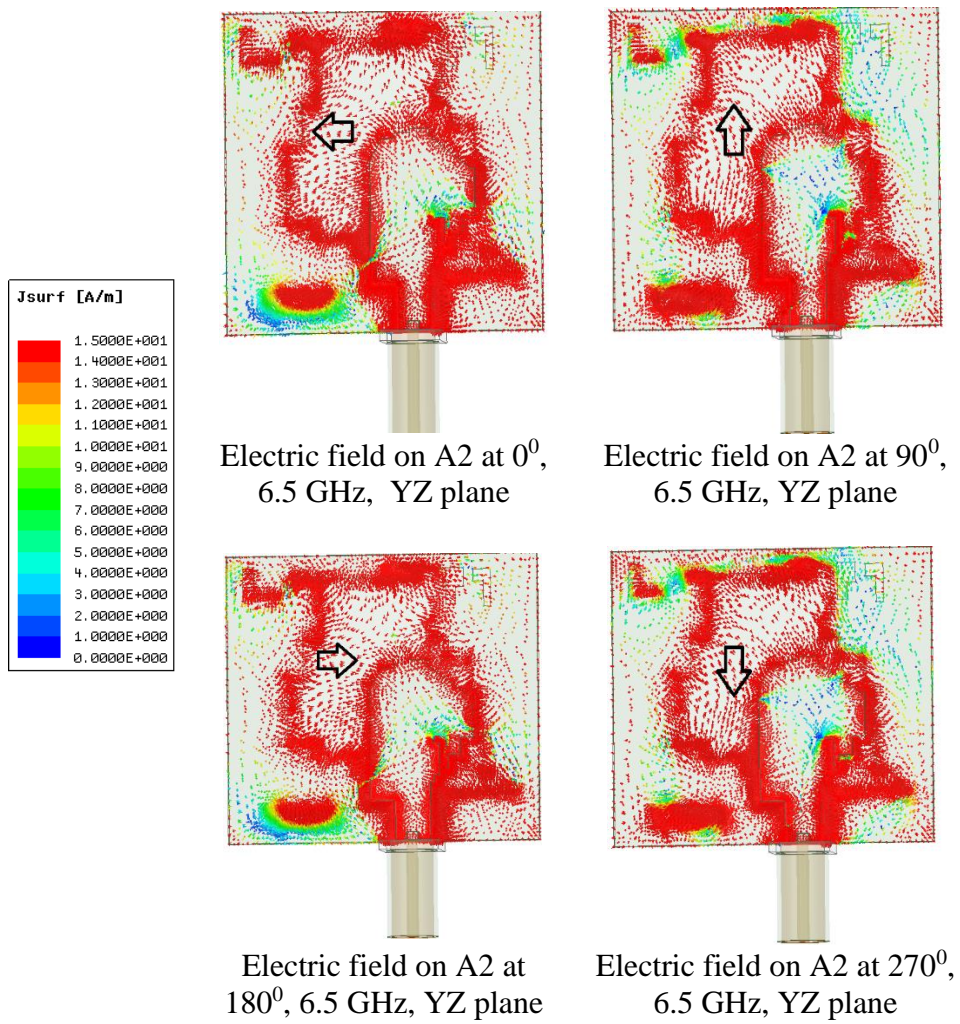


Figure 6.32. Electric field pattern on the proposed antenna A2

6.4.3 Measured results and discussion

Measurement of return loss and axial ratio

Selected substrate is FR4 ($\epsilon_r = 4.4$) with a size of $30 \times 33.5 \times 0.8$ mm³. The fabricated prototypes A1 and A2 were experimentally analysed using Agilent Vector Network Analyser PNAE 8362B, in the anechoic chamber. Return loss measurements of A1 and A2 are plotted along with the simulation values in Figure 6.33. It can be seen from this figure that the simulated $|S_{11}|$ plots coincide. Also, it is observed that there is close resemblance between measured and simulated results. Axial ratios of the antennas A1 and A2 were measured using the standard setup in the anechoic chamber. These measurements along with simulated values are plotted as depicted in Figure 6.34. A1 offered IBW of 9.67 GHz (2.46–12.13 GHz, 132.6%) and ARBW of 7 GHz (4–11 GHz, 93.33%). A2 offered IBW of 10.05 GHz (2.55–12.6 GHz, 132.7%) and ARBW of 7.3 GHz (3.9–11.2 GHz, 96.7%).

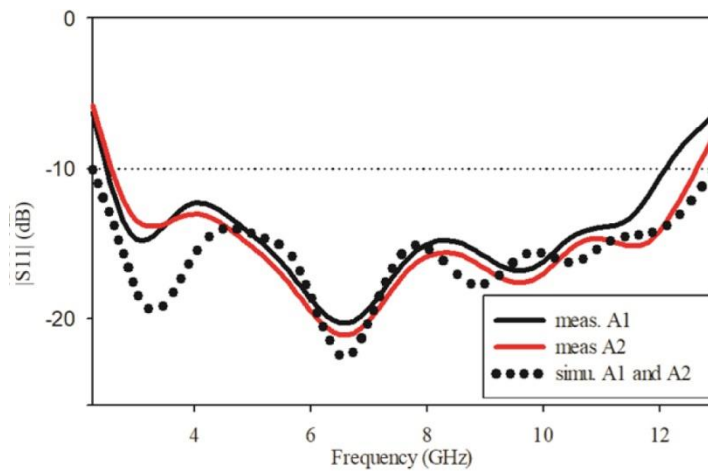


Figure 6.33. Measured and simulated $|S_{11}|$ plots of A1 & A2

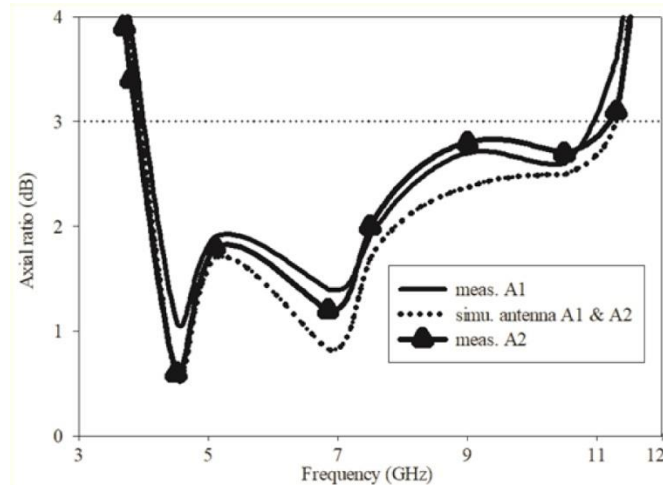


Figure 6.34. Measured and simulated axial ratio plots of A1 & A2

The CP band coverage of UWB spectrum (3.1 – 10.6 GHz) by A1 is 88% and that of A2 is 89.3 %. These are the maximum achieved values when compared with the antennas covered in the literature.

Measurement of gain and efficiency

Gain measurement using gain comparison method yielded average gain values of 3 dBi and 3.04 dBi for A1 & A2 respectively, in the operating frequency band. Peak gain values obtained were 4.0 dBi for A1 and 4.1 dBi for A2 at 8.72 GHz. Simulated and measured gain plots are depicted in Figure 35(a). The measured antenna efficiency plots are depicted in Figure 35(b). Peak values obtained were 92.71% at 3.3 GHz for A1 and 92.75% at 3.4 GHz for A2.

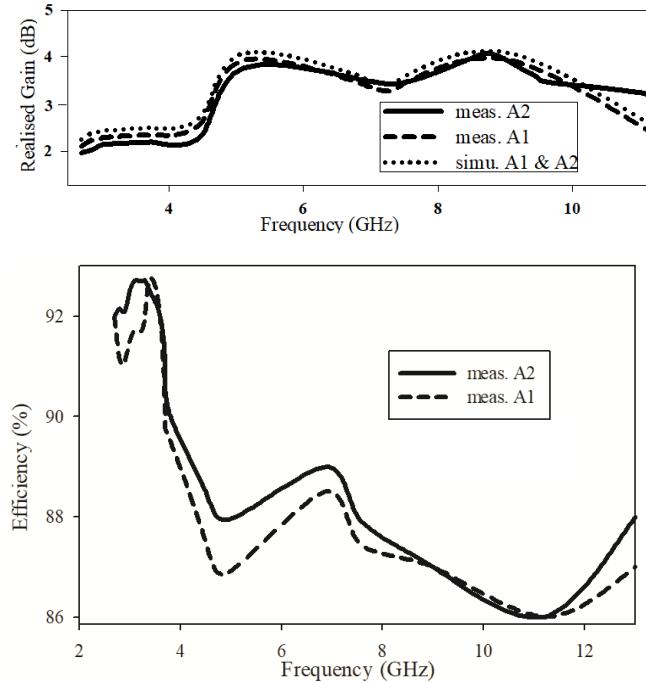


Figure 6.35. (a) Measured and simulated realized gain plots of the proposed A1 and A2 (b) Measured antenna efficiency plots of A1 and A2.

Measurement of group delay

Group delay measurements of A1 and A2 are shown in Figure 6.36. Measurements were carried out with two identical antennas each of A1 and A2, initially placed face to face and then side by side. The measurement results of both A1 and A2 coincide. It is observed that the group delay variations are less than 0.1 ns for both the antennas and are stable in the entire UWB spectrum. Consequently, it is inferred that the input signal suffers negligible time delay in the operating range.

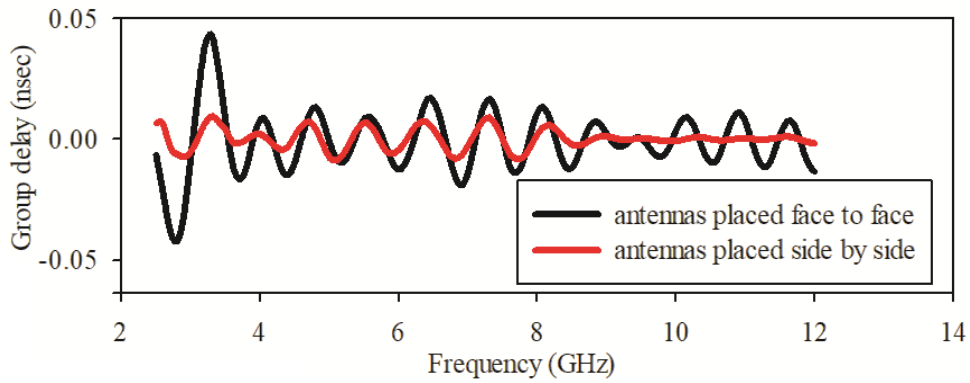


Figure 6.36. Measured group delay plots of the proposed A1 and A2

Measurement of radiation pattern

The simulated and measured far-field normalized radiation patterns of A1 and A2 in both XZ-plane and YZ-plane at frequencies 4.5 GHz, 6.85 GHz, and 7.5 GHz are plotted in Figure 6.37 and Figure 6.38. It is observed that the co polarization is RHCP for A1 and LHCP for A2, whereas the cross polarisation is LHCP for A1 and RHCP in the case of A2. The antenna has a wide half-power beam width at each measured frequency. The cross polarisation level is lower than 20 dB. More than 20 dB isolation was observed between corresponding RHCP and LHCP patterns of both A1 and A2. Moreover, the radiation patterns of the antennas are stable and symmetrical in both XZ and YZ planes.

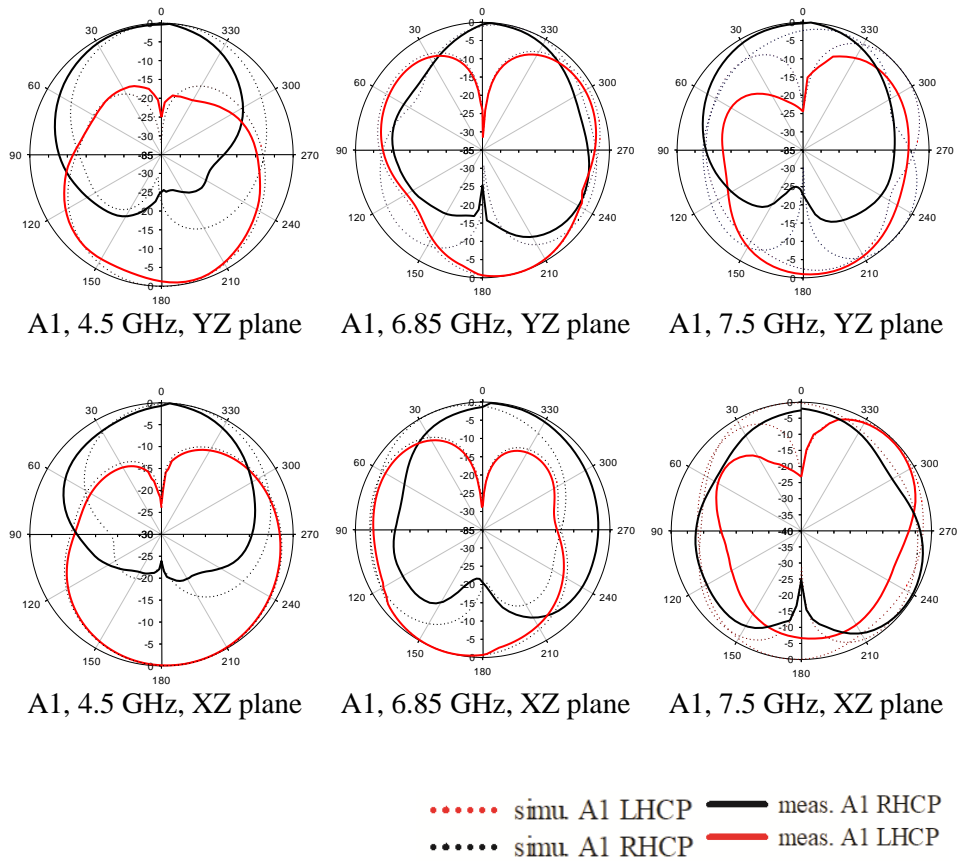


Figure 6.37. Normalised radiation patterns of A1 at three different frequencies

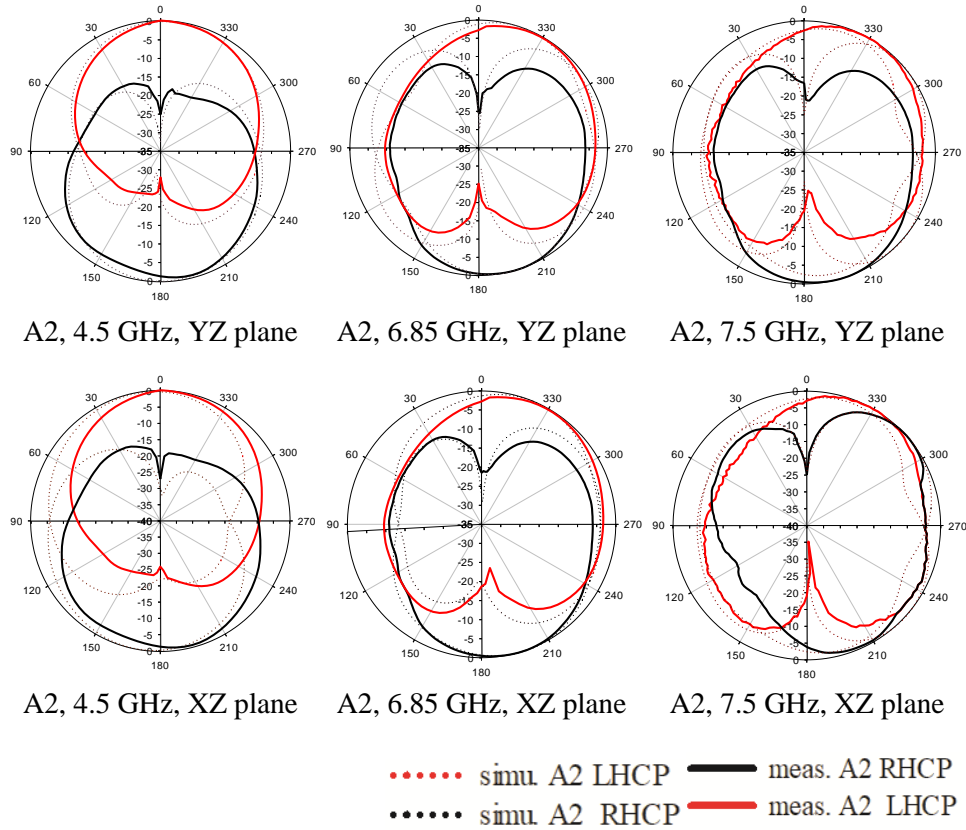
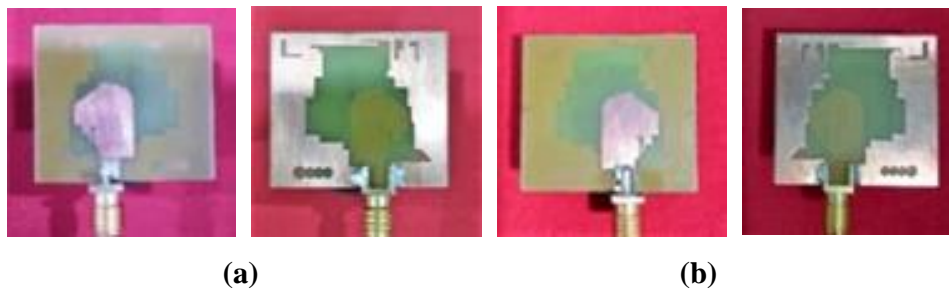


Figure 6.38. Normalised radiation patterns of A2 at three different frequencies

These antennas offered omnidirectional patterns, highly suitable for UWB communication. All measured results match very closely with the simulations. Performance comparison of the proposed antennas, is done as shown in Table 6.3 . The last column shows superior percentage in CP coverage of UWB spectrum by A1 and A2. The photographs of fabricated antennas are depicted in Figure 6.39.

Table 6.3. Performance comparison of antenna prototypes A1 and A2

Antennas under study	Size (mm ³)	IBW (GHz)	ARBW (GHz)	% CP of UWB
[24]	100×100×1.6	2.38 -2.54	2.45 -2.86	0
[25]	25×25×0.8	2.76-14.82	4.2-6.13	25.7
[26]	25×25×0.8	3-11.1	5.05-7.1	27.33
[27]	20×20×0.8	2.95-14	3.73-7.1	44.9
[28]	25×25×1.6	3.5-9.25	4.6-6.9	30.7
[29]	40×40×1.0	3.72-9.2	4.5-8.0	46.7
[30]	47.7×58×0.254	5.0-7.0	5.0-6.0	13.3
[31]	28×28×1.6	3.25-8	4.4-6.67	30.27
[32]	42×44×0.8	2.19-4.6	2.2-4.9	24.00
[33]	25×25×1.5	3.2-8.5	3.3-8.1	64.00
[34]	54×54×0.8	1.68-3.97	1.89-3.95	11.33
This work A1	30×33.5×0.8	2.46-12.13	4.0-11.0	88.0
This work A2	30×33.5×0.8	2.55-12.60	3.9-11.2	89.3

**Figure 6.39.** Photographs of fabricated antenna prototypes. Top and bottom views of (a) A1 (b) A2**Table 6.4.** Validation of different substrates (Simulated values)

Substrate	ϵ_r	h mm	IBW, GHz	ARBW, GHz
Taconic35	3.5	0.8	2.57- 12	4.25 – 8.07
Rogers04350	3.66	0.8	2.55 - 12	4.21 – 8.13
RogersTMM4	4.5	0.8	2.5 – 11.5	3.9 – 10.8
RogersTMM4	6	0.8	2.4 – 10.9	3.7 - 11

Chapter summary

The ultra-wideband circularly polarized patch antennas have been analyzed in this chapter. The key inferences derived from the studies can be summarized as below.

Printed asymmetric circularly polarised microstrip line fed antennas radiating with opposite senses of polarisation to each other, having wide IBW and ARBW are proposed. Wide slot patch antennas can be conveniently used to produce circular polarisation. With asymmetric structures these antenna prototypes exhibit nearly 90 percentage CP band coverage of the UWB spectrum. These antennas exhibit moderate average gain, very good efficiency, omni directional radiation pattern and marginal group delay, suitable for UWB applications. When validated with different substrates, it is found that substrates with lower dielectric constants exhibit the same impedance band but less axial ratio bandwidth. This may be due to the height factor. Here the height is taken to be the same. If it was increased proportionately, it would have given more axial ratio bandwidth. Reverse is true for substrates with higher dielectric constants.

References

- [1] Zhang, L., S. Gao, Q. Luo, P. R. Young, et al., "Single-feed ultra-wideband circularly polarized antenna with enhanced front-to-back ratio," *IEEE Trans. Antennas Propag.*, Vol. 64, 355–360, 2016.
- [2] Mao, S.-G., J.-C. Yeh, and S.-L. Chen, "Ultrawideband circularly polarized spiral antenna using integrated balun with application to time-domain target detection," *IEEE Trans. Antennas Propag.*, Vol. 57, No. 7, 1914–1920, 2009.

- [3] Nakano, H. and J. Yamauchi, “Printed slot and wire antennas: a review,” *Proceedings of the IEEE*, Vol. 100, No. 7, 2158–2168, 2012.
- [4] Wu, J., X. Ren, Z. Li, and Y. Yin, “Modified square slot antennas for broadband circular polarization,” *Progress In Electromagnetics Research C*, Vol. 38, 1–14, 2013.
- [5] Shokri, M., V. Rafii, S. Karamzadeh, Z. Amiri, and B. Virdee, “Miniaturised ultra-wideband circularly polarised antenna with modified ground plane,” *Electron. Lett.*, Vol. 50, 1786–1788, 2014.
- [6] Karamzadeh, S., V. Rafii, M. Kartal, and M. Dibayi, “Circularly polarized square slot antenna,” *ACES Journal*, Vol. 30, No. 3, 327–331, 2015.
- [7] Karamzadeh, S., V. Rafii, M. Kartal, H. Saygin, “Compact UWB CP square slot antenna with two corners connected by a strip line”, *Electron. Lett*, Vol.52, 10-12, 2016.
- [8] Mubarak Sani Ellis, Zhiqin Zhao, Jiangniu Wu, Xiaoxiang Ding, Zaiping Nie and Qing Huo Liu, “A novel simple and compact microstrip fed circularly polarized wide slot antenna with wide axial ratio bandwidth for C band applications”, *IEEE Trans. Antennas Propag.*, Vol. 64, No. 4, 1552-1555, 2016.
- [9] Kang Ding, Cheng Gao, Tongbin Yu, Dexin Qu: ‘Wideband CP slot antenna with backed FSS reflector’, *IET Microw. Antennas Propag.* , Vol. 11, No.7, 1045-1050, 2017.
- [10] Tapas Mondal, Sandip Maity, Rowdra Ghatak and Sekhar Ranjan Bhadra Chaudhuri, “Design and analysis of a wideband circularly polarised perturbed psi-shaped antenna”, *IET Microw. Antennas Propag.*, Vol.12, No.9, 1582-1586, 2018.
- [11] Mehrdad Nosrati and Negar Tavassolian, “Miniaturized circularly polarized square slot antenna with enhanced axial-ratio bandwidth using an antipodal Y-strip”, *IEEE Antennas and Wireless Propagation Letters*, Vol.16, 817-820, 2017.

- [12] Hui-Fen Huang and Bin Wang, “A Simple V-shaped slot antenna with broadband circular polarization”, *Progress In Electromagnetics Research Letters*, Vol. 67, 67–73, 2017.
- [13] Zhe Wu, Gen Ming Wei, Xi Li, and Lin Yang, “A Single-Layer and Compact Circularly Polarized Wideband Slot Antenna Based on Bent Feed”, *Progress In Electromagnetics Research Letters*, Vol. 72, 39–44, 2018.
- [14] Son Trinh-Van, Youngoo Yang, Kang-Yoon Lee and Keum Cheol Hwang, “Broadband circularly polarized slot antenna loaded by a multiple-circular-sector”, *Sensors*, Vol. 18, 1576- 1588, 2018.
- [15] R. Xu, J.-Y. Li, J. Liu, S.-G. Zhou, , K. Wei, and Z.-J. Xing, “A simple design of compact dual-wideband square slot antenna with dual-sense circularly polarized radiation for WLAN/Wi-Fi Communications”, *IEEE Trans. Antennas Propag.*, Vol. 66, No. 9, 4884 - 4889, 2018.
- [16] Adam Narbudowicz, Matthias John, Vit Sipal,” Design Method for Wideband CircularlyPolarized Slot Antennas” *Ieee Transactions On Antennas And Propagation*, Vol. 63, No. 10, pp 4271-4277,October 2015
- [17] Jia-Yi Sze, Chung-I. G. Hsu, Zhi-Wei Chen, and Chi-Chaan Chang “Broadband CPW-Fed Circularly Polarized Square Slot Antenna With Lightning-Shaped Feedline and Inverted-L Grounded Strips”. *IEEE Transactions On Antennas And Propagation*, Vol. 58, No. 3, March 2010
- [18] Pourahmadazar, J., and Mohammadi, S.:” Compact circularly-polarisedslot antenna for UWB applications”, *Electron. Lett.*, 2011, 47, (15), pp. 837–838.
- [19] Sze, J.-Y., and Chang, C.-C.: “Circularly polarized square slot antenna with a pair of inverted-L grounded strips”, *IEEE Antennas Wirel. Propag. Lett.*, 2008, 7, pp. 149–151.

- [20] Pourahmadazar, J., Ghobadi, C., Nourinia, J., et al.: “Broadband CPW-fed circularly polarized square slot antenna with inverted-L strips for UWB applications”, *IEEE Antennas Wirel. Propag. Lett.*, 2011, 10, pp. 369–372.
- [21] Chou, C.C., Lin, K.-H., and Su, H.L.: “Broadband circularly polarized crosspatch-loaded square slot antenna”, *Electron. Lett.*, 2007, 43, (9), pp. 485–486.
- [22] Sze, J.-Y., Wang, J.-C., and Chang, C.-C.: “Axial-ratio bandwidth enhancement of asymmetric-CPW-fed circularly-polarised square slotantenna”, *Electron. Lett.*, 2008, 44, (18), pp. 1048–1049.
- [23] Shokri, M., Rafii, V., Karamzadeh, S., et al.: ‘Miniaturised ultrawideband circularly polarised antenna with modified ground plane’, *Electron. Lett.*, 2014, 50, (24), pp. 1786–1788
- [24] Jianjun Wu, Xueshi Ren, Zhaoxing Li, and Yingzeng Yin, “Modified square slot antennas for broadband circular polarization”, *Progress In Electromagnetics Research C*, Vol. 38, 1–14, 2013.
- [25] Shokri, M., V. Rafii, S. Karamzadeh, Z. Amiri, B. Virdee, “Miniaturised ultra-wideband circularly polarised antenna with modified ground plane”, *Electron. Lett*, Vol. 50, 1786-788, 2014.
- [26] Saeid Karamzadeh , Vahid Rafii , Mesut Kartal and Morteza Dibayi, “Circularly polarized square slot antenna”, *ACES Journal*, Vol. 30, No. 3, 327-331, 2015.
- [27] Karamzadeh, S., V. Rafii, M. Kartal, H. Saygin, “Compact UWB CP square slot antenna with two corners connected by a strip line”, *Electron. Lett*, Vol. 52, 10-12, 2016.
- [28] Mubarak Sani Ellis, Zhiqin Zhao, Jiangniu Wu, Xiaoxiang Ding, Zaiping Nie and Qing Huo Liu, “A novel simple and compact microstrip fed circularly polarized wide slot antenna with wide axial ratio bandwidth for C band applications”, *IEEE Trans. Antennas Propag.*, Vol. 64, No. 4, 1552-1555, 2016.

- [29] Kang Ding, Cheng Gao, Tongbin Yu, Dexin Qu: ‘Wideband CP slot antenna with backed FSS reflector’, *IET Microw. Antennas Propag.*, Vol. 11, No.7, 1045-1050, 2017.
- [30] Tapas Mondal, Sandip Maity, Rowdra Ghatak and Sekhar Ranjan Bhadra Chaudhuri, ‘Design and analysis of a wideband circularly polarised perturbed psi-shaped antenna’, *IET Microw. Antennas Propag.*, Vol.12, No.9, 1582-1586, 2018.
- [31] Mehrdad Nosrati and Negar Tavassolian, ‘Miniaturized circularly polarized square slot antenna with enhanced axial-ratio bandwidth using an antipodal Y-strip’, *IEEE Antennas and Wireless Propagation Letters*, Vol.16, 817-820, 2017.
- [32] Hui-Fen Huang and Bin Wang, ‘A Simple V-shaped slot antenna with broadband circular polarization’, *Progress In Electromagnetics Research Letters*, Vol. 67, 67–73, 2017.
- [33] Zhe Wu, Gen Ming Wei, Xi Li, and Lin Yang, ‘A Single-Layer and Compact Circularly Polarized Wideband Slot Antenna Based on Bent Feed’, *Progress In Electromagnetics Research Letters*, Vol. 72, 39–44, 2018.
- [34] Son Trinh-Van, Youngoo Yang, Kang-Yoon Lee and Keum Cheol Hwang, ‘Broadband circularly polarized slot antenna loaded by a multiple-circular-sector’, *Sensors*, Vol. 18, 1576- 1588, 2018.

.....✂.....

- 7.1 Thesis summary
- 7.2 Inferences from the investigations on the various antennas described
- 7.3 Suggestions for future works

This chapter provides glimpses of the research work done and highlights the research outcome. The conclusions arrived through theoretical, simulated and experimental investigations on different circularly polarised antennas are showcased. A few suggestions for the extension of future study and work are also mentioned.

7.1 Thesis Summary and Conclusions

The aim of this research work was to design and develop compact single band, multi band and ultra-wide band circularly polarised antennas. This thesis presents a detailed study on the design, development and characterisation of eight different types of single band, one dual band and three different types of ultra-wide band circularly polarised antennas, for wireless applications. The analysis of the patch geometries was elaborated upon. The prime objective of the designs was to achieve circular polarization in the predetermined band. The generation of CP was better

understood by the detailed analysis of evolution. The development of the geometrical structure, location of slots and strips on the structures and the dependence of various geometrical parameters upon the antenna performance were first investigated. The reflection characteristics, circular polarisation behaviour, simulation studies of current/field distribution and characteristic mode analysis confirm their dependence on the antenna dimensions. It is estimated that the circular polarisation behaviour is highly sensitive and the dimensions, structure of slots and strips are the decisive factors which affect the performance to a large extent. The performance of the antenna on various substrates of different thicknesses were studied and this helps to design the antenna on any chosen substrate of a particular thickness for the desired frequency range of operation.

A brief study of advantages, applications and an overview of the history of microstrip antenna technology, theory of circular polarisation, methods of evoking circular polarisation and the study of the theory of characteristic mode analysis were carried out in Chapter 1. A survey of the literature in the areas of single band, dual band and ultra-wide band circularly polarised antennas was carried out and the justification for the choice of the present research work is portrayed in chapter 2. Adopted methodologies and experimental techniques are elaborated upon in Chapter 3. Design and development of eight different circularly polarised compact single band polygonal patch geometries with polygonal slots for wireless applications are described in Chapter 4. The circular polarisation behaviour in dual bands of a slot antenna is investigated and analysed using characteristic mode analysis in Chapter 5. Chapter 6

describes three different antennas which exhibit circular polarisation behaviour in ultra-wide band. The technique behind the percentage coverage CP characteristics is also elaborated upon.

7.2 Inferences arrived from the study of antennas developed

Major inferences arrived after the investigation of the developed antennas, in this piece of research work, are summarized below.

Inferences on single band CP antennas

- Eight different compact single band polygonal patch antennas, which exhibit circular polarisation characteristics are developed.
- Out of this, six antennas developed are having central hexagonal slot on their structure.
- This central hexagonal slot perturbation method is found to be effective in generating circular polarisation characteristics.
- Rest two antennas used central elliptical slot for generating CP characteristics.
- All the antennas provided symmetrical radiation patterns with wide angle half power beam widths, good 10 dB impedance bandwidth and 3 dB axial ratio bandwidth, circular polarization characteristics and reasonable gain values.
- The antennas are compact, simple to design cost effective and suitable for wide angle coverage wireless applications at 2.45 GHz.
- Observed that increase in the number of sides of the polygon, with which the antennas are made, improve CP characteristics.

This is because the number of sides of the polygonal patch affect the electrical length and hence the resonant frequency, which in turn, resonates TM_{01} and TM_{10} modes. These orthogonal modes give rise to the CP behaviour.

- Whereas, the CP characteristics deteriorate, when the number of sides of the polygon increase beyond polygon and hence the polygon tend to be circular in shape.
- It is found in literature that a circular patch with central elliptical slot exhibit CP characteristics, but to a less extent when compared to the polygonal patch antennas developed in this piece of research work.
- As stated previously, the central irregular hexagonal slot has a good effect on yielding circular polarisation characteristics.
- The CP performance is disturbed as the axial ratio characteristics rise above 3 dB level, when the aspect ratio of the central irregular hexagonal slot exceeds the value 1.62.
- The CP performance is highly sensitive with respect to the dimensions of the central slot and the location of the feed point.
- Two antennas incorporated two circular slots symmetrically placed with respect to the central slot, on the polygonal patch. These slots also contribute to the axial ratio bandwidths.
- Introduction of slots in the central portion of patch and symmetrically on both sides of it, can be successfully utilized to control the CP behaviour, compactness and possible to tune the operating frequency to the band of interest.

- The design equations are validated and authenticated by the actual fabrication.
- The antennas developed are novel and simple in their structure, easy to analyse, compact, cost effective and exhibit good circular polarisation characteristics.

Inferences on dual band CP antenna

A detailed analysis of the developed dual band circularly polarized patch antenna is done and following are the observations.

- A slot antenna is a good candidate for broad band CP generation
- Microstrip antennas having wide slot give good CP results.
- Instead of introducing single rectangular slot or crossed slot on a patch antenna, a modified slot shape can be used to improve the CP bandwidth of patch antennas.
- Asymmetric slots and strips either on the feed or on the ground give good IBW and ARBW.
- Dimensions and shape of the slot critically affect the generation of the orthogonal components of the electric field.
- Slot antennas having perturbations prove to be a better choice.
- To have good CP radiation properties, symmetric structure is not mandatory.
- Slot antennas have bidirectional radiation characteristics and their Q factor is also low.
- Asymmetric structures provide good CP bandwidth.

- Null current locations may be sorted out and help to improve design.
- The location of feed point has got an effect on CP characteristics
- The CP characteristics pertained to two bands is substantiated with simulation methods.
- Characteristic mode analysis is done extensively to resolve the CP mechanism in two bands. Many characteristic mode frequencies are sorted out in the range of 2.5GHz to 14GHz. Hence frequencies that contributed to CP behaviour have been analysed.

Inferences on circularly polarised UWB antennas

Four different circularly polarised UWB antennas are investigated and the inferences are summarised below.

- Two antennas are coplanar waveguide fed and two are microstrip line fed.
- All antennas have wide slot ground and lacks symmetric geometrical structure.
- The structures described proved to have improved results, compared to other antennas under study.
- Two CPW fed antennas, one having a hexagonal slot and the other, pentadecagonal slot, proved to have better CP performances.

- A stub projected from the ground and the slot radiator proved to have better contributions towards CP. Feed structure enhances the same.
- Two antennas developed are having opposite sense of polarisations.
- For a maximum CP band coverage of UWB, asymmetric structures are good enough.
- They are good in terms of gain, efficiency, Omni directional radiation pattern and group delay, which in turn are advantageous for UWB applications.
- The size of the radiating slot, methods of perturbations, dimensions location of slots etc., affect the CP performance
- The design strategy adopted here prove to be superior to other strategies for a better CP coverage of UWB.
- Conventional structures like spiral and travelling wave structures, need a big size compared to the antennas developed in this work.
- The dimensions of the slots and strips are very sensitive with reference to CP behaviour.
- The measurement of group delay shows that the variations are less than 0.1 ns and stable in the entire UWB spectrum. Therefore, the conclusion is that negligible time delay is there for the input signal.

7.3 Suggestions for future research work in this field

- Energy requirements have got paramount importance owing to increase in population, industrial development, technology advancement and the resulting needs of human beings. Consequently, new paradigms are needed to be explored which satisfy our energy needs in our daily life. Hence exploring new sources to extract energy from the surroundings and to convert into electrical energy has become a hot topic for research. Antenna is one of the most crucial components in RF energy harvesting system to extract maximum power. Rectifying antenna (rectenna) which can convert RF energy to DC can now play an important role in energy harvesting. The planar CP antennas are good candidates for energy harvesting due to their advantages. The CP antennas developed here may be applied to RF energy harvesting systems.
- Stacking may be employed to enhance the gain of single band CP antennas developed in this piece of research, without altering CP characteristics.
- Radome may be incorporated without affecting the CP performance, for enhanced gain, especially in RF energy harvesting applications.
- 100% CP coverage of the UWB spectrum is possible with improvised design without compromising dimensions.
- It is possible to form arrays with the asymmetric CP antenna structures, such that maximum gain and full band coverage of UWB are realised.

- The designs of the antennas described have been implemented on FR4 substrate only. Instead of using such lossy substrates, the design may be checked on low temperature co-fired ceramic (LTCC) substrates, which can be directly integrated with monolithic microwave circuits.
- Further miniaturization of the existing structures may be realised.
- Time domain analysis of the circularly polarised UWB antennas may be carried out for a better study.
- Characteristic mode analysis of only one antenna is done here. It may be extended to all the antennas for a better study.

.....❧.....

||| List of Publications |||

Journal Publications

- 1) **K.C.Prakash**, S.Mathew, R.Anitha, P.V.Vinesh, M.P. Jayakrishnan, P.Mohanan and K.Vasudevan Circularly Polarised dodecagonal patch antenna with polygonal slot for RFID applications Progress in Electromagnetics Research C, Vol.61, 9-15,2016.
- 2) **Prakash K.C**, Vinesh P.V., Jayakrishnan M.P., Dinesh R., Mohammad Ameen and Vasudevan K. Hexagonal Circularly Polarized Patch Antenna For Rfid Applications International Journal on Cybernetics & Informatics (IJCI) Vol. 5, No. 2, April 2016
- 3) **Prakash K. C**, Vinesh P. V, Vivek R, Mohammad Ameen, and Vasudevan K Circularly Polarised Hexagonal Patch Antenna With Polygonal Slot for RFID Applications Journal Of Communications Software and Systems, Vol. 12, No. 2, June 2016
- 4) **K C. Prakash**, P V. Vinesh, Manoj M, S.Mathew, P.Mohanan, and K Vasudevan, "Printed Circularly Polarised Asymmetric Ultra-Wideband Antenna", Progress In Electromagnetics Research M, Vol. 74, 179–189, 2018
- 5) R.Anitha, P.V. Vinesh, **K.C.Prakash**, P.Mohanan, K.Vasudevan A Compact Quad Element Slotted Ground Wideband Antenna for MIMO Applications, IEEE Transactions on Antennas and Propagation Vol. 64, No. 10, Oct. 2016.

Conference Publications

- 1) **Prakash K.C**, Vivek R. Kurup, Vinesh P.V, Mohammad Ameen, Jayakrishnan M. P, Anitha. R, Sumitha Mathew and K.Vasudevan Dodecagonal Circularly Polarized Patch Antenna for RFID Applications, Proceedings of fifth International IEEE Applied Electromagnetics conference, 18-21 December 2015, IIT, Guwahati (published in IEEE xplorer).

- 2) **Prakash K.C**, Vinesh P.V., Jayakrishnan M.P., Dinesh R., Mohammad Ameen and Vasudevan K, Hexagonal Circularly Polarized Patch Antenna For Rfid Applications, Proceedings of International Conference on Computing & CommuniCation ICC16, 18th January 2016, MA College of Engineering, Kothamangalam, Kerala.
- 3) **Prakash K.C**, Vinesh P.V., Vivek R., Mohammad Ameen and Vasudevan K, Circularly Polarized Decagonal Patch Antenna with Polygonal slot for RFID Applications, Proceedings of National Conference NCRTCIS16, Sree ayyappa College, Eramallikkara
- 4) **Prakash K.C**, Vinesh P.V, Sumitha Mathew, Mohammad Ameen, Vasudevan K.Circularly Polarised Tridecagonal Patch Antenna for Power Harvesting Applications, proceedings of International Conference on Computing Communication and signal Processing ICCSP2016, published by Mc Graw Hill Education, New Delhi, ISBN-13,978-93- 5260-127-1
- 5) **Prakash K.C**, Vinesh P.V, Sumitha Mathew, Mohammad Ameen, Vasudevan K. Novel Circularly Polarised Antenna for Power Harvesting applications Proceedings of International Conference on Signal Processing and Advanced Communication SPACC16, Aug 10-11, College of engineering, Cherthala
- 6) **Prakash K.C**, Vinesh P.V, Vivek R, Mohammad Ameen and Vasudevan K, Circularly Polarised Hexadecagonal Patch Antenna for Power Harvesting Applications, Proceedings of 8th National Conference on VLSI, Signal Processing and Communication , July 21-22, 2016, Viswajyothi College of Engineering and Technology, Vazhakkulam, Kerala.

- 7) **Prakash K.C**, Mohammad Ameen, Manoj M, Sumitha Mathew, Anitha R, Vinesh P.V, Vivek.R, Vasudevan.K, A Compact UWB Circularly Polarized Hexagonal Slot Antenna for Wireless Applications, Proceedings of International Symposium on antennas and Propagation APSYM2016, 15-17 Dec2016, pp197-200, ISBN: 978-93-80095-85-8.
- 8) Sumitha Mathew, **K.C Prakash**, Vivek R Kurup,K. Vasudevan “ Reduced Cross Polarisation Using Sectoral Slots in the Ground Plane of a Sectoral Patch antenna proceedings of International Conference on Computing Communication and signal Processing ICCSP2016, published by Mc Graw Hill Education, New Delhi, ISBN-13,978-93-5260-127-1.
- 9) Mohammad Ameen, **Prakash K.C**, Sumitha Mathew, Manoj M, K. Vasudevan, A compact pZi shaped Microstripantenna for WLAN, TD-LTE and Wi Max applications proceedings of International Conference on Computing Communication and signal Processing ICCSP2016, published by Mc Graw Hill Education, New Delhi, ISBN-13,978-93-5260-127-1.
- 10) Mohammad Ameen, **Prakash K.C**, Sumitha Mathew, Manoj m K, Vasudevan K, A Compact Wideband Square Slot Antenna with Enhanced Bandwidth for 5.2/5.8 GHz WLAN Applications, Proceedings of International Conference on Signal Processing and Advanced Communication SPACC16, Aug 10-11, College of engineering, Cherthala
- 11) Sumitha Mathew, **K.C Prakash**, Vivek R Kurup,K. Vasudevan, Annular ring patch antenna with omnidirectional radiation pattern for WiMAX applications , Proceedings of International Conference on Signal Processing and Advanced Communication SPACC16, Aug 10-11, College of Engineering, Cherthala.

- 12) Mohammad Ameen, **Prakash K. C**, Sumitha Mathew, Vinesh P. V, Anitha. R, P. Mohanan and K. Vasudevan A Compact S-Shaped 2x1MIMO Antenna for WLAN/WiMAX Applications, Proceedings of fifth International IEEE Applied Electromagnetics conference, 18-21 December 2015, IIT, Guwahati (published in IEEE xplorer).
- 13) Vinesh. P. V, Anitha. R, **Prakash. K. C**, Sumitha Mathew, P. Mohanan and K. Vasudevan A Compact L-slot loaded Planar Inverted F Antenna for GPS and WLAN Applications, Proceedings of fifth International IEEE Applied Electromagnetics conference, 18-21 December 2015, IIT, Guwahati (published in IEEE xplorer)
- 14) Mohammad Ameen, Sumitha Mathew, **Prakash K.C**, Manoj M, Mohanan P, Vasudevan.K, A Two Layer Circularly Polarised High Gain Antenna for 5.2 GHz LAN Applications, Proceedings of International Symposium on antennas and Propagation APSYM2016, 15-17 Dec2016, pp197-200, ISBN: 978-93-80095-85-8
- 15) Vinesh P.V, **Prakash K.C**, Mohammed Ameen, Sumitha Mathew, Anitha R, Vivek R, K.Vasudevan “ Compact Wide Band Planar inverted F antenna for LTE applications”, proceedings of 12th International Conference on MicrowAVES, ANTENNA Propagation and remote sensing ICMARS 2017, jodhpur, India Feb 15-17, 2017
- 16) Manoj M, Remsha R, Mohammed Ameen **Prakash K.C**, Mohammed Ameen, K.Vasudevan and P.Mohanan, “A novel Dualband ultra Compact Artificial Magnetic conductor backed antenna for wireless applications“ proceedings of 12th International Conference on MicrowAVES, ANTENNA Propagation and remote sensing ICMARS 2017, jodhpur, India Feb 15-17, 2017
- 17) Sumitha Mathew, **Prakash K.C**, Vinesh P.V Mohammed Ameen, K.Vasudevan “Slotted Ground Sectoral patch antenna with low cross polarization and enhanced gain” proceedings of 12th International Conference on MicrowAVES, ANTENNA Propagation and remote sensing ICMARS 2017, jodhpur, India Feb 15-17, 2017

- 18) **Prakash K.C**, Mohammad Ameen, Manoj M, Vinesh P.V, Vivek.R, Vasudevan.K “A Compact UWB Circularly Polarized Penta Decagonal Slot Antenna for Energy Harvesting Applications “proceedings of National Conference On Communication, Antennas And Signal Processing –NCCAS 2017, Acharya Nagarjuna University, Nagarjuna Nagar, Guntur , 24-25 March 2017.
- 19) **Prakash K.C**, Sreethu Suresh, K.Vasudevan, “ Circularly Polarised UWB antenna for RF Power Harvesting Applications”, National Conference on Recent Trends in Energy and Environment, NCEE2019, ISBN 978-81-936117-9-1, Feb 2019

.....❧.....

Curriculum Vitae

PRAKASH K.C

Designation	Associate Professor Sree Ayyappa College Eramallikkara P.O Thiruvandoor Via Chengannur, Alappuzha Dist., Kerala 689109 keyceepee@gmail.com
-------------	--

EDUCATION

Pursuing Ph.D in the area of Microstrip Antennas	Cochin University of Science and Technology, India
M.Sc Electronics with Specialisation in Artificial Intelligence and Robotics	Dept. of Electronics, Cochin University of Science and Technology, India 81.17%, Rank III, 1993
B.Sc Physics	Christian College, Chengannur affiliated to University of Kerala, Thiruvananthapuram, Kerala 93.8%, Rank IV, 1990
Pre-Degree	Christian College, Chengannur affiliated to University of Kerala, Thiruvananthapuram, Kerala 80.22%, 1987
S.S.L.C	Devaswom Board High School, Cherianad. Board of Public Exams, Kerala 81.17%, 1985

IT SKILL AND COMPETENCY

Operating Systems	Linux, Windows
Languages	C
Office Packages	MS Office '2010
Software Simulators	Ansyz HFSS'18.2, CST Microwave studio

TEACHING EXPERIENCE

25-10-1993 to 16-09-1995 Lecturer in Electronics Science,
College of Applied Science (Managed by
IHRD), Calicut

18-09-1995 to 08-06-1998 Lecturer in Electronics Science,
W.M.O Arts and Science College, (Govt.
Aided College, Affiliated to University of
Calicut), Muttill, Wayanad

09-06-1998 – till date Associate Professor, Sree Ayyappa
College (Managed by Travancore
Devaswom Board, Govt. Aided College,
Affiliated to University of Kerala),
Eramallikkara, Chengannur

PROFESSIONAL MEMBERSHIPS / REVIEWERSHIP

- Member, IEEE
 - Life Member, Institute of Electronics and Telecommunication Engineers (IETE)
 - Reviewer, Progress in Electromagnetic Research (PIER) Journals.
-

PERSONAL DETAILS

Age & Date of Birth 49 years, 31.05.1970, Male

Permanent Address Sreegeham,
Mampra P.O, PIN 689 508
Kodukulanji Via
Chengannur, Alapuzha Dist, Kerala

Nationality Indian

AREAS OF INTEREST

Electromagnetic Field Theory, Microstrip
Antennas, Circular Polarisation, RF
energy harvesting

PUBLICATIONS

International Journals	5
International/National Conferences	19

AWARDS

Secured the best paper award in the National Conference on VLSI, Signal Processing and Communication conducted by Viswajyothy College of Engineering and Technology, Vazhakulam, held on 21st and 22nd August, 2016.

REFERENCES

Dr. K .Vasudevan	Professor Emeritus, Department of Electronics, CUSAT, Pin -682021 Email:vasudevankdr@gmail.com Phone:+91 9447357328
Dr. P Mohanan	Professor Emeritus, Department of Electronics, CUSAT, 682021. Email: drmohan@cusat.ac.in Phone:+91 9447325765
Dr. K.S. Anilkumar	Principal Sree Ayyappa College, Eramalikkara P.O, Thiruvandoor Via, Chengannur, Alappuzha Dist., KERALA 689109 ksanilksitm@gmail.com, +919447410591

.....✍.....

